

NONLINEAR DYNAMICS AND CHAOTIC PHENOMENA

FLUID MECHANICS AND ITS APPLICATIONS

Volume 42

Series Editor: R. MOREAU

MADYLAM

Ecole Nationale Supérieure d'Hydraulique de Grenoble

Boîte Postale 95

38402 Saint Martin d'Hères Cedex, France

Aims and Scope of the Series

The purpose of this series is to focus on subjects in which fluid mechanics plays a fundamental role.

As well as the more traditional applications of aeronautics, hydraulics, heat and mass transfer etc., books will be published dealing with topics which are currently in a state of rapid development, such as turbulence, suspensions and multiphase fluids, super and hypersonic flows and numerical modelling techniques.

It is a widely held view that it is the interdisciplinary subjects that will receive intense scientific attention, bringing them to the forefront of technological advancement. Fluids have the ability to transport matter and its properties as well as transmit force, therefore fluid mechanics is a subject that is particularly open to cross fertilisation with other sciences and disciplines of engineering. The subject of fluid mechanics will be highly relevant in domains such as chemical, metallurgical, biological and ecological engineering. This series is particularly open to such new multidisciplinary domains.

The median level of presentation is the first year graduate student. Some texts are monographs defining the current state of a field; others are accessible to final year undergraduates; but essentially the emphasis is on readability and clarity.

For a list of related mechanics titles, see final pages.

Nonlinear Dynamics and Chaotic Phenomena

An Introduction

by

BHIMSEN K. SHIVAMOGGI

*Departments of Mathematics and Physics,
University of Central Florida,
Orlando, Florida, U.S.A.*



SPRINGER-SCIENCE+BUSINESS MEDIA, B.V.

A C.I.P. Catalogue record for this book is available from the Library of Congress

ISBN 978-90-481-4926-1 ISBN 978-94-017-2442-5 (eBook)
DOI 10.1007/978-94-017-2442-5

Printed on acid-free paper

All Rights Reserved

©1997 Springer Science+Business Media Dordrecht

Originally published by Kluwer Academic Publishers in 1997

Softcover reprint of the hardcover 1st edition 1997

No part of the material protected by this copyright notice may be reproduced or utilized in any form or by any means, electronic or mechanical,
including photocopying, recording or by any information storage and
retrieval system, without written permission from the copyright owner

अज्ञानतिमिरान्धस्य ज्ञानाङ्गनशलगक्या ।
चक्षुरुन्मीलितं येन तस्मै श्रीगुरवे नमः ॥

Salutations to that guru who opened the eye of the one blind due to the (cover) darkness of ignorance with the needle (coated) with ointment of knowledge.

— Skanda Purāna

To Jayashree, Vasudha and Rohini

TABLE OF CONTENTS

Introduction to Chaotic Behavior in Nonlinear Dynamics	1
Phase-Space Dynamics	3
Conservative Dynamical Systems	3
Dissipative Dynamical Systems	4
Routes to Chaos	8
Turbulence in Fluids	11
1. Nonlinear Differential Equations	13
1.1. Deterministic Problems	14
1.2. Equilibrium Points and Stability	15
(i) Liapunov- and Asymptotic Stability	21
(ii) The Center Manifold Theorem	25
1.3. Phase-plane Analysis	32
1.4. Fully Nonlinear Evolution	49
1.5. Non-autonomous Systems	51
2. Bifurcation Theory	61
2.1. Stability and Bifurcation	62
2.2. Saddle-Node, Transcritical and Pitchfork Bifurcations	65
2.3. Hopf Bifurcation	78
2.4. Bifurcation Theory of One-Dimensional Maps	85
2.5. Appendix	88
3. Hamiltonian Dynamics	93
3.1. Hamilton's Equations	94
3.2. Phase Space	98
3.3. Canonical Transformations	105
3.4. The Hamilton-Jacobi Equation	112
3.5. Action-Angle Variables	118
3.6. Infinitesimal Canonical Transformations	121
3.7. Poisson's Brackets	122
4. Integrable Systems	127
4.1. Separable Hamiltonian Systems	127
4.2. Integrable Systems	129
4.3. Dynamics on the Tori	137
4.4. Canonical Perturbation Theory	140
4.5. Kolmogorov-Arnol'd-Moser Theory	149
4.6. Breakdown of Integrability and Criteria for Transition to Chaos	160
(i) Local Criteria	160
(ii) Local Stability vs. Global Stability	163

	(iii) Global Criteria	166
4.7.	Magnetic Island Overlap and Stochasticity in Magnetic Confinement Systems	171
4.8	Appendix: The Problem of Internal Resonance in Nonlinearly-Coupled Systems	177
5.	Chaos in Conservative Systems	197
5.1.	Phase-Space Dynamics of Conservative Systems	197
5.2.	Poincaré's Surface of Section	198
5.3.	Area-preserving Mappings	205
5.4.	Twist Maps	207
5.5.	Tangent Maps	211
5.6.	Poincaré-Birkhoff Fixed-Point Theorem	214
5.7.	Homoclinic and Heteroclinic Points	217
5.8.	Quantitative Measures of Chaos	224
	(i) Liapunov Exponents	225
	(ii) Kolmogorov Entropy	229
	(iii) Autocorrelation Function	231
	(iv) Power Spectra	232
5.9.	Ergodicity and Mixing	233
	(i) Ergodicity	233
	(ii) Mixing	236
	(iii) Baker's Transformation	239
6.	Chaos in Dissipative Systems	247
6.1.	Phase-Space Dynamics of Dissipative Systems	247
6.2.	Strange Attractors	251
6.3.	Fractals	254
6.4.	Multi-fractals	263
6.5.	Analysis of Time Series Data	274
6.6.	The Lorenz Attractor	276
	(i) Equilibrium Solutions and Their Stability	277
	(ii) Slightly Supercritical Case	280
	(iii) Existence of an Attractor	284
	(iv) Chaotic Behavior of the Nonlinear Solutions	284
6.6.	Period-Doubling Bifurcations	286
	(i) Difference Equations	286
	(ii) The Logistic Map	289
Appendix 6.1:	The Hausdorff-Besicovitch Dimension	310
Appendix 6.2:	The Derivation of Lorenz's Equations	312
Appendix 6.3:	The Derivation of Universality for One-Dimensional Maps	314

7.	Fractals and Multi-Fractals in Turbulence	319
7.1.	Scale Invariance of the Navier-Stokes Equations and the Kolmogorov (1941) Theory	328
7.2.	The β -model for Turbulence	332
7.3.	The Multi-fractal Models	336
7.4.	The Random- β Model	340
7.5.	The Intermediate Dissipation Range	348
8.	Singularity Analysis and the Painlevé Property of Dynamical Systems	353
8.1.	The Painlevé Property	353
8.2.	Singularity Analysis	357
8.3.	The Painlevé Property for Partial Differential Equations	367
	Exercises	375
	References	385
	Index	399

Preface

Following the formulation of the laws of mechanics by Newton, Lagrange sought to clarify and emphasize their geometrical character. Poincaré and Liapunov successfully developed analytical mechanics further along these lines. In this approach, one represents the evolution of all possible states (positions and momenta) by the flow in phase space, or more efficiently, by mappings on manifolds with a symplectic geometry, and tries to understand qualitative features of this problem, rather than solving it explicitly.

One important outcome of this line of inquiry is the discovery that vastly different physical systems can actually be abstracted to a few universal forms, like Mandelbrot's fractal and Smale's horse-shoe map, even though the underlying processes are not completely understood. This, of course, implies that much of the observed diversity is only apparent and arises from different ways of looking at the same system. Thus, modern nonlinear dynamics¹ is very much akin to classical thermodynamics in that the ideas and results appear to be applicable to vastly different physical systems.

Chaos theory, which occupies a central place in modern nonlinear dynamics, refers to a deterministic development with chaotic outcome. Computers have contributed considerably to progress in chaos theory via impressive complex graphics. However, this approach lacks organization and therefore does not afford complete insight into the underlying complex dynamical behavior. This dynamical behavior mandates concepts and methods from such areas of mathematics and physics as nonlinear differential equations, bifurcation theory, Hamiltonian dynamics, number theory, topology, fractals, and others.

This book has grown out of my lecture notes for an interdisciplinary graduate level course on nonlinear dynamics which I have taught for the past several years to a mix of students in applied mathematics, physics, and engineering. I have endeavored to describe the basic concepts, language and results of nonlinear dynamical systems. This book is accessible, therefore, to first-year graduate students in applied mathematics, physics, and engineering, and is useful, of course, to any theoretically inclined researcher in the physical sciences and engineering. In order to allow an interdisciplinary readership, I have adopted an informal style, kept the mathematical

¹ In view of the ubiquity of nonlinear phenomena, it is rather awkward to call the subject nonlinear dynamics. As Stanislaus Ulam put it (Gleick (1987)), "Calling the subject nonlinear dynamics is like calling zoology 'non-elephant studies'".

formalism to a minimum, and omitted much detail. Thus, I have stated a few theorems for which the proofs are only sketched or are replaced by illustrative examples which make the general principles plausible.

The book starts with a discussion of nonlinear ordinary differential equations, bifurcation theory, and Hamiltonian dynamics. It then embarks on a systematic discussion of the traditional topics of modern nonlinear dynamics – integrable systems, Poincaré maps, chaos, fractals and strange attractors. The Baker's transformation, the logistic map and the Lorenz system are discussed in detail in view of their central place in the subject. Then, there is a detailed discussion of the application of fractals and multi-fractals to fully-developed turbulence – a problem whose understanding has been considerably enriched by the application of the concepts and methods of modern nonlinear dynamics. Finally, there is a discussion of the Painlevé property of nonlinear differential equations which seems to provide a test of integrability. On the application side, one may discern a special emphasis on some aspects of fluid dynamics and plasma physics reflecting my continued involvement in these areas of physics. I have provided a few exercises that range from simple applications to occasional considerable extension of the theory. Finally, the list of references given at the end of the book contains primarily books and papers I have used in developing my lecture material (and this book). This list is not to be construed as complete (experts may notice omission of many important papers).

Orlando
1997

Bhimsen K. Shivamoggi

Acknowledgments

I want to place it on record right from the outset that without the help, support and encouragement of several individuals this book would never have seen the light of day.

My first gratitude is to Professor Peter Rautenstrauch, our Assistant Chairman, and Professor Larry Andrews, our former Graduate Coordinator, who were very instrumental in getting our graduate course on Nonlinear Dynamics off the ground several years ago and sustained their valuable support as this course developed and evolved further. I wish to thank our Department Chairman, Professor John Cannon, for his enormous support and encouragement of this project.

In the preparation of this course/manuscript material, I have enormously drawn from the ideas, procedures and treatments developed by several eminent authors - V.I. Arnol'd, M.V. Berry, M.J. Feigenbaum, J. Ford, U. Frisch, M. Hénon, B. Mandelbrot, R.M. May, J. Moser, D. Ruelle, and others. I have acknowledged the various sources, in this connection, in the References, given at the end of this book and wish to apologize to any others I may have inadvertently missed. I wish to express my gratitude to Professor K. Sreenivasan for his suggestions and providing me with some unpublished data presented in Chapter 7. I wish also to thank my students and colleagues who rendered valuable assistance as the course material was developed. Most of the manuscript was read by Professors John Cannon, Earl Dowell, and David Rollins who made valuable suggestions. Some sections of the manuscript were also read by Professors Larry Andrews, Ram Mohapatra, and Mike Taylor. I wish to acknowledge the benefit I have had from the enlightening discussions with Professor Mahinder Uberoi on the problem of turbulence. I wish to thank Professor Ronald Phillips for introducing me to the fractal aspects of turbulence. But, the responsibility for any defects in this book are mine alone. I wish to express my thanks to my colleague Professor Jagdish Chavda of our Art Department for his assistance in the reproduction of original figures.

My sincere thanks are due to Jackie Callahan for the exemplary patience, dedication, and skill with which she did the whole typing job and the support she gave to me for this whole project as well. My thanks are due to Ronee Trantham for her excellent job in doing the figures. My thanks are also due to Kluwer Academic Publishers for their cooperation with this whole project. Last, but by no means least, my immense thanks are due to my wife, Jayashree and my daughters, Vasudha and Rohini for their enormous understanding and cooperation with this endeavor as I sat away occupied with this work week after week, month after month, almost forever! Therefore, I dedicate this book to my wife and daughters as a token of my love and gratitude.

Bhimsen K. Shivamoggi

INTRODUCTION TO CHAOTIC BEHAVIOR IN NONLINEAR DYNAMICS

Newtonian dynamics, until recently, twice founded in assuming something which was not infinite to be infinite: the speed of light, c , and the reciprocal of Planck's constant, $1/h$. Reformulations remedying these assumptions led first to special relativity and then to quantum mechanics. Special relativity set to rest the Newtonian illusion of absolute space and time while quantum theory ended the Newtonian illusion of absolute objectivity in a measurement process. It was further realized that Newtonian dynamics entails a third tacitly assumed infinity, namely, one of infinite computational and observational precision. Reformulation of Newtonian dynamics remedying this assumption has led to chaos theory. The impact of chaos theory on science may be as significant as the first two, particularly since the concepts and results of chaos theory are applicable to a wide variety of physical, chemical and biological systems.

In the Newtonian view of mechanics, dynamical systems have a deterministic behavior, i.e., their evolution is completely determined by well-defined equations of motion in conjunction with precise knowledge of the conditions of the system at one time. All events abstracted as orbits of bodies under forces, are therefore completely predictable. Laplace (1776) even claimed that "we ought to regard the present state of the universe as the effect of its preceding state and as the cause of its succeeding state". But, then there is the age old fact that it is almost impossible to determine in practice the outcome of flipping a coin or rolling a dice. Indeed, Maxwell (1873) expressed doubts regarding Laplacian determinism and made the following prophetic remark – "it is manifest that the existence of unstable conditions renders impossible the prediction of future events, if our knowledge of the present state is only approximate, and not accurate." Poincaré's (1892) studies of the three-body problem in celestial mechanics further established that a purely deterministic law may materialize in a totally random series of observations, if part of the information is withheld, as it must be in any practical situation. To quote Poincaré, "...even in the case that the natural laws no longer held any secrets for us, we could only know the initial situation approximately.... It may happen that small differences in initial conditions produce very great ones in the final phenomena." We cannot attribute this apparent randomness to the influence of unknown factors *like noise* (because there are none) that preclude a causal evolution nor to infinite degrees of freedom with an underlying randomness (because two degrees of freedom are sufficient) that force a necessary human ignorance about the details of the process concerned. Chaos theory, which is concerned with chaotic outcomes in deterministic evolutions, has eliminated the Laplacian fantasy of deterministic predictability.

Lorenz (1963) confirmed that relatively simple deterministic systems of equations can exhibit solutions whose details are unpredictable over long times because of the amplification in time of arbitrarily small uncertainties in the state of the system. As Ekeland (1987) put it, "like the Queen of England, determinism reigns but does not govern!"

Chaos is a term that is now used to describe unpredictable long-term behavior present in simple deterministic nonlinear dynamical systems. It is now recognized that chaotic behavior in nonlinear dynamical systems is the rule rather than the exception. Indeed, Newtonian determinism assures us that chaotic solutions exist and are unique, but they are nonetheless so complex that they are virtually indistinguishable from realizations of truly random processes in the sense of extreme sensitivity to initial conditions (extremely small changes in the initial conditions leading to completely different outcomes)¹. The resemblance of chaotic orbits to truly random processes further entails the equality of time-average of any continuous function along the orbits converging to the average with respect to the invariant probability distribution of the system, for a set of positive measure of initial conditions. The ubiquity of chaos places limitations on our image of Nature in an essential way which may be considered to be rather similar to those caused by the Heisenberg uncertainty principle in quantum theory. Indeed, long ago, Plato (in the Book VII of his Republic) warned that humans are condemned to sense the true reality only through its imperfect projections into the world of appearances in much the same way as the prisoners in a cave sensed real things via their shadows on the cave wall!

The study of chaos has flowered during the past two decades, with a strong impetus coming from the discovery of scale invariant "universal" properties involved in the transition to chaos (Feigenbaum, (1978)) and the experimental observation of these properties (Libchaber, Fauve, and Laroche, (1983)), (see also Proccacia (1988) for a review). Universality implies that there are basic properties of the system (such as critical exponents near the transition to chaos) that depend only on some global properties of the system, and hence calls for renormalization group considerations (Feigenbaum, (1978)) based on the scale invariance.

¹ The extreme sensitivity of chaotic systems to small perturbations also implies that such systems present greater flexibility in their performance. Thus, one may use small feedback perturbations to control trajectories in chaotic systems (Shinbrot et al. (1993)) over a large region of the state space of the system. Such a possibility does not exist for nonchaotic systems which typically require a large control to produce a large effect.

Phase-Space Dynamics

For each degree of freedom of a system, there are two dynamical quantities: position and velocity. The state of a system of n degrees of freedom is given by a representative point in the $2n$ -dimensional phase space with n position coordinates and n velocity coordinates. The motion of the system is then described by the trajectory of the representative point in the phase space. Dynamical systems for which the total energy is conserved are called conservative systems, and those (like many in the real world) for which, this is not true are called dissipative systems.

Conservative Dynamical Systems

Liouville's Theorem shows that, for conservative dynamical systems, the volume of phase space occupied by an ensemble of states remains constant with time. The time evolution of a conservative system is described by a trajectory lying on a surface described by the conservation of energy in the phase space. A dynamical system is said to be ergodic if, left to itself for long enough, its trajectory will pass close to nearly all the points on the surface described by the conservation of energy.

A classical system is called integrable if it has as many constants of motion as the degrees of freedom, say n . Integrable systems are not ergodic since the constants of motion provide sufficient geometric constraint to the phase flow to force all the trajectories to lie on n -dimensional integral surfaces called "invariant tori" embedded in the $(2n - 1)$ -dimensional energy surface. Nonintegrable systems seem to exhibit ergodic behavior of some type due to the breakdown of the invariant tori. The introduction of even a small perturbation to an integrable system can lead to breakup of some invariant tori, and one finds regimes of irregular motion embedded in regimes of regular motion. As the perturbation increases, the regimes of irregular motion grow in size. This was observed in the numerical experiments of Hénon and Heiles (1964). The Kolmogorov-Arnol'd-Moser Theory (Kolmogorov (1954), Arnol'd (1963), and Moser (1962)) establishes what types of perturbations are likely to destroy the invariant tori. In order to understand this process better, we note that the invariant tori are covered by families of closed orbits. In a surface of section of the energy surface, a single one of these orbits would generate a pattern of fixed points lying on a smooth curve. On perturbation this smooth curve is broken up. According to the Poincaré-Birkhoff Fixed Point Theorem (Birkhoff, (1927)), one would find, in its place, pairs of elliptic and hyperbolic fixed points. The elliptic fixed points correspond to stable closed orbits and each is surrounded by smooth invariant curves corresponding to higher order tori. On the other hand, hyperbolic fixed points correspond to unstable closed orbits. The invariant tori in the neighborhood of such resonance points are destroyed, and chaos in the form of

transverse homoclinic orbits and horseshoes (see Chapter 5) shows up in the motion in such gaps. These resonances and the stochastic layers associated with them get wider with the increasing perturbation so that the invariant tori separating them become increasingly squeezed and distorted, and at a sufficiently large perturbation they disappear. The neighboring resonances then merge and overlap and chaos fills the whole space. Indeed, Chirikov (1979) proposed that such multiple overlap of nonlinear resonances is the cause of the onset global chaos in the system.

The standard method to test the integrability of a given dynamical system is indirect and is based on a geometric approach which considers the topological structure of the dynamical trajectories in phase space. This technique was given by Poincaré, (1892) and makes use of the fact that the evolution of a conservative Hamiltonian system in the phase space can be considered as an area-preserving mapping of the energy surface onto itself. In this method, given an orbit starting from a point x_o on the $(2n - 1)$ dimensional energy surface, one chooses an $(2n - 2)$ dimensional manifold S called the Poincaré surface of section passing through x_o and transverse to the orbit. Starting from x_o , the orbit will come back and hit the surface of section S at x_1 , and again at x_2 , etc. The successive iterates x_1, x_2, \dots of an initial point x_o on S reveal whether or not the system is integrable. If it is, the successive iterates x_1, x_2, \dots lie on a smooth closed curve C on S . If it is not, the successive iterates x_1, x_2, \dots constitute a set of randomly scattered points on S . The disadvantage of this method is that one needs to numerically integrate the orbits on the computer which can be an elaborate procedure. There appears to be no general direct method yet for testing the integrability of a given dynamical system.² The Painlevé criterion (Hillé (1976); Ablowitz, Ramani, and Segur (1980)), which exploits the fact that the integrability of a dynamical system is intimately linked with its analytical structure (i.e., the behavior of the solution in the complex plane), has been proposed as such a test, but the proof of this conjecture is still open.

Dissipative Dynamical Systems

In dissipative dynamical systems, the volume of phase space occupied by an ensemble of states decreases with time. This volume contraction simplifies the long-term topological structure of trajectories, so a complex dynamical system with phase space spanned by many degrees of freedom can settle to a final motion in a subspace of only a few dimensions.

Dissipative systems typically exhibit a start-up transient, after which the motion settles on to some form of long-term recurrent behavior, termed an attractor which is a set that attracts the nearby orbits. An attractor is also the closure of the set of points

² There exists, however, a method (due to Whittaker (1964)) to construct integrable Hamiltonians for a restricted class of problems.

visited asymptotically by the orbit. (A conservative system can never have an attractor, since its evolution does not involve volume contraction in phase space.) One such form of steady-state response is the stationary equilibrium point. In this simplest form of attractor, all motion has ceased and local trajectories converge to a fixed point, as for example in the motion of a simple pendulum.

Some systems do not come to rest in the long term but instead cycle periodically through a sequence of states. An example is, the pendulum clock, in which energy lost to friction is replaced by a mainspring or weights. The pendulum repeats the same motion over and over again. In the phase space such a motion corresponds to a cycle, or periodic orbit. No matter how the pendulum is set swinging, the cycle approached in the long-term limit is the same. Such attractors are therefore called limit cycles.

A system may have several attractors. If that is the case, different initial conditions may evolve to different attractors. The set of points that evolve to an attractor is called its basin of attraction. The pendulum clock has two such basins: small displacements of the pendulum from its rest position result in a return to rest; with large displacements, however, the clock begins to tick as the pendulum executes a stable oscillation.

The next most complicated form of attractor is a torus. This shape describes motion made up of two independent oscillations, sometimes called quasi-periodic motion. The orbit winds around the torus in phase space, one frequency determined by how fast the orbit circles the torus the short way, the other determined by how fast the orbit circles the long way around. Attractors may also be higher-dimensional tori since, they represent the combination of more than two oscillations.

The important feature of quasi-periodic motion is that in spite of its complexity it is predictable. Even though the orbit may never exactly repeat itself, if the frequencies that make up the motion have no common divisor, the motion remains regular. Orbits that start on the torus near one another remain near one another, and long-term predictability is guaranteed.

Until fairly recently, fixed points, limit cycles and tori were the only known attractors. In 1963, Lorenz discovered a chaotic, or strange attractor embedded in the convective flow described by a system of three nonlinear ordinary differential equations. The solutions of these equations show a random character for certain ranges of the governing parameters and the limit set of the representative points of the solutions in phase space is a strange attractor which is not a simple geometric object as a torus. This strange attractor describes the unpredictable motion which, the given deterministic dissipative system settles down to. Thanks to the dissipative nature of the motion, strange attractors are sets of lower dimensions than the system phase space in which they are embedded. The basic mechanism responsible for randomness is the sensitive dependence of solutions on initial conditions. Two orbits with nearly identical initial conditions diverge exponentially fast and so stay close together for only a short time.

The exponential divergence of adjacent trajectories does have a significant effect when observing trajectories with less than infinite precision. Any uncertainty in the

initial position leads to an error in the evolving position that increases exponentially as the true and approximate trajectories spread apart. The combination of sensitivity to initial data and only approximate information about initial data makes accurate long-term prediction impossible. Indeed, for a given degree of precision in the initial conditions, there is a "predictability horizon" as Lighthill (1987) put it. This is a time after which solutions with initial conditions that are nearest neighbors to the accuracy of specification being used become remote from one another. On the other hand, some short-range predictability also becomes possible, if the system in question is deterministic rather than random. This is apparent by noting that, it is possible to predict the future state of the system for a length of time which is determined by the accuracy with which the present state of the system is known.

The chaotic behavior arises through a simple stretching and folding operation occurring in the phase space. Exponential divergence is a local feature: Because attractors have finite size, two orbits on a chaotic attractor cannot diverge exponentially forever but must be confined globally. Consequently, the attractor must fold over onto itself. Although orbits diverge and follow increasingly different paths, they eventually must pass close to one another again. The orbits on a chaotic attractor are shuffled by this process which is the cause of the randomness of the chaotic orbits. The process of stretching and folding happens repeatedly, creating folds within folds ad infinitum, and leads to an infinitely-layered structure. The cross-sections through these layers are fractals (a term coined by Mandelbrot (1977)), in structure so that a chaotic attractor is, in other words, a fractal like a Cantor set: an object that has a self-similar structure which is maintained on all scales and which gives this object a noninteger or "fractal" dimension. Thus, a chaotic attractor has a much more complicated structure than a predictable attractor such as a point, a limit cycle or a torus³. Observed at large scales, a chaotic attractor is not a smooth surface but one with folds on it. In the presence of a chaotic attractor, one can describe the motion itself as a random walk in the space of allowed unstable periodic orbits. Furthermore, for a system with several attractors, the boundary separating two basins of attraction may also be a fractal (Grebogi et al. 1987).

May (1976) showed that there is a close correspondence between motion on a strange attractor and motion described by noninvertible one-dimensional maps. Noninvertible maps of the unit interval onto itself undergo a sequence of bifurcations as a parameter is varied such that the period of an attracting periodic orbit doubles repeatedly, accumulating at a critical parameter value beyond which the behavior is

³ In fact, Cantor's set theory and Peano's space-filling curve marked the break of modern mathematics with classical mathematics that was predicated on the regular geometric structures of Euclid. It came, at first, as a bit of surprise, when these pathological structures were manifest all around us in nature. Indeed, as Mandelbrot (1977) noted, even "the human tissue is a bona fide fractal surface...Lebesgue-Osgood monsters are the very substance of our flesh!"

chaotic. Feigenbaum (1978) has shown that this process has universal features treatable by the method of renormalization groups. Similarly, when a parameter is changed in a dissipative system, the system may change from periodic motion to the chaotic motion on a strange attractor. In many cases this change proceeds by successive doublings of the period of the singly periodic motion to some limit, beyond which the attractor changes character and becomes chaotic.

The first experimental evidence of the existence of chaotic attractors underlying random motion in fluid flows was given by Gollub and Swinney (1975). This evidence was indirect because they focused not on the attractor itself but rather on statistical properties characterizing the attractor. Gollub and Swinney examined the Couette flow between two concentric rotating cylinders. As the angular velocity of the inner cylinder increases, the fluid shows progressively more complex flow patterns. Gollub and Swinney measured the velocity of the fluid at a given spot⁴. As they increased the rotation rate, they observed transitions from a velocity that is constant in time to a periodically-varying velocity and finally to an aperiodically-varying velocity. At low rates of rotation, the flow of the fluid did not change in time: the underlying attractor was a fixed point. As the rotation rate was increased, the fluid began to oscillate with one independent frequency, corresponding to a limit-cycle attractor (a periodic orbit), and as the rotation rate was increased further, the oscillation took on two independent frequencies, corresponding to a two-dimensional torus attractor. According to Landau's (1959) theory for the onset of turbulence, as the rotation rate was increased this pattern would continue: more distinct frequencies would gradually appear as a result of successive Hopf bifurcations. The resulting motion would be quasi-periodic and would not show any sensitive dependence on the initial conditions. However, in the experiment, at a critical rotation rate, after only a finite number of bifurcations, a continuous range of frequencies suddenly appeared, and the irregular fluid motion near the transition was found to be described by deterministic chaotic attractors, in accordance with the scenario advanced by Ruelle and Takens (1971). The Ruelle-Takens scenario envisages a sequence of transitions generating successively an attracting $(n+1)$ -torus from an attracting n -torus, $n = 0, 1, 2, \dots$ with a strange attractor lying arbitrarily close to any uniform motion on an n -torus, $n \geq 3$. Thus, it appears that the onset of turbulence may be identified with a kind of low-dimensional chaos. However, once a strange attractor for the problem in question has been identified, this proposition

⁴ The time series of the velocity at a point in the fluid can be experimentally measured using the laser Doppler velocimetry. A laser beam scattered by small solid particles suspended in the fluid and moving with it is slightly Doppler-shifted due to the motion of the fluid. The instantaneous local fluid velocity is then obtained by measuring this small frequency shift. A time series of the local fluid velocity is obtained by repeating this measurement.

envisages linking up the ergodic theory on the strange attractor with the statistical theory of turbulence.

Routes to Chaos

In view of the great variety of chaotic behavior observed in experiments on nonlinear systems, it would be premature at this time to make sweeping generalizations about routes to chaos. Nevertheless, it is encouraging that a small number of common transition scenarios through bifurcation sequences are beginning to emerge from experiments. Two major routes are:

- (i) Period doubling: The transition process is not a single bifurcation but an infinite sequence of them: The starting point is an attracting periodic orbit which loses stability at a first critical value R_1 of the parameter, R . It then produces a new attracting periodic orbit in much the same way as an attracting periodic orbit is produced in the Hopf bifurcation. The new orbit follows the old one closely but goes around it twice before closing. Thus, the period of the stable oscillation for R just above R_1 is twice that for R just below R_1 : Hence the name, period-doubling bifurcation. As the parameter R is further increased, at a second critical value R_2 , the system has an attracting periodic orbit that follows four times around the fundamental orbit before closing, i.e., a stable oscillation with period about four times the base period. This orbit in turn undergoes a period doubling bifurcation (at $R = R_3$) producing an oscillation with period about eight times the base period, and in fact the cascade continues ad infinitum in a finite parameter interval. The parameter value R to which the sequence of doublings converges represents the onset of chaotic behavior.

The period-doubling route to chaos has been observed in Rayleigh-Bénard convection. This is a thermoconvection experiment in which a horizontal layer of fluid is heated from below. The signals shown in Figure 1 (due to Libchaber et al. (1983)) were obtained from a cell with an aspect ratio of 4, containing mercury, immersed in a magnetic field. The system is displaced from equilibrium by increasing the vertical temperature gradient, which is expressed by the dimensionless Rayleigh number R . At a critical value R_c of R , the heat-conducting fluid at rest becomes unstable to convection and a spatially periodic horizontal roll pattern appears. At a value close to $2R_c$, another instability sets in, and stationary convection disappears in favor of oscillatory convection (which can be attributed to a wave propagating along the roll axes), so that any variable measured at any point in space exhibits an oscillating signal. As R is further increased this periodic regime becomes

unstable and there appears a new periodic state with double the period. Figure 1 shows the succession of signals of the temperature at a point in the fluid bifurcating out upon increasing R - the period doubling where the length of one period, defined by a basic pattern repeated indefinitely, doubled at each successive instability until a completely chaotic motion resulted. This sequence exhibited a quantitative universality discovered earlier for one-dimensional maps by Feigenbaum (1978). The successive critical values of R for at least four period doublings seemed to form a geometric series with the same convergence rate -

$$\lim_{n \rightarrow \infty} \frac{R_n - R_{n-1}}{R_{n+1} - R_n} = 4.66902\dots$$

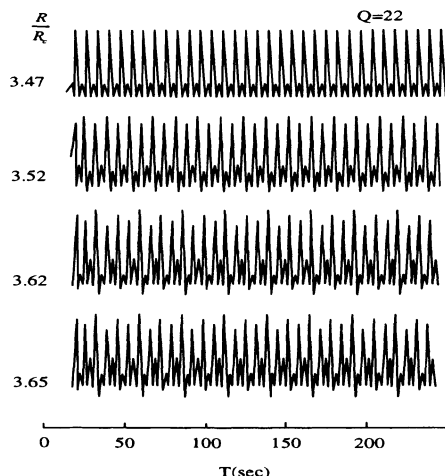


Figure 1. Period-doubling cascade in a thermoconvection experiment. The lines segments show the length of one period of basic pattern repeating as a function of the control parameter R/R_c . (Due to Libchaber et al. (1983)) (By courtesy of Elsevier Science Publishers)

However, because of the relatively large value of the limiting ratio, all but the first few R_n 's can be expected to be very close together, and this makes the observation of successive period doublings and physical measurement of the ratio extremely difficult. Unless the parameter can be controlled extraordinarily well, what will be observed are one or two period doublings

and then a chaotic behavior. In fact, up to now, the limiting ratio does not appear to have been measured in any physical system.

Still, a legitimate question is – why should a spatially extended system, such as a fluid undergoing thermal convection, exhibit a behavior similar to that of simple maps that contain none of the physics? The answer to this question lies in the fact that the experiments were done on highly dissipative, spatially constrained systems which acted as if they had only a few degrees of freedom.

- (ii) **Intermittency:** Some systems exhibit a transition from periodic (for some parameter R less than a critical value R_c) to a chaotic behavior (for $R > R_c$) characterized by an occasional burst of noise (Pomeau and Manneville (1980)). For R only slightly greater than R_c , there are long intervals of periodic behavior between short bursts of chaos, but with increasing R the intervals between the bursts decrease; it becomes more and more difficult and finally impossible to recognize the periodic behavior. This route to chaos has also been observed in Rayleigh-Benard convection under variant conditions (Libchaber and Maurer (1980)). Numerical computation due to Grebogi et al. (1987) (see Figure 2) shows that prior to the burst of chaos the amplitude of the subharmonic grows continuously, while at the instant of the burst of chaos, the amplitude of the subharmonic increases abruptly along with a concomitant decrease in the amplitude of the fundamental. For the intermittency scenario, Manneville and Pomeau (1979) also discovered a universal scaling law, similar in form to that for the period-doubling sequence, relating the average duration of regular motion to the deviation of the control parameter from its tangent bifurcation (see Chapter 6) value.

It should be noted that a given system may show more than one route to chaos depending on the values of the control parameters or the initial conditions. This is due to the fact that the basins of attractors are tremendously interlocked.

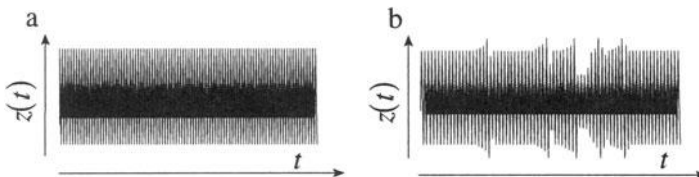


Figure 2. Intermittency in the numerical calculation of the Lorenz equations as the control parameter γ increases from (a) $\gamma = 166.00$ to (b) $\gamma = 166.2$. (Due to Grebogi et al. (1987)) (By courtesy of the American Association for Advancement of Science)

Turbulence in Fluids

The dynamical systems approach, which is concerned with the global behavior of all the solutions rather than the particular behavior of a given solution, has not solved the age old problem of turbulence in fluids which is both spatially and temporally chaotic and is characterized by a continuous range of length scales.⁵ However, the dynamical processes leading to fully-developed turbulence are believed to consist of stretching and folding of the sheet like structures in the physical space in a manner qualitatively similar to what happens in establishing a strange attractor in phase space. Indeed, if the basic mechanism underlying the observed chaotic behavior in fluid turbulence is one which does not require consideration of many degrees of freedom, then it might be useful to model it by simple deterministic finite-dimensional dynamical systems which show chaotic behavior in the sense of sensitivity to initial conditions (Lanford, 1982). This has the operational advantage that the embedding space is low dimensional and so accurate characterizations are generally possible. Indeed, experiments (Swinney and Gollub (1978)) have indicated that some features of the early stages of the transition to turbulence in certain fluid flows can be understood, at least qualitatively, via low-degree-of-freedom dissipative dynamical systems. It should be noted, however, that a dissipative system may have infinitely many attractors, each having its basin of attraction. Therefore, an attractor model of turbulence poses difficulties for the widely believed picture of turbulence, according to which the details of the flow are not predictable while the statistical properties are; the attractor model forces even the statistical properties to depend on the initial conditions! Nevertheless, chaos considerations have provided new methods of characterizing turbulent behavior, such as the measurement of the average Liapunov exponent (which measures the exponential rate at which two trajectories started at nearby initial conditions diverge), the entropy (which measures the average rate at which an orbit loses information about its initial condition), and the fractal dimension of the strange attractor associated with turbulence.

⁵ This aspect provides a certain similarity of turbulence to the problem of phase transitions and critical phenomena in condensed matter physics in that, at a critical point, many of the precise details of the interactions between constituent subunits play essentially no role in determining the bulk properties of the system. More particularly, at a critical point, the correlation $C(r)$ between subunits separated by a distance r shows a power-law decay, $C(r) \sim r^{-\eta}$, signifying the absence of a characteristic scale in the system. Besides, the characteristic exponent η depends essentially on the dimension of the system and on the general symmetry properties of the constituent subunits, and not on other details of the system. This has provided the *raison d'être* for the application of scaling and universality arguments and the renormalization group methods to the problem of turbulence. The latter approach is further supported by the infinitely-nested self-similar structure believed to be present in a fully-developed turbulence.

CHAPTER 1

NONLINEAR DIFFERENTIAL EQUATIONS

Traditionally all the macroscopic phenomena observed in nature have been studied via solutions of differential equations which are described by smooth and continuous curves. This approach works very well for a class of problem like the planetary motion where the orbits are regular geometric objects (namely, ellipses). However, there is a class of problems like the fluid turbulence which involves growth of objects of irregular shape and cannot be studied via smooth solutions of differential equations.

On the other hand, nonlinear differential equations present altogether interesting possibilities. Essentially new phenomena occur in nonlinear problems, which have no place in the corresponding linear problems. Therefore, in the following, we will venture not so much to introduce methods of improving the accuracy obtainable by the linear problem, but to focus attention on those features of the nonlinearities that result in distinctively new phenomena (some of which also serve to remedy the defects produced by the linear problem)! Among the latter are (Hagedorn (1988)):

- existence of solutions of periodic problems for all values of the frequency rather than only a set of characteristic values;
- dependence of amplitude on frequency;
- removal of resonance infinities;
- appearance of jump phenomena;
- onset of chaotic motions.

However, linear systems possess explicit solutions, so they can be used to approximate the motion near equilibrium points of nonlinear systems. As we will see in Chapter 5, for the discrete analogues, one may similarly use linear maps to approximate the motion near periodic orbits of nonlinear systems.

1.1. Deterministic Problems

Let D be a domain¹ in R^n and let $f: D \rightarrow R^n$ be a smooth function. A dynamical system is defined as a system of n first-order differential equations in n variables, $\mathbf{x} = (x_1, \dots, x_n)$:

$$\dot{\mathbf{x}}(t) = \mathbf{f}(\mathbf{x}) \quad (1)$$

with the initial condition

$$\mathbf{x}(0) = \mathbf{x}_o, \quad (2)$$

and hence provides for a deterministic evolution of the state of a system in time.² Equation (1) defines a flow³ $\phi_t: R^n \rightarrow R^n$ where $\mathbf{x}(t) = \phi_t(\mathbf{x}_o)$ and has a family of solution curves or trajectories generated by the initial conditions (2), which fill D . It is customary to think of certain geometric structures called manifolds on which solutions "flow" in time. The solution $\mathbf{x}(t)$ remains on the particular trajectory that passes through (2) for all time t . The behavior of $\mathbf{x}(t)$ as $t \rightarrow \pm\infty$ may be found by following the trajectory.

If

* \mathbf{x}_o is a point other than a singular point where

$$\dot{\mathbf{x}} = \mathbf{f}(\mathbf{x}) = \mathbf{0}^4 \quad (3)$$

* $\mathbf{f}(\mathbf{x})$ satisfies the Lipschitz property, i.e.,

$$|\mathbf{f}(\mathbf{y}) - \mathbf{f}(\mathbf{x})| \leq \kappa |\mathbf{y} - \mathbf{x}|$$

¹ For cases with more general phase spaces like finite-dimensional manifolds such as tori, the above discussion is still valid, albeit in a local coordinate system.

² The initial-value problem given by (1) and (2) is said to be well-posed if the solution $\mathbf{x}(t)$ exists and is free of singularities in $t > 0$ and, in addition, it depends continuously on the initial condition (2). This initial-value problem, on the other hand, is said to be ill-posed if the solution $\mathbf{x}(t)$ exists only for analytic initial condition (2) and, even when it does exist, it develops singularities in a finite time.

³ The concept of flow here is predicated on the resemblance of the solution trajectories to the paths followed by particles of a flowing fluid.

⁴ The trajectories corresponding to (3) are single points because $\phi_t(\mathbf{x}_o) = \mathbf{x}_o$ for all t .

for some $\kappa < \infty$,

then there exists an interval $0 < t < T$, in which equation (1) has a unique solution $\mathbf{x}(t)$ satisfying the initial condition (2).

The uniqueness of the solution $\mathbf{x}(t)$ implies that no two trajectories cross. Moreover, the trajectories vary smoothly over D except at singular points.

This leads to topological constraints on the trajectories in D and precludes complex dynamical behaviors in the one- and two-dimensional cases. Consequently, a chaotic behavior can occur only in the three- and higher-dimensional cases.

1.2. Equilibrium Points and Stability

Consider the autonomous system (for which, time plays the role of the independent variable and does not appear explicitly in the equation of motion),

$$\dot{x}_i = f_i(x_1, x_2, \dots, x_n); \quad i = 1, 2, \dots, n. \quad (4)$$

An equilibrium point is a fixed point $(\bar{x}_1, \bar{x}_2, \dots, \bar{x}_n)$ of the flow ϕ_t for all t and corresponds to

$$f_i(\bar{x}_1, \bar{x}_2, \dots, \bar{x}_n) = 0; \quad i = 1, 2, \dots, n. \quad (5)$$

An equilibrium point is stable if it attracts nearby solutions, unstable if it repels nearby solutions. More precisely, the equilibrium point $\bar{\mathbf{x}}$ is stable if for every neighborhood U of $\bar{\mathbf{x}}$ there is a neighborhood U_1 of $\bar{\mathbf{x}}$ such that every solution $\mathbf{x}(t) \in U$ for all $t > 0$, if $\mathbf{x}(0) \in U_1$. The equilibrium point $\bar{\mathbf{x}}$ is unstable if there exists a neighborhood U of $\bar{\mathbf{x}}$ such that for all neighborhoods $U_1 \subset U$ of $\bar{\mathbf{x}}$ there exists an orbit based at $\mathbf{x}(0) \in U_1$ which leaves U for some $t > 0$.

In order to investigate the linear stability of the system near a given equilibrium point $\bar{\mathbf{x}}$, we expand as follows:

$$x_i = \bar{x}_i + \delta x_i \quad (6)$$

so,

$$f_i(x_1, x_2, \dots, x_n) = f_i(\bar{x}_1, \bar{x}_2, \dots, \bar{x}_n) + \sum_{j=1}^n \delta x_j \left. \frac{\partial f_i}{\partial x_j} \right|_{\substack{x_i = \bar{x}}} + \dots \quad (7)$$

Using (6) and (7), to first order in the displacement δx_i , we obtain, from equation (4), the linear equation –

$$\delta \dot{x}_i = \sum_{j=1}^n \frac{\partial f_i}{\partial x_j} \Bigg|_{x_i=\bar{x}_i} \delta x_j \quad (8a)$$

or

$$\delta \dot{x} = A \delta x \quad (8b)$$

where A is the Jacobian matrix evaluated at the equilibrium point \bar{x}_j ,

$$A_{ij} = \frac{\partial f_i}{\partial x_j} \Bigg|_{x_i=\bar{x}_i} . \quad (9)$$

Thus, the local nonlinear flow near \bar{x}_j is approximated by the linear flow governed by equation (8)b which has the solution –

$$\delta x(t) = e^{tA} \delta x(0) . \quad (10)$$

The time-evolution operator e^{tA} may be defined by its power series

$$e^{tA} = I + tA + \frac{1}{2} t^2 A^2 + \dots \quad (11)$$

An n -dimensional linear system has n linearly independent solutions. If the eigenvalues of A are non-degenerate, then it can be diagonalized⁵, and we can write (10) in the form

⁵ If an eigenvalue λ_k is μ_k -fold degenerate and has only $\gamma_k < \mu_k$ linearly independent eigenvectors associated with it, then $\text{rank } \{A - \lambda_k I\} = n - \gamma_k$ and the matrix A cannot be diagonalized. The best one can do in such a situation is to reduce A to a Jordan canonical form; in this form, there is a Jordan block of order, say $n \times n$,

$$B_k = \begin{bmatrix} \lambda_k & 1 & & 0 \\ & \lambda_k & \ddots & \\ & & \ddots & \\ 0 & & & \lambda_k \end{bmatrix}$$

corresponding to each eigenvector, the sum of the dimensions of all the Jordan blocks associated with λ_k being μ_k . In order to calculate e^{tB_1} , we write (Arnol'd, (1973)),

$$B_k = \lambda_k I + J$$

where,

$$J = \begin{bmatrix} 0 & 1 & & 0 \\ & \ddots & \ddots & \\ & & \ddots & \\ 0 & & & 0 \end{bmatrix}$$

Noting that,

$$J^k = \begin{bmatrix} 0 & \cdots & 1 & 0 \\ & \ddots & \ddots & 1 \\ & & \ddots & \\ 0 & & & 0 \end{bmatrix} \text{ and } J^n = [0]$$

we have,

$$\delta \mathbf{x}(t) = \sum_{k=1}^n c_k e^{\lambda_k t} \mathbf{e}_k, \text{ no sum on k} \quad (12)$$

where $(\mathbf{e}_k, \lambda_k)$ is an eigenpair of \mathbf{A} , namely,

$$\mathbf{A}\mathbf{e}_k = \lambda_k \mathbf{e}_k, \text{ so } e^{t\mathbf{A}}\mathbf{e}_k = e^{\lambda_k t} \mathbf{e}_k \quad (13)$$

and the set $\{\mathbf{e}_1, \dots, \mathbf{e}_n\}$ is assumed to span \mathbb{R}^n , so $\delta \mathbf{x}(0) = \sum_{k=1}^n c_k \mathbf{e}_k$.

The equilibria given by (5) are stable if $\operatorname{Re} \lambda_k \leq 0$ for all k , and unstable if $\operatorname{Re} \lambda_k > 0$ for some k .

$$e^{t\mathbf{A}} = \begin{bmatrix} 1 & t & t^2/2! & \cdots & t^{n-1}/(n-1)! \\ & \ddots & \ddots & \ddots & \ddots \\ & & \ddots & \ddots & t^2/2! \\ & & & \ddots & t \\ 0 & & & & 1 \end{bmatrix}.$$

Next, noting that, for two matrices \mathbf{A} and \mathbf{B} which commute,

$$e^{\mathbf{A}+\mathbf{B}} = e^{\mathbf{A}} e^{\mathbf{B}}$$

we have,

$$e^{t\mathbf{B}_k} = \begin{bmatrix} e^{\lambda_k t} & te^{\lambda_k t} & \frac{t^2}{2!} e^{\lambda_k t} & \cdots & \frac{t^{n-1}}{(n-1)!} e^{\lambda_k t} \\ e^{\lambda_k t} & \ddots & \ddots & \ddots & \ddots \\ & \ddots & \ddots & \ddots & \ddots \\ & & \ddots & \ddots & \frac{t^2}{2!} e^{\lambda_k t} \\ 0 & & & & e^{\lambda_k t} \end{bmatrix}.$$

EXAMPLE 1

Consider a second-order system

$$\begin{cases} \dot{x} = P(x, y) \\ \dot{y} = Q(x, y) \end{cases}.$$

The equilibrium points of this system are found from

$$\begin{cases} P(\bar{x}_k, \bar{y}_k) = 0 \\ Q(\bar{x}_k, \bar{y}_k) = 0 \end{cases}.$$

The nature of the equilibrium points (\bar{x}_k, \bar{y}_k) are found by examining the linearizations of the above system in the neighborhood of each point (\bar{x}_k, \bar{y}_k) . The latter are found by writing Taylor expansions of $P(x, y)$ and $Q(x, y)$ around (\bar{x}_k, \bar{y}_k) :

$$\begin{pmatrix} \delta \dot{x}_k \\ \delta \dot{y}_k \end{pmatrix} = A \begin{pmatrix} \delta x_k \\ \delta y_k \end{pmatrix} + O\left(\begin{pmatrix} \delta x_k \\ \delta y_k \end{pmatrix}^2\right)$$

where,

$$A \equiv \begin{pmatrix} \left(\frac{\partial P}{\partial x}\right)_k & \left(\frac{\partial P}{\partial y}\right)_k \\ \left(\frac{\partial Q}{\partial x}\right)_k & \left(\frac{\partial Q}{\partial y}\right)_k \end{pmatrix}.$$

EXAMPLE 2

Consider the Jacobian matrix A given by (Arnol'd, (1973))

$$A = \begin{bmatrix} 1 & 1 \\ 1 & 1 \end{bmatrix}$$

in some basis (ξ_1, ξ_2) . The eigenvalues of A are $\{2, 0\}$ and the eigenvectors are $e_1 = \xi_1 + \xi_2$ and $e_2 = \xi_1 - \xi_2$. Diagonalizing A by a real linear transformation using the basis (e_1, e_2) , we have

$$e^{tA} = \begin{bmatrix} e^{2t} & 0 \\ 0 & 1 \end{bmatrix}.$$

The general solution is then given by

$$\delta x(t) = c_1(1, 1)e^{2t} + c_2(1, -1)$$

or

$$\delta x(t) = (c_1 e^{2t} + c_2, c_1 e^{2t} - c_2).$$

EXAMPLE 3

Consider

$$\ddot{x} + x = 0, \quad x(0) = a, \quad \dot{x}(0) = b.$$

Putting $y = \dot{x}$, this can be written as

$$\begin{pmatrix} \dot{x} \\ \dot{y} \end{pmatrix} = \begin{pmatrix} 0 & 1 \\ -1 & 0 \end{pmatrix} \begin{pmatrix} x \\ y \end{pmatrix}$$

with $x(0) = a$, $y(0) = b$. Putting $w = (x, y)^T$, this becomes

$$\dot{w} = Aw, \quad A = \begin{pmatrix} 0 & 1 \\ -1 & 0 \end{pmatrix}$$

with $w(0) = (a, b)^T$.

Thus,

$$w = e^{tA}w(0).$$

Note,

$$e^{tA} = \sum_{n=0}^{\infty} \frac{t^n A^n}{n!}$$

with,

$$A^{2n} = \begin{pmatrix} (-1)^n & 0 \\ 0 & (-1)^n \end{pmatrix}, \quad A^{2n+1} = \begin{pmatrix} 0 & (-1)^n \\ (-1)^{n+1} & 0 \end{pmatrix}.$$

Thus,

$$e^{tA} = \begin{pmatrix} \sum_n \frac{(-1)^n t^{2n}}{(2n)!} & \sum_n \frac{(-1)^n t^{2n+1}}{(2n+1)!} \\ \sum_n \frac{(-1)^{n+1} t^{2n+1}}{(2n+1)!} & \sum_n \frac{(-1)^n t^{2n}}{(2n)!} \end{pmatrix} = \begin{pmatrix} \cos t & \sin t \\ -\sin t & \cos t \end{pmatrix}$$

and hence,

$$\left. \begin{aligned} x(t) &= a \cos t + b \sin t \\ y(t) &= -a \sin t + b \cos t \end{aligned} \right\}.$$

(i) Liapunov and Asymptotic Stability:

The notion of stability applies to different aspects of a dynamical system. Thus, it can refer to individual fixed points (local stability), to trajectories (asymptotic stability),

to families of trajectories (existence of an attractor), or to the whole dynamical system (uniqueness of the attractor). The notion of stability is of two types depending on whether the perturbations considered are those of states (dynamic stability) or of the system parameters (structural stability). In the following, we shall concern ourselves with only the dynamic stability.

The notion of local stability can be formalized as follows:

DEFINITION: The fixed point $P(\mathbf{x} = \bar{\mathbf{x}})$ is a Liapunov stable equilibrium of the system for all neighborhoods U of P if there exists a neighborhood U_1 of $P \subset U$ such that $\mathbf{x} = \phi_t(\mathbf{x}_0)$ belongs to U for all times if \mathbf{x}_0 belongs to U_1 . Furthermore, \mathbf{x} converges uniformly to $\bar{\mathbf{x}}$ (with respect to t) as \mathbf{x}_0 tends to $\bar{\mathbf{x}}$.

DEFINITION: The fixed point $P(\mathbf{x} = \bar{\mathbf{x}})$ is an asymptotically stable equilibrium of the system, if and only if, there exists a neighborhood U of P such that for all \mathbf{x}_0 belonging to U , we have

$$\lim_{t \rightarrow \infty} \phi_t(\mathbf{x}_0) = P$$

and for $t > s$,

$$\phi_t(U) \subset \phi_s(U).$$

For the linear problem (8), the equilibrium $\bar{\mathbf{x}}$ is asymptotically stable if and only if $\operatorname{Re}(\lambda_k) < 0$ for each eigenvalue λ_k of \mathbf{A} (see Theorem below).

The Liapunov stability may be established by exhibiting a C^1 function $V(\mathbf{x}) : U \rightarrow \mathbb{R}$, called the Liapunov function, defined in a neighborhood U of $\bar{\mathbf{x}}$, such that

- (i) $V(\bar{\mathbf{x}}) = 0$ and $V(\mathbf{x}) > 0$, if $\mathbf{x} \neq \bar{\mathbf{x}}$,
- (ii) $\frac{d}{dt} V(\mathbf{x}) \leq 0$ for $\mathbf{x} \in U$.

This idea is similar to that of proving a series to be convergent by finding a convergent series which bounds the given series. One may establish asymptotic stability by requiring the condition (ii) to be, instead

$$\frac{d}{dt} V(\mathbf{x}) < 0 \text{ for } \mathbf{x} \in U.$$

EXAMPLE 4

Consider the damped Duffing oscillator described by (Hagedorn, 1988)

$$\ddot{x} + k \dot{x} + x - x^3 = 0$$

or written as a system of equations

$$\left. \begin{array}{l} \dot{x}_1 = x_2 \\ \dot{x}_2 = -k x_2 - x_1 + x_1^3 \end{array} \right\}.$$

In order to investigate the Liapunov stability of the solution $(0, 0)$, consider the energy of the corresponding undamped system as the Liapunov function –

$$V(x_1, x_2) = \frac{1}{2} (x_2^2 + x_1^2) - \frac{1}{4} x_1^4.$$

Observe that

$$\left. \begin{array}{l} V(0, 0) = 0, \\ V(x_1, x_2) > 0 \text{ in a neighborhood of } (0, 0), \\ \text{and} \\ \frac{d}{dt} V(x_1, x_2) = \frac{\partial V}{\partial x_1} \dot{x}_1 + \frac{\partial V}{\partial x_2} \dot{x}_2 = -k x_2^2 \leq 0. \end{array} \right\}$$

Therefore, the solution $(0, 0)$ is Liapunov stable.

The Liapunov functions are not easy to find in practice. However, one may use the concept of Liapunov functions to sketch a proof of asymptotic stability.

THEOREM 1.1

Suppose that all of the eigenvalues of $A = \left[\frac{\partial f_i}{\partial x_j} \right]_{x=\bar{x}}$ have negative real parts. Then, the equilibrium solution, \bar{x} , of $\dot{x} = f(x)$ is asymptotically stable.

Proof: Let \bar{x} be a fixed point of equation (4) which may be moved to the origin by introducing $y = x - \bar{x}$. Taylor-expanding equation (4) about the fixed point $\bar{y} = 0$, we obtain

$$\dot{y} = A(\bar{x})y + R(y), \quad |R(y)| = O(|y|^2). \quad (14)$$

We choose a Liapunov function

$$V(y) = \frac{1}{2}|y|^2 \quad (15)$$

which automatically satisfies the condition (i). We have

$$\frac{d}{dt} V(y) = \sum_{j=1}^n \frac{\partial}{\partial y_j} V(y) \dot{y}_j = (y^T A(\bar{x})y) + (y^T R(y)). \quad (16)$$

If all of the eigenvalues of A have negative real parts, then

$$(y^T A(\bar{x})y) < 0 \text{ for all } y.$$

So, by choosing $|y|$ sufficiently small, we have

$$\frac{d}{dt} V < 0 \quad (17)$$

which implies that the fixed point \bar{x} is asymptotically stable.

The importance of the notion of asymptotic stability arises from the result (Hirsch and Smale, (1974)) that if \bar{x} is asymptotically stable for the linear system (8), then it will also be asymptotically stable for the original nonlinear system (4) within a certain stable neighborhood of the initial condition x_0 . But, the linear problem (8) provides no information about the size of this stable neighborhood around x_0 for the nonlinear problem.

It may be noted, however, that even if the equilibrium \bar{x} is not asymptotically stable it is possible to show that the linear problem (8) can describe the qualitative features of the original nonlinear problem (4) in some sense near the equilibrium \bar{x} . This possibility becomes effective when all the eigenvalues of A lie away from the imaginary axis in the complex- λ plane. In this case the fixed point \bar{x} is called a hyperbolic fixed point (see Section 1.3). For this case, the nonlinear flow can be shown to be locally isomorphic to the linear flow at \bar{x} (Hartman-Grobman Theorem).

THEOREM 1.2 (Hartman and Grobman)

Let $x = \bar{x}$ be a hyperbolic fixed point of the nonlinear problem (4), and let ϕ_t denote the nonlinear flow associated with equation (4) and $\tilde{\phi}_t$ denote the corresponding linear flow associated with equation (8). Then, there exists a homeomorphism⁶ $\Psi : R^n \rightarrow R^n$, defined on some neighborhood U of \bar{x} , locally mapping the nonlinear flow ϕ_t onto the linear flow $\tilde{\phi}_t$, around \bar{x} , i.e.,

$$(\Psi \circ \phi_t)(x) = (\tilde{\phi}_t \circ \Psi)(x) \quad (18)$$

for all (x, t) such that x and $\phi_t(x) \in U$. (For the proof, see Guckenheimer and Holmes, (1986).)

In other words, there exists a neighborhood of a hyperbolic fixed point \bar{x} where the nonlinear flow ϕ_t is topologically equivalent to the linear flow $\tilde{\phi}_t$, around \bar{x} .

Note that the Hirsch-Smale result stating that linear asymptotic stability implies nonlinear asymptotic stability is clearly contained in the above Theorem because, if $\text{Re}(\lambda_k) < 0$ for all k , so that $\Psi(x) \in E_s$, then $(\tilde{\phi}_t \circ \Psi)(x) \rightarrow \bar{x}$ as $t \rightarrow \infty$.

According to the Hartman-Grobman Theorem, there is a one-to-one correspondence between any qualitative changes in the local nonlinear dynamics and the concomitant linear dynamics. Note that this result also paves the way for local bifurcations whenever the equilibria lose hyperbolicity.

(ii) The Center-Manifold Theorem

DEFINITION: Let $S \subset R^n$ be a set. Then, S is said to be invariant under the vector field $\dot{x} = f(x)$ if, for any $x_0 \in S$, we have $x(t) \in S$, for all t . If, in addition, S is a C^r manifold, then S is said to be a C^r invariant manifold.

(13) implies that the linear subspaces of R^n generated by the eigenvectors of A , called the eigenspaces E_λ of A , are invariant under the flow map e^{tA} , i.e., if $x(0) \in E_\lambda$, then $x(t) \in E_\lambda$ for all t . One may divide this invariant subspace into three different invariant manifolds according as $\text{Re}(\lambda_k)$ is less than, equal to, or greater than zero:

⁶ A homeomorphism is a continuous, one-to-one mapping with a continuous inverse.

- stable manifold E_s is the subspace spanned by the eigenvectors $\{\mathbf{e}_k\}$ such that $\operatorname{Re}(\lambda_k) < 0$,

$$E_s = \operatorname{span}\left\{\mathbf{e}_k \in R^n \mid (\mathbf{A} - \lambda_k \mathbf{I}) \cdot \mathbf{e}_k = \mathbf{0} \text{ and } \operatorname{Re}(\lambda_k) < 0\right\}$$

- center manifold E_c is the subspace spanned by the eigenvectors $\{\mathbf{e}_k\}$ such that $\operatorname{Re}(\lambda_k) = 0$,

$$E_c = \operatorname{span}\left\{\mathbf{e}_k \in R^n \mid (\mathbf{A} - \lambda_k \mathbf{I}) \cdot \mathbf{e}_k = \mathbf{0} \text{ and } \operatorname{Re}(\lambda_k) = 0\right\}$$

- unstable manifold E_u is the subspace spanned by the eigenvectors $\{\mathbf{e}_k\}$ such that $\operatorname{Re}(\lambda_k) > 0$,

$$E_u = \operatorname{span}\left\{\mathbf{e}_k \in R^n \mid (\mathbf{A} - \lambda_k \mathbf{I}) \cdot \mathbf{e}_k = \mathbf{0} \text{ and } \operatorname{Re}(\lambda_k) > 0\right\}.$$

Corresponding to E_s and E_u , the dynamics has the following simple asymptotic property:

If $\mathbf{x}(t) \in E_s$, then $\mathbf{x}(t) \rightarrow \bar{\mathbf{x}}$, as $t \rightarrow \infty$;

if $\mathbf{x}(t) \in E_u$, then $\mathbf{x}(t) \rightarrow \bar{\mathbf{x}}$, as $t \rightarrow -\infty$.

The importance of the invariant manifolds of the linear flow in the neighborhood of an equilibrium point $\bar{\mathbf{x}}$ arises from the fact that they are locally tangent to the corresponding manifolds of the nonlinear flow.

THEOREM 1.3 (Center Manifold Theorem)

Let $f(\mathbf{x})$ be a C^r vector field on R^n which satisfies $f(\bar{\mathbf{x}}) = \mathbf{0}$. The spectrum of $\partial f_i / \partial x_j \Big|_{x_i = \bar{x}_i}$ is divided into three groups σ_s, σ_c and σ_u with the generalized eigenspaces E_s, E_c and E_u , respectively, where

$$\lambda_k \in \begin{cases} \sigma_s, \operatorname{Re}(\lambda_k) < 0 \\ \sigma_c, \operatorname{Re}(\lambda_k) = 0. \\ \sigma_u, \operatorname{Re}(\lambda_k) > 0 \end{cases}$$

Then, there exist C^r stable and unstable manifolds W_s and W_u tangent to E_s and E_u at \bar{x} and a C^{r-1} center manifold W_c tangent to E_c at \bar{x} which are invariant under the nonlinear flow generated by f . The manifolds W_s and W_u are unique, but W_c may not be. (For the proof, see Marsden and McCracken, (1976)).

Figure 1.1 shows the relationship between the linear eigenspaces and the invariant manifolds of the nonlinear flow (4). Note that the flow directions on the center manifold are not shown because they cannot be determined by the linear flow at \bar{x} .

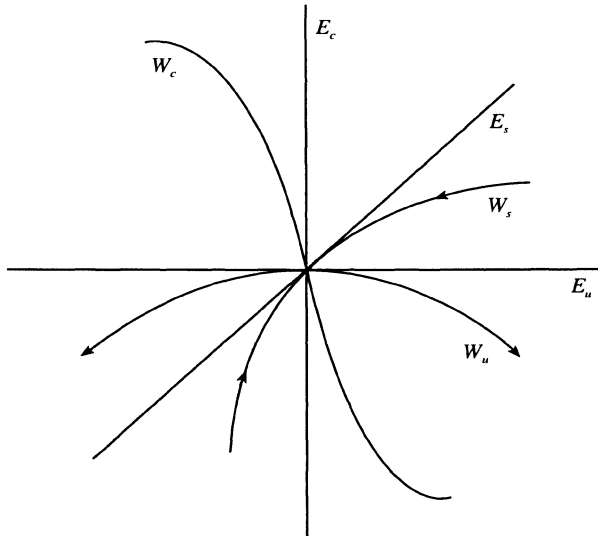


Figure 1.1. The stable, unstable and center manifolds.

EXAMPLE 5

Consider the system (Guckenheimer and Holmes, (1986)),

$$\left. \begin{array}{l} \dot{x} = x \\ \dot{y} = -y + x^2 \end{array} \right\}$$

Note that, for this system, the eigenspace E_s corresponds to the y -axis and E_u corresponds to the x -axis. Eliminating t from the system, we obtain the equation of the orbits,

$$x \frac{dy}{dx} + y = x^2$$

the solution of which is

$$y = \frac{x^3}{3} + \frac{c}{x}.$$

The Center Manifold Theorem states that the unstable manifold W_u is tangent to the x -axis at the origin, so it is given by,

$$W_u : y = \frac{x^3}{3}.$$

The stable manifold W_s is still the y -axis, (see Figure 1.2).

The uniqueness of solutions of differential equations of the type (4) dictates that the stable (or the unstable) manifolds of two distinct fixed points cannot intersect; further, the stable (or unstable) manifold cannot intersect itself either. However, a stable manifold can intersect an unstable manifold belonging to distinct or the same fixed point.

However, at points where the manifolds of bifurcating solutions (see Chapter 2) intersect, flows may switch from one manifold to another and exchange stability between manifolds indicating the occurrence of a bifurcation. The central manifold W_c plays a very important role in bifurcation theory because of its locally attracting property implying that the entire flow ($-\infty < t < \infty$) will lie on the center manifold whenever part of it lies in a neighborhood U of the fixed point \bar{x} . (Such a property does not exist for the stable/unstable manifolds W_s and W_u because $x(t)$ grows without bound as $|t| \rightarrow \infty$ on these manifolds.)

Thanks to the nonlinearity, a global analytic description of the dynamics on the center manifold is not possible, so one settles for a local description on the center

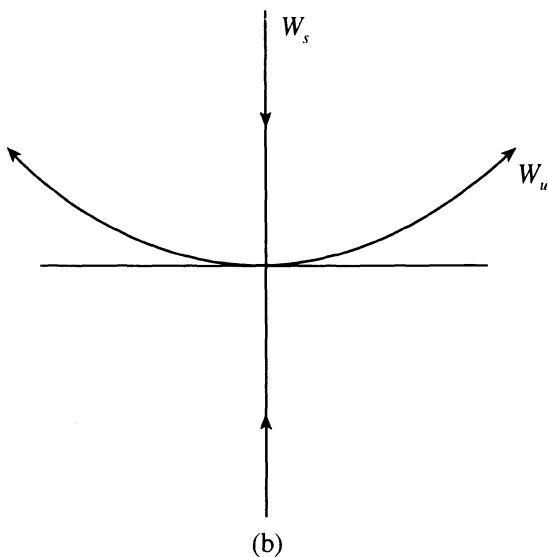
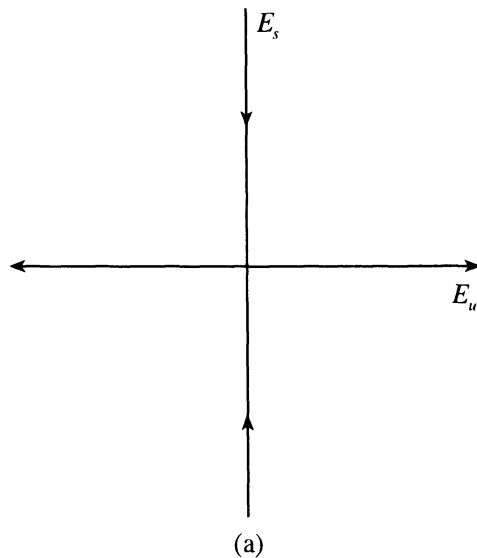


Figure 1.2. (a) Linearized motion for the system $\dot{x} = x$, $\dot{y} = y + x^2$.
(b) Stable and unstable manifolds $W_{s,u}$ for the full nonlinear system.

eigenspace E_c near the equilibrium \bar{x} . Choosing the local coordinate system such that $x = (x_1, x_2)$ where $x_1 \in E_c$ and $x_2 \in E_s \oplus E_u$, let us write equation (4) as

$$\delta \dot{x}_1 = B \delta x_1 + N_1(\delta x_1, \delta x_2) \quad (19a)$$

$$\delta \dot{x}_2 = C \delta x_2 + N_2(\delta x_1, \delta x_2)^7 \quad (19b)$$

where B is an $n_c \times n_c$ matrix with all eigenvalues on the imaginary axis, C is an $(n_s + n_u) \times (n_s + n_u)$ matrix with all eigenvalues off the imaginary axis, and N_1, N_2 denote the nonlinear terms. Here,

$$n_s = \dim(W_s), n_c = \dim(W_c), n_u = \dim(W_u).$$

DEFINITION: A manifold $W_c(\bar{x}, U)$ in a neighborhood U of the equilibrium \bar{x} is said to be a local central manifold for equation (19), if

- (i) $W_c(\bar{x}, U)$ is invariant under the flow of equation (19), and
- (ii) $W_c(\bar{x}, U)$ is a graph of a function $h(\delta x_1) = \delta x_2$ and is tangent to E_c at \bar{x} , i.e.,

$$W_c(\bar{x}, U) = \left\{ (\delta x_1, \delta x_2) \mid \delta x_2 = h(\delta x_1), (\delta x_1, \delta x_2) \in U \right\} \quad (20)$$

where the function $h(\delta x_1)$ satisfies

$$h(\mathbf{0}) = \mathbf{0}, \left. \frac{\partial h(\delta x_1)}{\partial \delta x_1} \right|_{\delta x_1=0} = \mathbf{0} \quad . \quad (21)$$

The local center manifold is then found by differentiating the relation $\delta x_2 = h(\delta x_1)$ with respect to t, and using equation (19), (21) leads to

⁷For a two-dimensional problem, equation (19) takes the obvious form

$$\dot{x}_1 = f_1(x_1, x_2)$$

$$\dot{x}_2 = -x_2 + f_2(x_1, x_2).$$

$$C \cdot h(\delta x_1) + N_2(\delta x_1, h(\delta x_1)) = \nabla_{\delta x_1} h(\delta x_1) \cdot [B \delta x_1 + N_1(\delta x_1, h(\delta x_1))]. \quad (22)$$

The dynamics on the local center manifold, from equations (19)a and (20), is then described by

$$\delta \dot{x}_1 = B \delta x_1 + N_1(\delta x_1, h(\delta x_1)). \quad (23)$$

Observe the reduction in the dimensionality of the flow when described on the local center manifold.

EXAMPLE 6

Consider the two-dimensional flow (Hale and Kocak, (1991)),

$$\left. \begin{aligned} \dot{x}_1 &= ax_1^3 + x_1x_2 \\ \dot{x}_2 &= -x_2 + (x_2^2 + x_1x_2 - x_1^3) \end{aligned} \right\}.$$

This flow has equilibrium at $(x_1, x_2) = (0, 0)$ and the eigenspaces are given by

$$\begin{aligned} E_s &= \{(x_1, x_2) \mid x_1 = 0\}, \\ E_c &= \{(x_1, x_2) \mid x_2 = 0\}. \end{aligned}$$

The local center manifold is given by

$$x_2 = h(x_1)$$

where the function $h(x_1)$, from equation (17), satisfies the following equation –

$$-h(x_1) + [h^2(x_1) + x_1h(x_1) - x_1^3] = \frac{\partial h}{\partial x_1} \cdot [ax_1^3 + x_1h(x_1)].$$

Now, in accordance with (15), we may approximate $h(x_1)$, near $x_1 = 0$, by expanding it as a power series of the form

$$h(x_1) = c_2 x_1^2 + c_3 x_1^3 + O(x_1^4).$$

Substituting this expression in the above equation, and collecting terms with equal powers of x_1 , we obtain

$$c_2 = 0, \quad c_3 = -1.$$

So, the local center manifold is given by

$$h(x_1) = -x_1^3 + O(x_1^4).$$

The flow on the local center manifold is then described by

$$\dot{x}_1 = ax_1^3 - x_1^4 + O(x_1^5)$$

which is one-dimensional, as expected!

1.3. Phase-Plane Analysis

The study of differential equations is based on two approaches:

- (i) construction of explicit solutions;
- (ii) search for qualitative information about the global behavior of solutions.

The second approach was initiated by Poincaré and involves what is known as phase-plane analysis. This is based on the fact that local analysis near equilibrium points can indicate global properties of the solution.

EXAMPLE 7

Consider a simple harmonic oscillator governed by

$$\ddot{x} + \omega^2 x = 0. \quad (24)$$

Equation (24) has the solution,

$$\left. \begin{aligned} x &= A \sin(\omega t + \varphi) \\ y &\equiv \dot{x} = A\omega \cos(\omega t + \varphi) \end{aligned} \right\}. \quad (25)$$

The locus of this solution in the xy -plane is an ellipse (see Figure 1.3),

$$\frac{x^2}{A^2} + \frac{y^2}{A^2\omega^2} = 1 \quad (26)$$

with t as a parameter.

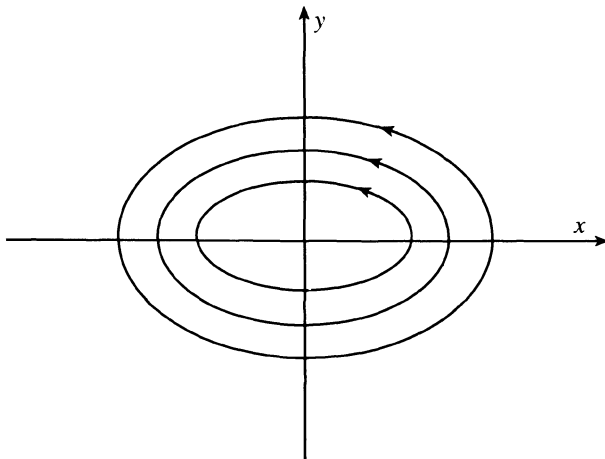


Figure 1.3. Phase curves for the simple harmonic oscillator.

A solution curve, plotted on the xy -plane, called the phase plane, is called a trajectory, which is oriented by the parameter t , and the direction of increasing t is indicated by the arrowheads. For a given set of initial conditions, the response of the system can be viewed as the motion of a point along a trajectory. Due to the uniqueness of solutions, at most one trajectory passes through each point in the xy -plane, with the exception of the equilibrium point which is at the origin $x = y = 0$. This equilibrium point is called a center⁸ (also called an elliptic fixed point) since all trajectories near it form a continuous family of closed curves about it. Closed trajectories generally correspond to periodic solutions, and vice versa.

The collection of trajectories in phase plane is called a phase portrait. The phase portrait provides a global qualitative picture of the dynamics and changes as the parameters in the given problem (equations of motion and boundary conditions) change.

⁸ The center is said to be structurally unstable because arbitrarily small perturbations on the system can turn it into a focus.

THE INITIAL-VALUE PROBLEM

The phase-plane concept is introduced as the natural setting for formulating the initial-value problem. The initial-value problem for a second-order equation, such as (24), is as follows – find a solution $x(t)$ satisfying

$$t = 0 : x = x_o, \dot{x} = y_o. \quad (27)$$

In the phase plane, (27) specifies a point $P_0(x_0, y_0)$, and the initial-value problem is that of finding a trajectory which passes through the point $P_0(x_0, y_0)$ for $t = 0$. For any point $P_0(x_0, y_0)$, the solution of the initial-value problem exists and is unique, whether singular or not.

EXAMPLE 8

Consider a damped harmonic oscillator governed by

$$\ddot{x} + k\dot{x} + \omega^2 x = 0, \quad k > 0 \quad (28)$$

which can be alternatively written as

$$\left. \begin{array}{l} \dot{x} = y \\ \dot{y} = -k y - \omega^2 x \end{array} \right\}. \quad (29)$$

We will now follow Struble (1962) and look for a solution of the form,

$$x \sim e^{\lambda t} \quad (30)$$

We then obtain

$$\lambda_1 = -\frac{k}{2} - \sqrt{\left(\frac{k}{2}\right)^2 - \omega^2}, \quad \lambda_2 = -\frac{k}{2} + \sqrt{\left(\frac{k}{2}\right)^2 - \omega^2}. \quad (31)$$

(31) indicates three cases according as $\omega^2 \gtrless \left(\frac{k}{2}\right)^2$, and a fourth case when $\omega^2 < 0$.

Case (i) $\omega^2 > \left(\frac{k}{2}\right)^2$.

We now have

$$\left. \begin{aligned} x &= Ae^{-\frac{kt}{2}} \sin(\omega_1 t + \varphi) \\ y \equiv \dot{x} &= -\frac{k}{2} Ae^{-\frac{kt}{2}} \sin(\omega_1 t + \varphi) + \omega_1 A e^{-\frac{kt}{2}} \cos(\omega_1 t + \varphi) \end{aligned} \right\} \quad (32)$$

where,

$$\omega_1 \equiv \sqrt{\omega^2 - \left(\frac{k}{2}\right)^2}.$$

Let us introduce two new dependent variables,

$$\left. \begin{aligned} u &= \omega_1 x = \omega_1 A e^{-\frac{kt}{2}} \sin(\omega_1 t + \varphi) \\ v &= y + \frac{k}{2} x = \omega_1 A e^{-\frac{kt}{2}} \cos(\omega_1 t + \varphi) \end{aligned} \right\}. \quad (33)$$

The solution curve (32), viewed in the uv -plane, is a spiral (see Figure 1.4), since we have, from (33),

$$\left. \begin{aligned} u^2 + v^2 &= \omega_1^2 A^2 e^{-kt} \\ \frac{u}{v} &= \tan(\omega_1 t + \varphi) \end{aligned} \right\}. \quad (34)$$

We have from equations (29) and (33),

$$\left. \begin{aligned} \dot{u} &= -\frac{k}{2} u + \omega_1 v \\ \dot{v} &= -\omega_1 u - \frac{k}{2} v \end{aligned} \right\} \quad (35)$$

(33) shows that the origin in the uv -plane corresponds to the origin in the xy -plane, and is a position of equilibrium. It is called a focus⁹ since the trajectories near it spiral in or out of it.

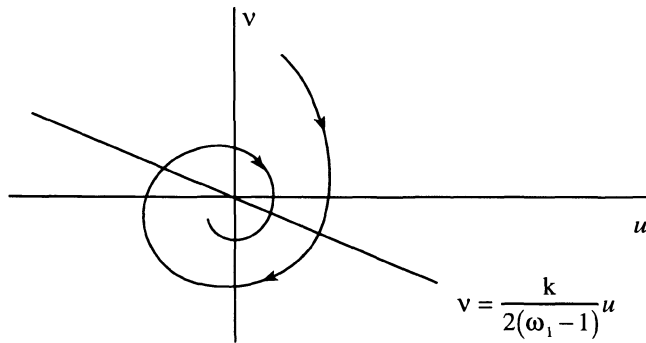


Figure 1.4. The solution curve in the uv -plane for the damped harmonic oscillator in the underdamped case.

In order to obtain the trajectory in the xy -plane, note that the eigenvectors of the transformation (33) namely,

$$\left. \begin{array}{l} u = \alpha x \\ v = \alpha y \end{array} \right\} \quad (36)$$

are given by

$$\left. \begin{array}{l} \alpha = 1 : x = 0, (\text{the } v - \text{axis}) \\ \alpha = \omega_1 : \frac{k}{2}x + (1 - \omega_1)y = 0, \left(\text{the line } v = \frac{k}{2(\omega_1 - 1)}u \right) \end{array} \right\} \quad (37)$$

⁹ The canonical form for a focus is

$$\dot{x} = ax + y, \quad \dot{y} = -x + ay.$$

If $a < 0$, one has a stable focus, while if $a > 0$, one has an unstable focus.

and correspond to those that are not rotated under the transformation (33). Whereas the lengths of the vectors parallel to the first eigenvector are unchanged under this transformation, the lengths of the vectors parallel to the second eigenvector are stretched by the factor ω_1 . Thus, one obtains a distorted spiral in the xy -plane (see Figure 1.5) from the logarithmic spiral in the uv -plane by moving the intercepts with the line

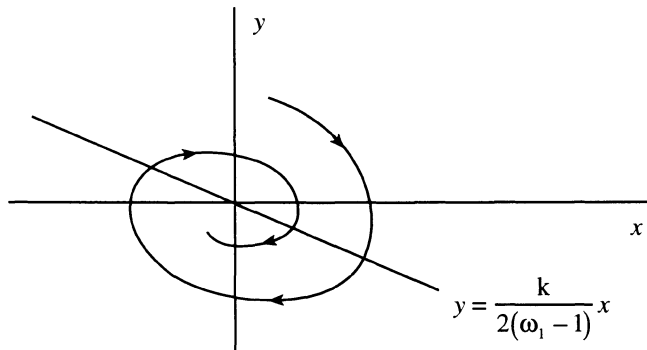


Figure 1.5. The solution curve in the xy -plane for the damped harmonic oscillator in the underdamped case.

$v = \frac{k}{2(\omega_1 - 1)} u$ outward in proportion to $1/\omega_1$, while leaving the intercepts on the v -axis unchanged.

Case (ii) $\omega^2 < (k/2)^2$.

Let us introduce here

$$\left. \begin{array}{l} u = \omega^2 x - \lambda_1 y \\ v = \omega^2 x - \lambda_2 y \end{array} \right\} \quad (38)$$

we then have from equations (29) and (38),

$$\left. \begin{array}{l} \dot{u} = \lambda_1 u \\ \dot{v} = \lambda_2 v \end{array} \right\} \quad (39)$$

so that

$$\left. \begin{aligned} u &= u_o e^{\lambda_1 t} \\ v &= v_o e^{\lambda_2 t} \end{aligned} \right\}. \quad (40)$$

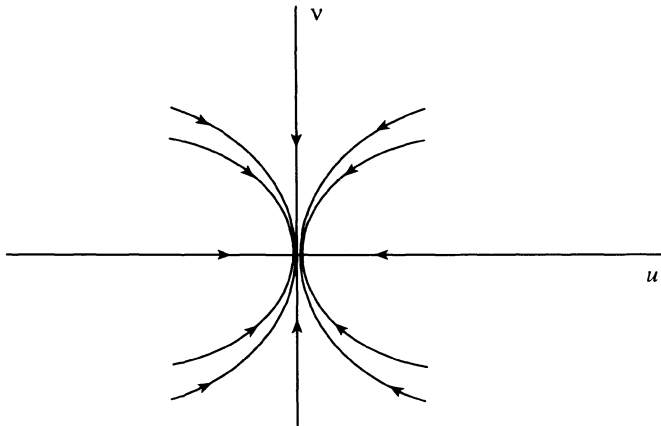


Figure 1.6. The solution curve in the uv -plane for the damped harmonic oscillator in the overdamped case.

Thus, the trajectories lie along the curves $u \sim v^{\frac{\lambda_1}{\lambda_2}}$, and are asymptotic to the v -axis (see Figure 1.6) since

$$\frac{u}{v} \sim e^{(\lambda_1 - \lambda_2)t} \rightarrow 0 \text{ as } t \rightarrow \infty. \quad (41)$$

The trajectories approach the origin $u = v = 0$ as $t \rightarrow \infty$.

In order to find the trajectories in the xy -plane, note, from (38), that the u -axis maps to the line $y = \frac{\omega^2}{\lambda_2} x$, while the v -axis maps to the line $y = \frac{\omega^2}{\lambda_1} x$. The origin $x = y = 0$,

which the trajectories approach as $t \rightarrow \infty$ (see Figure 1.7), is called a node¹⁰.

¹⁰ The canonical form for a stable node is

$$\dot{x} = -x, \quad \dot{y} = ay \quad (a < 0)$$

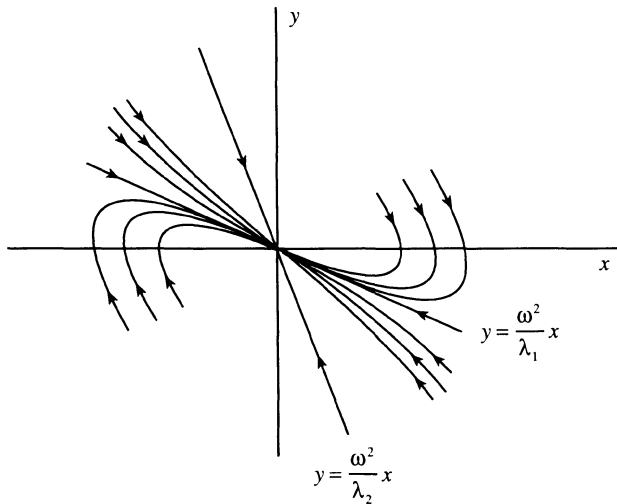


Figure 1.7. The solution curve in the xy -plane for the damped harmonic oscillator in the overdamped case.

Case (iii) $\omega^2 = (k/2)^2$

Let us now introduce

$$\left. \begin{aligned} u &= \omega^2 x - \lambda_1 y = \left(\frac{k}{2}\right)^2 x + \left(\frac{k}{2}\right)y \\ v &= \left(\frac{k}{2}\right)x \end{aligned} \right\}. \quad (42)$$

(compare with (38)). We then have from equations (29) and (42),

$$\left. \begin{aligned} \dot{u} &= -\left(\frac{k}{2}\right)u \\ \dot{v} &= u - \left(\frac{k}{2}\right)v \end{aligned} \right\}. \quad (43)$$

from which

while that for an unstable node is

$$\dot{x} = x, \quad \dot{y} = ay \quad (a > 0).$$

$$\left. \begin{aligned} u &= u_o e^{-\frac{kt}{2}} \\ v &= u_o t e^{-\frac{kt}{2}} + v_o e^{-\frac{kt}{2}} \end{aligned} \right\}. \quad (44)$$

Thus, each trajectory in the uv -plane approaches the origin as $t \rightarrow \infty$. Further, we have from (44),

$$\frac{v}{u} = t + \frac{v_o}{u_o} \quad (45)$$

which shows that each trajectory is asymptotic to the v -axis (see Figure 1.8).

Also, from equation (43), we have

$$\frac{dv}{du} = \frac{\dot{v}}{\dot{u}} = -\frac{2}{k} + \frac{v}{u} \quad (46)$$

we have,

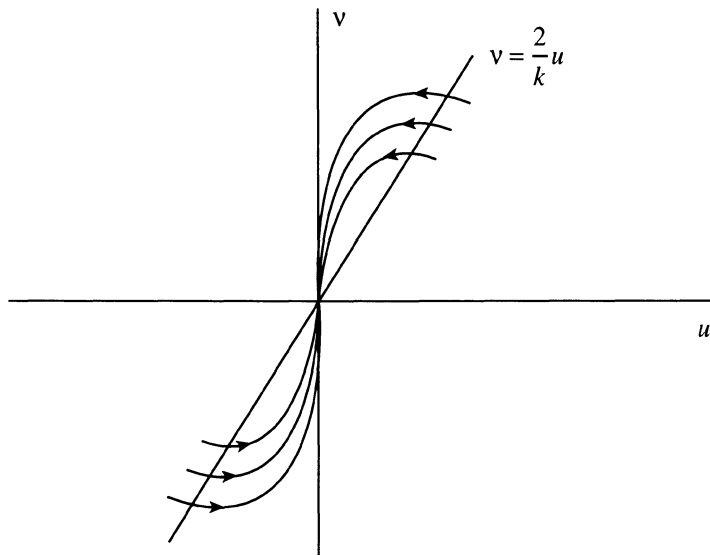


Figure 1.8. The solution curve in the uv -plane for the damped harmonic oscillator in the critical damped case.

$$\frac{dv}{du} = 0 \text{ along the line } v = \frac{2u}{k} \quad (47)$$

(see Figure 1.8).

In order to find the trajectories in the xy -plane, note, from (42), that the v -axis maps to the line $y = -\frac{kx}{2}$, and the line $v = \frac{2u}{k}$ maps to the x -axis. The origin $x = y = 0$ which the trajectories approach as $t \rightarrow \infty$ is again a node, (see Figure 1.9).

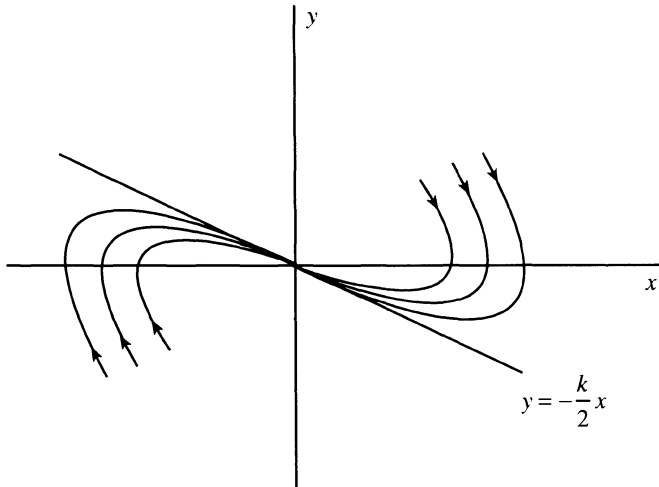


Figure 1.9. The solution curve in the xy -plane for the damped harmonic oscillator in the critically damped case

Case (iv) $\omega^2 = -\sigma^2$.

Let us now introduce (as in (38))

$$\left. \begin{aligned} u &= -\sigma^2 x - \lambda_1 y \\ v &= -\sigma^2 x - \lambda_2 y \end{aligned} \right\}. \quad (48)$$

We then obtain from equations (29) and (48),

$$\left. \begin{aligned} \dot{u} &= \lambda_1 u \\ \dot{v} &= \lambda_2 v \end{aligned} \right\} \quad (49)$$

(which are the same as (39)) so that

$$\left. \begin{array}{l} u = u_o e^{\lambda_1 t} \\ v = v_o e^{\lambda_2 t} \end{array} \right\} \quad (50)$$

where,

$$\lambda_1 = -\frac{k}{2} - \sqrt{\left(\frac{k}{2}\right)^2 + \sigma^2} < 0, \quad \lambda_2 = -\frac{k}{2} + \sqrt{\left(\frac{k}{2}\right)^2 + \sigma^2} > 0.$$

Thus, we have from (50),

$$\left. \begin{array}{l} t \rightarrow \infty : u \rightarrow 0, v \rightarrow \infty \\ \text{and } \frac{u}{v} \sim e^{(\lambda_1 - \lambda_2)t} \rightarrow 0 \end{array} \right\}. \quad (51)$$

The trajectories in the uv -plane appear as shown in Figure 1.10.

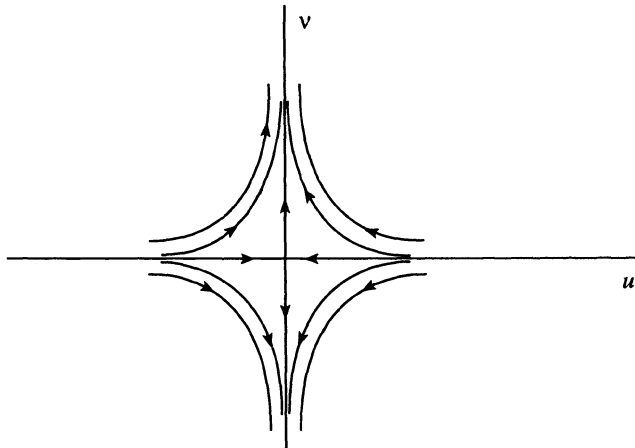


Figure 1.10. The solution curve in the uv -plane for the hyperbolic case.

Note that the trajectories do not approach origin as $t \rightarrow \infty$, but they approach the v -axis asymptotically.

In order to determine the trajectories in the xy -plane, note, from (48), that the u -axis maps to the line $y = -\frac{\sigma^2}{\lambda_2}x$, and the v -axis maps to the line $y = -\frac{\sigma^2}{\lambda_1}x$. The origin $x = y = 0$ is called the saddle point¹¹ (or a hyperbolic point), (see Figure 1.11). Thus, the saddle point is an equilibrium point which is approached by two orbits as $t \rightarrow \infty$ and two others as $t \rightarrow -\infty$.

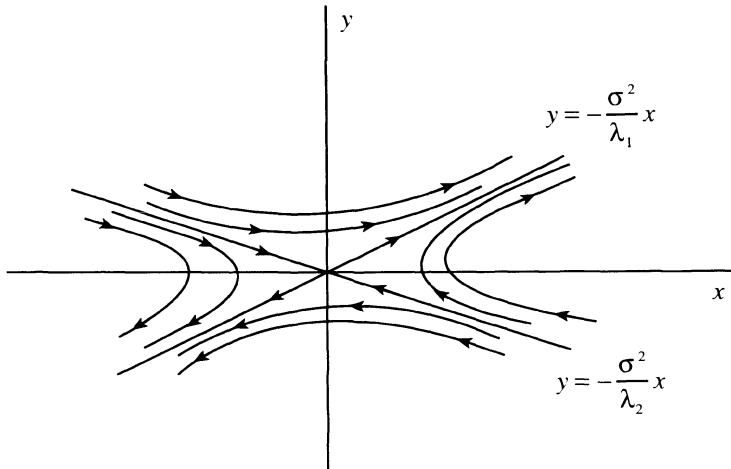


Figure 1.11. The solution curve in the xy -plane for the hyperbolic case.

EXAMPLE 9

Consider an oscillator with a weakly nonlinear restoring force governed by

$$\ddot{x} + \omega^2 x + \beta x^3 = 0 \quad (52)$$

where $|\beta|$ is a small constant and represents a small deviation from the linear problem. Equation (52) is called Duffing's equation.

One integration of equation (52) gives

¹¹ The canonical form for a saddle point is

$$\dot{x} = x, \quad \dot{y} = -y.$$

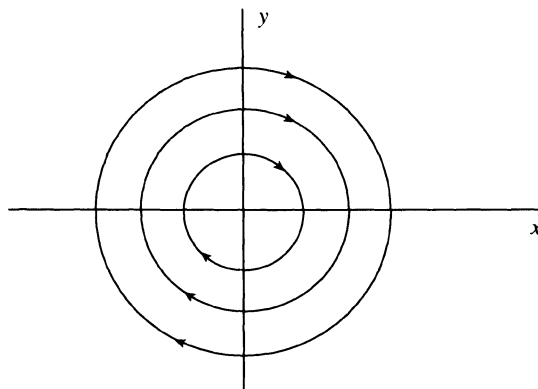


Figure 1.12. The solution curves in the xy -plane for the Duffing's equation in the hard spring ($\beta > 0$) case.

$$y^2 + x^2 \left(\omega^2 + \frac{\beta x^2}{2} \right) = c, \quad y = \dot{x}. \quad (53)$$

For $\beta > 0$, the trajectories in the phase plane are closed curves representing periodic solutions (see Figure 1.12). The origin is the only one singular solution and is a center.

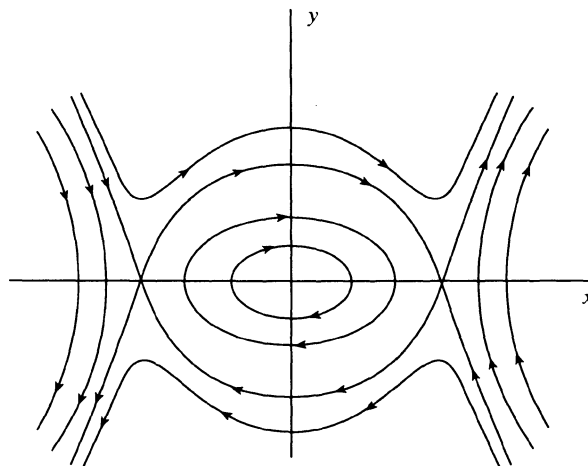


Figure 1.13. The solution curves in the xy -plane for the Duffing's equation in the soft spring case.

For $\beta < 0$, there are three singular solutions – the origin and the points $(\pm \sqrt{\omega^2/(-\beta)}, 0)$. The origin is a center, while each of the other two are saddle points, (see Figure 1.13).

EXAMPLE 10

The equation of motion for a simple pendulum (Figure 1.14) is

$$\ddot{\theta} + \omega^2 \sin \theta = 0, \quad \omega^2 \equiv \frac{g}{l} \quad (54)$$

where l is the length of the string and g is the gravitational constant.

The first integral of equation (54) is

$$\frac{1}{2} \dot{\theta}^2 - \omega^2 \cos \theta = E' \quad (55)$$

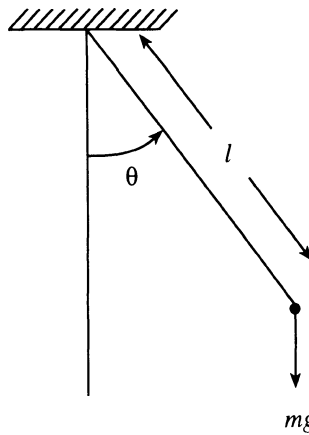


Figure 1.14. The simple pendulum.

where E' is proportional to the total energy of the system. The trajectories given by this integral are shown in Figure 1.15. Owing to the periodic term in equation (54), there are infinitely many equilibrium points: the centers are located along the θ -axis at even multiples of π while the saddle points are located at odd multiples of π . The closed

trajectories near each center represent the oscillatory motions of the system about the stable equilibrium position (upright pendulum) called the librations. Here, the period is a function of the amplitude of the motion. The saddle points correspond to unstable equilibrium positions (inverted pendulum), while the wavy curves, far away from the θ -axis correspond to neutrally stable equilibrium positions (rotating pendulum). For small energies, the pendulum will oscillate about a center. As the energy increases, the pendulum will execute larger librations until such a point is reached as when the pendulum goes right over the top and starts to execute rotational motion which gets faster as the energy increases further. The pair of trajectories that separate the librational and rotational motions and meet at the saddle points is called the separatrix¹². The separatrix corresponds to the pendulum being released from a vertical position ($\theta = -\pi$) passing through zero and slowly reaching the vertical position ($\theta = +\pi$) again. In practice, this particular solution is never achieved, since, as will be seen later, it takes an infinite time to go from $\theta = -\pi$ to $\theta = +\pi$.

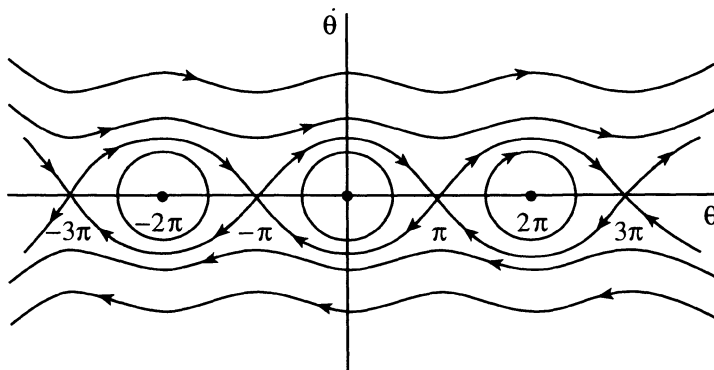


Figure 1.15. The trajectories in the $(\theta, \dot{\theta})$ phase space of a simple pendulum, Equation (54). The nearly elliptical trajectories represent librations. The trajectories outside the two separatrices represent rotational motions.

We obtain from (55), by a quadrature,

¹² Such an organization of the phase space by centers or elliptic points surrounded by the separatrices meeting at the saddle points or hyperbolic points is typical for integrable dynamical systems. Indeed, the representation of the motion of a general integrable two-degree-of freedom system on a Poincaré surface of section looks like a distorted version of the phase-plane portrait of the simple pendulum (see Chapter 5).

$$t = \int_{\alpha}^{\theta} \frac{d\theta'}{\sqrt{2(E' + \omega^2 \cos \theta')}} = \sqrt{\frac{1}{2\omega^2}} \int_{\alpha}^{\theta} \frac{d\theta'}{\sqrt{\cos \theta' - \cos \alpha}} \quad (56)$$

where,

$$\cos \alpha = -\frac{E'}{\omega^2}.$$

Putting,

$$\cos \theta = 1 - 2k^2 \sin^2 \varphi, \quad k = \sin \frac{\alpha}{2} = \sqrt{\frac{1}{2} \left(1 + \frac{E'}{\omega^2} \right)}. \quad (57)$$

(56) becomes

$$t = \frac{1}{\omega} \int_{\alpha}^{\varphi} \frac{d\varphi'}{\sqrt{1 - k^2 \sin^2 \varphi'}} \quad (58)$$

which can be inverted in terms of the Jacobi elliptic function

$$sn(\omega t, k) = \sin \varphi = \frac{1}{k} \sin \frac{\theta}{2}. \quad (59)$$

In order to find the period, the range of integration is taken from the equilibrium position $\theta = 0$ to the turning point $\theta_{\alpha} = \cos^{-1} \left(-\frac{E'}{\omega^2} \right) = \alpha$ which corresponds from $\varphi = 0$ to $\varphi = \pi/2$, and the period T is 4 times this integral:

$$T(k) = \frac{4}{\omega} \int_{\alpha}^{\pi/2} \frac{d\varphi}{\sqrt{1 - k^2 \sin^2 \varphi}} = \frac{4}{\omega} F\left(\frac{\pi}{2}, k\right) \quad (60)$$

where $F\left(\frac{\pi}{2}, k\right)$ is the complete elliptic integral.

For small oscillations, $k \rightarrow 0$, and noting that

$$k \rightarrow 0 : F\left(\frac{\pi}{2}, k\right) \rightarrow \frac{\pi}{2}. \quad (61)$$

(60) gives the result corresponding to a simple harmonic motion

$$T \approx 2\pi/\omega. \quad (62)$$

On the other hand, for motion along the separatrix, we have from (55), $E' = \omega^2$ so that $k = 1$, and then the period T becomes infinite –

$$T = \frac{4}{\omega} \int_{0}^{\pi/2} \frac{d\varphi}{\sqrt{1 - \sin^2 \varphi}} = \frac{4}{\omega} F\left(\frac{\pi}{2}, 1\right) = \infty. \quad (63)$$

In order to obtain amplitude-dependent corrections to the linear result, let $k \ll 1$, so that we have from (60),

$$T = \frac{4}{\omega} \int_{0}^{\pi/2} \left[1 + \frac{k^2}{2} \sin^2 \varphi + \frac{3k^4}{8} \sin^4 \varphi + \dots \right] d\varphi \quad (64)$$

from which,

$$T = \frac{2\pi}{\omega} \left(1 + \frac{k^2}{4} + \frac{9k^4}{64} + \dots \right). \quad (65)$$

Noting that,

$$k = \sin \frac{\alpha}{2} = \frac{\alpha}{2} - \frac{\alpha^3}{48} + \dots \quad (66)$$

(65) becomes

$$T = \frac{2\pi}{\omega} \left(1 + \frac{\alpha^2}{16} + \frac{11\alpha^4}{3072} + \dots \right). \quad (67)$$

(67) describes the amplitude-dependent corrections to the linear period.

1.4. Fully Nonlinear Evolution

It is quite possible that the predictions made by the linearized stability analysis in the foregoing will not be borne out by the full nonlinear equations. Elliptic fixed points, as predicted by a linearized stability analysis, are particularly susceptible to a breakdown under nonlinear perturbation.

EXAMPLE 11

Consider the system (Bender and Orszag (1978))

$$\left. \begin{aligned} \dot{x} &= -y + x(x^2 + y^2) \\ \dot{y} &= x + y(x^2 + y^2) \end{aligned} \right\}. \quad (68)$$

The linearized stability analysis of equation (68) predicts that $x = y = 0$ is an elliptic fixed point. However, the full nonlinear equation (68) predicts an unstable spiral emanating from the origin. This result follows from the exact solution: First, note that, we have from equation (68),

$$x\dot{x} + y\dot{y} = (x^2 + y^2)^2 \quad (69)$$

from which, putting,

$$r^2 = x^2 + y^2 \quad (70)$$

equation (69) becomes

$$\frac{1}{2} \frac{d}{dt}(r^2) = r^4. \quad (71)$$

Equation (71) has the solution,

$$r(t) = \frac{r(0)}{\sqrt{1 - 2\{r(0)\}^2 t}} \quad (72)$$

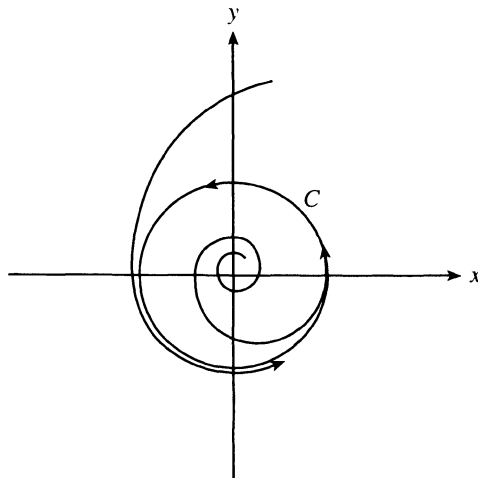


Figure 1.16. Limit cycle.

which shows that $r(t)$ grows with time; it actually goes to infinity when $t = \frac{1}{2\{r(0)\}^2}$!

This is an example of subcritical instability, which refers to the development of instability in a linearly-stable regime when the nonlinearities become sufficiently strong.

Another type of fully nonlinear behavior which will be missed by a linearized analysis is that of a limit cycle. A limit cycle in \mathbb{R}^2 is a closed curve C that is periodic and attracts the orbit of all solutions as t increases without bound (see Figure 1.16).

EXAMPLE 12

Consider the system

$$\left. \begin{aligned} \dot{x} &= x + y - x(x^2 + y^2) \\ \dot{y} &= -x + y - y(x^2 + y^2) \end{aligned} \right\}. \quad (73)$$

The linearized stability analysis of equation (73) predicts that $x = y = 0$ is an unstable focus (all orbits are repelled exponentially from this point). However, the full nonlinear equation (73) predicts a limit cycle enclosing the origin. This result follows from the substitution: $R(t) = r^2 = x^2 + y^2$, which leads to a Riccati equation –

$$\dot{R} + 2R^2 - 2R = 0. \quad (74)$$

On writing equation (74) as

$$\dot{R} = 2R(1 - R)$$

one observes that

$$\dot{R} \geq 0 \text{ when } R \leq 1.$$

The exact solution of equation (74) may be obtained by substituting,

$$R = \frac{\dot{f}}{2f} \quad (75)$$

to obtain

$$\ddot{f} - 2\dot{f} = 0 \quad (76)$$

so,

$$f = c_1 e^{2t} + c_2. \quad (77)$$

Therefore,

$$R(t) = x^2 + y^2 = \frac{c_1 e^{2t}}{c_1 e^{2t} + c_2} = \frac{1}{1 + ce^{-2t}} \quad (78)$$

which shows evolution into a limit cycle of radius 1 as $t \rightarrow \infty$. ($R = 1$ is, in fact, a stationary solution of equation (75)!) This is an example of supercritical equilibrium, which refers to the development of a nonlinear saturation in a linearly-unstable regime.

1.5. Non-autonomous Systems

A common example of nonautonomous system is one in which a system is subjected to an external time-dependent force $F(t)$. An example is the driven, nonlinear oscillator

$$\ddot{x} + \omega^2 x + \beta x^3 = \varepsilon F(t) \quad (79)$$

where ε can be considered to be a "coupling parameter". In the limit $\varepsilon \rightarrow 0$, the system becomes autonomous. In this limit, the phase space is two-dimensional, but for $\varepsilon \neq 0$, the phase space becomes three dimensional. In order to see this, consider the specific case of a periodic driving force, i.e.,

$$\ddot{x} + \omega^2 x + \beta x^3 = \varepsilon \cos \Omega t. \quad (80)$$

Introducing $z = \Omega t$ as a third dependent variable, equation (80) can be written as the system

$$\left. \begin{array}{l} \dot{x} = y \\ \dot{y} = -\omega^2 x - \beta x^3 + \varepsilon \cos z \\ \dot{z} = \Omega \end{array} \right\} \quad (81)$$

The extra dimension shown by the system (76) can lead to completely new types of behavior, particularly when the driving force is sufficiently strong (i.e., ε is large) because of a feedback between both the fundamental motion and its harmonics and the external field. In this regime, the solution can start to exhibit chaotic¹³ (though deterministic – since the solution is uniquely determined by the initial conditions) behavior, oscillating in time in an apparently random manner, (see Figure 1.17).

DEFINITION: A chaotic solution to a deterministic equation is one which shows extreme sensitivity to initial conditions (extremely small changes in the initial conditions leading to completely different outcomes) and whose evolution through phase space appears to be quite random, as measured by positive algorithmic complexity or entropy (see Chapter 5). Other properties of a chaotic solution are broad-band spectra and decaying correlations.

¹³ According to the Poincaré-Bendixson Theorem (see Chapter 6), the only possible attracting solutions in a two-dimensional phase space are periodic solutions (limit cycles) and steady states and are therefore non-chaotic. Geometrically, this can be seen by noting that, in a two-dimensional phase space, the solution curves (or trajectories) cannot undergo self-intersection, as this would violate the uniqueness of solution (except at the equilibrium points). By contrast, in a three-dimensional phase space, the solution curves can avoid self-intersection by going off in the third dimension, thereby rendering the topological structure of the trajectories quite complex in this case.

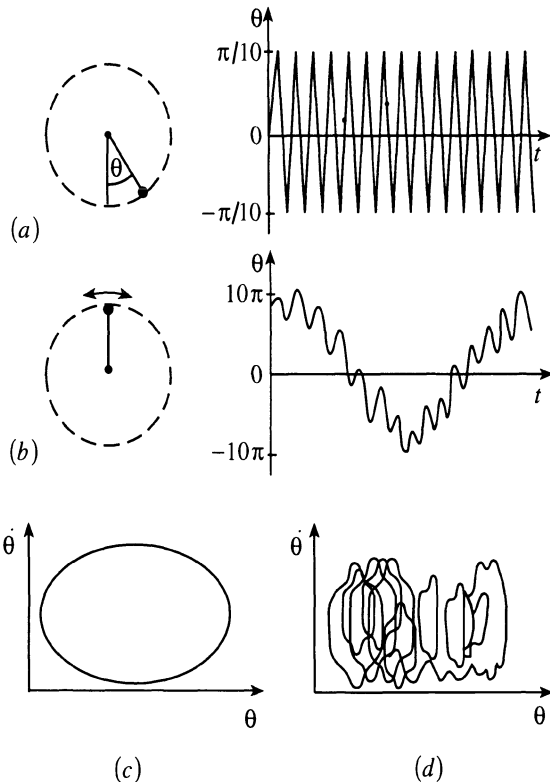


Figure 1.17. Transition to chaos in a driven pendulum. a) Regular motion at small values of the amplitude ε of the driving torque. b) Chaotic motion at $\varepsilon = \varepsilon_0$. c) and d) Regular and irregular trajectories in phase space $(\theta, \dot{\theta})$ which correspond to a) and b). (Due to Schuster, 1989) (By courtesy of VCH Publishers)

EXAMPLE 13

Consider forced oscillations of the Duffing system:

$$\ddot{x} + x = \varepsilon x^3 + \varepsilon F_o \cos \lambda t, \quad |\varepsilon| \ll 1. \quad (82)$$

Let us look for a solution of the form (Struble, (1962)),

$$x = A(t) \cos(t - \theta(t)) + \varepsilon x_1 + \varepsilon^2 x_2 + \dots \quad (83)$$

The motivation behind this prescription is the expectation that solution of the above equation for $\varepsilon \neq 0$ (but small ε) is very nearly a simple harmonic of the form $A \cos(t - \theta)$, which it would identically be if $\varepsilon = 0$. The perturbations induced by the terms with $\varepsilon \neq 0$ on the right hand side of the above equation are then expected to be reflected in –

- show changes in the amplitude A and phase θ of the near harmonic.
- higher harmonics through the x_k 's.

Thus, we obtain

$$\begin{aligned} & (2A\dot{\theta} + \ddot{A} - A\dot{\theta}^2) \cos(t - \theta) + (A\ddot{\theta} + 2A\dot{\theta}\dot{A} - 2\dot{A}) \sin(t - \theta) \\ & + \varepsilon(\ddot{x}_1 + x_1) + \dots = \varepsilon A^3 \cos^3(t - \theta) + \varepsilon F_o \cos \lambda t + \dots \end{aligned} \quad (84)$$

Now, since the nonlinearity and excitation are taken to be weak, we may assume that $A(t)$ and $\theta(t)$ are slowly-varying in time so that $\ddot{A}, \dot{A}^2, \dot{\theta}\dot{A}, \dot{\theta}^2$ and $\ddot{\theta}$ are quantities of higher order in ε than \dot{A} and $\dot{\theta}$. Further, grouping the various terms by the coefficients of $\cos(t - \theta)$ and $\sin(t - \theta)$ and requiring the x_k 's to take on the higher harmonics, we have at $0(\varepsilon)$:

$$\dot{\theta} = -\frac{3}{8}\varepsilon A^2 \quad (85)$$

$$\dot{A} = 0 \quad (86)$$

$$\ddot{x}_1 + x_1 = \frac{A^3}{4} \cos 3(t - \theta) + F_o \cos \lambda t \quad (87)$$

etc.

If $\lambda \neq 1$, equations (85)-(87) give the solution

$$\left. \begin{array}{l} \theta = \theta_o + \frac{3\varepsilon A^2 t}{8} \\ A = \text{const} \\ x_1 = -\frac{A^3}{32} \cos 3(t - \theta) + \frac{F_o}{1 - \lambda^2} \cos \lambda t \end{array} \right\} \quad (88)$$

which shows that to $O(\varepsilon)$, the amplitude of the near harmonic is not affected by the excitation.

However, if $\lambda \approx 1$, the solution (88) breaks down. In order to treat this case, we need to allow the excitation to affect the amplitude of the near harmonic especially during a resonance. For this purpose, we write

$$\begin{aligned}\varepsilon F_o \cos \lambda t &= \varepsilon F_o \cos[(\lambda - 1)t + \theta] \cos(t - \theta) + \\ &\quad - \varepsilon F_o \sin[(\lambda - 1)t + \theta] \sin(t - \theta).\end{aligned}\tag{89}$$

Using (89), we now obtain from equation (84),

$$\dot{\theta} = \frac{3}{8} \varepsilon A^2 + \frac{\varepsilon F_o}{2A} \cos[(\lambda - 1)t + \theta]\tag{90}$$

$$\dot{A} = \frac{\varepsilon F_o}{2} \sin[(\lambda - 1)t + \theta]\tag{91}$$

$$\ddot{x}_1 + x_1 = \frac{A^3}{4} \cos 3(t - \theta).\tag{92}$$

Equation (91) shows that the change in A is, however, slow.

We have from equation (92),

$$x_1 = -\frac{A^3}{32} \cos 3(t - \theta)\tag{93}$$

which is well behaved at $\lambda = 1$!

Putting,

$$\Phi = (\lambda - 1)t + \theta\tag{94}$$

equations (90) and (91) become

$$\dot{\Phi} = \frac{3}{8} \varepsilon A^2 + (\lambda - 1) + \frac{\varepsilon F_o}{2A} \cos \Phi\tag{95}$$

$$\dot{A} = \frac{\varepsilon F_o}{2} \sin \Phi. \quad (96)$$

Putting, further,

$$a = A \cos \Phi, \quad b = A \sin \Phi \quad (97)$$

equations (95) and (96) give

$$\dot{a} = -\left[\frac{3}{8} \varepsilon (a^2 + b^2) + (\lambda - 1) \right] b \quad (98)$$

$$\dot{b} = \frac{\varepsilon F_o}{2} + \left[\frac{3}{8} \varepsilon (a^2 + b^2) + (\lambda - 1) \right] a. \quad (99)$$

The equilibrium solutions of equations (98) and (99) correspond to

$$b = 0 \quad (100)$$

$$\frac{\varepsilon F_o}{2} + \left[\frac{3}{8} \varepsilon a^2 + (\lambda - 1) \right] a = 0. \quad (101)$$

Let us write equation (101) in the form,

$$(a + \mu)(a^2 - \mu a + v) = 0 \quad (102)$$

where,

$$v - \mu^2 = \frac{8}{3} \left(\frac{\lambda - 1}{\varepsilon} \right), \quad \mu v = \frac{4}{3} F_o > 0.$$

Since $(v - \mu^2)$ should change sign depending on whether $\lambda \leq 1$, we require $v > 0$. Further, since $\mu v > 0$, this implies $\mu > 0$.

The roots of equation (102) are

$$a = -\mu, \quad \frac{\mu \pm \sqrt{\mu^2 - 4v}}{2}. \quad (103)$$

(103) implies

- $v > \mu^2$: One real root $a = -\mu$,
- $v < \mu^2$: three real roots $a = -\mu, \sigma_1, \sigma_2$ with $\sigma_1 < 0, \sigma_2 > 0$.

Thus, if $\left(\frac{\lambda-1}{\varepsilon}\right) > 0$, there is one equilibrium point, and if $\left(\frac{\lambda-1}{\varepsilon}\right) < 0$, there will be three equilibrium points.

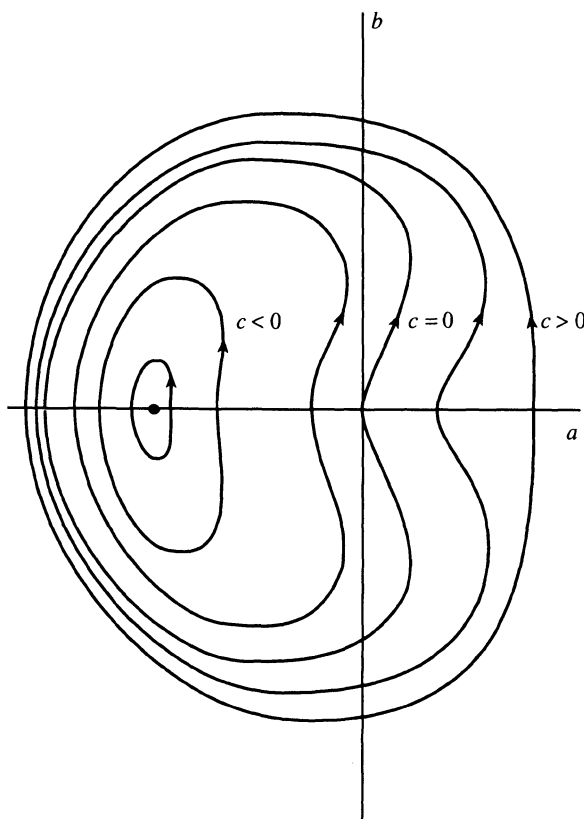


Figure 1.18. The solution curves in the ab -plane for the forced Duffing's oscillator in the case $\frac{\lambda-1}{\varepsilon} > 0$.

We have from equations (98) and (99),

$$\left\{ \frac{\varepsilon F_o}{2} + \left[\frac{3}{8} \varepsilon (a^2 + b^2) + (\lambda - 1) \right] a \right\} da = - \left[\frac{3}{8} \varepsilon (a^2 + b^2) + (\lambda - 1) \right] b db$$

which leads to the integral

$$F_o a + \left(\frac{\lambda - 1}{\varepsilon} \right) (a^2 + b^2) + \frac{3}{16} (a^2 + b^2)^2 = \text{const.} = c. \quad (104)$$

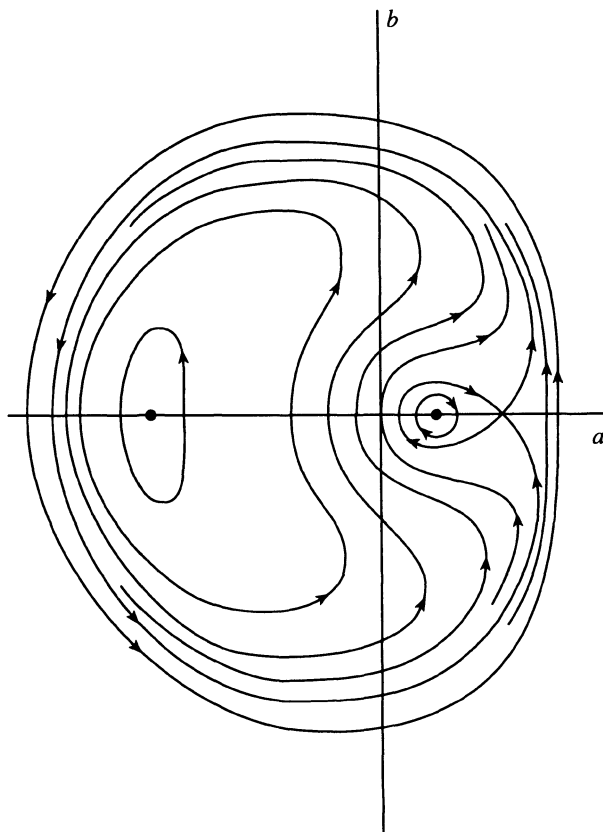


Figure 1.19. The solution curves in the ab -plane for the forced Duffing's oscillator in the case $\frac{\lambda - 1}{\varepsilon} < 0$.

(104) shows that all solutions are bounded, since the term $\frac{3}{16}(a^2 + b^2)^2$ completely dominates all others for large a and b .

The quartic curves described by (104), if $\left(\frac{\lambda - 1}{\varepsilon}\right) > 0$, form a family of closed paths centered about the equilibrium point $a = -\mu = -A$, $b = 0$, (see Figure 1.18). If $\left(\frac{\lambda - 1}{\varepsilon}\right) < 0$, there will be three equilibrium points – two centers and a saddle point, (see Figure 1.19).

Thus, if $\lambda \approx 1$, for the nonlinear problem, there exist bounded, periodic responses entrained at the impressed frequency so that the resonance infinities have been removed by the nonlinearity. This is because the frequency of the natural oscillation varies with amplitude due to the nonlinearity so that the natural oscillation does not remain in step with the excitation. The amplitude-frequency relationships for these responses are shown in Figure 1.20. The stability of a given branch is determined in the sense that $|A|$ increases as F_0 increases and instability if the reverse prevails. Whereas the stable states correspond to centers, the unstable states correspond to saddle points. For a given

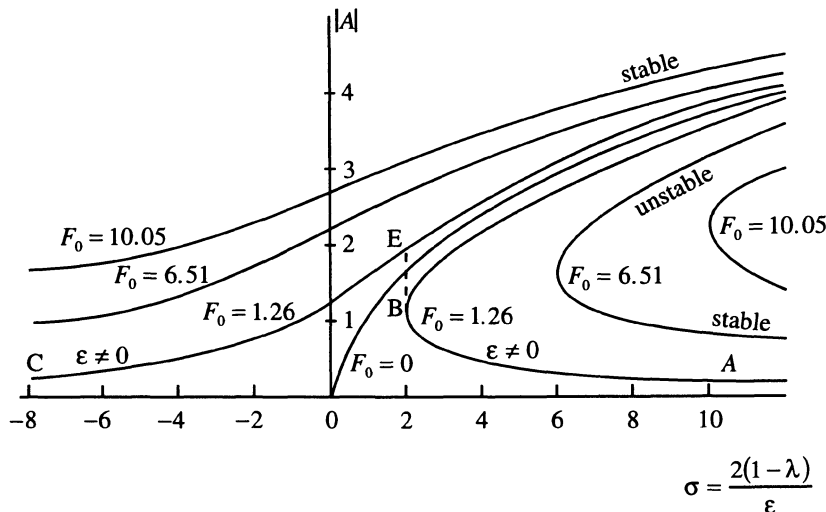


Figure 1.20. The amplitude-frequency response for the forced Duffing's oscillator. (Adapted from Struble (1962)) (By courtesy of McGraw-Hill Publishing Company)

impressed frequency, there can be more than one steady-state response. The initial conditions determine which of the possible responses actually develops. As λ increases from below 1, $|A|$ increases along AB . At B , $|A|$ jumps abruptly to the value corresponding to E , afterwards decreasing along EC as λ increases further¹⁴.

Consider next the case with $\lambda t = 3(t - \theta)$. Then, the principal term of the response (83) is a subharmonic of the impressed harmonic. The second-order solution x_2 then shows that resonance occurs for $\lambda \approx 3$, which is called the subharmonic resonance.

¹⁴ When there is some damping present in the system, these jump phenomena lead to a dynamic hysteresis effect – the response of the system depends on its past history so that the system responds differently when λ is increased than when λ is decreased.

CHAPTER 2

BIFURCATION THEORY

At points where the manifolds of bifurcating solutions intersect, flows may switch from one manifold to another, and sometimes take on new qualitative behavior by exchanging stability between manifolds. This signifies the occurrence of a bifurcation. Bifurcation or branching occurs in a system when the state of the system depends on some parameter and as that parameter varies the state branches to another state at some critical value of the parameter with usually a concomitant change of stability. The nature of the bifurcation is therefore determined by the dynamics on the center manifold at the bifurcation point. Further, the normal-forms reduction on the central manifold proves to be convenient for a discussion of local bifurcation because, as we saw in Chapter 1, this causes a reduction in dimensionality and, therefore, proves especially helpful in the bifurcation analysis of high-dimensional systems, (Crawford, (1991)). On the other hand, when there is a multiplicity of solutions, the solution sought out by the system is determined by stability considerations. The bifurcation theory is a study of non-uniqueness, and specifically a study of how the multiplicity of solutions varies with the parameter and the stability properties of the bifurcating solutions. Here, we will consider local bifurcation theory that addresses phenomena near a single point, (see Wiggins (1988) for a discussion of global bifurcations which often involve homoclinic and heteroclinic connections (Chapter 5)).

Bifurcations are classified according to how the stability of an equilibrium solution changes. There are two ways in which this can occur. An eigenvalue of the system linearized about this solution can pass through zero, or a pair of non-zero eigenvalues may cross the imaginary axis. The first case corresponds to a saddle-node or tangent bifurcation and describes the birth or collapse of two equilibria (like a stable node coalescing with a saddle and annihilating it). This corresponds to a manifold associated with a given fixed point intersecting itself. (On the other hand, when manifolds associated with different fixed points intersect, an exchange of stability occurs – this corresponds to a transcritical bifurcation or a pitchfork bifurcation.) The second case corresponds to the so-called Hopf bifurcation and describes the birth of a family of periodic orbits (limit cycle) following the change in stability of a focus. The type of bifurcation involved in a given problem is identified usually by developing the corresponding canonical form.

Consider the nonlinear problem –

$$Au = \lambda u \quad (1)$$

with the corresponding linear problem having an eigensolution u_o for an eigenvalue λ_o . The bifurcation theory investigates the nonlinear solutions in the neighborhood of this known solution, and in particular, the dependence of the various branches on λ in the neighborhood of the branch point. Notice the connection between the nonlinear branch points and the eigenvalues of the linearized problem. On the other hand, according to the Hartman-Grobman Theorem (Chapter 1), the loss of hyperbolicity of the equilibria implies that the local behavior of the flow cannot be described by the linearized flow.

2.1. Stability and Bifurcation

The goal of bifurcation theory is to determine the existence and stability of various branches of solutions like fixed points and periodic orbits. The various equilibria emerge from one another in a continuous manner as the bifurcation parameter μ varies across the bifurcation point so that the local dynamics is contained in a suitably defined center manifold at the bifurcation point.

Consider the first-order autonomous differential equation describing flow in a one-dimensional phase space R ,

$$\frac{du}{dt} = f(u; \mu), \quad t > 0 \quad (2)$$

where μ is a real parameter, and f is a given analytic function of u and μ with continuous partial derivatives of all order with respect to u and μ .

The equilibrium solution $u = u_o$ of equation (2) is found from

$$f(u; \mu) = 0. \quad (3)$$

Corresponding to one value of μ , several equilibrium solutions u_o may exist. This is guaranteed by the Implicit Function Theorem¹ which allows the solutions of equation (3) to become non-unique whenever $\partial f / \partial u = 0$. On the other hand, if $\partial f / \partial u \neq 0$, $\lambda = 0$

¹ **THEOREM:** Suppose that $f(u; \mu): R \times R \rightarrow R$ is a C^1 function satisfying

$$f(u_o; \mu_c) = 0 \text{ and } \frac{\partial f}{\partial u}(u_o; \mu_c) \neq 0.$$

Then, there exists a solution of the implicit equation $f(u; \mu) = 0$ given by $u = g(\mu)$ in some open subset W of μ_c .

$\lambda = 0$ is not an eigenvalue of the linear problem associated with equation (2) so that small changes in μ will not eliminate the existence of the equilibrium solution $u(\mu)$, which lies on a local branch of the equilibria.

The graph of equation (3) is called the branching or bifurcation diagram. The intersecting branches are the bifurcating solutions and the points of intersection, which correspond to change of stability, are called bifurcation points.

For a fixed value of μ , it is of interest to know the stability of any equilibrium solutions that exist for that value of μ . It is also of interest to know how the stability of equilibrium solutions changes as μ varies. Often an equilibrium solution $u_o(\mu)$ will be stable for $\mu < \mu_c$ and unstable for $\mu \geq \mu_c$, where μ_c is some critical value of μ . Thus, as μ is increased slowly, the equilibrium solution $u_o(\mu)$ becomes unstable at μ_c and the system in question can no longer remain in the state $u_o(\mu)$. As μ exceeds μ_c , the system may therefore branch to another stable solution. The supercritical branches are stable while the subcritical branches are unstable. The bifurcation theory seeks to explore how the stability of various equilibria changes as μ is varied near μ_c . This issue, of course, depends on the nonlinear nature of the problem in an essential way.

In order to determine stability of the equilibrium solution $u_o(\mu)$, consider a small perturbation $\hat{u}(t)$ about $u_o(\mu)$, so that

$$u(t) = u_o(\mu) + \hat{u}(t) \quad (4)$$

Equation (2) then becomes

$$\frac{d\hat{u}}{dt} = f(u_o + \hat{u}; \mu). \quad (5)$$

Linearizing f in \hat{u} , equation (5) becomes

$$\frac{d\hat{u}}{dt} \approx f_u(u_o; \mu)\hat{u} \quad (6)$$

from which, we have

$$\hat{u}(t) = ce^{f_u(u_o; \mu)t}. \quad (7)$$

Thus, if $f_u(u_o; \mu) < 0$, u_o is stable and vice versa. The bifurcation point μ_c is here defined by $f_u(u_o; \mu) = 0$ along with $f(u_o; \mu) = 0$. Now, noting that, by the Implicit

Function Theorem, the latter implies $\mu = \mu(u_o)$ whenever $f_\mu(u_o; \mu) \neq 0$, we have on differentiating $f(u_o; \mu) = 0$ with respect to u_o ,

$$f_{u_o} + f_\mu \frac{d\mu}{du_o} = 0. \quad (8)$$

(8) shows that $\frac{d\mu}{du_o} = 0$ at a bifurcation point if $f_\mu \neq 0$ there.

In higher dimensions, one has, in place of equation (2),

$$\frac{d\mathbf{u}}{dt} = \mathbf{f}(\mathbf{u}; \mu). \quad (9)$$

Let $\mathbf{u}_o(\mu)$ be an equilibrium point of equation (9), so that

$$\mathbf{f}(\mathbf{u}_o(\mu); \mu) = \mathbf{0}. \quad (10)$$

The stability of $\mathbf{u}_o(\mu)$ is then determined by the eigenvalues $\lambda_1(\mu), \lambda_2(\mu), \dots, \lambda_n(\mu)$ of the matrix

$$\mathbf{A}(\mu) = \frac{\partial \mathbf{f}(\mathbf{u}_o(\mu); \mu)}{\partial \mathbf{u}}. \quad (11)$$

If all the eigenvalues have a negative real part, then $\mathbf{u}_o(\mu)$ is stable. On the other hand, if one or more eigenvalues have a positive real part, then $\mathbf{u}_o(\mu)$ is unstable. Further, if the eigenvalues depend on the parameter μ , this stability may change as the parameter μ varies. In fact, the value of $\mu = \mu_c$, say, for which

$$\left. \begin{array}{l} \operatorname{Re} \lambda_i(\mu_c) = 0 \text{ for some } i \\ \operatorname{Re} \lambda_j(\mu_c) < 0 \text{ for all } j \neq i \end{array} \right\}$$

define the bifurcation points. It is apparent that a bifurcation point can arise in two ways:

- (i) $\lambda_1(\mu)$ is real-valued, $\lambda_1(\mu_c) = 0$, and $\operatorname{Re} \lambda_i(\mu_c) < 0$ for $i = 2, \dots, n$;
- (ii) $\lambda_1(\mu)$ and $\lambda_2(\mu)$ form a complex conjugate pair, so that $\lambda_1(\mu) = \overline{\lambda_2(\mu)} = \alpha(\mu) + i\beta(\mu)$, $\alpha(\mu_c) = 0$, $\beta(\mu_c) \neq 0$ and $\operatorname{Re} \lambda_i(\mu_c) < 0$ for $i = 3, \dots, n$.

Note that for a one-dimensional system, only Case (i) can occur. Case (i) is called the saddle-node bifurcation. Case (ii) is called the Hopf bifurcation. Figure 2.1 shows the schematic diagram of the variation of the eigenvalues as μ varies through μ_c in cases (i) and (ii) for a two-dimensional system.

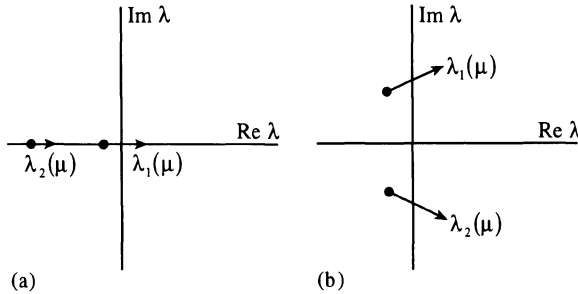


Figure 2.1. Schematic diagrams for (a) one-dimensional bifurcation and (b) Hopf bifurcation.

Case (i) corresponds to the transition of the critical point $u_o(\mu)$ from a stable node into a saddle point. Case (ii) corresponds to the transition of the critical point $u_o(\mu)$ from a stable focus into an unstable focus and appearance of a periodic solution. This requires an increase in the dimension of the center manifold so the Hopf bifurcation involves a change in the dimension of the stable and unstable manifolds about the bifurcation point as μ varies through μ_c and the real parts of a conjugate pairs of eigenvalues $\lambda, \bar{\lambda}$ cross the imaginary axis.

2.2. Saddle-Node, Transcritical and Pitchfork Bifurcations

Let us consider first a few examples.

EXAMPLE 1

Consider the equation

$$\frac{du}{dt} = f(u; \mu) = \mu - u^2. \quad (12)$$

The branches of critical points of equation correspond to

$$\mu - u^2 = 0 \quad (13)$$

which are

$$u_{o_1} = \sqrt{\mu}, \quad u_{o_2} = -\sqrt{\mu}. \quad (14)$$

These two branches of critical points intersect at the bifurcation point at $\mu = 0$. The existence of two branches (14) is allowed by the Implicit Function Theorem, because $f_u = -2u = 0$ at $u = 0$.

We have, from equation (12),

$$f_u(u_{o_i}; \mu) = -2u_{o_i}, \quad i = 1 \text{ and } 2. \quad (15)$$

Therefore, the critical point is stable or unstable, according as $u_{o_i} \gtrless 0$. Thus, a single branch of critical points undergoes a transition from a stable to an unstable state, and there is an exchange of stability at $u_{o_i} = 0$. Note that, here $f_\mu = 1 \neq 0$ at the bifurcation point, so (8) implies that $d\mu/d_{u_o} = 0$ there. This also implies that, there exists a unique fixed-point curve $\mu = \mu(u)$ through the bifurcation point $(u, \mu) = (0, 0)$ so that, as μ is varied, the two critical points u_{o_1} and u_{o_2} move toward each other, collide and destroy one another. This is an example of saddle-node bifurcation (see Figure 2.2). Equation (12) is the canonical form of the saddle-node bifurcation. Saddle-node bifurcation provides the mechanism by which critical points (or equilibria) are created or destroyed.

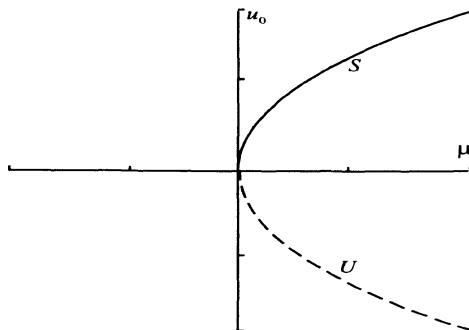


Figure 2.2. Saddle-mode bifurcation.

EXAMPLE 2

Consider the logistic equation (see Chapter 6),

$$\frac{du}{dt} = f(u; \mu) = \mu u - u^2. \quad (16)$$

Equation (16) is used as a simple model to describe population growth of a given species, the number of individuals of which is represented by u (May, 1976). When u is sufficiently small the population grows or dies exponentially according as $\mu \gtrless 0$. If the population grows then, after sometime, it will have become so large that food shortage or predator activity takes effect and the growth rate will drop. The nonlinear term in equation (16) represents this moderation of the exponential population growth rate.

The branches of critical points of equation (16) are found from

$$\mu u - u^2 = 0 \quad (17)$$

which are

$$u_{o_1} = 0, \quad u_{o_2} = \mu. \quad (18)$$

These two branches of critical points intersect at the bifurcation point at $\mu = 0$. The existence of two branches (18) is allowed by the Implicit Function Theorem, because $f_u = \mu - 2u = 0$ at $\mu = 0$ and $u = 0$.

We have, from equation (16),

$$f_u(u_{o_1}; \mu) = \mu, \quad f_u(u_{o_2}; \mu) = -\mu \quad (19)$$

Therefore, the critical point u_{o_1} is stable if $\mu < 0$ and unstable if $\mu > 0$, whereas u_{o_2} is stable if $\mu > 0$ and unstable if $\mu < 0$. Thus, the two branches have opposite stabilities and exchange stability at the bifurcation point $\mu = 0$. Note that, here $f_\mu = u = 0$ at the bifurcation point, so (8) implies that $d\mu/du_{o_0}$ may be non-zero there. This is an example of transcritical bifurcation (see Figure 2.3)². Equation (16) is the canonical form of transcritical bifurcation.

² Equation (16) has the following exact solution –

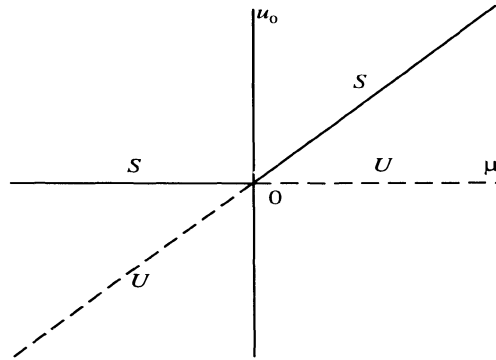


Figure 2.3. Transcritical bifurcation.

EXAMPLE 3

Consider the equation

$$\frac{du}{dt} = f(u, \mu) = \mu u - u^3. \quad (20)$$

Equation (20) was introduced by Landau (1944) to describe the effect of non-linearities on a hydrodynamic instability, the amplitude of a perturbation being represented by u .

The branches of critical points of equation (20) are found from

$$\mu u - u^3 = 0 \quad (21)$$

which are

$$u_{o_1} = 0, \quad u_{o_2} = \sqrt{\mu}, \quad u_{o_3} = -\sqrt{\mu}. \quad (22)$$

$$u(t) = \begin{cases} \frac{\mu u_o}{u_o + (\mu - u_o)e^{-\mu t}}, & \mu \neq 0 \\ \frac{u_o}{1 + u_o t}, & \mu = 0 \end{cases}$$

where $u_o = u(t=0)$. This shows that, as $t \rightarrow \infty$,

$$u(t) \rightarrow \begin{cases} \mu, & \mu > 0 \\ 0, & \mu \leq 0, \end{cases}$$

as can also be appreciated from equation (16), or Figure 2.3, for that matter!

(22) shows that, if $\mu \leq 0$, there is only one branch, while, if $\mu > 0$, there are three branches. These two branches of critical points intersect at the bifurcation point at $\mu = 0$. The existence of two branches (22) is allowed by the Implicit Function Theorem, because $f_u = \mu - 3u^2 = 0$ at $\mu = 0$ and $u = 0$.

We have, from equation (20),

$$f_u(u_{o_1}; \mu) = \mu, \quad f_u(u_{o_{2,3}}; \mu) = -2\mu \quad (23)$$

Therefore, the critical point u_{o_1} is stable if $\mu < 0$ and unstable if $\mu > 0$, whereas $u_{o_{2,3}}$ are stable if $\mu > 0$ and unstable if $\mu < 0$. These two branches have opposite stabilities and exchange stability at the bifurcation point $\mu = 0$. Note that, here $f_\mu = u = 0$ at the bifurcation point, but $\frac{d\mu}{du_o}$ is still zero there. This is an example of supercritical pitchfork bifurcation (see Figure 2.4a). One obtains a subcritical pitchfork bifurcation (see Figure 2.4b) if one changes the minus sign in equation (20) to a positive sign³.

³ Equation (20) has the following exact solution –

$$u(t) = \begin{cases} \frac{\sqrt{\mu} u_o}{\sqrt{u_o^2 + (\mu - u_o^2)e^{-2\mu t}}}, & \mu \neq 0 \\ \frac{u_o}{\sqrt{1+2u_o^2 t}}, & \mu = 0 \end{cases}$$

where $u_o = u(t=0)$. This shows that, as $t \rightarrow \infty$,

$$u(t) \rightarrow \begin{cases} \sqrt{\mu}, & \mu > 0 \\ 0, & \mu \leq 0 \end{cases}$$

the first of which describes the advent of a supercritical equilibrium following an initial exponential growth of the perturbation.

Equation (20), with a positive sign instead, has the following exact solution –

$$u(t) = \begin{cases} \frac{\sqrt{-\mu} u_o}{\sqrt{u_o^2 + (-\mu - u_o^2)e^{-2\mu t}}}, & \mu \neq 0 \\ \frac{u_o}{\sqrt{1-2u_o^2 t}}, & \mu = 0 \end{cases}$$

When $\mu < 0$, this shows

$$u(t) \rightarrow 0 \text{ as } t \rightarrow \infty, \text{ if } |u_o| < \sqrt{-\mu}$$

$$u(t) \rightarrow \infty \text{ as } t \rightarrow \frac{1}{\sqrt{-2\mu}} \ln\left(\frac{u_o^2}{u_o^2 + \mu}\right), \text{ if } |u_o| > \sqrt{-\mu},$$

(The bifurcation is called subcritical/supercritical when new equilibria occur for the values of the parameter at which the original equilibrium is stable/unstable.) Equation (20) is the canonical form of the pitchfork bifurcation. Pitchfork bifurcation is generic to problems that have symmetry, (note that equation (20) is invariant under the change of variables $u \rightarrow -u$).

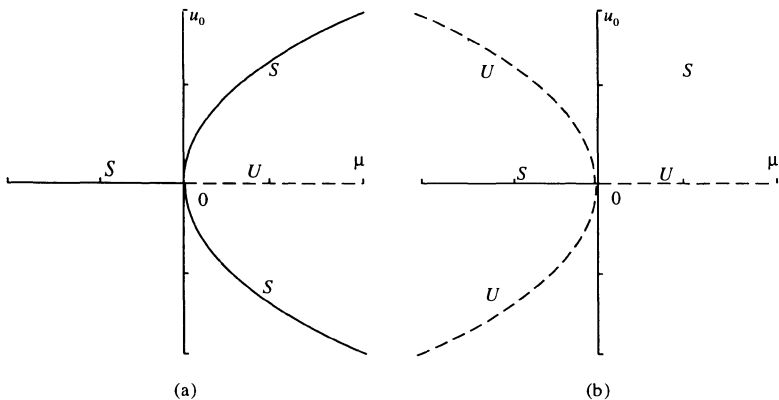


Figure 2.4. Pitchfork bifurcation, (a) supercritical pitchfork, (b) subcritical pitchfork.

Thus, the bifurcation points for transcritical and pitchfork bifurcations are determined by locating the points where the branches of critical points intersect, while saddle-node bifurcations are found by locating the points where $\frac{d\mu}{du_o} = 0$.

These results can now be summarized by the following Theorem:

THEOREM 2.1

Consider a first-order autonomous equation

$$\frac{du}{dt} = f(u; \mu). \quad (2)$$

Let $f(u_o; \mu)$ be an analytic function of u_o and μ in a neighborhood of $u_o = \mu = 0$, and suppose that $u_o = \mu = 0$ is a bifurcation point so that

which describe the possibility of a subcritical instability whenever the perturbation amplitude exceeds a threshold.

$$f(0;0) = f_u(0;0) = 0. \quad (24)$$

Then,

- (i) if $f_\mu(0;0) \neq 0$, there exists in some neighborhood of the bifurcation point $u_o = \mu = 0$, a single branch of critical points which undergoes a saddle-node bifurcation at this point;
- (ii) if $f_\mu(0;0) = 0$ and $D \equiv f_{\mu\mu}(0;0)f_{uu}(0;0) - f_{u\mu}^2(0;0) > 0$, the point $u_o = \mu = 0$ is an isolated bifurcation point; if $D < 0$, there are two branches of critical points which intersect and exchange stability at the bifurcation point $u_o = \mu = 0$; in the latter case, the bifurcation is either transcritical or pitchfork.

Proof: Since $f(u_o; \mu)$ is analytic, we have, in the neighborhood of the bifurcation point $u_o = \mu = 0$, on using (24), the Taylor series –

$$f(u_o; \mu) = \alpha\mu + \frac{1}{2}a\mu^2 + b\mu u_o + \frac{1}{2}cu_o^2 + O(u_o^3, u_o^2\mu, u_o\mu^2, \mu^3) \quad (25)$$

where,

$$\left. \begin{aligned} \alpha &= f_\mu(0;0), \quad a = f_{\mu\mu}(0;0), \\ b &= f_{u\mu}(0;0), \quad c = f_{uu}(0;0) \end{aligned} \right\}. \quad (26)$$

Thus,

$$\left. \begin{aligned} f_u(u_o; \mu) &= b\mu + cu_o + O(u_o^2, u_o\mu, \mu^2) \\ f_\mu(u_o; \mu) &= \alpha + a\mu + bu_o + O(u_o^2, u_o\mu, \mu^2) \end{aligned} \right\}.$$

- (i) In this case $\alpha \neq 0$, and the Implicit Function Theorem provides for a solution $\mu = \mu(u_o)$ of

$$f(u_o; \mu) = 0 \quad (3)$$

which is an analytic function of u_o and such that $\mu(0) = 0$. On using (24), (25) then gives

$$\left. \begin{aligned} \mu &= -\frac{c}{2\alpha} u_o^2 + O(u_o^3) \\ f_u &= cu_o + O(u_o^2) \end{aligned} \right\}. \quad (27)$$

(27) shows that if $c \neq 0$, f_u changes sign and stability is exchanged at the bifurcation point near which the branch of critical points has the shape of a parabola. Besides, $\frac{d\mu}{du_o} = 0$ at the bifurcation point, as is necessary, since $f_\mu(0,0) = \alpha \neq 0$ here. Thus, this case corresponds to a saddle-node bifurcation.

(ii) For the case $\alpha = 0$, and $D = ac - b^2 > 0$, the quadratic form

$$\frac{1}{2}a\mu^2 + b\mu u_o + \frac{1}{2}cu_o^2$$

cannot vanish for any real values of μ and u_o except $\mu = u_o = 0$. Therefore, the point $\mu = u_o = 0$, which is a solution of (3), is an isolated bifurcation point.

In order to consider the case $D < 0$, let us first assume that $c \neq 0$, and introduce

$$u_o = \mu v \quad (28)$$

and define

$$g(v; \mu) = \frac{f(u_o; \mu)}{\mu^2} = \frac{1}{2}a + bv + \frac{1}{2}cv^2 + O(\mu). \quad (29)$$

The critical points of equation (2) are then given by

$$g(v; \mu) = 0. \quad (30)$$

Since,

$$g_v(v; 0) = cv + b = \pm\sqrt{-D} \neq 0$$

the Implicit Function Theorem provides for two distinct solutions $v_1(\mu)$ and $v_2(\mu)$ of (30) which are analytic functions of μ and such that $v_1(0) = v_1$ and $v_2(0) = v_2$, where v_1 and v_2 are solutions of

$$g(v; 0) = 0$$

and are given by

$$v_{1,2} = \frac{-b \pm \sqrt{-D}}{c}. \quad (31)$$

This establishes the existence of two distinct branches of critical points $u_o = \mu v_1(\mu)$ and $u_o = \mu v_2(\mu)$ which intersect at the bifurcation point, have slopes there given by v_1 and v_2 and so exchange stabilities at the bifurcation point. Thus, this case corresponds to a transcritical bifurcation.

Noting that

$$f_{u_o}(u_o; \mu) = cu_o + b\mu = \mu(cv + b) = \pm\mu\sqrt{-D} + O(\mu^2)$$

we see that the two branches above have opposite stabilities, and exchange stability at the bifurcation point.

If, on the other hand, $c = 0, D < 0$ implies $b \neq 0$. In this case, we introduce

$$\mu = u_o w \quad (32)$$

and define

$$h(u_o; w) = \frac{f(u_o; u_o w)}{u_o^2} = \frac{1}{2} aw^2 + bw + O(u_o). \quad (33)$$

The critical points of (2) are then given by

$$h(u_o, w) = 0 \quad (34)$$

which are

$$w = 0, -\frac{2b}{a}.$$

Since,

$$h_w(0, w) = aw + b = \pm b \neq 0$$

the Implicit Function Theorem provides for two distinct solutions $w_1(u_o)$ and $w_2(u_o)$ of (34) which are analytic functions of u_o and such that $w_1(0) = 0, w_2(0) = -\frac{2b}{a}$. This establishes the existence of two distinct branches of critical points $\mu = u_o w_1(u_o)$ and $\mu = u_o w_2(u_o)$ which intersect at the bifurcation point. We have for the first branch $\mu = 0(u_o^2)$ or $\mu = \beta u_o^2$, say, which is a parabola. On the other hand, we have for the second branch $\mu = 0(u_o)$ or $\mu = -\left(\frac{2b}{a}\right)u_o$, which is a straight line. Now, the slopes of the above two branches, from (8), are given by

$$\begin{aligned} f_{u_o}(u_o; \mu) &= -f_\mu(u_o; u_o w) \frac{d\mu}{du_o} \\ &= -2b\mu + O(\mu^2), b\mu + O(\mu^2). \end{aligned}$$

So, the above two branches have opposite stabilities and exchange stabilities at the bifurcation point. Further, the parabolic branch is either always stable (if $b\beta > 0$) or always unstable (if $b\beta < 0$) so that one has a supercritical pitchfork bifurcation if $b\beta > 0$, or a subcritical pitchfork bifurcation if $b\beta < 0$.

EXAMPLE 4

Consider a bead of mass m sliding without friction on a circular wire or hoop of radius R (Figure 2.5). The hoop is constrained to rotate about a vertical diameter with constant angular velocity ω . The equation of motion of the bead subject to its weight mg and the centrifugal force $mr\omega^2$ is

$$mR\ddot{\theta} = mR\omega^2 \sin \theta \cdot \cos \theta - mg \sin \theta. \quad (35)$$

Equilibrium prevails, therefore, when

$$mR\omega^2 \sin \theta \cdot \cos \theta - mg \sin \theta = 0$$

or

$$\theta_o = 0, \quad \theta_i = \cos^{-1} \frac{g}{R\omega^2}. \quad (36)a$$

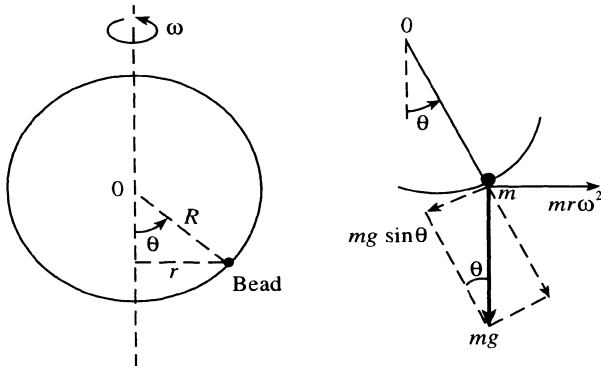


Figure 2.5. Bead on a rotating hoop.

In the neighborhood of the bifurcation point $\omega_c = \sqrt{g/R}$, (36)a becomes

$$\theta_o = 0, \quad \theta_1^2 \approx \frac{4}{\sqrt{g/R}} \left(\omega - \sqrt{\frac{g}{R}} \right) \quad (36b)$$

so that the branch corresponding to θ_1 is locally a parabola near the bifurcation point.

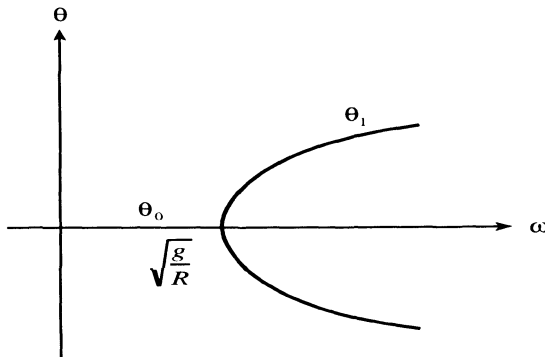


Figure 2.6. Equilibrium solutions for a bead sliding without friction on a circular wire.

In Figure 2.6, the two equilibrium solutions are sketched as functions of ω . (36) shows that if $\omega \leq \sqrt{g/R}$, then the only equilibrium solution is $\theta_o = 0$; however, if

$\omega > \sqrt{g/R}$, then there are three possible equilibrium solutions. The equilibrium solutions bifurcate at the bifurcation point $\omega_c = \sqrt{g/R}$.

When there is a multiplicity of solutions, the solution sought out by the system is determined by stability considerations.

In order to determine the stability of θ_o , consider a small perturbation $\hat{\theta}$ about θ_o , and write

$$\theta = \theta_o + \hat{\theta} \quad (37)$$

and linearizing in $\hat{\theta}$, equation (35) becomes

$$mR\ddot{\hat{\theta}} \approx (mR\omega^2 - mg)\hat{\theta}$$

or

$$\ddot{\hat{\theta}} + \left(\frac{g}{R} - \omega^2\right)\hat{\theta} = 0 \quad (38)$$

from which it is obvious that θ_o is stable if $\omega < \sqrt{g/R}$ and unstable if $\omega > \sqrt{g/R}$.

Similarly, the stability of θ_1 may be determined by writing

$$\theta = \theta_1 + \hat{\theta} \quad (39)$$

and linearizing equation (35) again in $\hat{\theta}$; we then obtain

$$mR\ddot{\hat{\theta}} \approx -m \left[\frac{(R\omega^2)^2 - g^2}{R\omega^2} \right] \hat{\theta}$$

or

$$\ddot{\hat{\theta}} + \left[\frac{(R\omega^2)^2 - g^2}{R^2\omega^2} \right] \hat{\theta} = 0 \quad (40)$$

from which it is obvious that θ_1 is stable if $\omega > \sqrt{g/R}$ and unstable if $\omega < \sqrt{g/R}$.

Thus, if ω starts from zero and is slowly increased, the bead will remain at the bottom of the hoop (corresponding to θ_o) until the critical value $\omega_c = \sqrt{g/R}$ is reached. As ω becomes larger than ω_c , θ_o becomes unstable and the bead will quickly bifurcate to a branch corresponding to θ_1 , (see Figure 2.6).

In the phase plane of $\dot{\theta}, \theta$, as ω increases and passes through $\omega_c = \sqrt{g/R}$, the stable center at the origin bifurcates into an unstable saddle at the origin and two non-zero stable centers located on the θ -axis, (see Figure 2.7). This is an example of pitchfork bifurcation.

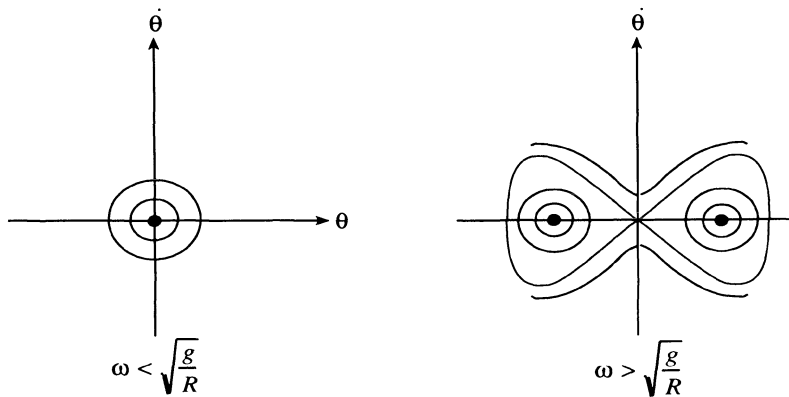


Figure 2.7. The bifurcation of the stable center at the origin into an unstable saddle as the angular velocity ω increases.

It may be noted that saddle-node bifurcation and Hopf bifurcation (see Section 3.3) are the generic bifurcations in dynamical systems. Under perturbations, transcritical bifurcation breaks up and pitchfork bifurcation breaks down into saddle-node bifurcation, as shown in Figure 2.8, (see Exercise 1). As shown in Figure 2.8, the breakdown of a pitchfork bifurcation leads to one equilibrium state that evolves smoothly as the control parameter increases and to another disconnected state that exists above a critical value of the parameter. The disconnected state can only be reached via a discontinuous jump in the parameter and disappears catastrophically below a critical value of the parameter.

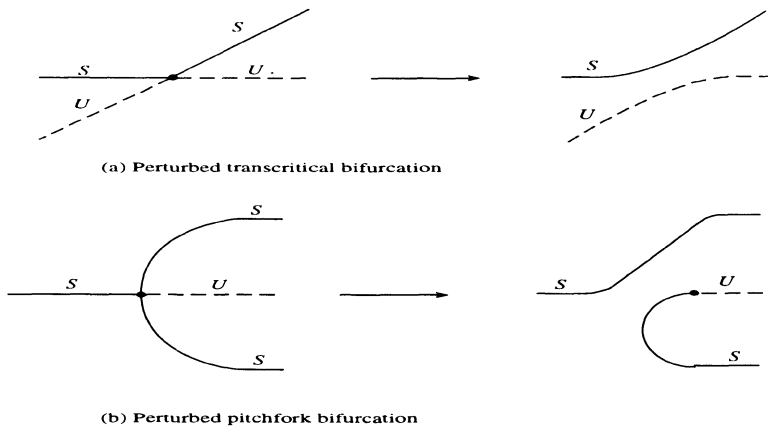


Figure 2.8. Break-up of bifurcations on perturbation.

2.3. Hopf Bifurcation

In order to permit the occurrence of Hopf bifurcation, the first-order system (9) must have dimension $n \geq 2$. Let us consider here, for illustration, only the planar case $n = 2$, when equation (9) becomes

$$\left. \begin{aligned} \frac{du}{dt} &= f(u, v; \mu) \\ \frac{dv}{dt} &= g(u, v; \mu) \end{aligned} \right\} \quad (41)$$

where f and g are analytic functions of u, v and μ .

The critical point $(u_o(\mu), v_o(\mu))$ of equation (41) corresponds to

$$\left. \begin{aligned} f(u_o(\mu), v_o(\mu); \mu) &= 0 \\ g(u_b(\mu), v_o(\mu); \mu) &= 0 \end{aligned} \right\} \quad (42)$$

and its stability is determined by the eigenvalues $\lambda_1(\mu)$ and $\lambda_2(\mu)$ of the matrix

$$\mathbf{A}(\mu) = \begin{bmatrix} f_u(u_o, v_o; \mu) & f_v(u_o, v_o; \mu) \\ g_u(u_o, v_o, \mu) & g_v(u_o, v_o, \mu) \end{bmatrix}. \quad (43)$$

One has for a Hopf bifurcation,

$$\lambda_1(\mu) = \overline{\lambda_2(\mu)} = \alpha(\mu) + i\beta(\mu) \quad (44)$$

where assuming, without loss of generality, the bifurcation point is $\mu = 0$, one has

$$\alpha(0) = 0, \quad \beta(0) \neq 0. \quad (45)$$

(45) implies that, in the neighborhood of $\mu = 0$, $\det \mathbf{A}(\mu) \neq 0$, so that, by the Implicit-Function Theorem, $u_o(\mu)$ and $v_o(\mu)$ are analytic functions of μ in a neighborhood of $\mu = 0$.

Putting

$$\hat{u} = u - u_o, \quad \hat{v} = v - v_o \quad (46)$$

and expanding f and g in powers of \hat{u} and \hat{v} , equation (41) becomes

$$\begin{bmatrix} \frac{d\hat{u}}{dt} \\ \frac{d\hat{v}}{dt} \end{bmatrix} = \mathbf{A}(\mu) \begin{bmatrix} \hat{u} \\ \hat{v} \end{bmatrix} + \begin{bmatrix} F(\hat{u}, \hat{v}; \mu) \\ G(\hat{u}, \hat{v}; \mu) \end{bmatrix} \quad (47)$$

where F and G are $O(\hat{u}^2, \hat{v}^2, \hat{u}\hat{v})$ as \hat{u} and $\hat{v} \rightarrow 0$, and are analytic functions of \hat{u} and \hat{v} .

To facilitate further discussion, let us suppose that $\mathbf{A}(\mu)$ has the following canonical form:

$$\mathbf{A}(\mu) = \begin{bmatrix} \alpha(\mu) & \beta(\mu) \\ -\beta(\mu) & \alpha(\mu) \end{bmatrix} \quad (48)$$

so that equation (47) becomes

$$\left. \begin{aligned} \frac{d\hat{u}}{dt} &= \alpha(\mu)\hat{u} + \beta(\mu)\hat{v} + F(\hat{u}, \hat{v}; \mu) \\ \frac{d\hat{v}}{dt} &= -\beta(\mu)\hat{u} + \alpha(\mu)\hat{v} + G(\hat{u}, \hat{v}; \mu) \end{aligned} \right\}. \quad (49)$$

Equation (49) shows that, in a small neighborhood at least of the bifurcation point, the origin $\hat{u} = 0, \hat{v} = 0$ in the \hat{u}, \hat{v} -plane is a focus (see footnote 6, Chapter 1) whose stability is determined by the sign of $\alpha(\mu)$. Since $\alpha(0) = 0$, this stability changes as μ passes through zero.

In order to facilitate discussion, let us introduce

$$z = \hat{u} + i\hat{v}, \quad \bar{z} = \hat{u} - i\hat{v} \quad (50)$$

so that equation (49) becomes

$$\frac{dz}{dt} = [\alpha(\mu) - i\beta(\mu)]z + N(z, \bar{z}; \mu) \quad (51)$$

where,

$$N(z, \bar{z}; \mu) = F(\hat{u}, \hat{v}; \mu) + iG(\hat{u}, \hat{v}; \mu) \sim O(|z|^2) \text{ as } |z| \rightarrow 0.$$

It is now a rather simple matter to show that (see Appendix), using a near-identity analytic transformation

$$\xi = z + S(z, \bar{z}; \mu) \quad (52)$$

where S is $O(|z|^2)$ as $|z| \rightarrow 0$, (51) can be reduced to the *normal* form

$$\frac{d\xi}{dt} = [\alpha(\mu) - i\beta(\mu)]\xi + [\gamma(\mu) + i\delta(\mu)]|\xi|^2\xi + O(|\xi|^4) \quad (53)$$

where $\gamma(\mu)$ and $\delta(\mu)$ are analytic functions of μ . Equation (53) implies that the nonlinear term $N(z, \bar{z}; \mu)$ in equation (51) can be transformed to remove all quadratic terms and all cubic terms except one, namely the term $|\xi|^2\xi$. Note that the latter term is the lowest-order nonlinear term which has the same phase as ξ , and is, therefore, the most dominant term producing resonance as $|\xi| \rightarrow 0$.

THEOREM 2.2

The first-order equation

$$\frac{d\xi}{dt} = [\alpha(\mu) - i\beta(\mu)]\xi + [\gamma(\mu) + i\delta(\mu)]|\xi|^2 \xi \quad (54)$$

for μ in a neighborhood of zero, has a family of periodic solutions of period $\frac{2\pi}{|\beta(\mu)|}$, as $\mu \rightarrow 0$, which are stable (or unstable) when $\alpha(\mu) > 0$ (or $\alpha(\mu) < 0$).

Proof: Introduce the polar coordinates (R, ϕ) by

$$\xi = R e^{i\phi} \quad (55)$$

so that equation (54) becomes

$$\left. \begin{aligned} \frac{dR}{dt} &= \alpha(\mu)R + \gamma(\mu)R^3 \\ \frac{d\phi}{dt} &= -\beta(\mu) + \delta(\mu)R^2 \end{aligned} \right\}. \quad (56)$$

Assuming that $\gamma(0) \neq 0$ so that $\gamma(\mu)$ is non-zero in a neighborhood of $\mu = 0$, the first of equation (56) has two critical points,

$$R = 0, \quad R^2 = -\frac{\alpha(\mu)}{\gamma(\mu)}. \quad (57)$$

The stability of these solutions is determined by the sign of $\lambda_1(\mu)$, where

$$\lambda_1 = \frac{\partial}{\partial R} (\alpha R + \gamma R^3) \text{ at } \alpha R + \gamma R^3 = 0 \quad (58)$$

or

$$\lambda_1 = \begin{cases} \alpha, & \text{for } R = 0 \\ -2\alpha, & \text{for } R^2 = -\frac{\alpha}{\gamma} \end{cases}. \quad (59)$$

(59) shows that the two branches (57) have opposite stabilities. Observe that the second branch of (57), (noting that $\alpha(\mu) \sim \alpha'(0)\mu$ as $\mu \rightarrow 0$, with the generic condition $\alpha'(0) \neq 0$)⁴, is a pitchfork bifurcation, (see Figure 2.9).

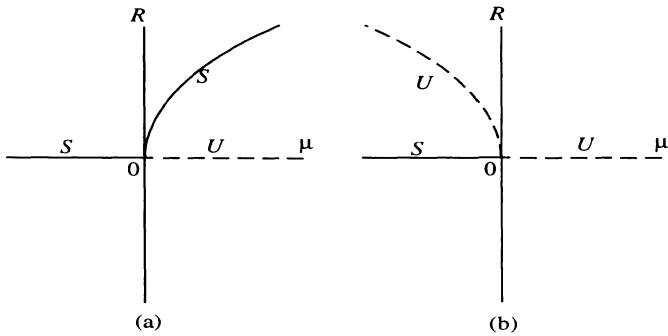


Figure 2.9. The bifurcation diagram for a Hopf bifurcation: (a) supercritical and (b) subcritical.

Further, the second of equation (56), for the second branch of (57), leads to

$$\phi = \phi_o + \omega(\mu)t \quad (60)$$

where,

$$\omega = -\beta - \frac{\delta\alpha}{\gamma}.$$

Thus, the second branch of (57) corresponds to a periodic solution, with period $2\pi/\omega(\mu)$ or $2\pi/|\beta(0)|$ as $\mu \rightarrow 0$.

⁴ $\alpha'(0) \neq 0$ implies that the eigenvalues cross the imaginary axis with non-zero speed so that the stability of the fixed point $(0,0)$ changes at a finite speed as μ passes through zero. This transversality condition leads to the existence of a unique center manifold passing through $(u,v) = (0,0)$, $\mu = 0$ in $R^2 \times R$ (Marsden and McCracken (1976)).

Therefore, in a supercritical Hopf bifurcation, as μ varies through the bifurcation point $\mu = 0$, the branch $R = 0$ becomes an unstable focus and leads to a periodic solution. Note that the pitchfork bifurcation at $\mu = 0$ for the first of equation (56) corresponds to a Hopf bifurcation for the full system (54). Thus, Hopf bifurcation is generically a pitchfork bifurcation.

However, in a subcritical Hopf bifurcation, as μ varies through the bifurcation point $\mu = 0$, the branch $R = 0$ becomes an unstable focus but goes into no periodic solution. Indeed, subcritical Hopf bifurcations provide a mechanism for the onset of chaos (like in the Lorenz model, see Section 6.6).

EXAMPLE 5

Consider the first-order system of equations

$$\left. \begin{array}{l} \dot{x} = -y - x(x^2 + y^2 - \mu) \\ \dot{y} = x - y(x^2 + y^2 - \mu) \end{array} \right\}. \quad (61)a,b$$

The linearized version of (61) is

$$\left. \begin{array}{l} \dot{x} = \mu x - y \\ \dot{y} = x + \mu y \end{array} \right\} \quad (62)a,b$$

for which,

$$x, y \sim e^{\lambda t}, \quad \lambda = \mu \pm i. \quad (63)$$

If $\mu < 0$, then $\operatorname{Re}(\lambda) < 0$, and $(0, 0)$ is a stable focus; if $\mu = 0$, then $\lambda = \pm i$, and $(0, 0)$ is a center; if $\mu > 0$, then $\operatorname{Re}(\lambda) > 0$, and $(0, 0)$ is an unstable focus. Further, $\frac{\partial \lambda(\mu)}{\partial \mu} \Big|_{\mu=0} = 1 \neq 0$ so that the eigenvalues cross the imaginary axis with non-zero speed.

The nonlinear problem (61) can be solved exactly by putting

$$x = r \cos \theta, \quad y = r \sin \theta \quad (64)$$

and noting,

$$x\dot{x} + y\dot{y} = r\dot{r}, \quad x\dot{y} - y\dot{x} = r^2\dot{\theta}. \quad (65)$$

We then obtain from equations (61)

$$\left. \begin{aligned} \dot{r} &= r(\mu - r^2) \\ \dot{\theta} &= 1 \end{aligned} \right\}. \quad (66)a,b$$

We have, from equation (66)b,

$$\theta = t + t_o. \quad (67)$$

For the case $\mu > 0$, equation (66)a has the solution –

$$r = \frac{\sqrt{\mu}}{\sqrt{1 + ce^{-2\mu t}}} \quad (68)$$

where,

$$c = \frac{\mu}{[r(t=0)]^2} - 1.$$

(68) shows the existence of a limit cycle at $r = \sqrt{\mu}$, for $\mu > 0$ (see Figure 2.10), via a supercritical pitchfork bifurcation. (Observe that $r = \sqrt{\mu}$ is, in fact, a stationary

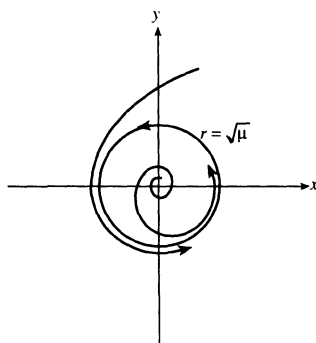


Figure 2.10. The limit cycle for the system (61) when $\mu > 0$.

solution of equation (66)a!) This is, of course, consistent with the linear result (63) that $(0, 0)$ is an unstable focus for $\mu > 0$.

Thus, as μ passes through the bifurcation point $\mu = 0$, the origin changes from a stable focus to an unstable focus and there appears a new periodic solution bifurcating from $\mu = 0$.

For the case $\mu = 0$, equation (66)a becomes

$$\dot{r} = -r^3 \quad (69)$$

from which, we have

$$r = \frac{1}{\sqrt{2t + c}}. \quad (70)$$

(70) shows that $(0, 0)$ is actually a stable focus, at variance with the linear result (63), so that the linearized version of equation (61) breaks down as $\mu \rightarrow 0$.

For the case $\mu < 0$, say $\mu = -k^2$, equation (66)a has the solution –

$$r = \frac{k}{\sqrt{\frac{1}{c} e^{2k^2 t} - 1}}. \quad (71)$$

(71) shows that $(0, 0)$ is a stable focus in accordance with the linear result (63).

2.4. Bifurcation Theory for One-Dimensional Maps

Area-preserving maps sometimes provide a superior alternative to differential-equations approach because of the ease with which the iterations can be carried out over hundreds of thousands of mapping periods (see Chapter 5). Here, one constructs a discrete map from the flow generated by a continuous time system by sampling the flow at discrete times $t_n = t_o + n\tau$ ($n = 0, 1, 2, \dots$),

$$x_{n+1} = f(x_n) \quad (72)$$

where,

$$x_n = x(t_n).$$

We will now give a brief account of the bifurcation theory for one-dimensional maps of the form –

$$f_\lambda(x) = f(x, \lambda) : R \times R \rightarrow R. \quad (73)$$

To simplify the discussion, we take the fixed point to be at $x = 0$ and the bifurcation to occur at $\lambda = 0$.

THEOREM 2.3

Let $f : R \times R \rightarrow R$ be a one-parameter family of C^2 maps satisfying

$$\left. \begin{array}{l} f(0, 0) = 0, \frac{\partial f}{\partial x}(0, 0) = 1, \\ \frac{\partial^2 f}{\partial x^2}(0, 0) > 0, \frac{\partial f}{\partial \lambda}(0, 0) > 0 \end{array} \right\}. \quad (74)$$

Then, there exists intervals $(\lambda_1, 0), (0, \lambda_2)$ and a number $k > 0$ such that:

- (i) there are two fixed points in $(-k, k)$, with $x \gtrless 0$ being unstable/stable, if $\lambda \in (\lambda_1, 0)$;
- (ii) there are no fixed points in $(-k, k)$, if $\lambda \in (0, \lambda_2)$ (Saddle-node bifurcation, Figure 2.11).

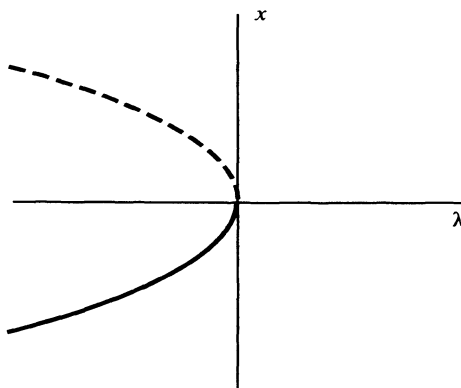


Figure 2.11. Saddle-node bifurcation (dashed curve represents unstable fixed points).

THEOREM 2.4

Let $f: R \times R \rightarrow R$ be a one-parameter family of C^2 maps satisfying

$$\left. \begin{aligned} f(0, \lambda) &= 0, \frac{\partial f}{\partial x}(0, 0) = 1, \\ \frac{\partial^2 f}{\partial x \partial u}(0, 0) &> 0, \frac{\partial^2 f}{\partial x^2}(0, 0) > 0 \end{aligned} \right\}. \quad (75)$$

Then, there exist two branches of fixed points for $\lambda \approx 0$. The first branch is $x = 0$ for all λ and is stable/unstable if $\lambda \lesssim 0$, while the second branch has $x(\lambda) \neq 0$ if $\lambda \neq 0$, with $x(0) = 0$, and is stable/unstable if $\lambda \gtrsim 0$ (Transcritical bifurcation, Figure 2.12).

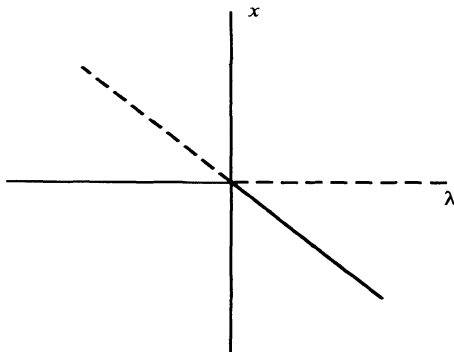


Figure 2.12. Transcritical bifurcation (dashed lines represent unstable fixed points).

THEOREM 2.5

Let $f: R \times R \rightarrow R$ be a one-parameter family of C^3 maps satisfying,

$$\left. \begin{aligned} f(-x, \lambda) &= -f(x, \lambda), \frac{\partial f}{\partial x}(0, 0) = 1, \\ \frac{\partial^2 f}{\partial x \partial u}(0, 0) &> 0, \frac{\partial^3 f}{\partial x^3}(0, 0) < 0 \end{aligned} \right\}. \quad (76)$$

Then, there exist intervals $(\lambda_1, 0), (0, \lambda_2)$ and a number $k > 0$ such that:

- (i) there is a single stable fixed point at the origin in $(-k, k)$, if $\lambda \in (\lambda_1, 0)$;
- (ii) there are three fixed points in $(-k, k)$, the one at the origin is unstable while the other two are stable, if $\lambda \in (0, \lambda_2)$.

(Pitch-fork bifurcation, Figure 2.13)

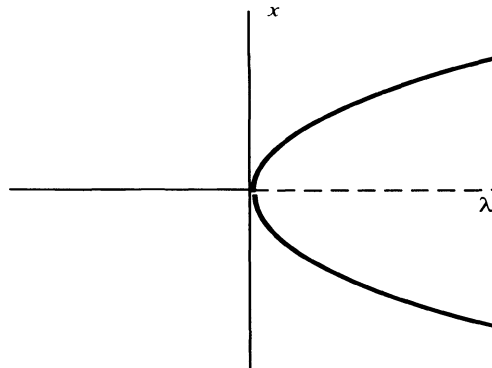


Figure 2.13. Pitchfork bifurcation (dashed line represents unstable fixed points).

See Rasband (1990) for proofs of these Theorems.

Iterated maps, unlike continuous flows, can possess non-hyperbolic fixed points with the eigenvalue equal to -1 . This leads to some bifurcation scenarios, like the period-doubling bifurcations, that are unique to iterated maps.

2.5. Appendix

Consider the reduction to *normal* form of the equation (Grimshaw, 1990) –

$$\frac{dz}{dt} = [\alpha(\mu) - i\beta(\mu)]z + N(z, \bar{z}; \mu) \quad (\text{A.1})$$

where,

$$N(z, \bar{z}; \mu) = \frac{1}{2}n_1 z^2 + n_2 z\bar{z} + \frac{1}{2}n_3 \bar{z}^2 + O(|z|^3).$$

For this purpose, let us introduce a near-identity transformation

$$w = z + Q(z, \bar{z}; \mu) \quad (\text{A.2a})$$

with the inverse,

$$z = w - Q(w, \bar{w}; \mu) \quad (\text{A.2b})$$

where,

$$Q(z, \bar{z}; \mu) = \frac{1}{2} q_1 z^2 + q_2 z \bar{z} + \frac{1}{2} q_3 \bar{z}^2.$$

We have from (A.2),

$$\frac{dw}{dt} = \frac{dz}{dt} + (q_1 z + q_2 \bar{z}) \frac{dz}{dt} + (q_2 z + q_3 \bar{z}) \frac{d\bar{z}}{dt}$$

which, on using (A.1) and (A.2), becomes

$$\frac{dw}{dt} = (\alpha - i\beta)w + \frac{1}{2} \hat{n}_1 w^2 + \hat{n}_2 w \bar{w} + \frac{1}{2} \hat{n}_3 \bar{w}^2 + O(|w|^3) \quad (\text{A.3})$$

where,

$$\begin{aligned} \hat{n}_1 &= n_1 + (\alpha - i\beta)q_1, \quad \hat{n}_2 = n_2 + (\alpha + i\beta)q_2, \\ \hat{n}_3 &= n_3 + (\alpha + 3i\beta)q_3. \end{aligned}$$

Now, since $\beta(0) \neq 0$, we may choose q_1, q_2 and q_3 in such a way that

$$\hat{n}_1 = \hat{n}_2 = \hat{n}_3 = 0 \quad (\text{A.4})$$

in a neighborhood of the bifurcation point $\mu = 0$.

Using (A.4), equation (A.3) becomes

$$\frac{dw}{dt} = (\alpha - i\beta)w + M(w, \bar{w}; \mu) \quad (\text{A.5})$$

where,

$$M(w, \bar{w}; \mu) = \frac{1}{3} m_1 w^3 + m_2 w^2 \bar{w} + m_3 w \bar{w}^2 + \frac{1}{3} m_4 \bar{w}^3 + O(|w|^4).$$

In order to reduce equation (A.5) further, let us introduce another near-identity transformation

$$\xi = w + R(w, \bar{w}; \mu) \quad (\text{A.6a})$$

with the inverse

$$w = \xi - R(\xi, \bar{\xi}; \mu) \quad (\text{A.6b})$$

where,

$$R(w, \bar{w}; \mu) = \frac{1}{3} r_1 w^3 + r_2 w^2 \bar{w} + r_3 w \bar{w}^2 + \frac{1}{3} r_4 \bar{w}^3.$$

We have from (A.6),

$$\frac{d\xi}{dt} = \frac{dw}{dt} + (r_1 w^2 + 2r_2 w \bar{w} + r_3 \bar{w}^2) \frac{dw}{dt} + (r_2 w^2 + 2r_3 w \bar{w} + r_4 \bar{w}^2) \frac{d\bar{w}}{dt}$$

which, on using (A.5) and (A.6), becomes

$$\frac{d\xi}{dt} = (\alpha - i\beta)\xi + \frac{1}{3} \hat{m}_1 \xi^3 + \hat{m}_2 \xi^2 \bar{\xi} + \hat{m}_3 \xi \bar{\xi}^2 + \frac{1}{3} \hat{m}_4 \bar{\xi}^3 + O(|\xi|^4) \quad (\text{A.7})$$

where,

$$\begin{aligned} \hat{m}_1 &= m_1 + 2(\alpha - i\beta)r_1, \quad \hat{m}_2 = m_2 + 2\alpha r_2, \\ \hat{m}_3 &= m_3 + 2(\alpha + i\beta)r_3, \quad \hat{m}_4 = m_4 + 2(\alpha + i\beta)r_4. \end{aligned}$$

Now, again since $\beta(0) \neq 0$, we may choose r_1, r_3 and r_4 in such a way that

$$\hat{m}_1 = \hat{m}_3 = \hat{m}_4 = 0 \quad (\text{A.8a})$$

in a neighborhood of the bifurcation point $\mu = 0$. However, r_2 cannot be chosen in any way to make $\hat{m}_2 = 0$ because, $\alpha(0) = 0$. So, let us choose $r_2 = 0$ giving

$$\hat{m}_2 = m_2 = \gamma(\mu) + i\delta(\mu), \text{ say.} \quad (\text{A.8b})$$

Using (A.8), equation (A.7) becomes

$$\frac{d\xi}{dt} = [\alpha(\mu) - i\beta(\mu)]\xi + [\gamma(\mu) + i\delta(\mu)]|\xi|^2 \xi + O(|\xi|^4) \quad (\text{A.9})$$

as advertised in the text.

CHAPTER 3

HAMILTONIAN DYNAMICS

The goal of a physical theory is not only to give a precise mathematical formulation of observed phenomena but also to describe these effects with a minimum of fundamental postulates and in the most unified manner possible. Hamilton's principle, which adopts a variational approach, is, in this sense, more fundamental than the Newtonian formulation.

Variational principles in physics always have had great appeal. The search for such principles is predicated on the belief that nature acts in such a way that certain important quantities are minimized during the course of a physical process. According to Fermat's principle of least time, a light ray always travels from one point to another in a medium by a path that requires the least time of transit. The laws of reflection and refraction then follow as direct consequences of this principle.

Hamilton's principle states that of all the possible paths along which a dynamical system may move from one point to another within a specified time interval, the actual path followed is that which minimizes the time integral of the Lagrangian function for the system. The integral statement embodied in Hamilton's principle is equivalent to the differential statement of mechanics contained in Newton's equations. However, it is possible to make a distinction between these two viewpoints on philosophical grounds. The Newtonian formulation is based on the notion that a certain effect is always traceable to a certain cause. On the other hand, Hamilton's principle associates the motion of a body to the attempt of nature to achieve a certain purpose, viz., to minimize the time integral of the Lagrangian function for the system.

The advantages of the Hamiltonian formulation lie not in its use as a calculational tool, but rather in the deeper insight it affords into the formal structure of mechanics. The symplectic structure of the phase space associated with the constancy of the integral $\oint \mathbf{p} \cdot d\mathbf{q}$ (\mathbf{q} being the position vector and \mathbf{p} the momentum) around any closed loop in phase space is a case in point (the Hamiltonian formulation manifestly preserves phase-space volumes). An immediate consequence of this aspect is the recurrence of almost every bounded orbit in phase space.

3.1. Hamilton's Equations

Consider a system of n degrees of freedom which is described by a Lagrangian L^1 which is a function of the generalized coordinates $q_j, (j = 1, 2, \dots, n)$, the generalized velocities $\dot{q}_j (j = 1, 2, \dots, n)$, and the time t –

$$L = L(q_j, \dot{q}_j, t). \quad (1)$$

Then, the actual motion of the system from a position $q_j^{(1)}$ at time t_1 to a position $q_j^{(2)}$ at time t_2 can be determined from Hamilton's principle of least action which requires that the integral of the Lagrangian function takes the minimum possible value between the initial time t_1 and the final time t_2 for the actual path. More precisely, the actual path in configuration space between two configurations $q_j(t_1)$ and $q_j(t_2)$ at times t_1 and t_2 , respectively, is that which makes the time integral of the Lagrangian function stationary with respect to variations δq_j of the path which vanish at the end points, i.e.,

$$\delta\Phi = \delta \int_{t_1}^{t_2} L(q_j, \dot{q}_j, t) dt = 0. \quad (2)$$

The functional Φ is called Hamilton's principal function (or the action integral) for the path $q(t)$.

Using the techniques of variational calculus, (2) can be expressed as²

¹ Lagrangian of a system is typically the difference between the kinetic energy and the potential energy of the system.

² In order to calculate the first variation of the action functional Φ , one compares the values of Φ that correspond to neighboring paths $q(t)$ anchored on the same end points at $t = t_1$ and t_2 or

$$\delta q(t) = 0 \text{ for } t = t_1 \text{ and } t_2.$$

Thus,

$$\delta\Phi = \int_{t_1}^{t_2} L(q_j + \delta q_j, \dot{q}_j + \delta \dot{q}_j, t) dt - \int_{t_1}^{t_2} L(q_j, \dot{q}_j, t) dt.$$

Expanding the integrand of the first integral to $O(\delta q_i)$ and $O(\delta \dot{q}_i)$, we obtain

$$\delta\Phi = \sum_{j=1}^n \int_{t_1}^{t_2} \left[\frac{\partial L}{\partial q_j} - \frac{d}{dt} \left(\frac{\partial L}{\partial \dot{q}_j} \right) \right] \delta q_j dt = 0, \quad j = 1, 2, \dots, n. \quad (3)$$

Because of the arbitrariness of δq_j between $t = t_1$ and $t = t_2$ equation (3) leads to Lagrange's equations

$$\frac{\partial L}{\partial q_j} - \frac{d}{dt} \left(\frac{\partial L}{\partial \dot{q}_j} \right) = 0, \quad j = 1, 2, \dots, n. \quad (4)$$

If we introduce generalized momenta according to

$$p_j = \frac{\partial L}{\partial \dot{q}_j}, \quad j = 1, 2, \dots, n. \quad (5)$$

Lagrange's equations (4) become

$$\dot{p}_j = \frac{\partial L}{\partial q_j}, \quad j = 1, 2, \dots, n. \quad (6)$$

$$\delta\Phi = \sum_{j=1}^n \int_{t_1}^{t_2} \left(\frac{\partial L}{\partial q_j} \delta q_j + \frac{\partial L}{\partial \dot{q}_j} \delta \dot{q}_j \right) dt.$$

Assuming that $\delta \dot{q}_j = \frac{d}{dt}(\delta q_j)$, and integrating the second term by parts, one obtains

$$\delta\Phi = \sum_{j=1}^n \left\{ \left[\frac{\partial L}{\partial \dot{q}_j} \delta q_j \right] \Big|_{t=t_1}^{t=t_2} + \int_{t_1}^{t_2} \left[\frac{\partial L}{\partial q_j} - \frac{d}{dt} \left(\frac{\partial L}{\partial \dot{q}_j} \right) \right] \delta q_j dt \right\}$$

or

$$\delta\Phi = \sum_{j=1}^n \int_{t_1}^{t_2} \left[\frac{\partial L}{\partial q_j} - \frac{d}{dt} \left(\frac{\partial L}{\partial \dot{q}_j} \right) \right] \delta q_j dt.$$

EXAMPLE 1

Show that two Lagrangians, L and \hat{L} , differing only by the total time derivative of a function of q and t , describe the same motion.

If we have

$$\hat{L}(q, \dot{q}, t) = L(q, \dot{q}, t) + \frac{d}{dt} f(q, t) = L(q, \dot{q}, t) + \frac{\partial f}{\partial q} \dot{q} + \frac{\partial f}{\partial t} \quad (7)$$

this will lead to

$$\frac{\partial \hat{L}}{\partial \dot{q}} = \frac{\partial L}{\partial \dot{q}} + \frac{\partial f}{\partial q}, \quad \frac{\partial \hat{L}}{\partial q} = \frac{\partial L}{\partial q} + \frac{d}{dt} \left(\frac{\partial f}{\partial q} \right). \quad (8)$$

(8) then gives

$$\frac{d}{dt} \left(\frac{\partial \hat{L}}{\partial \dot{q}} \right) - \frac{\partial \hat{L}}{\partial q} = \frac{d}{dt} \left(\frac{\partial L}{\partial \dot{q}} \right) - \frac{\partial L}{\partial q} = 0. \quad (9)$$

Thus, the Lagrangian, for a given motion, can be determined uniquely to only within the additive total time derivative of a scalar function f since the latter will not contribute to the variation of the time integral of the Lagrangian.

Therefore, if $q(t)$ satisfies the equations of motion obtained from \hat{L} it also satisfies those obtained from L .

Note, however, these two Lagrangians define different momenta:

$$\bar{p} = \frac{\partial \hat{L}}{\partial \dot{q}} = \frac{\partial L}{\partial \dot{q}} + \frac{\partial f}{\partial q} = p + \frac{\partial f}{\partial q}. \quad (10)$$

Let us now use q_j, p_j, t as the independent variables (q_j and p_j are called the conjugate variables) rather than q_j, \dot{q}_j, t . Noting that

$$\begin{aligned}
\delta L &= \sum_j \frac{\partial L}{\partial q_j} \delta q_j + \sum_j \frac{\partial L}{\partial \dot{q}_j} \delta \dot{q}_j + \frac{\partial L}{\partial t} \delta t \\
&= \sum_j \dot{p}_j \delta q_j + \sum_j p_j \delta \dot{q}_j + \frac{\partial L}{\partial t} \delta t \\
&= \delta \left(\sum_j p_j \dot{q}_j \right) + \sum_j \dot{p}_j \delta q_j - \sum_j \dot{q}_j \delta p_j + \frac{\partial L}{\partial t} \delta t.
\end{aligned} \tag{11}$$

We have

$$\delta \left(\sum_j p_j \dot{q}_j - L \right) = - \sum_j \dot{p}_j \delta q_j + \sum_j \dot{q}_j \delta p_j - \frac{\partial L}{\partial t} \delta t \tag{12}$$

which describes a Legendre transformation from L to the Hamiltonian H^3 ,

$$H = H(q_j, p_j, t) = \sum_j p_j \dot{q}_j - L. \tag{13}$$

We have from (13)

$$\delta H = \sum_j \frac{\partial H}{\partial q_j} \delta q_j + \sum_j \frac{\partial H}{\partial p_j} \delta p_j + \frac{\partial H}{\partial t} \delta t \tag{14}$$

which, on comparing with equation (12), leads to Hamilton's equations –

$$\left. \begin{aligned}
\dot{q}_j &= \frac{\partial H}{\partial p_j}, \\
\dot{p}_j &= - \frac{\partial H}{\partial q_j}, \\
\frac{\partial H}{\partial t} &= - \frac{\partial L}{\partial t},
\end{aligned} \right\}_{j=1,2,\dots,n}. \tag{15a}$$

³ H is typically the energy of the system.

The relation between the partial derivatives of the conjugate variables, described by equation (15), is called symplectic. Observe that if a particular coordinate is cyclic, i.e., it does not appear explicitly in H , the corresponding momentum is a constant of the motion. Similarly, if L does not depend on t explicitly, H is a constant of motion and we have conservation of energy. (In general, the deduction of H as a constant of the motion and the identification of H as the total energy are two separate matters.) This provides a fundamental principle underlying the structure of mechanics; which is known as Noether's Theorem: "*invariance under translation in time and space leads to conservation of energy H and momenta (p_j) , respectively.*"

3.2. Phase Space

For each degree of freedom of the system, note that there are now two quantities, q_j and p_j , that assume independent roles. The state of the system is then given by a representative point in a space of $2n$ -dimensions, called the phase space, with coordinates $(q_1, q_2, \dots, q_n, p_1, p_2, \dots, p_n)$. As the state of the system changes, the q_j and the p_j change in physical space with t , and the representative point moves in this $2n$ -dimensional phase space, which is the set of all states of the system. The motion of the system can then be described by the trajectory of the representative point in the phase space. In this space, the equations representing the motion of the representative point are

$$\dot{p}_j = -\frac{\partial H}{\partial q_j}, \quad \dot{q}_j = \frac{\partial H}{\partial p_j}; \quad j = 1, 2, \dots, n. \quad (15b)$$

EXAMPLE 2

Consider a simple pendulum, for which we have for small angular deflections, the Lagrangian

$$L = \frac{1}{2}ml^2\dot{\theta}^2 - \frac{1}{2}mgl\theta^2 \quad (16)$$

where l is the length of the pendulum.

Since L does not depend explicitly on t , we have for the Hamiltonian,

$$H = \frac{p_\theta^2}{2ml^2} + \frac{\theta^2}{2/mgl} = \text{const} = E \quad (17)$$

where $p_\theta = ml^2\dot{\theta}$ (p_θ is not the θ -component of p , it is the momentum conjugate to θ). For a given E , fixed by the initial conditions, the representative point P is restricted to move in the two-dimensional (θ, p_θ) phase space on an ellipse (Figure 3.1).

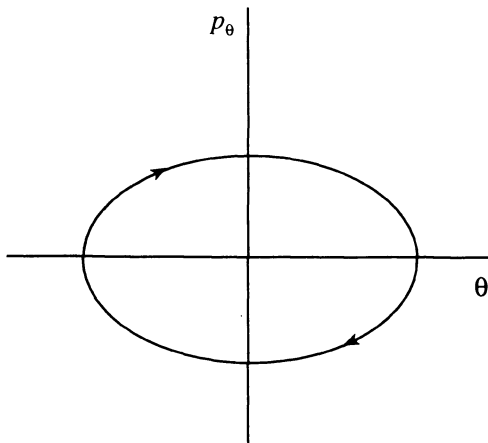


Figure 3.1. Solution curve for a small oscillations of a simple pendulum.

Suppose, now that a large number of identical one-dimensional systems, similar to the one considered in the above example, of different energies E are present. Each system has a representative point in the pq -plane, tracing out a curve, so there are several trajectories for different values of E .

Consider an area element $dpdq$ at a given point (p, q) in the pq -plane; within this area element $dpdq$, there will be many representative points at any instant. Suppose the density of such points is $\rho(p, q, t)$. The totality of such points move in much the same way as an element of fluid flowing over the plane. Consider a fixed element of area as shown in Figure 3.2. The number of representative points moving per unit time into $dpdq$ on its left edge will be

$$\rho \dot{q} dp.$$

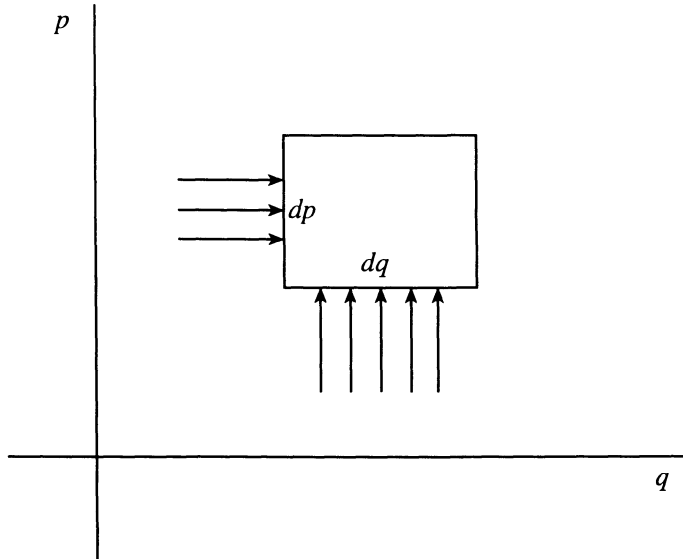


Figure 3.2. Flow through an element in the phase space.

The number of points moving out of $dpdq$ through its right edge will be

$$\left[\rho \dot{q} + \frac{\partial}{\partial q} (\rho \dot{q}) dq \right] dp.$$

Hence, the net increase in the number of representative points in $dpdq$ due to flow in the q -direction will be

$$-\frac{\partial}{\partial q} (\rho \dot{q}) dpdq.$$

In a similar way, the net gain due to flow in the p -direction will be

$$-\frac{\partial}{\partial p} (\rho \dot{p}) dpdq.$$

The total increase per unit time in density in $dpdq$ is, therefore,

$$-\left[\frac{\partial}{\partial p}(\rho \dot{p}) + \frac{\partial}{\partial q}(\rho \dot{q}) \right] dp dq$$

which is equal to

$$\frac{\partial \rho}{\partial t} dp dq.$$

Hence, we have the conservation equation

$$\frac{\partial \rho}{\partial t} + \left[\frac{\partial}{\partial p}(\rho \dot{p}) + \frac{\partial}{\partial q}(\rho \dot{q}) \right] = 0 \quad (18)a$$

or

$$\frac{\partial \rho}{\partial t} + \left[\dot{p} \frac{\partial \rho}{\partial p} + \dot{q} \frac{\partial \rho}{\partial q} \right] + \rho \left[\frac{\partial \dot{p}}{\partial p} + \frac{\partial \dot{q}}{\partial q} \right] = 0. \quad (18)b$$

Using Hamilton's equations (15), equation (18)b becomes

$$\frac{\partial \rho}{\partial t} + \dot{p} \frac{\partial \rho}{\partial p} + \dot{q} \frac{\partial \rho}{\partial q} = 0. \quad (19)$$

If $\rho = \rho(p, q, t)$, then the rate of change of ρ as seen by an observer moving with a representative point, from equation (19), is

$$\frac{d\rho}{dt} = \frac{\partial \rho}{\partial t} + \dot{p} \frac{\partial \rho}{\partial p} + \dot{q} \frac{\partial \rho}{\partial q} = 0. \quad (20)$$

This leads to Liouville's Theorem: "*The density of representative points remains constant as one moves along with these points in the phase space.*"

The result deduced above for a system with one degree of freedom may be generalized readily for systems with n degrees of freedom:

$$\frac{\partial \rho}{\partial t} + \sum_{j=1}^n \left(\frac{\partial \rho}{\partial p_j} \dot{p}_j + \frac{\partial \rho}{\partial q_j} \dot{q}_j \right) = 0. \quad \text{4} \quad (21)$$

Let us consider now the evolution of phase-space volumes during the motion of a system of n degrees of freedom. Consider a volume V enclosed by some closed surface S in the phase space, and let the surface S evolve by having each point on it follow a trajectory generated by Hamilton's equations, written in the form

$$\frac{dx_i}{dt} = f_i(x_1, x_2, \dots, x_{2n}), \quad i = 1, 2, \dots, 2n. \quad (22)$$

The rate of change of V in this process is given by

$$\frac{dV}{dt} = \iint_S \sum_{i=1}^{2n} \frac{dx_i}{dt} \hat{n}_i \prod_{j=1, j \neq i}^{2n} dx_j \quad (23)$$

where \hat{n} is the unit normal to S . Using the divergence Theorem, (23) becomes

$$\frac{dV}{dt} = \iiint_V \sum_{i=1}^{2n} \frac{\partial f_i}{\partial x_i} \prod_{j=1}^{2n} dx_j. \quad (24)$$

EXAMPLE 3

For a conservative Hamiltonian system, we have

$$\sum_{i=1}^{2n} \frac{\partial f_i}{\partial x_i} = \sum_{i=1}^n \left(\frac{\partial \dot{q}_i}{\partial q_i} + \frac{\partial \dot{p}_i}{\partial p_i} \right) = 0 \quad (25)$$

so that (24) gives

⁴ The Liouville equation for many interacting particles contains too much dynamical information to be of practical interest. Therefore, one typically seeks a reduced macroscopic description of the detailed underlying microscopic dynamics.

$$\frac{dV}{dt} = 0 \quad (26)$$

implying that the phase-space volumes are preserved in time.

EXAMPLE 4

Consider a dissipative system given by

$$\ddot{x} + k\dot{x} + \omega^2 x = 0, \quad k > 0 \quad (27)$$

which is equivalent to

$$\left. \begin{aligned} \dot{x}_1 &= x_2 \\ \dot{x}_2 &= -kx_2 - \omega^2 x_1 \end{aligned} \right\}. \quad (28)$$

We have, here,

$$\sum_{i=1}^2 \frac{\partial f_i}{\partial x_i} = \frac{\partial \dot{x}_1}{\partial x_1} + \frac{\partial \dot{x}_2}{\partial x_2} = -k. \quad (29)$$

Using (29), (24) gives

$$\frac{dV}{dt} = -kV \quad (30)$$

from which

$$V(t) = V(0)e^{-kt} \quad (31)$$

implying that the phase-space volumes now shrink exponentially in time.

Thus, for a conservative Hamiltonian system, the quantity $\prod_{i=1}^n dp_i dq_i$ is the

measure on phase space conserved by the Hamiltonian phase flow. This aspect immediately leads to the recurrence of almost every bound orbit in phase space.

THEOREM 3.1 (Poincaré's Recurrence Theorem):

Let T be an area-preserving, continuous isomorphism defined by a Hamiltonian phase flow $(p(t), q(t))$ within a bounded region D . Then, in any neighborhood W which lies in D , there exists a trajectory through a point (p, q) in W which returns to W , i.e., $T^{[s]}(p, q)$ (which denotes T iterated s times) is in W for some integer $s > 0$. Further, this recurrence occurs infinitely often⁵.

Proof: Under the isomorphism T , W is mapped successively onto (see Figure 3.3)

$$T(W), T^{[2]}(W), \dots$$

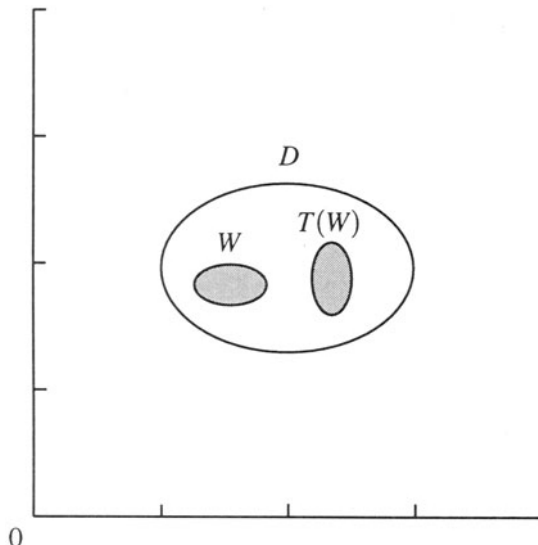


Figure 3.3. Mapping of an area element W by the isomorphism T .

All of these images have the same area and all lie in a bounded region D . Consequently, the images cannot be all mutually disjoint and must have nonzero intersections since D

⁵ Alternatively, one may define a point (p, q) to be a wandering point of the map T if there exists a neighborhood W of (p, q) and a number N for which $(T^{[s]}W) \cap W = \emptyset$ for all $s > N$, otherwise (p, q) is defined to be a non-wandering point. Poincaré's Recurrence Theorem may then be restated as follows: For a Hamiltonian system with bounded motion, all points are non-wandering.

is bounded (otherwise, D would have an infinite area). Thus, there exist integers $k, \ell \geq 0$ with $k > \ell$ such that the intersection of $T^{[k]}(W)$ with $T^{[\ell]}(W)$ is not empty. Since T is an invertible map, this implies that the intersection of $T^{[s]}(W)$ and W is not empty, with $s = k - \ell$. Therefore, there exists a trajectory through a point (p, q) in W which returns to W . Repetition of this argument applied to the intersection of $T^{[s]}(W)$ and W shows that this recurrence occurs infinitely often.

3.3. Canonical Transformations

Hamilton's principle has the advantage of being independent of the coordinate system used to describe the system, but has the apparent disadvantage of referring to the state of the system at two distinct times rather than at a single time. However, the latter feature permits describing the motion of a dynamic system as the development in time of a canonical transformation (which therefore preserves (2)) generated by the Hamiltonian. On the other hand, canonical transformations can be of practical use in simplifying the integration of Hamilton's equations.

Let $L(q_i, \dot{q}_i, t)$ and $\bar{L}(\bar{q}_i, \dot{\bar{q}}_i, t)$ be two Lagrangian functions involving the same number of degrees of freedom. Let q_i and \bar{q}_i be related so that a path in the q_i -space for which the time integral of L is stationary corresponds to a path in \bar{q}_i -space for which the time integral of \bar{L} is stationary. Then these two Lagrangians provide two different descriptions of the same system. This implies that

$$\bar{L}(\bar{q}_i, \dot{\bar{q}}_i, t) = L(q_i, \dot{q}_i, t) - \frac{d}{dt} \psi(q_i, \bar{q}_i, t) \quad (32)$$

because, as we saw in EXAMPLE 1, L is unique to within an additive total derivative of a scalar function ψ . Thus, we have from (32),

$$\delta\bar{L}(\bar{q}_i, \dot{\bar{q}}_i, t) = \delta L(q_i, \dot{q}_i, t) - \frac{d}{dt} \delta\psi(q_i, \bar{q}_i, t)$$

or

$$\begin{aligned}
& \sum_i \frac{\partial \bar{L}}{\partial \bar{q}_i} \delta \bar{q}_i + \sum_i \bar{p}_i \delta \dot{\bar{q}}_i + \frac{\partial \bar{L}}{\partial t} \delta t \\
&= \sum_i \frac{\partial L}{\partial q_i} \delta q_i + \sum_i p_i \delta \dot{q}_i + \frac{\partial L}{\partial t} \delta t + \\
& - \frac{d}{dt} \left(\sum_i \frac{\partial \psi}{\partial q_i} \delta q_i + \sum_i \frac{\partial \psi}{\partial \bar{q}_i} \delta \bar{q}_i + \frac{\partial \psi}{\partial t} \delta t \right).
\end{aligned} \tag{33}$$

Choosing

$$p_i = \frac{\partial \psi}{\partial q_i}, \quad \bar{p}_i = -\frac{\partial \psi}{\partial \bar{q}_i}; \quad i = 1, 2, \dots, n, \tag{34}$$

we find, from (33) that the Lagrange equations remain form invariant under a group of canonical transformations generated by the function $\psi(q_i, \bar{q}_i, t)$.⁶

Using (32) and (34), the new Hamiltonian is then given by

$$\begin{aligned}
\bar{H} &= \sum_i \bar{p}_i \dot{\bar{q}}_i - \bar{L} = \sum_i p_i \dot{q}_i - L + \frac{\partial \psi}{\partial t} \\
&= H(q_i, p_i, t) + \frac{\partial}{\partial t} \psi(q_i, \bar{q}_i, t).
\end{aligned} \tag{35}$$

ψ is called the generating function, and we have from (34) and (35),

$$d\psi = \sum_i p_i dq_i - \sum_i \bar{p}_i d\bar{q}_i - (H - \bar{H}) dt. \tag{36}$$

The canonical transformations may be used in a practical way to make the integration of Hamilton's equations as simple as possible. The optimal case is the one in which all the \bar{q}_i 's are cyclic so that

$$\bar{H} = \bar{H}(\bar{p}_i, t). \tag{37}$$

Hamilton's equations can then be readily integrated, since

⁶ Note that the coordinates and momenta do not remain necessarily distinct under such transformations.

$$\left. \begin{aligned} \dot{\bar{p}}_i &= -\frac{\partial \bar{H}}{\partial \bar{q}_i} = 0 \\ \dot{\bar{q}}_i &= \frac{\partial \bar{H}}{\partial \bar{p}_i} = f_i(\bar{p}_1, \bar{p}_2, \dots, \bar{p}_n), \text{ say} \end{aligned} \right\} \quad (38)$$

from which

$$\left. \begin{aligned} \bar{p}_i &= \text{const}, \\ \bar{q}_i &= f_i t + \delta_i \end{aligned} \right\} i = 1, 2, \dots, n. \quad (39)$$

EXAMPLE 5

Consider a simple harmonic oscillator, given by

$$H = \frac{1}{2m} (p^2 + m^2 \omega^2 q^2). \quad (40)$$

Let us make a canonical transformation through the generating function

$$\psi(q, \bar{q}) = \frac{1}{2} m \omega q^2 \cot \bar{q} \quad (41)$$

(which will be systematically derived by the Hamilton-Jacobi method in EXAMPLE 10) so that we have, according to (34),

$$\left. \begin{aligned} p &= \frac{\partial \psi}{\partial q} = m \omega q \cot \bar{q} \\ \bar{p} &= -\frac{\partial \psi}{\partial \bar{q}} = \frac{m \omega q^2}{2} \operatorname{cosec}^2 \bar{q} \end{aligned} \right\} \quad (42)$$

from which,

$$\left. \begin{aligned} q &= \sqrt{\frac{2\bar{p}}{m\omega}} \sin \bar{q} \\ p &= \sqrt{2m\bar{p}\omega} \cos \bar{q} \end{aligned} \right\}. \quad (43)$$

Note that the mixup of the momenta and coordinates in (43) simply highlights the absence of independent status of generalized coordinates and momenta.

Thus, the new Hamiltonian \bar{H} is given by

$$\bar{H} = H + \frac{\partial \psi}{\partial t} = \omega \bar{p}. \quad (44)$$

Observe that the canonical transformation (41) has accomplished integration of Hamilton's equations by transforming H to \bar{H} for which \bar{q} is a cyclic coordinate so that \bar{p} is a constant. Thus,

$$\bar{p} = \frac{E}{\omega} \text{ and } \bar{q} = \omega(t - t_o) \quad (45)$$

which, from (43), give the well known solution of the original problem,

$$\left. \begin{aligned} q &= \frac{\sqrt{2mE}}{m\omega} \sin \omega(t - t_o) \\ p &= \sqrt{2mE} \cos \omega(t - t_o) \end{aligned} \right\}. \quad (46)$$

EXAMPLE 6

Show that a transformation generated by $\psi(q, \bar{q})$ is area-preserving.

The Jacobian of the transformation is given by

$$\begin{aligned} \frac{\partial(\bar{q}, \bar{p})}{\partial(q, p)} &= \frac{\partial(\bar{q}, \bar{p})}{\partial(q, \bar{q})} \frac{\partial(q, \bar{q})}{\partial(q, p)} = \frac{\partial(\bar{q}, \bar{p})}{\partial(q, \bar{q})} \left[\frac{\partial(q, p)}{\partial(q, \bar{q})} \right]^{-1} \\ &= -\frac{\partial \bar{p}}{\partial q} \left| \left[\frac{\partial p}{\partial \bar{q}} \right]_q \right|^{-1} = \frac{\partial^2 \psi}{\partial q \partial \bar{q}} \left[\frac{\partial^2 \psi}{\partial \bar{q} \partial q} \right]^{-1} = 1 \end{aligned} \quad (47)$$

where we have used (34). Therefore, the transformation generated by $\psi(q, \bar{q})$ is area-preserving.

It may be noted that this result also follows from

$$\oint_C d\psi = \oint_C \left(\frac{\partial \psi}{\partial q} dq + \frac{\partial \psi}{\partial \bar{q}} d\bar{q} \right) = \oint_C (pdq - \bar{p}d\bar{q}) = 0 \quad (48)$$

from which, on using Green's Theorem, we have

$$\iint_R dpdq = \iint_R d\bar{p}d\bar{q} \quad (49)$$

where R is the area enclosed by a curve C in the phase plane.

Now, corresponding to variations δq_i in q_i , and Δt in t , recall that one has for the change in action Φ (see equation (2)) along the path of motion

$$\delta\Phi = \int_{t_1}^t \sum_i \left[\frac{\partial L}{\partial q_i} - \frac{d}{dt} \left(\frac{\partial L}{\partial \dot{q}_i} \right) \right] \delta q_i dt + \left[\sum_i \frac{\partial L}{\partial \dot{q}_i} \delta q_i + L \Delta t \right]_{t_1}^t. \quad (50)$$

Noting,

$$\Delta q_i = \delta q_i + \dot{q}_i \Delta t. \quad (51)$$

and using equation (4), (50) becomes

$$\delta\Phi = \left[\left(-\sum_i \frac{\partial L}{\partial \dot{q}_i} \dot{q}_i + L \right) \Delta t + \sum_i \frac{\partial L}{\partial \dot{q}_i} \Delta q_i \right]_{t_1}^t = \left[-H \Delta t + \sum_i p_i \Delta q_i \right]_{t_1}^t. \quad (52)$$

Writing H , p_i and q_j for the values of these quantities at time t , and \bar{H}, \bar{p}_j and \bar{q}_j for their values at $t = t_1$, and letting $\Delta q_j = dq_j, \Delta \bar{q}_j = d\bar{q}_j$ and $(\Delta t)_{t=t_1} = (\Delta t)_{t=t_2} = dt$, we have from (52)

$$d\Phi = \sum_j p_j dq_j - \sum_j \bar{p}_j d\bar{q}_j - (H - \bar{H})dt. \quad (53)$$

On comparing (53) with (36), we see that the principal function between time t_1 and t is the generating function of the canonical transformation from the initial values of the coordinates and momenta to the values of the coordinates and momenta at time t . Therefore, the state of the system at any time may be thought of as having been obtained from the initial state by the canonical transformation generated by the principal function up to that time. In other words, the Hamiltonian flows are one-parameter (namely, the time t) families of canonical transformations.

Other Generating Functions:

One may find other types of generating functions by making Legendre transformations. Thus, letting

$$\psi(q_j, \bar{q}_j, t) = \psi'(p_j, \bar{q}_j, t) + \sum_j p_j q_j \quad (54)$$

and using (36), we have,

$$d\psi = d\psi' + \sum_j (p_j dq_j + q_j dp_j) = \sum_j p_j dq_j - \sum_j \bar{p}_j d\bar{q}_j + (\bar{H} - H)dt. \quad (55)$$

(55) shows that $\psi'(p_j, \bar{q}_j, t)$ generates a canonical transformation according to

$$\left. \begin{aligned} q_j &= -\frac{\partial \psi'(p_j, \bar{q}_j, t)}{\partial p_j}, \bar{p}_j = -\frac{\partial \psi'(p_j, \bar{q}_j, t)}{\partial \bar{q}_j} \\ \bar{H}(\bar{q}_j, \bar{p}_j, t) &= H(q_j, p_j, t) + \frac{\partial \psi'(p_j, \bar{q}_j, t)}{\partial t} \end{aligned} \right\}. \quad (56)$$

Here (and also in the following), the primes on the generating function do not denote any differentiation.

Similarly, letting

$$\psi(q_j, \bar{q}_j, t) = \psi''(p_j, \bar{p}_j, t) + \sum_j (p_j q_j - \bar{p}_j \bar{q}_j) \quad (57)$$

we find that $\psi''(p_j, \bar{p}_j, t)$ generates a canonical transformation according to

$$\left. \begin{aligned} q_j &= -\frac{\partial \psi''(p_j, \bar{p}_j, t)}{\partial p_j}, \quad \bar{q}_j = \frac{\partial \psi''(p_j, \bar{p}_j, t)}{\partial \bar{p}_j} \\ \bar{H}(\bar{q}_j, \bar{p}_j, t) &= H(q_j, p_j, t) + \frac{\partial \psi''(p_j, \bar{p}_j, t)}{\partial t} \end{aligned} \right\}. \quad (58)$$

Finally, letting

$$\psi(q_j, \bar{q}_j, t) = \psi'''(q_j, \bar{p}_j, t) - \sum_j \bar{p}_j \bar{q}_j \quad (59)$$

we find that $\psi'''(q_j, \bar{p}_j, t)$ generates a canonical transformation according to

$$\left. \begin{aligned} p_j &= \frac{\partial \psi'''(q_j, \bar{p}_j, t)}{\partial q_j}, \quad \bar{q}_j = \frac{\partial \psi'''(q_j, \bar{p}_j, t)}{\partial \bar{p}_j} \\ \bar{H}(\bar{q}_j, \bar{p}_j, t) &= H(q_j, p_j, t) + \frac{\partial \psi'''(q_j, \bar{p}_j, t)}{\partial t} \end{aligned} \right\}. \quad (60)$$

EXAMPLE 7

The transformation from a fixed to a moving reference frame is given by

$$\bar{q} = q - a(t). \quad (61)$$

$a(t)$ being the distance between the origins at time t . If the Hamiltonian in the fixed reference frame is $\frac{p^2}{2m} + V(q)$ let us find the Hamiltonian, and the equations of motion in the moving reference frame (Percival and Richards (1982)).

A generating function for the transformation (61) is

$$\psi'''(q, \bar{p}, t) = \bar{p}[q - a(t)] \quad (62)$$

and so,

$$p = \frac{\partial \psi'''}{\partial q} = \bar{p}. \quad (63)$$

The transformed Hamiltonian is then

$$\bar{H}(\bar{q}, \bar{p}, t) = \frac{\bar{p}^2}{2m} + V(\bar{q} + a) - \bar{p}\dot{a} \quad (64)$$

and the equations of motion in the moving reference frame are

$$\left. \begin{aligned} \dot{\bar{q}} &= \frac{\partial \bar{H}}{\partial \bar{p}} = \frac{\bar{p}}{m} - \dot{a} \\ \dot{\bar{p}} &= -\frac{\partial \bar{H}}{\partial \bar{q}} = -\frac{\partial V}{\partial \bar{q}}(\bar{q} + a) \end{aligned} \right\} \quad (65)$$

from which, we have

$$m\ddot{\bar{q}} = -\frac{\partial V}{\partial \bar{q}}(\bar{q} + a) - m\ddot{a}. \quad (66)$$

The term $m\ddot{a}$ is the inertial force due to the acceleration of the moving reference frame.

3.4. The Hamilton-Jacobi Equation

Let us choose a canonical transformation so that $\bar{H} = \text{constant}$. Then, we may take $\bar{H} = 0$, which trivially integrates the canonical equations to give $\bar{p}_i = \text{constant}$ and $\bar{q}_i = \text{constant}$.

The Hamilton-Jacobi equation for the generating function ψ''' is

$$\frac{\partial \psi'''}{\partial t} + H\left(q_j, \frac{\partial \psi'''}{\partial q_j}, t\right) = 0; \quad j = 1, \dots, n. \quad (67)$$

Suppose there exists a solution of this equation of the form

$$\psi''' = S'''(q_j, \alpha_k, t); \quad j = 1, \dots, n \text{ and } k = 1, \dots, n+1, \quad (68)$$

where α_k 's are the constants of integration. Now, if S''' is a solution of the Hamilton-Jacobi equation so is $S''' + \alpha$, for a constant α . Thus, one of these α_k 's is irrelevant. So, (68) becomes

$$\psi''' = S'''(q_j, \alpha_j, t); \quad j = 1, \dots, n. \quad (69)$$

Since $\bar{p}_j = \text{constant}$, we may take

$$\bar{p}_j = \alpha_j; \quad j = 1, \dots, n. \quad (70)$$

We have, then,

$$p_i = \frac{\partial S'''(q_j, \alpha_j, t)}{\partial q_i} \quad (71a)$$

$$\bar{q}_i = \frac{\partial S'''(q_j, \alpha_j, t)}{\partial \alpha_i} = \beta_i = \text{constant}. \quad (71b)$$

(71b) may be inverted to give

$$q_j = q_j(\alpha_j, \beta_j, t). \quad (72)$$

Using (72), we then obtain from (71a)

$$p_i = p_i(\alpha_j, \beta_j, t) \quad (73)$$

(72) and (73) give the complete solution of the problem.

In order to see the physical significance of S''' , noting that $\bar{p}_i = \text{constant}$, we have

$$\frac{dS'''}{dt} = \sum_i \frac{\partial S'''}{\partial q_i} \dot{q}_i + \frac{\partial S'''}{\partial t} = \sum_i p_i \dot{q}_i - H = L \quad (74)$$

so that

$$S''' = \int L dt + \text{constant} . \quad (75)$$

Hence, S''' is simply the principal function! So, we see again that the principal function is the generator of a canonical transformation to constant coordinates and momenta.

In applying the Hamilton-Jacobi method to integrate the equations of motion, one uses the technique of separating the variables whereby one variable is separated at a time and a constant of integration appears with each separation. Indeed, the Hamilton-Jacobi equation for an n -degree of freedom system can be solved only if it is separable; i.e., the generating function can be written as a sum of n terms - each depending on only one coordinate.

EXAMPLE 8

Consider a one-dimensional force-free motion of a particle of mass m . We have

$$H = \frac{p^2}{2m} . \quad (76)$$

Since $q = x$ is a cyclic variable, $p = \text{constant} = \alpha$, say. The Hamilton-Jacobi equation for this system is

$$\frac{1}{2m} \left(\frac{\partial S'''}{\partial x} \right)^2 + \left(\frac{\partial S'''}{\partial t} \right) = 0 \quad (77)$$

where $S''' = S'''(x, \alpha)$. Equation (77) has the separable solution -

$$S''' = \alpha x - \frac{\alpha^2 t}{2m} . \quad (78)$$

The new constant coordinate β is then given by

$$\beta = \frac{\partial S'''}{\partial \alpha} = x - \frac{\alpha t}{m} \quad (79)$$

from which, we obtain the well known solution for the force-free motion:

$$x = \frac{\alpha t}{m} + \beta. \quad (80)$$

EXAMPLE 9

Consider the problem of a simple harmonic oscillator,

$$H = \frac{1}{2m} \left(p^2 + m^2 \omega^2 q^2 \right) = E. \quad (81)$$

The Hamilton-Jacobi equation for this problem is

$$\frac{1}{2m} \left[\left(\frac{\partial S'''}{\partial q} \right)^2 + m^2 \omega^2 q^2 \right] + \frac{\partial S'''}{\partial t} = 0. \quad (82)$$

Equation (82) admits a separable solution –

$$S'''(q, \alpha, t) = W(q, \alpha) - \alpha t \quad (83)$$

where α is a constant of integration, which, from the Hamilton-Jacobi equation

$$\frac{\partial S'''}{\partial t} + H = 0 \quad (84)$$

can be identified with the total energy E . The solution of equation (82) then reduces to quadratures. We have for $W(q, \alpha)$,

$$\frac{1}{2m} \left[\left(\frac{\partial W}{\partial q} \right)^2 + m^2 \omega^2 q^2 \right] = \alpha \quad (85)$$

from which,

$$W = \sqrt{2m\alpha} \int \sqrt{1 - \frac{m\omega^2 q^2}{2\alpha}} dq. \quad (86)$$

Using (86), (83) gives

$$S''' = \sqrt{2m\alpha} \int \sqrt{1 - \frac{m\omega^2 q^2}{2\alpha}} dq - \alpha t. \quad (87)$$

Using (87), we have

$$\beta = \frac{\partial S'''}{\partial \alpha} = \sqrt{\frac{m}{2\alpha}} \int \frac{dq}{\sqrt{1 - \frac{m\omega^2 q^2}{2\alpha}}} - t \quad (88)$$

from which,

$$\beta = \frac{1}{\omega} \sin^{-1} \sqrt{\frac{m\omega^2}{2\alpha}} q - t. \quad (89)$$

(89) can be inverted to give

$$q = \sqrt{\frac{2\alpha}{m\omega^2}} \sin \omega(t + \beta). \quad (90)$$

Next,

$$p = \frac{\partial S'''}{\partial q} = \frac{\partial W}{\partial q} = \sqrt{2m\alpha - m^2\omega^2 q^2} = \sqrt{2m\alpha} \cos \omega(t + \beta). \quad (91)$$

If, on the other hand, H is not an explicit function of t , then

$$H(q_i, p_i) = \text{constant} = \alpha_1, \text{ say.} \quad (92)$$

We now seek a canonical transformation generated by $\psi''' = W(q_i, \alpha_i)$ such that all the new momenta \bar{p}_i are constants, say α_i . The new Hamiltonian \bar{H} will then be equal to H or α_1 and will be cyclic in all the new coordinates \bar{q}_i . The new equations of motion are

$$\begin{aligned}\dot{\bar{q}}_i &= \frac{\partial \bar{H}}{\partial \bar{p}_i} = \frac{\partial \bar{H}}{\partial \alpha_i} = \begin{cases} 1, & i = 1 \\ 0, & i \neq 1 \end{cases} \\ \dot{\bar{p}}_i &= -\frac{\partial \bar{H}}{\partial \bar{q}_i} = 0; \quad i = 1, \dots, n\end{aligned}\quad (93)$$

The generating function $W(q_i, \alpha_i)$ produces the following transformation:

$$p_i = \frac{\partial W}{\partial q_i}, \quad \bar{q}_i = \frac{\partial W}{\partial \bar{p}_i} = \frac{\partial W}{\partial \alpha_i} \quad (94)$$

and satisfies the following equation:

$$H\left(q_i, \frac{\partial W}{\partial q_i}\right) = \alpha_1. \quad (95)$$

α_1 is called an isolating integral (Whittaker, 1965) since it isolates one degrees of freedom from the other $(n-1)$ degrees of freedom.

In order to see the physical significance of W , note that

$$\frac{dW}{dt} = \sum_i \frac{\partial W}{\partial q_i} \dot{q}_i = \sum_i p_i \dot{q}_i \quad (96)$$

so that

$$W = \sum_i \int p_i \dot{q}_i dt = \sum_i \int p_i dq_i \quad (97)$$

which is simply the action integral!

3.5. Action-Angle Variables

In cases where the motion is periodic, one may be interested in some average characteristics of the motion rather than the details of the motion. Toward this objective, one modifies the Hamilton-Jacobi approach slightly so that the integration constants α_i are not chosen to be the new momenta, but are used to define a set of n constants called action variables J_i .

Consider, for the sake of illustration, a system with one degree of freedom described by a Hamiltonian $H = H(q, \bar{p})$. Apply a canonical transformation generated by $S'''(q, \bar{p})$ so that

$$p = \frac{\partial S'''}{\partial q}, \quad \bar{q} = \frac{\partial S'''}{\partial \bar{p}}, \quad \bar{H} = H. \quad (98)$$

Hamilton's equations in the new coordinates are then

$$\dot{\bar{p}} = -\frac{\partial \bar{H}}{\partial \bar{q}}, \quad \dot{\bar{q}} = \frac{\partial \bar{H}}{\partial \bar{p}}. \quad (99)$$

Let $\bar{p} = \text{constant} = J$, say. Then $\bar{q} = \theta$ is a cyclic coordinate, and the Hamilton-Jacobi equation for the generating function S''' is

$$\bar{H} = \bar{H}(J) = H(q, p) = H\left(q, \frac{\partial S'''}{\partial q}\right) \quad (100)$$

with

$$\theta = \frac{\partial S'''}{\partial J} \quad (101)$$

and from equation (99), we have

$$\dot{\theta} = \frac{d\bar{H}}{dJ} = \omega, \text{ say,} \quad (102)$$

from which,

$$\theta = \omega t + \delta. \quad (103)$$

Note that if J has the dimension of action, θ is dimensionless and is called the angle variable.

Let us suppose now that q and p are periodic functions of t , and let us take J to be the action evaluated over one period

$$J = \frac{1}{2\pi} \oint pdq. \quad (104)$$

Note that during one period of the motion, θ increases by an amount

$$\Delta\theta = \oint d\theta = \oint \frac{\partial}{\partial q} \left(\frac{\partial S'''}{\partial J} \right) dq = \frac{\partial}{\partial J} \oint \frac{\partial S'''}{\partial q} dq = \frac{\partial}{\partial J} \oint p dq = 2\pi \quad (105)$$

so that ω is the frequency of the periodic motion. Since the integral $\oint pdq$ represents the area enclosed by an orbit of energy $H = E$ in the phase plane, each orbit is uniquely labelled by J , which is constant along every orbit. Each point on an orbit is labelled by a single-valued function of θ . Thus, the action-angle formulation enables us to calculate the frequencies of the periodic motions directly without finding the variations of the coordinates with time.

On using (98), (104) shows that

$$J = \frac{1}{2\pi} \oint \left(\frac{\partial S'''}{\partial q} \right) dq \quad (106)$$

or

$$\Delta S''' \equiv \oint dS''' = 2\pi J \quad (107)$$

indicating that S''' increases by $2\pi J$ during one period. The relation

$$S'''(q, \bar{p}) = S(q, \theta) + J\theta \quad (108)$$

then shows that $S(q, \theta)$ is a periodic function of θ with period 2π .

EXAMPLE 10

Consider a simple harmonic oscillator, given by

$$H = \frac{1}{2m} (p^2 + m^2 \omega^2 q^2). \quad (109)$$

The Hamilton-Jacobi equation for the generating function S''' is then

$$\frac{1}{2m} \left(\frac{\partial S'''}{\partial q} \right)^2 + \frac{1}{2} m^2 \omega^2 q^2 = H = \text{const} = E \quad (110)$$

from which,

$$S''' = \int^q \sqrt{2mE - m^2 \omega^2 q^2} dq \quad (111)$$

and

$$J = \frac{1}{2\pi} \oint \sqrt{2mE - m^2 \omega^2 q^2} dq = \frac{E}{\omega}. \quad (112)$$

Using (112), (111) becomes

$$S''' = \int \sqrt{2m\omega J - m^2 \omega^2 q^2} dq. \quad (113)$$

We have from (113),

$$\theta = \frac{\partial S'''}{\partial J} = m\omega \int \frac{dq}{\sqrt{2m\omega J - m^2 \omega^2 q^2}} = \sin^{-1} \sqrt{\frac{m\omega}{2J}} q \quad (114)$$

from which, we have

$$q = \sqrt{\frac{2J}{m\omega}} \sin \theta = \frac{\sqrt{2mE}}{m\omega} \sin \theta. \quad (115)$$

We have also from (113),

$$p = \frac{\partial S'''}{\partial q} = \sqrt{2mJ\omega} \cos \theta = \sqrt{2mE} \cos \theta. \quad (116)$$

Finally, we have, from (113), for the generating function $S = S(q, \bar{q})$,

$$S(q, \bar{q}) = S'''(q, J) - J\theta = \frac{1}{2}m\omega q^2 \cot \theta = \frac{1}{2}m\omega \bar{q}^2 \cot \bar{q}. \quad (117)$$

which was used earlier in EXAMPLE 5.

3.6. Infinitesimal Canonical Transformations

Let us consider a canonical transformation which is a continuous function of a parameter and reduces to an identity transformation at some initial value of the parameter. If the parameter is small enough to be treated as a first-order infinitesimal, then the transformed canonical variables differ only infinitesimally from the initial variables.

Consider a near-identity transformation generated by

$$\psi'''(q_j, \bar{p}_j, t) = \sum_j q_j \bar{p}_j + \varepsilon X(q_j, \bar{p}_j, t) \quad (118)$$

where ε is the small parameter. If,

$$\bar{p}_j = p_j + \delta p_j, \quad \bar{q}_j = q_j + \delta q_j \quad (119)$$

then $\psi'''(q_j, \bar{p}_j, t)$ generates an infinitesimal canonical transformation according to

$$\left. \begin{aligned} \delta q_j &= \varepsilon \frac{\partial X}{\partial \bar{p}_j} \approx \varepsilon \frac{\partial X}{\partial p_j} \\ \delta p_j &= -\varepsilon \frac{\partial X}{\partial q_j} \\ \bar{H}(\bar{q}_j, \bar{p}_j, t) &= H(q_j, p_j, t) + \varepsilon \frac{\partial X(q_j, \bar{p}_j, t)}{\partial t}. \end{aligned} \right\} \quad (120)$$

EXAMPLE 11

Let

$$X = H, \quad \varepsilon = \delta t \quad (121)$$

then (120) becomes

$$\left. \begin{aligned} \frac{\delta q_j}{\delta t} &= \dot{q}_j = \frac{\partial H}{\partial p_j} \\ \frac{\delta p_j}{\delta t} &= \dot{p}_j = -\frac{\partial H}{\partial q_j} \end{aligned} \right\}. \quad (122)$$

Hence, Hamilton's equations are themselves an infinitesimal canonical transformation generated by the Hamiltonian, H . Thus, the motion of a system may be regarded as a succession of infinitesimal canonical transformations generated by the Hamiltonian of the system. This implies that, the motion of a mechanical system corresponds to the continuous evolution or unfolding of a canonical transformation generated by the Hamiltonian and can be determined by constructing a global generating function S'' .

On the other hand, by using a succession of inverse infinitesimal canonical transformations one can annul the effect of motion and bring the variables back to their initial values. Thus, the canonically transformed variables will be constants. This has the effect of making the variables cyclic so that the equations of motion are trivially integrated.

3.7. Poisson's Brackets

Let us now determine the change in the functional form of a dynamical variable caused by an infinitesimal canonical transformation. Let $Y(q_i, p_i, t)$ be the dynamical variable in question, and let $X(q_i, p_i, t)$ be the generator of the infinitesimal canonical transformation, with

$$\delta q_i = \varepsilon \frac{\partial X}{\partial p_i}, \quad \delta p_i = -\varepsilon \frac{\partial X}{\partial q_i}. \quad (120)$$

The transformed dynamical variable is given by

$$\bar{Y}(\bar{q}_i, \bar{p}_i, t) = Y(q_i, p_i, t) + \delta Y(q_i, p_i, t) \quad (123)$$

where, we have, on using equation (120),

$$\begin{aligned} \delta Y(q_i, p_i, t) &= \sum_i \frac{\partial Y(q_i, p_i, t)}{\partial q_i} \delta q_i + \sum_i \frac{\partial Y(q_i, p_i, t)}{\partial p_i} \delta p_i + \frac{\partial Y(q_i, p_i, t)}{\partial t} \delta t \\ &= \varepsilon \sum_i \left(\frac{\partial Y}{\partial q_i} \frac{\partial X}{\partial p_i} - \frac{\partial X}{\partial q_i} \frac{\partial Y}{\partial p_i} \right) + \frac{\partial Y}{\partial t} \delta t \\ &\equiv \varepsilon [Y, X] + \frac{\partial Y}{\partial t} \delta t. \end{aligned} \quad (124)$$

Taking $\varepsilon = \delta t$ and $X = H$, (124) gives

$$\frac{dY}{dt} = [Y, H] + \frac{\partial Y}{\partial t}. \quad (125)$$

If Y does not depend on t explicitly, equation (125) becomes

$$\frac{dY}{dt} = [Y, H]. \quad (126)$$

Thus, Y is a constant of the motion, if and only if, its Poisson bracket with the Hamiltonian vanishes. On the other hand, by replacing Y by H and X by Y , we have, in place of (124),

$$\delta H = \varepsilon [H, Y] \quad (127)$$

which shows that a constant of motion generates an infinitesimal canonical transformation with respect to which H is invariant.

EXAMPLE 12

If $Y = q_i$ or p_i , we have from equation (126) –

$$\frac{dq_i}{dt} = [q_i, H], \quad \frac{dp_i}{dt} = [p_i, H]. \quad (128)$$

EXAMPLE 13

Let $\varepsilon = \delta q$ and $\delta p = 0$. Then we have from (120), $X = p$, so that the momentum p generates a canonical transformation which gives translations in the direction of the coordinate that is canonically conjugate to p . If p is conserved, then $[p, H] = 0$ so that H is independent of q . So, momentum conservation corresponds to the invariance of H under translations in the direction of the coordinate that is canonically conjugate to p .

Note the following results associated with Poisson's brackets:

$$\begin{aligned} [q_i, q_j] &= 0, \quad [p_i, p_j] = 0 \\ [q_i, p_j] &= \delta_{ij} \\ [q_i, X] &= \frac{\partial X}{\partial p_i}, \quad [p_i, X] = -\frac{\partial X}{\partial q_i}. \end{aligned} \quad (129)$$

These relations imply that any set of $2n$ canonically conjugate variables (q, p) constitute infinitesimal generators for a complete set of commuting translations in the $2n$ -dimensional phase-space (p_i generates translations along the q_i -axis while $-q_i$ generates translations along the p_i -axis).

Note further that equation (126) has the formal series solution:

$$Y(t) = Y_0 + t[Y, H]_0 + \frac{t^2}{2!}[[Y, H], H]_0 + \dots \quad (130)$$

where the subscript zero refers to the initial conditions at $t = 0$.

EXAMPLE 14

Consider a one-dimensional motion with a constant acceleration a , with the Hamiltonian given by (Goldstein, 1980)

$$H = \frac{p^2}{2m} - max. \quad (131)$$

We then have,

$$\left. \begin{aligned} [x, H] &= \frac{p}{m} \\ [[x, H], H] &= \frac{1}{m} [p, H] = a \\ [[[x, H], H], H] &= 0 \\ \text{etc.} & \end{aligned} \right\} \quad (132)$$

Using (132), we then obtain from (130),

$$x = x_o + t \frac{p_o}{m} + \frac{t^2}{2} a$$

where $p_o = p(t = 0)$. Putting, $p_o/m = v_o$, we obtain

$$x = x_o + v_o t + \frac{1}{2} a t^2 \quad (133)$$

which, of course, is the well known solution!

The above series solution (130) shows that one may use infinitesimal canonical transformations to build up finite canonical transformations, depending on a parameter, and thus construct solutions to the equations of motion.

EXAMPLE 15

The infinitesimal canonical transformations are built into the Poisson bracket relations. In order to see this, note

$$[\bar{q}_i, \bar{p}_i] = 1, \text{ no sum over } i. \quad (134)$$

Letting,

$$\bar{p}_i = p_i + \delta p_i, \quad \bar{q}_i = q_i + \delta q_i \quad (135)$$

(134) gives

$$\left(1 + \frac{\partial \delta q_i}{\partial q_i}\right) \left(1 + \frac{\partial \delta p_i}{\partial p_i}\right) - \frac{\partial \delta q_i}{\partial p_i} \frac{\partial \delta p_i}{\partial q_i} = 1 \quad (136)$$

from which, we have

$$\frac{\partial \delta q_i}{\partial q_i} + \frac{\partial \delta p_i}{\partial p_i} = 0. \quad (137)$$

Equation (137) implies

$$\delta q_i = \varepsilon \frac{\partial X}{\partial p_i}, \quad \delta p_i = -\varepsilon \frac{\partial X}{\partial q_i} \quad (138)$$

as advertized.

It may be readily verified that Poisson's brackets have the following properties:

$$[X, Y] = -[Y, X], \text{ so } [X, X] = 0 \quad (139)$$

$$[X, Y + Z] = [X, Y] + [X, Z] \quad (140)$$

$$[X, YZ] = Y[X, Z] + Z[X, Y] \quad (141)$$

$$[[X, Y], Z] + [[Z, X], Y] + [[Y, Z], X] = 0 \quad (142)$$

(142) is known as Jacobi's identity.

Another important property of Poisson's brackets, which is easy to verify, is their invariance with respect to a canonical transformation. Thus, the value of a Poisson's bracket is independent of the set of conjugate variables with respect to which it is evaluated. Therefore, the use of a subscript on the bracket is superficial and is normally omitted.

CHAPTER 4

INTEGRABLE SYSTEMS

Consider a conservative Hamiltonian system. One may specify the state of such a system by giving all the position and momentum coordinates (\mathbf{q}, \mathbf{p}) of a point in the system phase space, and the time evolution of the system is described by a trajectory lying on a surface described by the conservation of energy in the phase space. A dynamical system is said to be ergodic if left to itself for long enough, it will pass in an erratic manner close to nearly all the dynamical states compatible with conservation of energy.

A classical system is said to be integrable if it has as many integrals of motion as the degrees of freedom, say n . If the intersection of the level sets of these integrals is compact, then it is topologically an n -dimensional torus. Integrable systems are not ergodic since all their trajectories lie on these n -dimensional invariant tori embedded in the $(2n - 1)$ dimensional energy surface. Nonintegrable systems seem to exhibit ergodic behavior of some type due to the breakdown of the invariant tori. The introduction of even a small perturbation to an integrable system can lead to regimes of irregular motion embedded in regions of regular motion. As the perturbation increases, the regimes of irregular motion grow in size, and eventually fill the whole phase space¹.

4.1. Separable Hamiltonian Systems

The Hamilton-Jacobi equation for n degrees of freedom, as we saw in Chapter 3, cannot, in general, be solved unless it is separable (when it can be integrated by quadratures). The generating function for such systems can be written as a sum of n terms – each depending on only one coordinate, $q_k, k = 1, \dots, n$,

$$S'''(q_1, q_2, \dots, q_n, J_1, J_2, \dots, J_n) = \sum_{k=1}^n S_k'''(q_k, J_1, \dots, J_n) \quad (1)$$

¹ This picture appears to be supported by the spectacular success of the predictions of statistical mechanics which is predicated on the basic supposition that the Hamiltonian system with a large number of degrees of freedom in question is equally likely to be found, at each instant, at any point on the energy surface in the phase space.

where J_k are the new "momenta". An example of such separable systems is one in which the Hamiltonian is the sum of n -independent parts of the form

$$H(p_1, \dots, p_n, q_1, \dots, q_n) = \sum_{k=1}^n H_k(p_k, q_k). \quad (2)$$

The generating function (1) brings about a transformation according to

$$\left. \begin{aligned} p_k &= \frac{\partial S'''(q_k, J_1, \dots, J_n)}{\partial q_k} \\ \theta_k &= \frac{\partial S'''}{\partial J_k} = \sum_{l=1}^n \frac{\partial S'''(q_l, J_1, \dots, J_n)}{\partial J_k} \end{aligned} \right\} \quad (3)$$

where θ_k are the new "coordinates". Note that each p_k is a function of only one q_k . Furthermore, if the motion is periodic in each of the q_k , then one may take J_k to be the set of action variables:

$$J_k = \frac{1}{2\pi} \oint p_k dq_k, \text{ no sum on } k. \quad (4)$$

If the new coordinates θ_k (which are now the angle variables) are cyclic, then

$$\bar{H} = \bar{H}(J_1, \dots, J_n) = \sum_{k=1}^n E_k(J_1, \dots, J_n), \text{ say,} \quad (5)$$

and the Hamilton-Jacobi equation is

$$H_k \left(q_k, \frac{\partial S'''}{\partial q_k} \right) = E_k(J_1, \dots, J_n). \quad (6)$$

Hamilton's equations in the transformed variables are

$$\left. \begin{aligned} j_k &= -\frac{\partial \bar{H}}{\partial \theta_k} = 0 \\ \dot{\theta}_k &= \frac{\partial \bar{H}}{\partial J_k} = \omega_k \end{aligned} \right\} \quad (7)$$

from which,

$$\left. \begin{aligned} J_k &= \text{const} \\ \theta_k &= \omega_k t + \delta_k \end{aligned} \right\} k = 1, 2, \dots, n \quad (8)$$

where ω_k 's are the frequencies associated with various degrees of freedom.

4.2. Integrable Systems

It is now apparent that one way of integrating a Hamiltonian system of n degrees of freedom is to find n independent integrals of motion. If these constants are taken as n constant conjugate momenta, Hamilton's equations then become separable and are trivially integrated via quadratures.

If $F_i(p_j, q_j)$ is an integral of motion, then we have

$$[H, F_i] = 0. \quad (9)$$

DEFINITION: A Hamiltonian system of n degrees of freedom is said to be completely integrable if there exist n integrals of the motion F_1, \dots, F_n , which are in involution, i.e., the F_i 's all commute with each other,

$$[F_i, F_j] = 0, \quad i \text{ and } j = 1, \dots, n. \quad (10)$$

One of these integrals may be taken to be the Hamiltonian H .

The existence of the n integrals F_i means that the phase-space trajectories will lie on some n -dimensional manifold, M , in the $2n$ -dimensional phase space. Let us now define the "velocity" fields

$$\xi_i \equiv (\nabla_p F_i, -\nabla_q F_i), \quad i = 1, 2, \dots, n \quad (11)$$

in the $2n$ -dimensional phase space. For $F_i = H$, equation (11) defines the actual Hamiltonian flow, $\xi_i \equiv (\nabla_p H, -\nabla_q H) = (\dot{q}, \dot{p})$, which, due to the existence of the n integrals F_1, F_2, \dots, F_n , must entirely lie on the manifold M . Thus, ξ_i is tangent to M . In fact, on account of (10), each ξ_i is perpendicular to all normals to M ; because,

$$\xi_i \cdot (\nabla_q F_j, \nabla_p F_j) = [F_i, F_j] = 0 \text{ for all } i, j. \quad (12)$$

Therefore, all n "velocity" fields ξ_i are tangent to the manifold M . Further, since F_i 's are independent and in involution, ξ_i 's are all linearly independent. Let us now restrict ourselves to bounded motions for which the accessible region in phase space is finite. Then, we have the following topological Theorem due to Poincaré and Hopf.

THEOREM 4.1 (Poincaré and Hopf)

Let M be an n -dimensional compact manifold M , for which there exist n independent vector fields ξ_i 's tangent to it. Then, M has the topology of an n -dimensional torus².

The existence of these invariant tori (a trajectory starting out on one of these remains on it forever), in phase space, on the other hand, enables one to define action variables in a form invariant way. Since the n -torus shows n independent periodicities of period 2π , one can define n topologically independent closed paths C_k on the torus. The action variables can then be defined as

$$J_k = \frac{1}{2\pi} \oint_{C_k} \sum_{m=1}^n p_m dq_m; \quad k = 1, \dots, n \quad (13)$$

which can be used to label a torus uniquely.

Using the generating function $S'''(q_1, \dots, q_n, J_1, \dots, J_n)$, one obtains the conjugate angle variables

² An n -dimensional torus is defined as

$$T^n = S^1 \times S^1 \times \cdots \times S^1 \text{ (n products)}$$

where,

$$S^1 = \{x_1^2 + x_2^2 = 1\}.$$

$$\theta_k = \frac{\partial}{\partial J_k} S'''(q_1, \dots, q_n, J_1, \dots, J_n), k = 1, \dots, n, \quad (14)$$

which then serve as coordinates on this torus. Hamilton's equations in the action-angle variables are then given by (7). Note that a 1-torus is a circle, while a 2-torus is the surface of a doughnut, and an n -torus is a quasi-periodic motion.

If the system is completely integrable, the whole phase-space is filled with invariant tori, and a given trajectory will lie on one torus or another, forever. The transformation to action-angle variables is then global. A given set of initial conditions $(q_i(0), p_i(0))$ prescribes the actions J_i , and hence determines on which torus the trajectory lies.

For a conservative integrable system of n degrees of freedom, one may, therefore, identify the following important dimensions:

- (i) phase space: $2n$ -dimensional,
- (ii) energy shell: $(2n - 1)$ -dimensional,
- (iii) tori: n -dimensional.

This implies that for one-degree-of-freedom systems, the energy shell and tori are the same one-dimensional manifold. Therefore, these systems would be ergodic, i.e., any trajectory of the system explores the energy shell uniformly, which means that the time average³ of a given quantity, say, $f(\mathbf{p}, \mathbf{q})$, must equal its ensemble-average on the energy surface, i.e.,

$$\lim_{T \rightarrow \infty} \frac{1}{T} \int_{-T}^T f(\mathbf{p}(t), \mathbf{q}(t)) dt = \iint d\mathbf{p} d\mathbf{q} f(\mathbf{p}, \mathbf{q}) \delta(E - H(\mathbf{p}, \mathbf{q})) \quad (15)$$

³ It may be noted that the time average often depends on initial conditions, so it may vary from trajectory to trajectory. Nonetheless, there may be cases, like when the dynamical system has an attractor, with families of trajectories possessing the same time averages.

⁴ For a regular motion, this result would be sensitive to the choice of initial conditions. Because, if one chooses the ensemble of initial values such that they are bunched together, then due to the regularity of the motion, they will remain bunched together. As a result, the ensemble samples and the averages computed by them will not be statistically independent, and the result (15) will not hold. For a mixing motion (see Section 5.9), however, the result (15) would be insensitive to the choice of initial conditions. Because, the mixing motion spreads the samples of the ensemble uniformly over the energy surface even if they are very close to each other initially. As a result, these samples and the averages computed by them will be statistically independent, and the result (15) holds.

⁵ For a one-dimensional map

$$x_{n+1} = M(x_n)$$

with an attractor A and a basin of attraction B (see Chapter 6) and a natural measure μ , (15) takes the form

$$\lim_{T \rightarrow \infty} \frac{1}{T} \sum_{n=0}^T f(M^{[n]}(x_o)) = \int f(x) d\mu(x)$$

in some sense of convergence like pointwise, mean square, etc. Here, the weighting function $\delta(E - H(\mathbf{p}, \mathbf{q}))$ represents the "micro-canonical ensemble", i.e., the invariant measure on the energy shell $E = H$. (The existence of an invariant probability distribution for a Hamiltonian system is guaranteed by Liouville's Theorem and enables one to concentrate on those properties which hold for "almost all orbits" and ignore those properties which are not typical.) Next, for $n = 2$, the two-dimensional tori foliate the three-dimensional energy shell E , i.e., the two-dimensional tori effectively separate the three-dimensional energy shell into distinct open sets. Therefore, the irregular orbits, which wander through regions where rational tori have been destroyed (see Section 4.5) are trapped in the gaps between remaining irrational tori, and can explore a region of E which, while three-dimensional, is nevertheless restricted, and in particular, disconnected from other irregular regions in E . For $n \geq 3$, however, the tori do not foliate E , (for $n = 3$, for example, the tori are three-dimensional while the energy shell is five-dimensional)⁶. Then, the gaps between irrational tori form one single-connected region, and an irregular trajectory in one gap can escape to other gaps of the energy shell. This leads to the so-called Arnol'd diffusion which is a diffusive meandering of irregular trajectories through a network of tori on the energy shell E . The possibility of the Arnol'd diffusion means that, for $n > 2$, the existence of some invariant tori for perturbed motion is no guarantee of stability of motion, since irregularly wandering orbits, that are not trapped, exist arbitrarily close to the tori. This aspect is of great importance in the construction of particle accelerators and magnetically confined thermonuclear fusion devices (see Section 4.7).

EXAMPLE 1

Consider a particle moving in the field of a fixed center of force with the potential $V(r)$. In spherical-polar coordinates, the Lagrangian of a particle is

which states that the time average of $f(x)$ over an orbit emanating from an initial condition x_o on B is equal to the natural-measure weighted average of $f(x)$ over A .

⁶ This follows from the fact that, for an n degree-of-freedom system, the n -dimensional tori foliate the $(2n - 1)$ -dimensional energy surface if they are capable of being the boundaries of the latter region, i.e., are of dimension at least $(2n - 2)$, so

$$n \geq (2n - 2)$$

or

$$n \leq 2.$$

$$L = \frac{1}{2} \mu \left(\dot{r}^2 + r^2 \dot{\theta}^2 + r^2 \sin^2 \theta \cdot \dot{\phi}^2 \right) - V(r) \quad (16)$$

from which the momenta are given by

$$\left. \begin{aligned} p_r &= \frac{\partial L}{\partial \dot{r}} = \mu \dot{r} \\ p_\theta &= \frac{\partial L}{\partial \dot{\theta}} = \mu r^2 \dot{\theta} \\ p_\phi &= \frac{\partial L}{\partial \dot{\phi}} = \mu r^2 \sin^2 \theta \cdot \dot{\phi} \end{aligned} \right\}. \quad (17)$$

Here, μ is the so-called reduced mass of this system.

The Hamiltonian is then given by

$$H = \frac{1}{2\mu} \left(p_r^2 + \frac{p_\theta^2}{r^2} + \frac{p_\phi^2}{r^2 \sin^2 \theta} \right) + V(r). \quad (18)$$

Hamilton's equations are

$$\left. \begin{aligned} \dot{p}_r &= -\frac{\partial H}{\partial r} = \frac{1}{\mu r^3} \left(p_\theta^2 + \frac{p_\phi^2}{\sin^2 \theta} \right) - \frac{\partial V}{\partial r} \\ \dot{p}_\theta &= -\frac{\partial H}{\partial \theta} = \frac{1}{\mu r^2} \left(\frac{p_\phi^2 \cos \theta}{\sin^3 \theta} \right) \\ \dot{p}_\phi &= -\frac{\partial H}{\partial \phi} = 0 \end{aligned} \right\}. \quad (19)$$

We will solve the nonlinear equations (19) using the Hamilton-Jacobi formulation. Since H does not involve t , the Hamilton-Jacobi equation is

$$\frac{1}{2\mu} \left[\left(\frac{\partial S}{\partial r} \right)^2 + \frac{1}{r^2} \left(\frac{\partial S}{\partial \theta} \right)^2 + \frac{1}{r^2 \sin^2 \theta} \left(\frac{\partial S}{\partial \phi} \right)^2 \right] + V = E \quad (20)$$

S being the generating function.

Let us separate the variables as follows –

$$S(r, \theta, \phi) = S_1(r) + S_2(\theta) + S_3(\phi). \quad (21)$$

We then obtain from equation (20)

$$r^2 \sin^2 \theta \left[2\mu(E - V) - \left(\frac{dS_1}{dr} \right)^2 - \frac{1}{r^2} \left(\frac{dS_2}{d\theta} \right)^2 \right] = \left(\frac{dS_3}{d\phi} \right)^2 = p_\phi^2 = \text{const} = m^2 \quad (22)$$

which is apparent since ϕ is cyclic.

Further, we have from (22),

$$\left(\frac{dS_2}{d\theta} \right)^2 + \frac{m^2}{\sin^2 \theta} = 2r^2\mu(E - V) - r^2 \left(\frac{dS_1}{dr} \right)^2 = \text{const} = l^2 \quad (23)$$

from which,

$$\left. \begin{aligned} p_\theta &= \frac{dS_2}{d\theta} = \left(l^2 - \frac{m^2}{\sin^2 \theta} \right)^{\frac{1}{2}} \\ p_r &= \frac{dS_1}{dr} = \left[2\mu(E - V) - \frac{l^2}{r^2} \right]^{\frac{1}{2}} \end{aligned} \right\}. \quad (24)$$

Thus, there exist three constants – the angular momentum about the polar axis, the total angular momentum, and the energy –

$$\left. \begin{aligned} m &= p_\phi \\ l &= \left(\frac{m^2}{\sin^2 \theta} + p_\theta^2 \right)^{\frac{1}{2}} \\ E &= \frac{1}{2\mu} \left(p_r^2 + \frac{l^2}{r^2} \right) + V \end{aligned} \right\}. \quad (25)$$

The problem (16) is thus broken into three equivalent one-dimensional problems for the r, θ, ϕ motions, respectively.

If the motion is periodic, the action variables are

$$\left. \begin{aligned} J_\phi &= \frac{1}{2\pi} \oint p_\phi d\phi = \frac{m}{2\pi} \oint d\phi = m \\ J_\theta &= \frac{1}{2\pi} \oint p_\theta d\theta = \frac{1}{2\pi} \oint \left(l^2 - \frac{m^2}{\sin^2 \theta} \right)^{\frac{1}{2}} d\theta \\ J_r &= \frac{1}{2\pi} \oint p_r dr = \frac{1}{2\pi} \oint \left[2\mu(E - V) - \frac{l^2}{r^2} \right]^{\frac{1}{2}} dr \end{aligned} \right\}. \quad (26)$$

Since p_θ is real, we require, from (24), $|\sin \theta| \geq \frac{m}{l}$. Then (26) becomes

$$J_\theta = \frac{1}{\pi} \int_{\theta_{\min}}^{\theta_{\max}} \left(l^2 - \frac{m^2}{\sin^2 \theta} \right)^{\frac{1}{2}} d\theta = \frac{2l}{\pi} \int_{\theta_{\min}}^{\theta_{\max}} \left(1 - \frac{m^2}{l^2 \sin^2 \theta} \right)^{\frac{1}{2}} d\theta \quad (27)$$

where,

$$\theta_{\min} = \sin^{-1} \left(\frac{m}{l} \right), \quad \theta_{\max} = \pi - \theta_{\min}.$$

Putting,

$$u = \sin^2 \theta \quad (28)$$

(27) becomes

$$J_\theta = \frac{1}{\pi} \int_{m^2/l^2}^1 \left(\frac{l^2 u - m^2}{1-u} \right)^{\frac{1}{2}} \frac{du}{u}. \quad (29)$$

Putting,

$$u = \frac{1}{v} \quad (30)$$

(29) becomes

$$J_\theta = -\frac{1}{\pi} \int_{l^2/m^2}^1 \left(\frac{m^2 v - l^2}{1 - v} \right)^{\frac{1}{2}} \frac{dv}{v} \quad (31)$$

(29) and (31) imply that J_θ is an odd function in the argument $(l - m)$:

$$J_\theta = f_{odd}(l - m). \quad (32)$$

Now, note, from (27), that

$$m = 0 : J_\theta = \frac{2l}{\pi} \int_0^{\frac{\pi}{2}} d\theta = l. \quad (33)$$

(32) and (33) imply that

$$J_\theta = (l - m). \quad (34)$$

For a gravitational field, $V(r) = -\frac{K}{r}$, and for radial periodic motions, the integrand for J_r , in (26), must vanish for two values of r :

$$r_{\max, \min} = -\frac{K}{2E} \left[1 \pm \sqrt{1 + \frac{2El^2}{\mu K^2}} \right] \quad (35)$$

which are both positive if $E < 0$, i.e., the particle has insufficient kinetic energy to escape to infinity. Then, we have

$$J_r = \frac{1}{\pi} \int_{r_{\min}}^{r_{\max}} \left[2\mu \left(E + \frac{K}{r} \right) - \frac{l^2}{r^2} \right]^{\frac{1}{2}} dr = -l - \frac{\mu K}{\sqrt{-2\mu E}}. \quad (36)$$

Thus, we have from (26), (34) and (36),

$$J_r + J_\theta + J_\phi = -\frac{\mu K}{\sqrt{-2\mu E}} \quad (37)$$

from which, we have

$$E = -\frac{\mu K^2}{2(J_r + J_\theta + J_\phi)^2} = \bar{H}(J_r, J_\theta, J_\phi). \quad (38)$$

The frequencies of the r, θ, ϕ periodic motions are given by

$$\omega_r = \frac{\partial \bar{H}}{\partial J_r}, \quad \omega_\theta = \frac{\partial \bar{H}}{\partial J_\theta}, \quad \omega_\phi = \frac{\partial \bar{H}}{\partial J_\phi} \quad (39)$$

from which,

$$\omega_r = \omega_\theta = \omega_\phi = \frac{(-2E)^{3/2}}{K\sqrt{\mu}}. \quad (40)$$

It is to be noted that the degeneracy $\omega_\theta = \omega_\phi$ is characteristic of the central nature of the force field; the degeneracy $\omega_r = \omega_\theta = \omega_\phi$ is a peculiarity with the gravitational field.

4.3. Dynamics on the Tori

Thanks to the periodic nature of the Hamiltonian flow on tori, a given dynamical quantity $f(p_j, q_j)$ may be expressed as a multiple Fourier series in the angle variables $\theta_1, \dots, \theta_n$. For example, $q_i(t)$ may be expressed as

$$\begin{aligned} q_i(t) &= \sum_{k_1=-\infty}^{\infty} \dots \sum_{k_n=-\infty}^{\infty} a_{k_1 \dots k_n}^{(i)} e^{i(k_1 \theta_1 + \dots + k_n \theta_n)} \\ &= \sum_{k_1} \dots \sum_{k_n} a_{k_1 \dots k_n}^{(i)} e^{i(k_1 \omega_1 + \dots + k_n \omega_n)t + i(k_1 \delta_1 + \dots + k_n \delta_n)} \end{aligned} \quad (41)$$

where,

$$a_{k_1 \dots k_n}^{(i)}(J_1, \dots, J_n) = \int_0^{2\pi} d\theta_1 \dots \int_0^{2\pi} d\theta_n q_i(J_1, \dots, J_n, \theta_1, \dots, \theta_n) e^{-i(k_1 \theta_1 + \dots + k_n \theta_n)}. \quad (42)$$

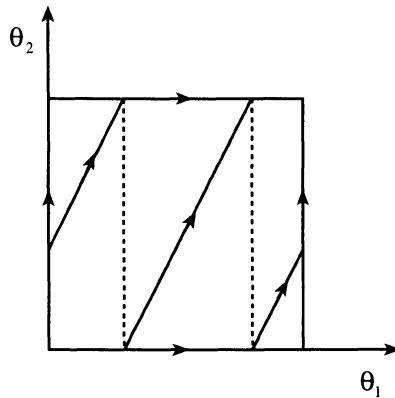


Figure 4.1. Equivalence between the flow on a 2-torus and mapping on a unit square.

If the frequencies are not commensurate, i.e., they are not rationally related, the motion on a given torus will never exactly repeat itself. Such orbits are called quasi-periodic, and a single orbit will wander all over the torus uniformly, and is dense there. This may be easily seen for the two-dimensional case, where, the two-dimensional torus is topologically equivalent to a square (Figure 4.1) with periodic boundary conditions. Let ω_1 and ω_2 be the frequencies of periodic motions about large circles and small circles, respectively. Any phase trajectory on the torus is represented on the square by a set of parallel line segments. If the ratio ω_1/ω_2 is irrational, then the line segments densely cover the square – this is the quasi-periodic orbit. On the other hand, if ω_1/ω_2 is rational, the motion will eventually repeat itself. Such orbits are called closed orbits, and are composed of a finite number of parallel line segments on the square – this is the periodic regime⁷. Note that the parallelness of the line segments on the square is dictated by deterministic nature of the system because divergence of the line segments would lead to their intersection, in violation of determinism.

⁷ A periodic motion can ensue in a system of coupled nonlinear oscillators as a consequence of the frequency locking effect: This refers to a self-synchronization of two coupled nonlinear oscillators so as to make their basic frequencies commensurate and to keep the system locked in this state over a range of parameters. One example of this effect is the locking of the moon's rotation rate to its orbital period caused by the dissipative tidal forces which leads to the same side of the moon always facing the earth!

DEFINITION: A completely integrable system is called nondegenerate if the Hessian satisfies the following condition:

$$\det \left| \frac{\partial \omega_i(J_1, \dots, J_n)}{\partial J_j} \right| = \det \left| \frac{\partial^2 \bar{H}(J_1, \dots, J_n)}{\partial J_i \partial J_j} \right| \neq 0. \quad (43)$$

This condition implies that the frequencies vary from torus to torus (as it behoves a nonlinear system). For a nondegenerate system, the set of tori covered with closed orbits, although dense, will be infinitely outnumbered by the tori covered with quasi-periodic orbits (because the rational numbers though dense make a set of zero Lebesgue measure⁸ in the space of real numbers).

DEFINITION: A completely integrable system is termed "isoenergetic nondegenerate" (due to Arnol'd (1978)) if the frequencies are independent functions of the action variables, i.e.,

$$\det \begin{vmatrix} \frac{\partial^2 \bar{H}}{\partial J_i \partial J_j} & \frac{\partial \bar{H}}{\partial J_i} \\ \frac{\partial \bar{H}}{\partial J_j} & 0 \end{vmatrix} \neq 0. \quad (44)$$

This condition ensures that the frequency ratios vary smoothly from torus to torus, which in turn guarantees the existence of a set of rational and irrational tori densely on every energy level surface. Note that, for $n = 2$, the above determinant becomes

⁸ A compact set is of Lebesgue measure zero if, for any $\varepsilon > 0$, it can be covered with a finite number of intervals of total length less than ε .

$$\det \begin{vmatrix} \frac{\partial^2 \bar{H}}{\partial J_1^2} & \frac{\partial^2 \bar{H}}{\partial J_1 \partial J_2} & \frac{\partial \bar{H}}{\partial J_2} \\ \frac{\partial^2 \bar{H}}{\partial J_2 \partial J_1} & \frac{\partial^2 \bar{H}}{\partial J_2^2} & \frac{\partial \bar{H}}{\partial J_1} \\ \frac{\partial \bar{H}}{\partial J_1} & \frac{\partial \bar{H}}{\partial J_2} & 0 \end{vmatrix} = \det \begin{vmatrix} \frac{\partial \omega_1}{\partial J_1} & \frac{\partial \omega_1}{\partial J_2} & \omega_1 \\ \frac{\partial \omega_2}{\partial J_1} & \frac{\partial \omega_2}{\partial J_2} & \omega_2 \\ \omega_1 & \omega_2 & 0 \end{vmatrix}$$

$$= -\omega_2^3 \det \begin{vmatrix} \frac{\partial}{\partial J_1} \left(\frac{\omega_1}{\omega_2} \right) & \frac{\partial}{\partial J_2} \left(\frac{\omega_1}{\omega_2} \right) \\ \frac{\omega_1}{\omega_2} & 1 \end{vmatrix} \neq 0. \quad (45)$$

4.4. Canonical Perturbation Theory

Completely integrable Hamiltonian systems are an exception rather than the rule (they actually form a set of measure zero). However, they play an important role in the treatment of nonintegrable systems because it often proves to be useful to represent a given Hamiltonian system in the form of an integrable part H_0 plus a small nonintegrable perturbation εH_1 :

$$H(\mathbf{p}, \mathbf{q}) = H_0(\mathbf{p}, \mathbf{q}) + \varepsilon H_1(\mathbf{p}, \mathbf{q}) \quad (46)$$

where ε is the perturbation parameter, $\varepsilon \ll 1$. This representation enables one to find approximate solutions to $H(\mathbf{p}, \mathbf{q})$ in the form of the exact solutions corresponding to H_0 plus small corrections due to the perturbation $H_1(\mathbf{p}, \mathbf{q})$. This idea is valid if there is a region of phase space in which the phase curves of H and H_0 may be continuously deformed into each other. (In other words, during small intervals of time, the perturbed system moves in an orbit of the same functional form as the unperturbed system but with parameters changing with time.) This is the case, if the perturbation serves only to add some higher harmonics and slightly modulate the amplitudes and shift the unperturbed frequencies⁹. Here, we will discuss the perturbation theory in canonical variables, but it

⁹ However, this is, generally, not the case; most multi-dimensional nonlinear systems are not integrable. In such systems, chaotic trajectories are densely distributed among the regular trajectories and have finite measure in the phase space. Perturbation theory cannot describe the complexity of this chaotic motion; formally the series diverge (see below). Nonetheless, one may still use the perturbation theory to obtain solutions that in some sense “approximate” the actual motion in nonlinear systems. If the actual trajectory is

may be mentioned that other perturbation theories, such as the Lie transform theory (Cary (1981)) are also available for this purpose.

EXAMPLE 2

Consider as the unperturbed system the force-free motion in one dimension of a particle of mass m (Goldstein (1980)). The unperturbed Hamiltonian is

$$H_o = \frac{p^2}{2m}. \quad (47)$$

Since $q = x$ is a cyclic variable, $p = \text{constant} = \alpha$, say. Using the generating function $S'''(x, \alpha)$, the Hamilton-Jacobi equation for this problem is

$$\frac{1}{2m} \left(\frac{\partial S'''}{\partial x} \right)^2 + \frac{\partial S'''}{\partial t} = 0 \quad (48)$$

from which,

$$S''' = \alpha x - \frac{\alpha^2 t}{2m}. \quad (49)$$

The new coordinate β (which is constant for the unperturbed problem) is then given by

$$\beta = \frac{\partial S'''}{\partial \alpha} = x - \frac{\alpha t}{m} \quad (50)$$

from which,

$$x = \frac{\alpha t}{m} + \beta \quad (51)$$

as expected!

Now introduce a perturbation on the Hamiltonian (47) –

chaotic or involves significant change in topology, then the perturbation solution may still approximate the motion in some coarse-grained sense, as when the chaotic motion is confined to a thin separatrix layer bounded by regular motion (Lichtenberg and Lieberman, 1992).

$$H_1 = \frac{kx^2}{2} = \frac{m\omega^2 x^2}{2} = \frac{m\omega^2}{2} \left(\frac{\alpha t}{m} + \beta \right)^2 \quad (52)$$

where k is a small parameter and $\omega^2 \equiv k/m$. The parameters α and β are constant in the unperturbed system but develop variations in time upon the introduction of the perturbation H_1 . The first approximation to the solution is obtained by replacing α and β on the right of the equations of motion

$$\left. \begin{aligned} \dot{\beta} &= \frac{\partial H_1}{\partial \alpha} = \omega^2 t \left(\frac{\alpha t}{m} + \beta \right) \\ \dot{\alpha} &= -\frac{\partial H_1}{\partial \beta} = -m\omega^2 \left(\frac{\alpha t}{m} + \beta \right) \end{aligned} \right\} \quad (53)$$

by their unperturbed values α_o and β_o . Let us take $\beta_o = 0$, for convenience. We then obtain from (53), for the first approximations α_1, β_1 to α, β , respectively:

$$\left. \begin{aligned} \dot{\beta}_1 &= \alpha_o \frac{\omega^2 t^2}{m} \\ \dot{\alpha}_1 &= -\omega^2 \alpha_o t \end{aligned} \right\} \quad (54)$$

from which,

$$\left. \begin{aligned} \alpha_1 &= \alpha_o - \frac{\omega^2 \alpha_o t^2}{2} \\ \beta_1 &= \frac{\alpha_o \omega^2 t^3}{3m} \end{aligned} \right\}. \quad (55)$$

The first-order approximations to the solution x and p , from (51) and (55), are thus given by

$$\left. \begin{aligned} x_1 &= \frac{\alpha_1 t}{m} + \beta_1 = \frac{\alpha_o}{m\omega} \left[\omega t - \frac{\omega^3 t^3}{6} \right] \\ p_1 &= \alpha_1 = \alpha_o \left[1 - \frac{\omega^2 t^2}{2} \right] \end{aligned} \right\}. \quad (56)$$

The second-approximation to the solution is next obtained by replacing α and β on the right of the equations of motion (53) by their first-order values α_1 and β_1 , given by (55). We then obtain

$$\left. \begin{aligned} \dot{\beta}_2 &= \frac{\alpha_o \omega^2}{m} \left(t^2 - \frac{\omega^2 t^4}{6} \right) \\ \dot{\alpha}_2 &= -\alpha_o \omega^2 \left(t - \frac{\omega^2 t^3}{6} \right) \end{aligned} \right\} \quad (57)$$

from which,

$$\left. \begin{aligned} \alpha_2 &= \alpha_o - \frac{\omega^2 \alpha_o t^2}{2} + \frac{\omega^4 \alpha_o t^4}{24} \\ \beta_2 &= \frac{\alpha_o \omega^2}{m} \left(\frac{t^3}{3} - \frac{\omega^2 t^5}{30} \right) \end{aligned} \right\}. \quad (58)$$

Using (58), the second-order approximations to x and p are

$$\left. \begin{aligned} x_2 &= \frac{\alpha_2 t}{m} + \beta_2 = \frac{\alpha_o}{m\omega} \left(\omega t - \frac{\omega^3 t^3}{3!} + \frac{\omega^5 t^5}{5!} \right) \\ p_2 &= \alpha_2 = \alpha_o \left(1 - \frac{\omega^2 t^2}{2!} + \frac{\omega^4 t^4}{4!} \right) \end{aligned} \right\}. \quad (59)$$

Note that these are the first three terms in the expansions of the exact solution –

$$x = \frac{\alpha_o}{m\omega} \sin \omega t, \quad p = \alpha_o \cos \omega t \quad (60)$$

in powers of $(\omega t)!$

As we just saw in EXAMPLE 2, the effect of the perturbation is to cause the parameters of the unperturbed system to vary with time. If the perturbation is small, the variation of the parameters within one period of the unperturbed motion will also be small. Thus, the perturbation theory is based on the premise that during small intervals of time the perturbed system moves along a route which has the same functional form as the unperturbed system but with parameters changing in time. The latter variation may be periodic or secular. In the latter case, the change in a parameter is cumulative so that no matter how small this change may be over a small interval of time, eventually the perturbed route will differ greatly from the unperturbed route. The periodic variations in the parameters on the other hand, do not materialize over long intervals of time because they can be eliminated by averaging the perturbation effects over the unperturbed period! This was the *raison d'être* for the action-angle formulation in Chapter 3.

Canonical perturbation theory exploits the special features provided by the action-angle formulation. While it is generally successful for autonomous systems of one degree of freedom, it reveals, for systems of two or more degrees of freedom, the intrinsic difficulties associated with solution of the "many-body" problem; formally, the series diverge. These difficulties, in fact, turn out to be related to chaotic behavior in an essential way.

Let us now consider first systems of one-degree-of freedom to illustrate the method. Let us express the system in terms of the action-angle variables (J, θ) of the zero-order system, i.e.,

$$H(J, \theta) = H_o(J) + \varepsilon H_1(J, \theta) + \varepsilon^2 H_2(J, \theta) + O(\varepsilon^3), \quad \varepsilon \ll 1. \quad (61)$$

The basic idea of canonical perturbation theory is to find a canonical transformation that takes $H(J, \theta)$ to a new Hamiltonian $\bar{H}(\tilde{J})$ which depends only on the new action variable \tilde{J} ; this would, of course, correspond to a completely integrable system.

Let $S''' = S'''(\theta, \tilde{J})$ be the generating function which brings about the canonical transformation $H(J, \theta) \rightarrow \bar{H}(\tilde{J})$ according to

$$J = \frac{\partial}{\partial \theta} S'''(\theta, \tilde{J}), \quad \varphi = \frac{\partial}{\partial \tilde{J}} S'''(\theta, \tilde{J}) \quad (62)$$

where φ is the new angle variable.

Using the relations (62), and expanding $\bar{H}(\tilde{J})$ in a perturbation series in ε , we obtain the time-independent Hamilton-Jacobi equation

$$\begin{aligned}
H_o \left(\frac{\partial S'''}{\partial \theta} \right) + \varepsilon H_1 \left(\frac{\partial S'''}{\partial \theta}, \theta \right) + \varepsilon^2 H_2 \left(\frac{\partial S'''}{\partial \theta}, \theta \right) + O(\varepsilon^3) \\
= \overline{H}(\tilde{J}) = \overline{H}_o(\tilde{J}) + \varepsilon \overline{H}_1(\tilde{J}) + \varepsilon^2 \overline{H}_2(\tilde{J}) + O(\varepsilon^3).
\end{aligned} \tag{63}$$

Let us now take $S'''(\theta, \tilde{J})$ to be a near-identity transformation given by

$$S'''(\theta, \tilde{J}) = \tilde{J}\theta + \varepsilon S'_1(\theta, \tilde{J}) + \varepsilon^2 S'_2(\theta, \tilde{J}) + O(\varepsilon^3) \tag{64}$$

which gives

$$\begin{aligned}
J &= \frac{\partial S'''}{\partial \theta} = \tilde{J} + \varepsilon \frac{\partial S'_1}{\partial \theta} + \varepsilon^2 \frac{\partial S'_2}{\partial \theta} + \dots \\
\varphi &= \frac{\partial S'''}{\partial \tilde{J}} = \theta + \varepsilon \frac{\partial}{\partial \tilde{J}} S'_1(\theta, \tilde{J}) + \varepsilon^2 \frac{\partial}{\partial \tilde{J}} S'_2(\theta, \tilde{J}) + \dots
\end{aligned} \tag{65}$$

We use the expansion (64) to expand out each term in the Hamilton-Jacobi equation (63) in a Taylor series, which then becomes

$$\begin{aligned}
H_o(\tilde{J}) + \varepsilon \left[\frac{dH_o}{d\tilde{J}} \left(\frac{\partial S'''}{\partial \theta} \right) + H_1 \right] + \varepsilon^2 \left[\frac{1}{2} \frac{d^2 H_o}{d\tilde{J}^2} \left(\frac{\partial S'''}{\partial \theta} \right)^2 + \frac{dH_o}{d\tilde{J}} \left(\frac{\partial S'_2}{\partial \theta} \right) + \frac{\partial H_1}{\partial \tilde{J}} \left(\frac{\partial S'_1}{\partial \theta} \right) + H_2 \right] \\
+ O(\varepsilon^3) = \overline{H}_o(\tilde{J}) + \varepsilon \overline{H}_1(\tilde{J}) + \varepsilon^2 \overline{H}_2(\tilde{J}) + O(\varepsilon^3).
\end{aligned} \tag{66}$$

From equation (66), we obtain,

$$\begin{aligned}
0(1): H_o(\tilde{J}) &= \overline{H}_o(\tilde{J}) \\
0(\varepsilon): \frac{dH_o}{d\tilde{J}} \left(\frac{\partial S'_1}{\partial \theta} \right) + H_1(\tilde{J}, \theta) &= \overline{H}_1(\tilde{J}) \\
0(\varepsilon^2): \frac{1}{2} \frac{d^2 H_o}{d\tilde{J}^2} \left(\frac{\partial S'_1}{\partial \theta} \right)^2 + \frac{dH_o}{d\tilde{J}} \left(\frac{\partial S'_2}{\partial \theta} \right) + \frac{\partial H_1}{\partial \tilde{J}} \left(\frac{\partial S'_1}{\partial \theta} \right) + H_2(\tilde{J}, \theta) &= \overline{H}_2(\tilde{J})
\end{aligned} \tag{67}$$

etc.

We thus have

$$\begin{aligned}
 0(1): \overline{H}_o(\tilde{J}) &= H_o(\tilde{J}) \\
 0(\varepsilon): \overline{H}_1(\tilde{J}) &= \omega_o(\tilde{J}) \frac{\partial}{\partial \theta} S_1'''(\theta, \tilde{J}) + H_1(\tilde{J}, \theta) \\
 0(\varepsilon^2): \overline{H}_2(\tilde{J}) &= \omega_o(\tilde{J}) \frac{\partial}{\partial \theta} S_2'''(\theta, \tilde{J}) + \frac{1}{2} \frac{d\omega_o}{dJ} \left[\frac{\partial}{\partial \theta} S_1'''(\theta, \tilde{J}) \right]^2 \\
 &\quad + \frac{\partial}{\partial J} H_1(\tilde{J}, \theta) \cdot \frac{\partial}{\partial \theta} S_1'''(\theta, \tilde{J}) + H_2(\tilde{J}, \theta)
 \end{aligned} \tag{68}$$

etc. Here, $\omega_o(\tilde{J}) \equiv \frac{dH_o}{d\tilde{J}}$.

At this point, we recognize the periodicity of the motion in θ and hence average equation (68) over θ . We then obtain for the $0(\varepsilon)$ problem in (68):

$$\overline{H}_1(\tilde{J}) = \langle H_1(\tilde{J}, \theta) \rangle \tag{69}$$

where,

$$\langle Q \rangle \equiv \frac{1}{2\pi} \int_0^{2\pi} Q d\theta. \tag{70}$$

If we Fourier expand, then, the periodic functions, with respect to θ , as follows –

$$\left. \begin{aligned}
 H_1(\tilde{J}, \theta) - \langle H_1(\tilde{J}, \theta) \rangle &= \sum_{k=1}^{\infty} A_k(\tilde{J}) e^{ik\theta} \\
 S_1'''(\theta, \tilde{J}) &= \sum_{k=1}^{\infty} B_k(\tilde{J}) e^{ik\theta}
 \end{aligned} \right\} \tag{71}$$

we obtain, from (68),

$$B_k(\tilde{J}) = \frac{i}{k\omega_o(\tilde{J})} A_k(\tilde{J}). \quad (72)$$

Using (72), (71) gives

$$S_1'''(\theta, \tilde{J}) = \sum_{k=1}^{\infty} \frac{iA_k(\tilde{J})}{k\omega_o(\tilde{J})} e^{ik\theta}. \quad (73)$$

Similarly, we obtain for the $O(\epsilon^2)$ problem in (68):

$$\overline{H}_2(\tilde{J}) = \left\langle H_2(\tilde{J}, \theta) \right\rangle + \frac{1}{2} \frac{d\omega_o}{d\tilde{J}} \left\langle \left[\frac{\partial}{\partial \theta} S_1'''(\theta, \tilde{J}) \right]^2 \right\rangle + \left\langle \frac{\partial}{\partial \tilde{J}} H_1(\tilde{J}, \theta) \cdot \frac{\partial}{\partial \theta} S_1'''(\theta, \tilde{J}) \right\rangle. \quad (74)$$

Using (74), (68) gives

$$\begin{aligned} \frac{\partial}{\partial \theta} S_2''(\theta, \tilde{J}) &= -\frac{1}{\omega_o(\tilde{J})} \left[\left\{ H_2(\tilde{J}, \theta) - \left\langle H_2(\tilde{J}, \theta) \right\rangle \right\} + \right. \\ &\quad + \frac{1}{2} \frac{d\omega_o}{d\tilde{J}} \left\{ \left[\frac{\partial}{\partial \theta} S_1'''(\theta, \tilde{J}) \right]^2 - \left\langle \left[\frac{\partial}{\partial \theta} S_1'''(\theta, \tilde{J}) \right]^2 \right\rangle \right\} \\ &\quad + \left. \left\{ \frac{\partial}{\partial \tilde{J}} H_1(\tilde{J}, \theta) \cdot \frac{\partial}{\partial \theta} S_1'''(\theta, \tilde{J}) + \right. \right. \\ &\quad \left. \left. - \left\langle \frac{\partial}{\partial \tilde{J}} H_1(\tilde{J}, \theta) \cdot \frac{\partial}{\partial \theta} S_1'''(\theta, \tilde{J}) \right\rangle \right\} \right] \end{aligned} \quad (75)$$

and so on.

The new action and angle variables are then given by (65) and the corrected frequency is given by

$$\omega(\tilde{J}) = \omega_o(\tilde{J}) + \epsilon \frac{d\overline{H}_1}{d\tilde{J}} + \epsilon^2 \frac{d\overline{H}_2}{d\tilde{J}} + \dots \quad (76)$$

Note that if ω_o is small, the effect of the perturbation can be quite large. Since the

n th-order correction has terms proportional to $1/\omega_o^n$, this difficulty gets compounded at the higher-order corrections. Usually, ω_o is small near a separatrix dividing phase-space into regions containing different types of motion. This problem, as we will see in Section 4.5, becomes much more serious for systems of n degrees of freedom ($n \geq 2$) because, then there are n fundamental frequencies. These frequencies and all their integer linear combinations occur in the denominator of the expressions for the various orders of corrections, so that, even if all the frequencies are large, a particular linear combination of them may be small. Thus, the convergence of perturbation expansions for systems of more than one degree of freedom is a very tricky problem.

EXAMPLE 3

Consider the motion of a simple pendulum executing oscillations about the downward vertical. For this problem, the unperturbed Hamiltonian is

$$H_o(p, q) = \frac{1}{2}(p^2 + \omega_o^2 q^2) \quad (77)$$

while the perturbation is

$$H_1(p, q) = -\omega_o^2 \left(\cos q - 1 + \frac{1}{2}q^2 \right). \quad (78)$$

In the action-angle formulation given by

$$q = \sqrt{\frac{2J}{\omega_o}} \sin \theta, \quad p = \sqrt{2J\omega_o} \cos \theta \quad (79)$$

(77) and (78) become

$$H_o(J) = J\omega_o. \quad (80)$$

$$H_1(J, \theta) = -\frac{1}{6}J^2 \sin^4 \theta. \quad (81)$$

We have, on averaging (80) and (81) over θ ,

$$\overline{H}_0(\tilde{J}) = \tilde{J} \omega_o. \quad (82)$$

$$\overline{H}_1(\tilde{J}) = \left\langle H_1(\tilde{J}, \theta) \right\rangle = -\frac{1}{6} \frac{\tilde{J}^2}{2\pi} \int_0^{2\pi} \sin^4 \theta \, d\theta = -\frac{1}{16} \tilde{J}^2. \quad (83)$$

We have from (82) and (83),

$$\overline{H}(\tilde{J}) = \tilde{J} \omega_o - \frac{1}{16} \varepsilon \tilde{J}^2 + O(\varepsilon^2). \quad (84)$$

The corrected frequency is then

$$\omega(\tilde{J}) = \frac{d\overline{H}}{d\tilde{J}} = \omega_o - \frac{1}{8} \varepsilon \tilde{J} + O(\varepsilon^2). \quad (85)$$

It may be verified that (85) is in agreement with the one derived previously in Example 8 in Chapter 1.

4.5. Kolmogorov-Arnol'd-Moser Theory

If a Hamiltonian is integrable, a continuous family of invariant tori exists. On introducing small perturbations, the majority of the invariant tori are preserved (the deformations being described by diffeomorphisms), while a small number break-up. As the perturbation increases the number of broken invariant tori increases, and eventually, the break-up becomes complete. The Kolmogorov-Arnol'd-Moser theory establishes what type of perturbations are likely to destroy the invariant tori and gives a sufficient condition for the existence of perturbed invariant tori. The latter condition is one of "sufficient incommensurability" of the winding number (which is the ratio of the natural frequencies of the unperturbed system) with respect to rational approximations when the perturbation is small enough. Though the KAM Theorem was a great theoretical breakthrough, its usefulness in applications is very limited. Because, according to this Theorem, any perturbation of strength greater than 10^{-48} will destroy all tori. However, numerical evidence shows the contrary.

Consider a perturbed nonlinear oscillator system with n degrees of freedom with the Hamiltonian

$$H(\mathbf{J}, \boldsymbol{\theta}) = H_o(\mathbf{J}) + \varepsilon H_1(\mathbf{J}, \boldsymbol{\theta}), \quad \varepsilon \ll 1 \quad (86)$$

where $\varepsilon H_1(\mathbf{J}, \boldsymbol{\theta})$ is a perturbation on an integrable part $H_o(\mathbf{J})$. If $H(\mathbf{J}, \boldsymbol{\theta})$ is integrable, then there must exist a canonical transformation generated by a function $S(\boldsymbol{\theta}, \mathbf{J})$, according to,

$$\mathbf{J} = \nabla_{\boldsymbol{\theta}} S'''(\boldsymbol{\theta}, \tilde{\mathbf{J}}), \quad \boldsymbol{\varphi} = \nabla_{\mathbf{J}} S'''(\boldsymbol{\theta}, \tilde{\mathbf{J}}) \quad (87)$$

such that

$$H\left(\nabla_{\boldsymbol{\theta}} S'''(\boldsymbol{\theta}, \tilde{\mathbf{J}}), \boldsymbol{\theta}\right) = \bar{H}(\tilde{\mathbf{J}}) \quad (88)$$

which is the time-independent Hamilton-Jacobi equation. Thus, the question of the continued existence of invariant tori reduces to the question of whether equation (88) can be solved. If this is possible, then the perturbation serves essentially to shift the frequencies and introduce small nonlinear harmonics to the motion.

Let us expand $\bar{H}(\tilde{\mathbf{J}})$ in a perturbation series in ε ,

$$\bar{H}(\tilde{\mathbf{J}}) = \bar{H}_0(\tilde{\mathbf{J}}) + \varepsilon \bar{H}_1(\tilde{\mathbf{J}}) \quad (89)$$

and take $S'''(\boldsymbol{\theta}, \tilde{\mathbf{J}})$ to be a near-identity transformation

$$S'''(\boldsymbol{\theta}, \tilde{\mathbf{J}}) = \tilde{\mathbf{J}} \cdot \boldsymbol{\theta} + \varepsilon S'_1(\boldsymbol{\theta}, \tilde{\mathbf{J}}). \quad (90)$$

We use the expansions (89) and (90) to expand out each term in equation (88) in a Taylor series, which then becomes

$$H_o(\tilde{\mathbf{J}}) + \varepsilon \left[\nabla_{\mathbf{J}} H_o(\tilde{\mathbf{J}}) \right] \cdot \nabla_{\boldsymbol{\theta}} S''' + \varepsilon H_1(\tilde{\mathbf{J}}, \boldsymbol{\theta}) = \bar{H}_0(\tilde{\mathbf{J}}) + \varepsilon \bar{H}_1(\tilde{\mathbf{J}}) \quad (91)$$

from which,

$$\left. \begin{aligned} 0(1) : & H_o(\tilde{\mathbf{J}}) = \bar{H}_o(\tilde{\mathbf{J}}) \\ 0(\varepsilon) : & \nabla_{\mathbf{J}} H_o(\tilde{\mathbf{J}}) \cdot \nabla_{\boldsymbol{\theta}} S''' + H_1(\tilde{\mathbf{J}}, \boldsymbol{\theta}) = \bar{H}_1(\tilde{\mathbf{J}}) \end{aligned} \right\}. \quad (92)$$

Recognizing the periodicity of the motion in $\boldsymbol{\theta}$, and averaging over $\boldsymbol{\theta}$, we obtain

from (92)

$$\overline{H}_1(\tilde{\mathbf{J}}) = \langle H_1(\tilde{\mathbf{J}}, \boldsymbol{\theta}) \rangle \quad (93)$$

where,

$$\langle Q \rangle \equiv \frac{1}{(2\pi)^n} \int_0^{2\pi} Q d\boldsymbol{\theta}. \quad (94)$$

If we Fourier expand, as follows –

$$\left. \begin{aligned} H_1(\tilde{\mathbf{J}}, \boldsymbol{\theta}) - \langle H_1(\tilde{\mathbf{J}}, \boldsymbol{\theta}) \rangle &= \sum_{\mathbf{m}(\neq 0)} H_{1_{\mathbf{m}}}(\tilde{\mathbf{J}}) e^{i\mathbf{m} \cdot \boldsymbol{\theta}} \\ S_1''(\boldsymbol{\theta}, \tilde{\mathbf{J}}) &= \sum_{\mathbf{m}(\neq 0)} S_{1_{\mathbf{m}}}''(\tilde{\mathbf{J}}) e^{i\mathbf{m} \cdot \boldsymbol{\theta}} \end{aligned} \right\} \quad (95)$$

then we obtain from (92),

$$S_1'''(\boldsymbol{\theta}, \tilde{\mathbf{J}}) = i \sum_{\mathbf{m}(\neq 0)} \frac{H_{1_{\mathbf{m}}}(\tilde{\mathbf{J}}) e^{i\mathbf{m} \cdot \boldsymbol{\theta}}}{\mathbf{m} \cdot \boldsymbol{\omega}_o(\tilde{\mathbf{J}})}$$

where $\boldsymbol{\omega}_o(\tilde{\mathbf{J}}) \equiv \nabla_j H_o(\tilde{\mathbf{J}})$ represent the frequencies of the unperturbed motions. Observe that this solution breaks down if $\boldsymbol{\omega}_o(\tilde{\mathbf{J}})$ are commensurable, i.e.,

$$\mathbf{m} \cdot \boldsymbol{\omega}_o(\tilde{\mathbf{J}}) = 0 \quad (96)$$

which describe the so-called resonant surfaces. (See Appendix for a discussion of the problem of internal resonances in nonlinearly-coupled systems.)

EXAMPLE 4

Consider a two degrees-of-freedom system

$$H = H_o(\mathbf{J}) + \sum_{m,n} H_{l_m}(\mathbf{J}) e^{i(m\theta_1 + n\theta_2)} \quad (97)$$

with an internal resonance at $\mathbf{J} = \mathbf{J}^*$, where

$$\frac{\omega_1(\mathbf{J}^*)}{\omega_2(\mathbf{J}^*)} = \frac{k}{\ell} \quad (98)$$

k and ℓ are two integers with no common divisors other than 1.

Let us now consider the dynamics of this perturbed Hamiltonian system near the internal resonance (98). For this purpose, we make a canonical transformation through a generating function

$$S'''(\boldsymbol{\omega}, \mathbf{I}) = (\ell \theta_1 - k\theta_2) I_1 + \theta_2 I_2 + \boldsymbol{\theta} \cdot \mathbf{J}^* \quad (99)$$

(99) implies

$$\begin{aligned} J_1 &= \frac{\partial S'''}{\partial \theta_1} = \ell I_1 + J_1^* \\ J_2 &= \frac{\partial S'''}{\partial \theta_2} = -kI_1 + I_2 + J_2^* \\ \varphi_1 &= \frac{\partial S'''}{\partial I_1} = (\ell \theta_1 - k\theta_2) \\ \varphi_2 &= \frac{\partial S'''}{\partial I_2} = \theta_2. \end{aligned} \quad (100)$$

Here $\boldsymbol{\varphi} = (\varphi_1, \varphi_2)$ is the new angle variable. (100) shows that φ_1 is a slowly-varying angle component which measures the deviation from resonance, and φ_2 is a rapidly-varying angle component, i.e., $\dot{\varphi}_1 \ll \dot{\varphi}_2$.

The new Hamiltonian is then given by

$$H = H_o(\mathbf{J}(I)) + \sum_{m,n} H_{l_m}(\mathbf{J}(I)) e^{i[m\varphi_1 + (km+n\ell)\varphi_2]}. \quad (101)$$

Averaging H with respect to the fast variable φ_2 , we have near a resonance surface,

$$\langle H \rangle = \frac{1}{2\pi} \int_0^{2\pi} H(I, \varphi_1, \varphi_2) d\varphi_2 = H_o(\mathbf{J}(I)) + \sum_p H_{1_{p\ell-pk}}(\mathbf{J}(I)) e^{ip\varphi_1}. \quad (102)$$

Let us next neglect the resonance harmonics by assuming

$$H_{1_{\ell-k}} \gg H_{1_{p\ell-pk}} \text{ for } p = 2, 3, \dots \quad (103)$$

and assuming further that

$$H_{1_{\ell-k}} = H_{1_{-\ell-k}} \quad (104)$$

(102) becomes

$$\langle H \rangle = H_o(\mathbf{J}(I)) + H_1(\mathbf{J}(I)) \cos \varphi_1 \quad (105)$$

where we have absorbed the factor 2 in $H_{1_{\ell-k}}$.

Let us expand H_o and H_1 about $I = \mathbf{O}$, and note, from (98) and (102), that

$$\left(\frac{\partial H_o}{\partial I_1} \right)^* = \left(\frac{\partial H_o}{\partial J_i} \right)^* \frac{\partial J_i}{\partial I_1} = \ell \omega_1(\mathbf{J}^*) - k \omega_2(\mathbf{J}^*) = 0$$

$$I_2 = \text{const.} \quad (106)$$

Assuming further that $H_{1_{\ell-k}}$ is only a slowly-varying function of I , (105) then becomes

$$\langle \bar{H} \rangle \approx \frac{1}{2} I_1^2 \left(\frac{\partial^2 H_o}{\partial I_1^2} \right)^* + H_1(\mathbf{0}) \cos \varphi_1 \quad (107)$$

where we have discarded the constant terms. (107) shows that the dynamics of a perturbed integrable Hamiltonian system near a resonance corresponds to that of a simple pendulum!

Note that since the rational numbers are dense¹⁰ (though they form a set of Lebesgue measure zero) inside the reals, the resonant surfaces are dense in the phase space. Kolmogorov (1954), Arnol'd (1963), and Moser (1963) argued that the invariant tori in the neighborhood of such resonant surfaces, are destroyed, and chaos shows up in the motion in such gaps. These gaps grow with the perturbation, and eventually fill the whole phase space. If, on the other hand, $\omega_o(\tilde{\mathbf{J}})$ are incommensurable, so that $m \cdot \omega_o(\tilde{\mathbf{J}})$ is bounded away from zero, the perturbed motion differs slightly from the unperturbed motion. The perturbed invariant tori now lie close to the unperturbed invariant tori so that the invariant tori continue to exist.

THEOREM 4.2

Let a perturbed nonlinear oscillator system be given by $H(\mathbf{J}, \theta) = H_o(\mathbf{J}) + \varepsilon H_i(\mathbf{J}, \theta)$, $\varepsilon \ll 1$. If ε is small enough and the frequencies ω_i 's are sufficiently incommensurable, the invariant tori of the perturbed system are "close to" those of the unperturbed system. However, such tori form a nowhere dense set.¹¹

On the other hand, if the system is nondegenerate so that $\omega_o(\tilde{\mathbf{J}})$ vary from torus to torus, even invariant tori with incommensurable $\omega_o(\tilde{\mathbf{J}})$ may not be able to resist destruction because of the fact that an invariant torus with commensurable $\omega_o(\tilde{\mathbf{J}})$ can exist arbitrarily close by. (This, in turn, follows from the fact that any irrational number can be approximated arbitrarily close by a rational number.)

The rational approximation of an irrational number is an age old problem that goes back to the times when one first considered measuring the diagonal of a square or the circumference of a circle. As an example of a rational approximation to an irrational number, consider the sequence of approximations of $\pi = 3.141592654\dots$, generated by the successive truncation of the decimal expansion,

¹⁰ That is, given an irrational number k , in any neighborhood of k , namely, $[k - \varepsilon, k + \varepsilon]$, one can always find a rational number no matter how small ε is. Indeed, every irrational number can be thought of as the limit of a sequence of rational numbers.

¹¹ A subset A of a set S is said to be nowhere dense in S if the complement of the closure of A is dense there. (A subset A of a set S is said to be dense in S if and only if the closure of A is S , the closure of a set A being the union of the set A with all its limit points. A point P is a limit point of a set A if there exists an infinite sequence of distinct points x_1, x_2, \dots in A such that $\lim_{n \rightarrow \infty} x_n = P$. A set A is said to be closed if it contains all of its limit points.)

$$\sigma \approx \frac{r}{s} = \frac{3}{1}, \frac{31}{10}, \frac{314}{100}, \frac{3141}{1000}, \dots \quad (108)$$

This rational approximation is very crude because the convergence rate is not faster than $1/s$:

$$\left| \sigma - \frac{r}{s} \right| < \frac{1}{s}. \quad (109)$$

It may be noted that the best rational approximations to irrational numbers are obtained by using continued fractions

$$\sigma = a_0 + \cfrac{1}{a_1 + \cfrac{1}{a_2 + \cfrac{1}{a_3 + \dots}}} \quad (110)$$

which provide a unique and convergent representation of an irrational number. The successive truncations of a continued fraction are just the following sequence of rational approximations that converge monotonically on σ :

$$\sigma_n = \frac{r_n}{s_n} = a_0 + \cfrac{1}{a_1 + \cfrac{1}{a_2 + \ddots \cfrac{1}{a_n}}}. \quad (111)$$

σ_n is called the n th-order convergent of σ . These are the best approximations in the sense that no rational r/s with $s \leq s_n$ is closer to σ than r_n/s_n . (The successive iterates r_n/s_n alternate about σ , however.) The rapidly-convergent continued fraction representation for π is

$$\pi = 3 + \cfrac{1}{7 + \cfrac{1}{15 + \cfrac{1}{1 + \cfrac{1}{292 + \dots}}}} \quad (112)$$

with the following sequence of successive approximants to π :

$$\sigma_1 = \frac{22}{7}, \sigma_2 = \frac{333}{106}, \sigma_3 = \frac{355}{113}, \text{ etc.} \quad (113)$$

The sequences σ_n converge to π , as $n \rightarrow \infty$, with successive approximants being alternately greater than or less than σ (see Figure 4.2). For these approximants, we have

$$\left| \sigma - \frac{r_n}{s_n} \right| < \frac{1}{s_n s_{n-1}} \quad (114)$$

so that the successive approximants converge as fast as $1/s^2$. Therefore, it is not difficult to approximate π by rationals.

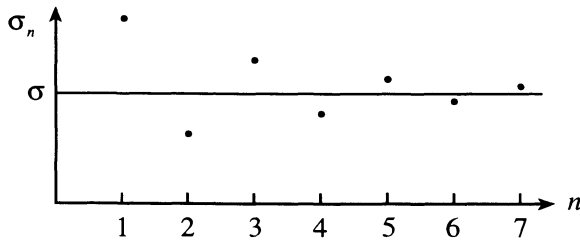


Figure 4.2. Rational approximations to π .

It turns out that the continued fraction representation converges faster if the sequence a_0, a_1, a_2, \dots diverges faster and vice versa. Transcendental numbers like π and e have very rapidly converging rational approximants. Quadratically irrational numbers, in contrast, have most slowly converging rational representations:

$$(a) \sqrt{3} = 1 + \cfrac{1}{1 + \cfrac{1}{2 + \cfrac{1}{1 + \dots}}}$$

$$(b) \sqrt{2} = 1 + \cfrac{1}{2 + \cfrac{1}{2 + \cfrac{1}{2 + \dots}}}$$

$$(c) \frac{\sqrt{5}-1}{2} = \cfrac{1}{1 + \cfrac{1}{1 + \cfrac{1}{1 + \dots}}} \quad (115)^{12}$$

12

These continued-fraction representations can be generated as follows:

(a) $x = \sqrt{3}$ can be written as

$$\begin{aligned} x &= 1 + \cfrac{2}{1+x} \\ &= 1 + \cfrac{2}{1+1+\cfrac{2}{1+1+\cfrac{2}{1+\dots}}} \end{aligned}$$

or

$$\sqrt{3} = 1 + \cfrac{1}{1 + \cfrac{1}{2 + \cfrac{1}{1 + \dots}}}$$

(b) $x = \sqrt{2}$ can be written as

$$\begin{aligned} x &= 1 + \cfrac{1}{2+x} \\ &= 1 + \cfrac{1}{2 + \cfrac{1}{2 + \cfrac{1}{2 + \dots}}} \end{aligned}$$

or

$$\sqrt{2} = 1 + \cfrac{1}{2 + \cfrac{1}{2 + \cfrac{1}{2 + \dots}}}$$

(c) Note that $\frac{\sqrt{5}-1}{2}$, called the golden mean number, can be expressed as follows:

$$\frac{\sqrt{5}-1}{2} = \frac{1+\sqrt{5}}{2} - 1$$

and $x = \frac{1+\sqrt{5}}{2}$ can be written as

$$x = 1 + \frac{x}{1+x} = 1 + \frac{1}{1 + \frac{1}{x}}$$

or

$$\frac{1+\sqrt{5}}{2} = 1 + \frac{1}{1 + \frac{1}{1 + \frac{1}{1 + \dots}}}$$

Therefore,

$$\frac{\sqrt{5}-1}{2} = \frac{1}{1 + \frac{1}{1 + \frac{1}{1 + \dots}}}$$

Thus, the golden mean number has the simplest possible continued fraction expansion.

It is of interest to note that the continued fraction for $\frac{\sqrt{5}-1}{2}$ is also generated by the Fibonacci numbers F_n , which are defined by

$$F_{n+1} = F_n + F_{n-1}; \quad F_0 = 0, \quad F_1 = 1; \quad n = 0, 1, 2, \dots$$

via a sequence of rationals W_n ,

$$W_n = \frac{F_n}{F_{n+1}} = \frac{F_n}{F_n + F_{n-1}} = \frac{1}{1 + W_{n-1}} = \frac{1}{1 + \underbrace{\frac{1}{1 + \dots}}_{n \text{ times}}}$$

which converge towards

$$W^* = \lim_{n \rightarrow \infty} W_n = \frac{1}{1 + W^*}$$

from which

$$W_{1,2}^* = \frac{\sqrt{5} \pm 1}{2}$$

These irrational numbers are, therefore, difficult to be approximated by rationals. However, they have an interesting pattern, as stated below.

THEOREM 4.3 (Lagrange)

Any periodic simple continued fraction is a quadratic irrational, and vice versa.

Thus, for any σ whatever, it is possible to find rationals r/s such that $|\sigma - r/s| < 0(s^{-2})$. Kolmogorov, Arnol'd and Moser Theory showed that tori having sufficiently irrational frequency ratios satisfying a Diophantine condition

$$\left| \frac{\omega_1}{\omega_2} - \frac{r}{s} \right| > \frac{K(\varepsilon)}{s^{5/2}} \text{ for all } r,s \quad (116)$$

where $K(\varepsilon) \rightarrow 0$ as $\varepsilon \rightarrow 0$, are preserved. The tori excluded by this condition and satisfying

$$\left| \frac{\omega_1}{\omega_2} - \frac{r}{s} \right| < \frac{K(\varepsilon)}{s^{5/2}} \text{ for some } r,s \quad (117)$$

are destroyed. Thus, the more closely the irrational frequency ratio of a torus can be approximated by a sequence of rationals, the smaller the perturbation required to destroy it. The condition (117) is less restrictive than the strict commensurability condition $n_1\omega_1 + n_2\omega_2 = 0$. However, (117) still allows a nonzero measure of the tori that are preserved. In order to see this consider all initial tori whose frequency ratios lie in the unit interval $[0,1]$ and delete from it zones of width $\frac{K}{s^{5/2}}$ about each rational r/s in $[0,1]$, which are s as many. The total length deleted thus is

$$\sum_{s=1}^{\infty} \frac{K}{s^{5/2}} s = K \sum_{s=1}^{\infty} \frac{1}{s^{3/2}} \approx K \quad (118)$$

which goes to zero as $\varepsilon \rightarrow 0$. Note that this is a crude overestimate of the "measure" of

Since, $1 > W^* > .5$, W_1^* is a spurious root and has to be discarded.

The above derivation also shows that irrational numbers may be represented by an elementary limit process resulting from a fixed-point equation.

destroyed tori because we have included separately rationals r/s whose deleted neighborhoods overlap.

On the other hand, the existence of a non-integrable Hamiltonian H in the neighborhood of every integrable Hamiltonian H_o implies that non-integrable Hamiltonians are dense in the set of analytic Hamiltonians.

4.6. Breakdown of Integrability and Criteria for Transition to Chaos

The notion of a critical value for the perturbation corresponding to the transition to chaos turns out to be a very tricky one because of the fact that the transition to chaos is never sharp though usually quite rapid. One finds irregular trajectories in regimes of predominantly regular motion and vice versa. Therefore, we have at this time only rather qualitative estimates for the "critical energy". Such estimates are deduced by using methods that are simpler to implement than a detailed trajectory-by-trajectory study.

(i) Local Criteria

Computer experiments indicate that the chaotic regions contain a dense set of unstable periodic orbits. Toda (1974) proposed a criterion to predict the onset of chaotic motion which is based on a linear stability analysis of nearby trajectories. This criterion attempts to determine the critical energy as the lowest energy at which adjacent trajectories will undergo local exponential separation in the sense of extreme sensitivity to initial conditions.

Consider a system of two degrees of freedom with a Hamiltonian given by

$$H(\mathbf{p}, \mathbf{q}) = \frac{\mathbf{p}^2}{2} + V(\mathbf{q}). \quad (119)$$

The equations of motion for this system are

$$\left. \begin{aligned} \dot{\mathbf{q}} &= \nabla_{\mathbf{p}} H = \mathbf{p} \\ \dot{\mathbf{p}} &= -\nabla_{\mathbf{q}} H = -\nabla_{\mathbf{q}} V \end{aligned} \right\}. \quad (120)$$

Consider two trajectories $(\mathbf{p}^{(1)}, \mathbf{q}^{(1)})$ and $(\mathbf{p}^{(2)}, \mathbf{q}^{(2)})$, with a separation given by

$$\xi = \mathbf{q}^{(1)} - \mathbf{q}^{(2)}, \quad \eta = \mathbf{p}^{(1)} - \mathbf{p}^{(2)}. \quad (121)$$

If the two trajectories are close to one another, one may linearize the equations of motion for ξ and η about the trajectory corresponding to the superscript (1). Thus, equations (120) give

$$\left. \begin{array}{l} \dot{\xi} = \eta \\ \dot{\eta} = -V(t) \cdot \xi \end{array} \right\} \quad (122)$$

where,

$$V(t) \equiv \left(\frac{\partial^2 V}{\partial q \partial q} \right)_{q=q^{(1)}}.$$

The local stability of this linearized motion is determined by the eigenvalues of the 4×4 matrix –

$$M = \begin{bmatrix} O & I \\ -V(t) & O \end{bmatrix}. \quad (123)$$

If any of these eigenvalues is real, the separation between the trajectories grows exponentially and the motion is unstable. On the other hand, if the eigenvalues are imaginary the motion is stable. Note that the character of the eigenvalues and hence the stability of motion can change as a function of time so that the stability properties of neighboring trajectories are assumed to follow the reference trajectory adiabatically. The eigenvalues of M are given by

$$\lambda = \pm \left[-b \pm \sqrt{b^2 - 4c} \right]^{\frac{1}{2}} \quad (124)$$

where,

$$b \equiv \frac{\partial^2 V}{\partial q_1^2} + \frac{\partial^2 V}{\partial q_2^2}, \quad c \equiv \frac{\partial^2 V}{\partial q_1^2} \frac{\partial^2 V}{\partial q_2^2} - \left(\frac{\partial^2 V}{\partial q_1 \partial q_2} \right)^2.$$

If we assume $b > 0$, the eigenvalues are all imaginary when $c > 0$ and two of them are real when $c < 0$ (c has the same sign as the Gaussian curvature of the potential V).

Thus, $c = 0$ is the boundary between the stable and unstable motion. In order to determine the lowest energy for which unstable motions exist one finds $q_1 = q_1(q_2)$ from $c = 0$ and substitutes this in the potential V to write it as a function of q_2 alone. One then minimizes the potential V with respect to q_2 to obtain the lowest energy for unstable motions (Cerjan and Reinhardt (1979)).

EXAMPLE 5

Consider the Hénon-Heiles potential

$$V(q_1, q_2) = \frac{1}{2}(q_1^2 + q_2^2) + q_1^2 q_2 - \frac{1}{3}q_2^3.$$

We have for this potential

$$c(q_1, q_2) = \frac{\partial^2 V}{\partial q_1^2} \frac{\partial^2 V}{\partial q_2^2} - \left(\frac{\partial^2 V}{\partial q_1 \partial q_2} \right)^2 = \left[1 - 4(q_1^2 + q_2^2) \right].$$

Solving $c = 0$, we obtain

$$q_1^2 = \frac{1}{4} - q_2^2.$$

Substituting this in $V(q_1, q_2)$, we obtain

$$V(q_2) = \frac{1}{8} + \frac{1}{4}q_2 - \frac{4}{3}q_2^3.$$

Putting $\frac{\partial V}{\partial q_2} = 0$, then gives

$$q_2 = \pm \frac{1}{4}$$

which then leads to the minimum value of the potential

$$V_{\min} = 0.167.$$

This compares favorably with the numerical estimate for the critical energy, namely, 0.11.

EXAMPLE 6

Consider the Toda Hamiltonian

$$H = \frac{1}{2} \left(\frac{P_1^2}{M_1} + \frac{P_2^2}{M_2} + \frac{P_3^2}{M_3} \right) + e^{-(Q_1 - Q_2)} + e^{-(Q_2 - Q_3)} + e^{-(Q_3 - Q_1)}.$$

By making a suitable canonical transformation and a change of variables, this Hamiltonian can be transformed to

$$H = \frac{1}{2} \left(\frac{p_1^2}{m_1} + \frac{p_2^2}{m_2} \right) + \frac{1}{24} \left[e^{2q_2 + 2\sqrt{3}q_1} + e^{2q_2 - 2\sqrt{3}q_1} \right] - \frac{1}{8}.$$

We have for this Hamiltonian,

$$c = \frac{\partial^2 V}{\partial q_1^2} \frac{\partial^2 V}{\partial q_2^2} - \left(\frac{\partial^2 V}{\partial q_1 \partial q_2} \right)^2 = \frac{1}{3} \left(e^{4q_2} + e^{-2q_2 + 2\sqrt{3}q_1} + e^{-2q_2 - 2\sqrt{3}q_1} \right).$$

Since $c > 0$ here, it follows that the eigenvalues of the matrix \mathbf{M} are all imaginary so that the motion is stable. However, numerical calculation (Casati and Ford (1975)) showed that irregular trajectories appear for the case $m_1 \neq m_2$.

EXAMPLE 6 shows that the Toda criterion is not always reliable. The shortcomings of the Toda criterion are –

- It is based on a test of local divergence of nearby trajectories, but the local divergence may not persist globally;
- it does not include any sense of measure as to the extent of instability, so one has no idea of how widespread is the chaos.

(ii) Local Stability vs. Global Stability

Just as local divergence of nearby trajectories may not persist globally, locally stable motion may be globally unstable. In order to see this clearly consider a linear oscillator with an "adiabatically switched" frequency (Arnol'd (1978), Tabor (1980)). One has, for this system, the following Hamiltonian

$$H = \frac{1}{2m} (p^2 + m^2 \omega^2 q^2). \quad (125)$$

The equations of motion are

$$\left. \begin{array}{l} \dot{q} = \frac{p}{m} \\ \dot{p} = -m\omega^2 q \end{array} \right\} \quad (126)$$

with the solution

$$\begin{bmatrix} q(t) \\ p(t) \end{bmatrix} = N \begin{bmatrix} q(0) \\ p(0) \end{bmatrix} \quad (127)$$

where,

$$N \equiv \begin{bmatrix} \cos \theta & \frac{1}{m\omega} \sin \theta \\ -m\omega \sin \theta & \cos \theta \end{bmatrix}, \quad \theta = \omega t$$

and $t = 0 : q = q(0), p = p(0)$.

Note that N represents an area-preserving mapping since

$$\det N = 1.$$

Let us now introduce the "adiabatic switching" of the frequency,

$$\omega = \begin{cases} \omega_1, & \text{for a period } t_1 \\ \omega_2, & \text{for a period } t_2 \end{cases} \quad (128)$$

so that the mapping N is a product of two mappings,

$$N = N_2 N_1 \quad (129)$$

where N_1 and N_2 are both area-preserving mappings given by

$$N_k = \begin{bmatrix} \cos \theta_k & \frac{1}{m\omega_k} \sin \theta_k \\ -m\omega_k \sin \theta_k & \cos \theta_k \end{bmatrix}, \quad \theta_k \equiv \omega_k t, \quad k = 1, 2.$$

The stability of the combined mapping N can be determined by examining its eigenvalues, which are given by

$$\lambda = \frac{1}{2} \left[(tr N) \pm \sqrt{(tr N)^2 - 4} \right] \quad (130)$$

where we have used the fact that

$$\det N = 1.$$

Thus, the motion is unstable if λ is real, i.e., if

$$|tr N| > 2$$

or

$$|\cos \theta_1 \cdot \cos \theta_2 - A \sin \theta_1 \cdot \sin \theta_2| > 1 \quad (131)$$

where,

$$A = \frac{1}{2} \left(\frac{\omega_2}{\omega_1} + \frac{\omega_1}{\omega_2} \right).$$

If there is no frequency-switching, i.e., if $\omega_1 = \omega_2$, (131) is not satisfied and hence the motion is locally stable.

On the other hand, if $\omega_1 \neq \omega_2$, putting

$$A = 1 + \varepsilon, \quad \varepsilon > 0$$

(131) becomes

$$|\cos(\theta_1 + \theta_2) - \varepsilon \sin \theta_1 \cdot \sin \theta_2| > 1 \quad (132)$$

which is satisfied when $(\theta_1 + \theta_2)$ is near an integer multiple of π . Thus, setting

$$\theta_1 + \theta_2 = n\pi + \delta; \quad n = 1, 2, \dots \quad (133)$$

and noting that

$$\cos(\theta_1 + \theta_2) \approx (-1)^n \cos \delta \approx (-1)^n \left(1 - \frac{\delta^2}{2}\right)$$

(132) becomes

$$\left|1 - \frac{\delta^2}{2} - \varepsilon(-1)^n \sin \theta_1 \cdot \sin \theta_2\right| > 1. \quad (134)$$

(134) is satisfied if

$$|\delta| < \sqrt{2|\varepsilon \sin \theta_1 \cdot \sin \theta_2|} \quad (135)$$

so that the motion is unstable.

Since this system shows only locally stable motions the above result demonstrates that locally stable motions can be globally unstable.

(iii) Global Criteria

Consider a Hamiltonian system given by

$$H = H_o(J) + \varepsilon \sum_{m,n} V_{mn}(J) \cos(m\theta - n\Omega t). \quad (136)$$

If the system is integrable the orbits lie on nested tori in the J, θ, t space with θ and t as the two periodic variables. Further, if the winding number of these orbits, defined by,

$$q(J) \equiv \frac{H'_o(J)}{\Omega} \quad (137)$$

is rational, the orbits are periodic and close on themselves, but when the winding number is irrational, the orbits never close on themselves and cover the tori ergodically.

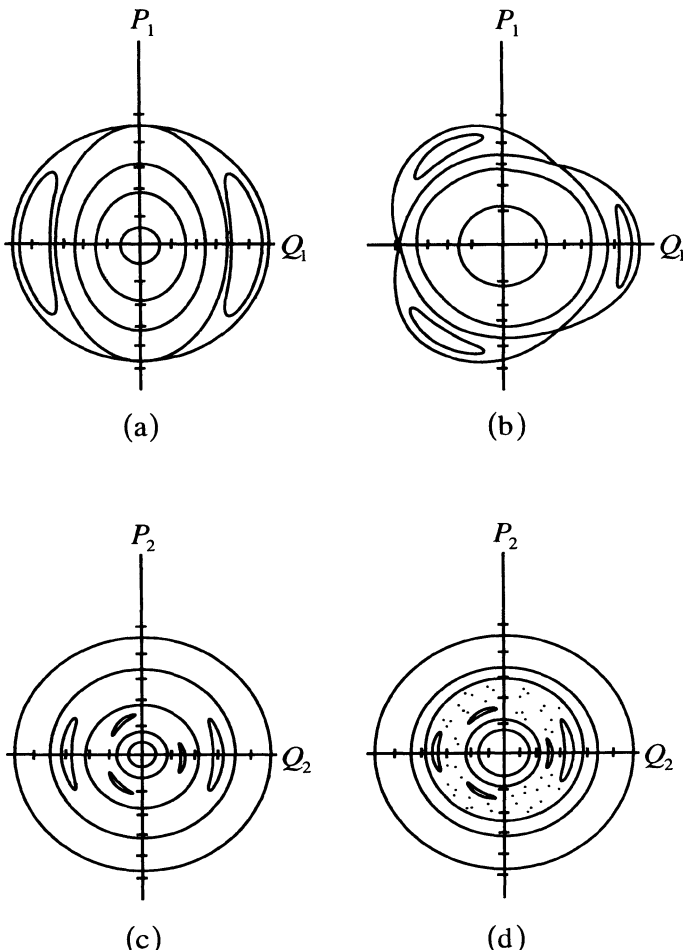


Figure 4.3. Surfaces of section of Walker-Ford resonant Hamiltonian: (a) only 2:2 resonance present ($\beta = 0$); (b) only 2:3 resonance present ($\alpha = 0$); (c) both resonances present ($\alpha = \beta = 0.02$) but widely separated at $E = 0.18$; and (d) the two resonant zones overlapping at $E = 0.2905$ and leading to the erratic splatter of points (which is generated by a trajectory started in the region of resonance overlap), (from Walker and Ford, 1969). (By courtesy of the American Physical Society.)

As the strength of the perturbation, namely ε , increases, the periodic orbits of the integrable limit are replaced by resonance regions of a finite width, each with a periodic orbit at the core and bounded by a separatrix (see Section 5.6). These resonances (and

the stochastic layers associated with them) get wider with increasing ε so that the invariant tori separating them become increasingly squeezed and distorted, and at a sufficiently large ε they disappear altogether. Chirikov (1979) proposed that the neighboring resonances then merge and overlap. The ratio of resonance width to distance between resonances is therefore the effective parameter determining the existence of the invariant tori. In the Chirikov theory, the invariant tori are taken to disappear when this overlap parameter is of order unity.

As an illustration of the resonance overlap theory, Walker and Ford (1969) considered the integrable Hamiltonian

$$H_o = J_1 + J_2 - J_1^2 - 3J_1J_2 + J_2^2$$

and investigated the effect of adding two resonances as follows –

$$H = H_o + \alpha J_1 J_2 \cos(2\theta_1 - 2\theta_2) + \beta J_1 J_2^{3/2} (2\theta_1 - 3\theta_2).$$

The effect of each resonance in isolation and together is shown in Figure 4.3. At low energies the two resonance regions are well separated. As the energy of the system is increased, the two resonance regions overlap and a random splatter of points appears on the surface of section. As the energy increases further, the size of this splatter region increases.

Chirikov's resonance-overlap criterion:

Consider a one-dimensional nonlinear oscillator perturbed by an external periodic force. On expressing the latter as a Fourier series in the action-angle variables, we then have

$$H = H_o(J) + \varepsilon \sum_{m,n} V_{mn}(J) e^{i(m\theta + n\phi)}, \quad \phi = \Omega t. \quad (138)$$

Let there be a resonance at $J = J^*$ such that

$$\frac{\omega(J^*)}{\Omega} = \frac{k}{\ell} \quad (139)$$

where,

$$\omega(J) \equiv \frac{\partial H_o}{\partial J} = -\dot{\theta}$$

and k and ℓ are integers with no common divisors other than 1. Thanks to the nonlinearity of H_o , one will of course have more than one resonance as in (139). However, in the interest of simplicity, we will consider the resonance in (139) in isolation and then investigate the behavior of the Hamiltonian (138) in its vicinity.

Thus, let us make a canonical transformation through a generating function

$$F'''(I, \theta) = (\ell\theta - k\phi)I + \theta J^*. \quad (140)$$

(140) implies

$$\left. \begin{aligned} J &= \frac{\partial F'''}{\partial \theta} = \ell I + J^* \\ \psi &= \frac{\partial F'''}{\partial I} = \ell\theta - k\phi \end{aligned} \right\}. \quad (141)$$

Note that ψ is a slowly-varying angle which measures the deviation from resonance.

The new Hamiltonian is then given by

$$\bar{H} = H_o(\ell I + J^*) + \varepsilon \sum_{m,n} V_{mn}(\ell I + J^*) e^{i[m\psi + (km+n\ell)\phi]} - k \Omega I. \quad (142)$$

Let us now average this Hamiltonian over the fast variable ϕ to eliminate the rapidly-oscillating non-resonant terms,

$$\begin{aligned} \langle \bar{H} \rangle &\equiv \frac{1}{2\pi} \int_0^{2\pi} \bar{H}(I, \psi, \phi) d\phi \\ &= H_o(\ell I + J^*) + \varepsilon \sum_p V_{p\ell, -pk}(\ell I + J^*) \cos p\psi - k \Omega J \end{aligned} \quad (143)$$

where we have assumed

$$V_{-\ell,k} = V_{\ell,-k}, \quad V_{o,o} = 0$$

and have absorbed the factor 2 in $V_{p\ell,-pk}$.

Next, let us neglect the resonance harmonics by assuming

$$V_{\ell,-k} \gg V_{p\ell,-pk} \text{ for } p = 2, 3, \dots$$

so that (143) becomes

$$\langle \bar{H} \rangle = H_o(\ell I + J^*) + \varepsilon V_{\ell,-k}(\ell I + J^*) \cos \psi - k \Omega I. \quad (144)$$

We now expand H_o and $V_{\ell,-k}$ about $I = 0$ and assume that $V_{\ell,-k}$ is only a slowly-varying function of I . Thus,

$$\langle \bar{H} \rangle = H_o(J^*) + \ell I \left(\frac{\partial H_o}{\partial I} \right)_o + \frac{\ell^2 I^2}{2} \left(\frac{\partial^2 H_o}{\partial I^2} \right)_o + \varepsilon V_{\ell,-k}(J^*) \cos \psi - k \Omega I. \quad (145)$$

Using the resonance condition (139) and dropping $H_o(J^*)$, (145) reduces to

$$\langle \bar{H} \rangle = \frac{I^2}{2M} + \varepsilon V_{\ell,-k} \cos \psi \quad (146)$$

where,

$$M^{-1} \equiv \ell^2 \left(\frac{\partial^2 H_o}{\partial I^2} \right)_o.$$

Observe that the resonant Hamiltonian (146) has the form of that for a pendulum. Noting that the separatrix in the phase plane portrait (see Figure 1.14) for the latter corresponds to

$$I_s = \pm \left(4M\varepsilon V_{\ell,-k} \right)^{1/2} \cos \frac{\psi}{2} \quad (147)$$

the resonance half-width is given by

$$\delta J^* = \ell \delta I^* = 2\ell \left(\varepsilon M V_{\ell,-k} \right)^{1/2}. \quad (148)$$

In terms of the frequency, the resonance half-width (148) corresponds to

$$\delta\omega^* = \frac{\partial\omega}{\partial J} \delta J^* = \frac{1}{\ell^2 M} 2\ell (\epsilon M V_{t,-k})^{1/2} = \frac{2}{\ell} \left(\frac{\epsilon V_{t,-k}}{M} \right)^{1/2}. \quad (149)$$

Let us now recognize that we have actually a multiplicity of resonances. Chirikov proposed that global chaos results if such resonance regions overlap, i.e., when the distance $\delta\Omega$ between resonance regions becomes smaller than the sum of the resonance half-widths. Thus, if $\delta\omega_1^*$ and $\delta\omega_2^*$ are the widths of two neighboring resonance regions and $\delta\Omega$ is their separation, then the two resonances overlap provided

$$\delta\omega_1^* + \delta\omega_2^* = \delta\Omega. \quad (150)$$

In practice, one calculates the width of each resonance region independently of the others – an approximation which is valid provided the nonlinearity is not very large¹³.

A difficulty with Chirikov's method of overlapping resonances is that it gives a critical value of the perturbation strength for a given energy whereas, in practice, one would like to know a critical energy for a given perturbation strength, (see Escande (1985), for further details).

An alternative method to predict global chaos was proposed by Greene (1979) wherein the breakup of an invariant torus having an irrational frequency ratio is related to the loss of stability of the neighboring closed orbits which have as their frequency ratios the rational iterates of the irrational frequency ratio of the torus. The application of this method to higher-dimensional systems is not clear yet.

4.7. Magnetic Island Overlap and Stochasticity in Magnetic Confinement Systems

In a controlled thermonuclear fusion device, a mixture of deuterium and tritium is raised to a sufficiently high temperature so that it can overcome the Coulomb barrier and undergo nuclear reactions and release not only large amounts of energy but enough neutrons to make tritium breeding feasible. However, since the temperatures are extreme ($\sim 10^8 K$) some non-material method of confining and thermally isolating the gas is needed and containment of the hot, ionized gas (called plasma) in an appropriate

¹³ Otherwise, the overall problem may significantly modify the width of each resonance region so that the resonance regions do not actually overlap despite the prediction of the single-resonance calculation to the contrary.

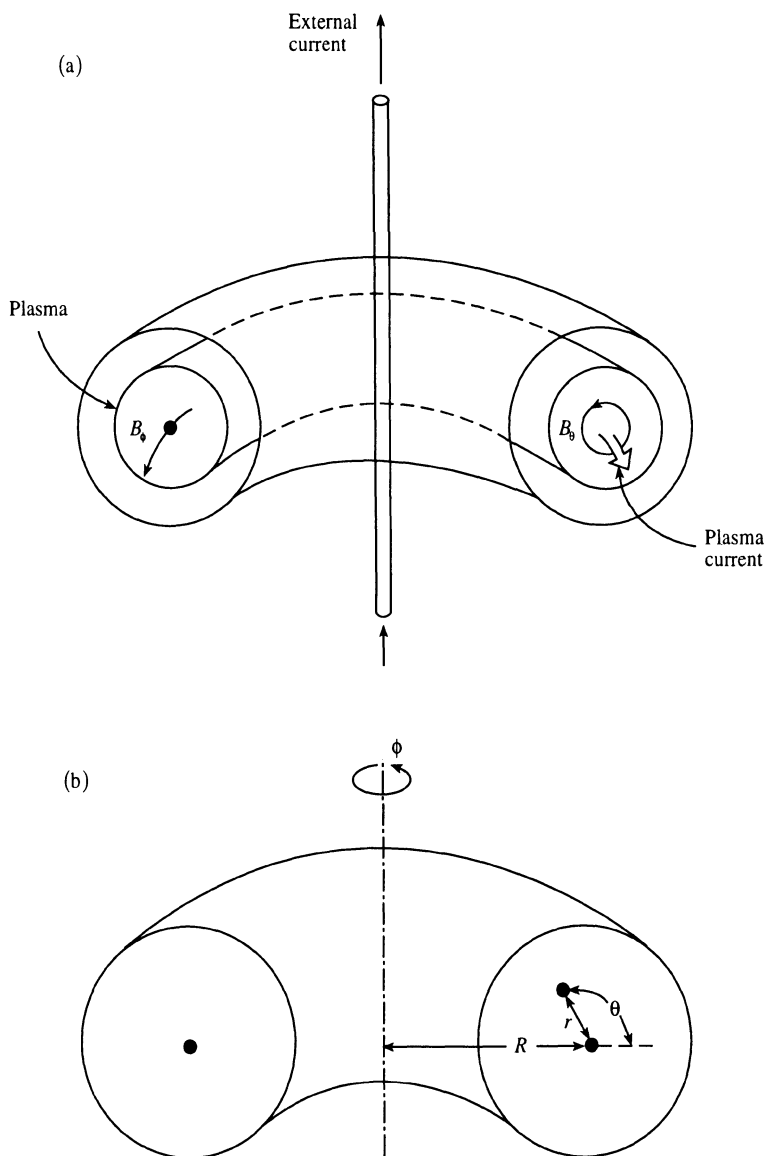


Figure 4.4. (a) A toroidal magnetic confinement system.
(b) Toroidal coordinates.

magnetic field configuration presents a promising approach¹⁴. In a strong magnetic field, the charged particles nearly follow the magnetic field lines so that the plasma confinement problem reduces to the prevention of the magnetic field lines from connecting the plasma interior to the walls of the device. At present, the tokamak is the most widely pursued magnetic-confinement device which has a plasma torus with magnetic-field producing coils wrapped around the minor circumference, in which, the magnetic field lines close on themselves around the major circumference. An external current-carrying coil produces a toroidal magnetic field B_ϕ (Figure 4.4). The toroidal current in the plasma which is induced by an external transformer creates a poloidal magnetic field B_θ . The field lines of the total magnetic field then lie on a nested set of tori.

The existence of toroidal magnetic surfaces, or at least the existence of approximate toroidal magnetic surfaces over a large fraction of the plasma volume on which the charged particles move about for a sufficient amount of time, is an essential requirement for long-term confinement. However, in confinement geometries that are not perfectly toroidally symmetric due to errors in magnetic coils or variations in the plasma current flow pattern, some of the nested set of toroidal magnetic surfaces break up into magnetic islands with stochastic separatrix layers. The magnetic field lines can then wander through the plasma chaotically in such regions thereby increasing the heat and particle loss from the plasma and degrading the plasma confinement.

There exists a close analogy between the magnetic field lines and the orbits of a Hamiltonian system. This is set forth by a characterization of the magnetic field lines in a toroidal confinement system in terms of the Hamiltonian given by

$$H = \int r B_\theta dr \quad (151)$$

and the action-angle variables

$$J = \int \frac{r}{R} B_\phi dr, \quad \theta \quad (152)$$

where R is the major radius of the torus and ϕ plays the role of the time variable. In the cylindrical approximation, i.e., to lowest order in r/R (which corresponds to $B_\phi = \text{constant}$, (White (1983))), the Hamilton's equations for the magnetic field lines are

¹⁴ However, efforts to produce a magnetically confined plasma have been considerably hampered by dynamic plasma instabilities which degrade the plasma confinement.

$$\frac{d\theta}{d\phi} = \frac{RB_\theta}{rB_\phi}, \quad \frac{dr}{d\phi} = \frac{RB_r}{B_\phi} \quad (153)$$

where,

$$B_\theta = \frac{\partial H}{\partial r}, \quad B_r = -\frac{1}{r} \frac{\partial H}{\partial \theta}. \quad (154)$$

(154), of course, implies

$$\nabla \cdot \mathbf{B} = 0 \quad (155)$$

which, in turn, means that the magnetic field lines should have the properties of area-preserving twist maps (see Section 5.4). (It may be noted that the magnetic field lines are made to twist as they progress around the torus in order to eliminate instabilities produced by the toroidal curvature.)

In terms of the action-angle variables (152), equations (153) become

$$\frac{d\theta}{d\phi} = \frac{\partial H}{\partial J}, \quad \frac{dr}{d\phi} = -\frac{\partial H}{\partial \theta}, \quad (156)$$

as expected.

In the cylindrical symmetric case, the Hamiltonian becomes

$$H = H_o(J) \quad (157)$$

so that the field lines lie on the one-dimensional tori $J = \text{constant}$ with

$$\theta = \omega\phi + \theta(0) \quad (158)$$

where,

$$\omega = \frac{\partial H_o}{\partial J}.$$

If the system in question corresponds to a nonlinear oscillator, then $\omega = \omega(J)$.

Upon introducing a symmetry-breaking perturbation $H_1(J, \theta, \phi)$ on the system (157), we have for the resulting system

$$H = H_o(J) + H_1(J, \theta, \phi). \quad (159)$$

Application of Kolmogorov, Arnol'd and Moser Theorem then shows that, for small perturbations, the magnetic field lines will continue to lie on smooth toroidal magnetic surfaces everywhere except for a finite volume proportional to $|H_1|$.

To make the discussion more precise, let us consider a perturbation consisting of a single harmonic:

$$H = H_o(J) + \varepsilon(J) \cos(m\theta + n\phi). \quad (160)$$

Let us make a canonical transformation through a generating function

$$F'''(J, \psi, \phi) = \left(J - J^* \right) \left(\frac{\psi - n\phi}{m} \right). \quad (161)$$

(161) implies

$$\left. \begin{aligned} I &= \frac{\partial F'''}{\partial \psi} = \frac{J - J^*}{m} \\ \theta &= \frac{\partial F'''}{\partial J} = \frac{\psi - n\phi}{m} \end{aligned} \right\}. \quad (162)$$

Note that ψ is a slowly-varying angle which measures the deviation from resonance.

The new Hamiltonian is then given by

$$\bar{H} = H + \frac{\partial F'''}{\partial \phi} = H - \frac{n}{m} (J - J^*). \quad (163)$$

Let us now expand \bar{H} about $I = 0$ and choose J^* such that

$$H'_o(J^*) = \frac{n}{m} \quad (164)$$

so that the terms linear in I vanish. Let us further assume that $\varepsilon(J)$ is a slowly-varying function of J ; we then obtain

$$\bar{H} = \frac{1}{2} H_o''(J^*) m^2 I^2 + \epsilon(J^*) \cos \psi. \quad (165)$$

The surfaces of constant H are then given in terms of the original variables by

$$J - J^* = \pm 2 \left[\frac{\epsilon(J^*)}{H_o''(J^*)} \right]^{1/2} \sin \left(\frac{m\theta + n\phi}{2} \right) \quad (166)$$

and show an island structure (Figure 4.5). The magnetic field lines within the magnetic island lie on a nested set of magnetic surfaces with their own magnetic axis.

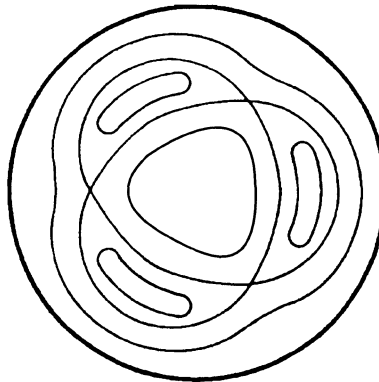


Figure 4.5. The island structure projected on to the $\phi = 0$ plane for $m = 3$.

If the perturbation consists of more than a single harmonic, then, at small amplitude, each harmonic produces narrow islands on its resonant surface, and the magnetic surfaces in the regions between the island structures remain essentially unchanged. However, if the amplitude of the multi-harmonic perturbation is increased, the islands become bigger and overlap with one another, and the magnetic field in the overlap regions becomes very stochastic, i.e., the magnetic field lines in such regions become ergodic.

4.8. Appendix

THE PROBLEM OF INTERNAL RESONANCES IN NONLINEARLY-COUPLED SYSTEMS

The problem of internal resonances in nonlinearly-coupled oscillator systems is of much interest in connection with redistribution of energy among the various natural modes of such a system. This energy sharing is usually brought about by resonant interactions among the natural modes of the system. The nature of the couplings among the latter plays a crucial role in such interactions.

Systems such as the one considered by Fermi *et al.* (1955), namely, a system of one-dimensional weakly-nonlinearly-coupled chain of oscillator with the Hamiltonian of the form

$$H = \frac{1}{2} \sum_{k=1}^{64} (p_k^2 + \omega_k^2 q_k^2) + \epsilon \sum_{j,k,l=1}^{64} A_{jkl} q_j q_k q_l. \quad (\text{A.1})$$

ϵ being chosen sufficiently small so that the nonlinear terms can be treated as a small perturbation on a primarily linear problem, are nonergodic for small values of ϵ so that they are amenable to analysis using a perturbation theory. One property of such systems is that there is, in general, no effective energy sharing without an internal resonance. One would therefore desire to solve analytically a nonlinear system of equations possessing internal resonances and show that the latter lead to an effective exchange of energy.

Jackson (1963) and Ford and Waters (1963) made such attempts for a problem of two coupled oscillators. In a straightforward perturbation theory, as we saw in Section 4.5, the internal resonances lead to the problem of small divisors which are associated

with terms having as factors $\left(\sum_{k=1}^N n_k \omega_k \right)^{-1}$. Jackson (1963) tried to remove the small divisors in the solution by introducing shifts in the frequencies ω_k so that the corrected frequencies were no longer commensurable. However, the frequency shifts arise whether or not small divisors in the solution exist so that this approach cannot describe adequately what happens during an internal resonance – such as the manner in which energy is exchanged among the oscillators.

In order to describe the internal resonances adequately, it is obvious that such a perturbation theory should include modulations of the amplitudes of the oscillators along with any corrections to the frequencies ω_k – which were most clearly seen in the numerical calculations of Ford and Waters (1963). Some perturbation theories for treating the problem of internal resonances in a system of two nonlinearly-coupled

oscillators adequately have been given by Kabakow (1968), van der Burgh (1976), Verhulst (1979), and Kevorkian (1980). These studies revealed that whereas the actions of the individual oscillators are nearly constant when the system does not show an internal resonance, the total action of the uncoupled system is found to be nearly constant when the system undergoes an internal resonance and allows for a significant redistribution of action between the two oscillators. The problem of higher-order internal resonances was considered by Shivamoggi and Varma (1988). The approximate invariant mentioned above to exist for the lowest-order internal resonance was found to continue to hold for the higher-order internal resonances.

Let us consider a system of two nonlinearly-coupled oscillators given by the generalized Hénon-Heiles Hamiltonian –

$$H = \frac{1}{2}(p_1^2 + p_2^2) + \frac{1}{2}(\omega_1^2 q_1^2 + \omega_2^2 q_2^2) + \varepsilon \left(q_1^2 q_2 - \frac{1}{3} q_2^3 \right) \quad (\text{A.2})$$

where ε is a small parameter characterizing the weakness of the couplings between the two oscillators.

Hamilton's equations for the two oscillators then follow from (A.2) –

$$\dot{q}_{1_u} + \omega_1^2 q_1 = -\varepsilon \cdot 2q_1 q_2 \quad (\text{A.3})$$

$$\dot{q}_{2_u} + \omega_2^2 q_2 = \varepsilon(q_2^2 - q_1^2). \quad (\text{A.4})$$

Let us look for solutions of the form

$$\begin{aligned} q_1(t; \varepsilon) &= A_1(t_1, t_2, \dots) \cos \phi_1(t, t_1, t_2, \dots) + \varepsilon u_1(t, t_1, t_2, \dots) + \varepsilon^2 u_2(t, t_1, t_2, \dots) + \dots \\ q_2(t; \varepsilon) &= A_2(t_1, t_2, \dots) \cos \phi_2(t, t_1, t_2, \dots) + \varepsilon v_1(t, t_1, t_2, \dots) + \varepsilon^2 v_2(t, t_1, t_2, \dots) + \dots \end{aligned} \quad (\text{A.5})$$

where $t_n = \varepsilon^n t$ are the slow-time scales that characterize the slow variations introduced by the weak couplings among the oscillators, and

$$\phi_s = \omega_s t - \theta_s(t_1, t_2); \quad s = 1, 2.$$

Note that (A.5) expresses the fact that the solutions of equations (A.3) and (A.4), for $\varepsilon \ll 1$, are very nearly equal to the set of harmonics represented by the first terms in the expansions of (A.5) which they would be if $\varepsilon \equiv 0$. The perturbations induced by the terms of $O(\varepsilon)$ in equations (A.3) and (A.4) may then be expected to show up as slow

variations in the A 's, and θ 's and as higher harmonics in the solution through the u_k 's and v_k 's.

In order to fully specify the solution, one needs to specify some initial conditions. However, we will not do this contingent upon the recognition that the periodic solutions derived in the following correspond to very special initial conditions.

Using (A.5), equations (A.3) and (A.4) give

$$\begin{aligned}
 & \left(2\epsilon\omega_1 A_1 \theta_{l_1} + 2\epsilon^2 \omega_1 A_1 \theta_{l_2} + 2\epsilon^3 \omega_1 A_1 \theta_{l_3} - \epsilon^2 A_1 \theta_{l_1}^2 + \right. \\
 & \quad \left. - 2\epsilon^3 A_1 \theta_{l_1} \theta_{l_2} + \epsilon^2 A_{l_1} + 2\epsilon^3 A_{l_1 l_2} \right) \cos \phi_1 + \\
 & + \left(-2\epsilon\omega_1 A_{l_1} - 2\epsilon^2 \omega_1 A_{l_2} - 2\epsilon^3 \omega_1 A_{l_3} + 2\epsilon^2 A_{l_1} \theta_{l_1} + \right. \\
 & \quad \left. + 2\epsilon^3 A_{l_2} \theta_{l_1} + 2\epsilon^3 A_{l_1} \theta_{l_2} + \epsilon^2 A_1 \theta_{l_1} + 2\epsilon^3 A_1 \theta_{l_1 l_2} \right) \sin \phi_1 + \\
 & + \epsilon(u_{l_1} + \omega_1^2 u_1) + \epsilon^2(2u_{l_1} + u_{l_2} + \omega_1^2 u_2) + \\
 & + \epsilon^3(2u_{l_2} + 2u_{l_1} + u_{l_1 l_2} + u_{l_3} + \omega_1^2 u_3) + \dots \\
 & = -\epsilon(2A_1 A_2 \cos \phi_1 \cos \phi_2) - \epsilon^2(2A_1 \cos \phi_1 \cdot v_1 + 2A_2 \cos \phi_2 \cdot u_1) \\
 & \quad - \epsilon^3(2A_1 \cos \phi_1 \cdot v_2 + 2A_2 \cos \phi_2 \cdot u_2 + 2u_1 v_1) + \dots
 \end{aligned} \tag{A.6}$$

$$\begin{aligned}
& \left(2\varepsilon\omega_2 A_2 \theta_{2_{1_1}} + 2\varepsilon^2 \omega_2 A_2 \theta_{2_{1_2}} + 2\varepsilon^3 \omega_2 A_2 \theta_{2_{1_3}} - \varepsilon^2 A_2 \theta_{2_{1_1}}^2 \right. \\
& \quad \left. - 2\varepsilon^3 A_2 \theta_{2_{1_1}} \theta_{2_{1_2}} + \varepsilon^2 A_{2_{1_1}} + 2\varepsilon^3 A_{2_{1_1}} \right) \cos \phi_2 + \\
& + \left(-2\varepsilon\omega_2 A_{2_{1_1}} - 2\varepsilon^2 \omega_2 A_{2_{1_2}} - 2\varepsilon^3 \omega_2 A_{2_{1_3}} + 2\varepsilon^2 A_{2_{1_1}} \theta_{2_{1_1}} + \right. \\
& \quad \left. + 2\varepsilon^3 A_{2_{1_2}} \theta_{2_{1_1}} + 2\varepsilon^3 A_{2_{1_1}} \theta_{2_{1_2}} + \varepsilon^2 A_2 \theta_{2_{1_1}} + 2\varepsilon^3 A_2 \theta_{2_{1_1}} \right) \sin \phi_2 + \\
& + \varepsilon \left(v_{1_u} + \omega_2^2 v_1 \right) + \varepsilon^2 \left(2v_{1_{1_1}} + v_{2_u} + \omega_2^2 v_2 \right) + \\
& + \varepsilon^3 \left(2v_{1_{1_2}} + 2v_{2_{1_1}} + v_{1_{1_1}} + v_{3_u} + \omega_2^2 v_3 \right) + \dots \\
& = \varepsilon \left(A_2^2 \cos^2 \phi_2 - A_1^2 \cos^2 \phi_1 \right) + \varepsilon^2 \left(2A_2 \cos \phi_2 \cdot v_1 - 2A_1 \cos \phi_1 \cdot u_1 \right) \\
& \quad + \varepsilon^3 \left(v_1^2 + 2A_2 \cos \phi_2 \cdot v_2 - u_1^2 - 2A_1 \cos \phi_1 \cdot u_2 \right) + \dots
\end{aligned} \tag{A.7}$$

By equating the coefficients of $\sin \phi_1, \cos \phi_1, \sin \phi_2, \cos \phi_2$ and the rest to zero separately, one obtains from equations (A.6) and (A.7) to $0(\varepsilon)$:

$$\theta_{1_{1_1}} = 0 \tag{A.8}$$

$$A_{1_{1_1}} = 0 \tag{A.9}$$

$$u_{1_u} + \omega_1^2 u_1 = -2A_1 A_2 \cos \phi_1 \cdot \cos \phi_2 \tag{A.10}$$

$$\theta_{2_{1_1}} = 0 \tag{A.11}$$

$$A_{2_{1_1}} = 0 \tag{A.12}$$

$$v_{1_u} + \omega_2^2 v_1 = A_2^2 \cos^2 \phi_2 - A_1^2 \cos^2 \phi_1 \tag{A.13}$$

On solving equations (A.8)-(A.13), one obtains

$$\begin{aligned} u_1 &= \frac{A_1 A_2}{(\omega_1 + \omega_2)^2 - \omega_1^2} \cos(\phi_1 + \phi_2) + \frac{A_1 A_2}{(\omega_1 - \omega_2)^2 - \omega_1^2} \cos(\phi_1 - \phi_2) \\ v_1 &= \frac{A_2^2 - A_1^2}{2\omega_2^2} - \frac{A_2^2}{6\omega_2^2} \cos 2\phi_2 + \frac{A_1^2/2}{(2\omega_1)^2 - \omega_2^2} \cos 2\phi_1 \end{aligned} \quad (\text{A.14})$$

where the A 's and θ 's are constants to $O(\varepsilon)$. Thus, in general the oscillators move as if they were uncoupled effectively, and there is no appreciable energy sharing among them. Note, however, that this solution breaks down when $\omega_2 = 2\omega_1$ which leads to small divisors in (A.14). This condition corresponds to an internal resonance in the system which, as we will see below, leads to considerable energy sharing in the system.

Let us now try to determine whether there are any higher-order resonances in this system. Towards this end, let us first assume that the lowest-order resonance is inoperative, i.e., $\omega_2 \neq 2\omega_1$. Then, to $O(\varepsilon^2)$, equations (A.6) and (A.7) give

$$\begin{aligned} 2\omega_1 A_1 \theta_{l_2} \cos \phi_1 - 2\omega_1 A_{l_2} \sin \phi_1 + 2u_{l_1} + u_{2_n} + \omega_1^2 u_2 \\ = -2A_1 \cos \phi_1 \cdot v_1 - 2A_2 \cos \phi_2 \cdot u_1 \end{aligned} \quad (\text{A.15})$$

$$\begin{aligned} 2\omega_2 A_2 \theta_{2_n} \cos \phi_2 - 2\omega_2 A_{2_n} \sin \phi_2 + 2v_{l_1} + v_{2_n} + \omega_2^2 v_2 \\ = 2A_2 \cos \phi_2 \cdot v_1 - 2A_1 \cos \phi_1 \cdot u_1 \end{aligned} \quad (\text{A.16})$$

Using (A.8), (A.9), (A.11), (A.12) and (A.14), equations (A.15) and (A.16) become

$$\begin{aligned} 2\omega_1 A_1 \theta_{l_2} \cos \phi_1 - 2\omega_1 A_{l_2} \sin \phi_1 + u_{2_n} + \omega_1^2 u_2 \\ = - \left[A_1 \frac{A_2^2 - A_1^2}{\omega_2^2} + \frac{A_1^3/2}{(2\omega_1)^2 - \omega_2^2} + \frac{A_1 A_2^2}{(\omega_1 + \omega_2)^2 - \omega_1^2} + \frac{A_1 A_2^2}{(\omega_1 - \omega_2)^2 - \omega_1^2} \right] \cos \phi_1 + \\ - \left[\frac{A_1 A_2^2}{6\omega_2^2} - \frac{A_1 A_2^2}{(\omega_1 + \omega_2)^2 - \omega_1^2} \right] \cos(\phi_1 + 2\phi_2) + \\ - \left[\frac{A_1 A_2^2}{6\omega_2^2} - \frac{A_1 A_2^2}{(\omega_1 - \omega_2)^2 - \omega_1^2} \right] \cos(\phi_1 - 2\phi_2) - \frac{A_1^3/2}{(2\omega_1)^2 - \omega_2^2} \cos 3\phi_1 \end{aligned} \quad (\text{A.17})$$

$$\begin{aligned}
& 2\omega_2 A_2 \theta_{1_2} \cos \phi_2 - 2\omega_2 A_{2_{1_2}} \sin \phi_2 + v_{2_n} + \omega_2^2 v_2 \\
& = \left[A_2 \frac{A_2^2 - A_1^2}{2\omega_2^2} - \frac{A_2^3}{6\omega_2^2} - \frac{A_1^2 A_2}{(\omega_1 + \omega_2)^2 - \omega_1^2} + \right. \\
& \quad \left. - \frac{A_1^2 A_2}{(\omega_1 - \omega_2)^2 - \omega_1^2} \right] \cos \phi_2 - \frac{A_2^3}{6\omega_2^2} \cos 3\phi_2 + \\
& - \left[\frac{A_1^2 A_2 / 2}{(2\omega_1)^2 - \omega_2^2} - \frac{A_1^2 A_2}{(\omega_1 + \omega_2)^2 - \omega_1^2} \right] \cos(2\phi_1 + \phi_2) + \\
& - \left[\frac{A_1^2 A_2 / 2}{(2\omega_1)^2 - \omega_2^2} - \frac{A_1^2 A_2}{(\omega_1 - \omega_2)^2 - \omega_1^2} \right] \cos(2\phi_1 - \phi_2)
\end{aligned} \tag{A.18}$$

from which, one obtains

$$\theta_{1_2} = -\frac{1}{2\omega_1} \left[\frac{A_2^2 - A_1^2}{2\omega_2^2} + \frac{A_1^2 / 2}{(2\omega_1)^2 - \omega_2^2} + \frac{A_2^2}{(\omega_1 + \omega_2)^2 - \omega_1^2} + \frac{A_2^2}{(\omega_1 - \omega_2)^2 - \omega_1^2} \right] \tag{A.19}$$

$$A_{1_{1_2}} = 0 \tag{A.20}$$

$$\begin{aligned}
u_2 &= \left[\frac{A_1 A_2^2}{6\omega_2^2} - \frac{A_1 A_2^2}{(\omega_1 + \omega_2)^2 - \omega_1^2} \right] \frac{\cos(\phi_1 + 2\phi_2)}{(\omega_1 + 2\omega_2)^2 - \omega_1^2} + \\
&+ \left[\frac{A_1 A_2^2}{6\omega_2^2} - \frac{A_1 A_2^2}{(\omega_1 - \omega_2)^2 - \omega_1^2} \right] \frac{\cos(\phi_1 - 2\phi_2)}{(\omega_1 - 2\omega_2)^2 - \omega_1^2} + \\
&+ \frac{A_1^3 / 2}{(2\omega_1)^2 - \omega_2^2} \frac{\cos 3\phi_1}{8\omega_1^2}
\end{aligned} \tag{A.21}$$

$$\theta_{2_{1_2}} = \frac{1}{2\omega_2} \left[\frac{A_2^2 - A_1^2}{\omega_2^2} - \frac{A_2^2}{6\omega_2^2} - \frac{A_1^2}{(\omega_1 + \omega_2)^2 - \omega_1^2} - \frac{A_1^2}{(\omega_1 - \omega_2)^2 - \omega_1^2} \right] \tag{A.22}$$

$$A_{2_{i_2}} = 0 \quad (\text{A.23})$$

$$\begin{aligned} v_2 = & \frac{A_2^3}{6\omega_2^2} \frac{\cos 3\phi_2}{8\omega_2^2} + \left[\frac{A_1^2 A_2 / 2}{(2\omega_1)^2 - \omega_2^2} - \frac{A_1^2 A_2}{(\omega_1 + \omega_2)^2 - \omega_1^2} \right] \frac{\cos(2\phi_1 + \phi_2)}{(2\omega_1 + \omega_2)^2 - \omega_2^2} + \\ & + \left[\frac{A_1^2 A_2 / 2}{(2\omega_1)^2 - \omega_2^2} - \frac{A_1^2 A_2}{(\omega_1 - \omega_2)^2 - \omega_1^2} \right] \frac{\cos(2\phi_1 - \phi_2)}{(2\omega_1 - \omega_2)^2 - \omega_2^2} \end{aligned} \quad (\text{A.24})$$

Inspection of (A.21) and (A.24) shows that in the $O(\varepsilon^2)$ problem, one has an internal resonance at $\omega_2 = \omega_1$. This corresponds to the case considered by Hénon and Heiles (1964).

Next, let us determine the internal resonances in the $O(\varepsilon^3)$ problem. First, let us assume that there are no internal resonances in the $O(\varepsilon)$ and $O(\varepsilon^2)$ problems, i.e., $\omega_2 \neq 2\omega_1$ and $\omega_2 \neq \omega_1$. Then, to $O(\varepsilon^3)$, equations (A.6) and (A.7) give

$$\begin{aligned} & 2\omega_1 A_1 \theta_{1_{i_3}} \cos \phi_1 - 2\omega_1 A_{1_{i_3}} \sin \phi_1 + 2u_{1_{i_2}} + u_{1_{i_1}} + u_{3_{i_3}} + \omega_1^2 u_3 \\ & = -2A_1 \cos \phi_1 \cdot v_2 - 2A_2 \cos \phi_2 \cdot u_2 - 2u_1 v_1 \end{aligned} \quad (\text{A.25})$$

$$\begin{aligned} & 2\omega_2 A_2 \theta_{2_{i_3}} \cos \phi_2 - 2\omega_2 A_{2_{i_3}} \sin \phi_2 + 2v_{1_{i_2}} + v_{1_{i_1}} + v_{3_{i_3}} + \omega_2^2 v_3 \\ & = v_1^2 + 2A_2 \cos \phi_2 \cdot v_2 - u_1^2 - 2A_1 \cos \phi_1 \cdot u_1 \end{aligned} \quad (\text{A.26})$$

Using (A.8), (A.9), (A.11), (A.12), (A.14), (A.19)-(A.24), and proceeding as before, one obtains from equations (A.25) and (A.26) –

$$\theta_{1_{i_3}} = 0 \quad (\text{A.27})$$

$$A_{1_{i_3}} = 0 \quad (\text{A.28})$$

$$\begin{aligned}
u_3 = & \left[\frac{2A_1 A_2 (\omega_1 + \omega_2)}{(\omega_1 + \omega_2)^2 - \omega_1^2} \left\{ \frac{1}{2\omega_1} \left[\frac{A_2^2 - A_1^2}{\omega_2^2} + \frac{A_1^2/2}{(2\omega_1)^2 - \omega_2^2} + \frac{A_2^2}{(\omega_1 + \omega_2)^2 - \omega_1^2} + \right. \right. \right. \right. \\
& \left. \left. \left. \left. + \frac{A_2^2}{(\omega_1 - \omega_2)^2 - \omega_1^2} \right] - \frac{1}{2\omega_2} \left[\frac{A_2^2 - A_1^2}{\omega_2^2} - \frac{A_2^2}{6\omega_2^2} - \frac{A_1^2}{(\omega_1 + \omega_2)^2 - \omega_1^2} - \frac{A_1^2}{(\omega_1 - \omega_2)^2 - \omega_1^2} \right] \right\} \right. \\
& \left. - \left\{ \frac{A_1^3 A_2 / 2}{(2\omega_1)^2 - \omega_2^2} - \frac{A_1^3 A_2}{(\omega_1 + \omega_2)^2 - \omega_1^2} \right\} \frac{1}{(2\omega_1 + \omega_2)^2 - \omega_2^2} + \right. \\
& \left. - \left\{ \frac{A_1 A_2^3}{6\omega_2^2} - \frac{A_1 A_2^3}{(\omega_1 + \omega_2)^2 - \omega_1^2} \right\} \frac{1}{(\omega_1 + 2\omega_2)^2 - \omega_1^2} + \right. \\
& \left. - \frac{A_2^2 - A_1^2}{\omega_2^2} \frac{A_1 A_2}{(\omega_1 + \omega_2)^2 - \omega_1^2} + \frac{A_2^2}{6\omega_2^2} \frac{A_1 A_2}{(\omega_1 - \omega_2)^2 - \omega_1^2} + \right. \\
& \left. - \frac{A_1^2 / 2}{(2\omega_1)^2 - \omega_2^2} \frac{A_1 A_2}{(\omega_1 - \omega_2)^2 - \omega_1^2} \right] \frac{\cos(\phi_1 + \phi_2)}{\omega_1^2 - (\omega_1 + \omega_2)^2} + \right. \\
& \left. + \left[\frac{2A_1 A_2 (\omega_1 - \omega_2)}{(\omega_1 - \omega_2)^2 - \omega_1^2} \left\{ \frac{1}{2\omega_1} \left[\frac{A_2^2 - A_1^2}{\omega_2^2} + \frac{A_1^2/2}{(2\omega_1)^2 - \omega_2^2} + \frac{A_2^2}{(\omega_1 + \omega_2)^2 - \omega_1^2} \right] + \right. \right. \right. \\
& \left. \left. \left. + \frac{A_2^2}{(\omega_1 - \omega_2)^2 - \omega_1^2} \right] + \frac{1}{2\omega_2} \left[\frac{A_2^2 - A_1^2}{\omega_2^2} - \frac{A_2^2}{6\omega_2^2} - \frac{A_1^2}{(\omega_1 + \omega_2)^2 - \omega_1^2} - \frac{A_1^2}{(\omega_1 - \omega_2)^2 - \omega_1^2} \right] \right\} \\
& \left. - \left\{ \frac{A_1^3 A_2 / 2}{(2\omega_1)^2 - \omega_2^2} - \frac{A_1^3 A_2}{(\omega_1 - \omega_2)^2 - \omega_1^2} \right\} \frac{1}{(2\omega_1 - 2\omega_2)^2 - \omega_2^2} + \right. \\
& \left. - \left\{ \frac{A_1 A_2^3}{6\omega_2^2} - \frac{A_1 A_2^3}{(\omega_1 - \omega_2)^2 - \omega_1^2} \right\} \frac{1}{(\omega_1 - 2\omega_2)^2 - \omega_1^2} + \right. \\
& \left. + \frac{A_2^2}{6\omega_2^2} \frac{A_1 A_2}{(\omega_1 + \omega_2)^2 - \omega_1^2} - \frac{A_1^2 / 2}{(2\omega_1)^2 - \omega_2^2} \frac{A_1 A_2}{(\omega_1 - 2\omega_2)^2 - \omega_1^2} + \right]
\end{aligned}$$

$$\begin{aligned}
& - \frac{A_2^2 - A_1^2}{\omega_2^2} \frac{A_1 A_2}{(\omega_1 - \omega_2)^2 - \omega_1^2} \left[\frac{\cos(\phi_1 - \phi_2)}{\omega_1^2 - (\omega_1 - \omega_2)^2} + \right. \\
& + \left[- \frac{A_1 A_2^3}{48 \omega_2^4} - \left\{ \frac{A_1 A_2^3}{6 \omega_2^2} - \frac{A_1 A_2^3}{(\omega_1 + \omega_2)^2 - \omega_1^2} \right\} \frac{1}{(\omega_1 + 2\omega_2)^2 - \omega_1^2} + \right. \\
& \quad \left. + \frac{A_2^2}{6 \omega_2^2} \frac{A_1 A_2}{(\omega_1 + \omega_2)^2 - \omega_1^2} \right] \frac{\cos(\phi_1 + 3\phi_2)}{\omega_1^2 - (\omega_1 + 3\omega_2)^2} \\
& + \left[- \frac{A_1 A_2^3}{48 \omega_2^4} - \left\{ \frac{A_1 A_2^3}{6 \omega_2^2} - \frac{A_1 A_2^3}{(\omega_1 - \omega_2)^2 - \omega_1^2} \right\} \frac{1}{(\omega_1 - 2\omega_2)^2 - \omega_1^2} + \right. \\
& \quad \left. + \frac{A_2^2}{6 \omega_2^2} \frac{A_1 A_2}{(\omega_1 - \omega_2)^2 - \omega_1^2} \right] \frac{\cos(\phi_1 - 3\phi_2)}{\omega_1^2 - (\omega_1 - 3\omega_2)^2} + \\
& + \left[- \left\{ \frac{A_1^3 A_2 / 2}{(2\omega_1)^2 - \omega_2^2} - \frac{A_1^3 A_2}{(\omega_1 + \omega_2)^2 - \omega_1^2} \right\} \frac{1}{(2\omega_1 + \omega_2)^2 - \omega_2^2} + \right. \\
& \quad \left. - \frac{1}{16\omega_1^2} \frac{A_2 A_1^3}{(2\omega_1)^2 - \omega_2^2} - \frac{A_1^2 / 2}{(2\omega_1)^2 - \omega_2^2} \frac{A_1 A_2}{(\omega_1 + \omega_2)^2 - \omega_1^2} \right] \frac{\cos(3\phi_1 + \phi_2)}{\omega_1^2 - (3\omega_1 + \omega_2)^2} + \\
& + \left[- \left\{ \frac{A_1^3 A_2 / 2}{(2\omega_1)^2 - \omega_2^2} - \frac{A_1^3 A_2}{(\omega_1 - \omega_2)^2 - \omega_1^2} \right\} \frac{1}{(2\omega_1 - \omega_2)^2 - \omega_2^2} - \frac{1}{16\omega_1^2} \frac{A_2 A_1^3}{(2\omega_1)^2 - \omega_2^2} + \right. \\
& \quad \left. - \frac{A_1^2 / 2}{(2\omega_1)^2 - \omega_2^2} \frac{A_1 A_2}{(\omega_1 - \omega_2)^2 - \omega_1^2} \right] \frac{\cos(3\phi_1 - \phi_2)}{\omega_1^2 - (3\omega_1 - \omega_2)^2} \tag{A.29}
\end{aligned}$$

$$\theta_{2_{\nu_i}} = 0 \tag{A.30}$$

$$A_{2_{\nu_i}} = 0 \tag{A.31}$$

$$\begin{aligned}
v_3 = & - \left[\frac{4A_2^2}{6\omega_2^2} \left\{ \frac{A_2^2 - A_1^2}{\omega_2^2} - \frac{A_2^2}{6\omega_2^2} - \frac{A_1^2}{(\omega_1 + \omega_2)^2 - \omega_1^2} + \right. \right. \\
& \left. \left. - \frac{A_1^2}{(\omega_1 - \omega_2)^2 - \omega_1^2} \right\} + \frac{A_2^4}{48\omega_2^4} - \frac{A_2^2(A_2^2 - A_1^2)}{6\omega_2^4} + \right. \\
& \left. - \left\{ \frac{A_1^2 A_2^2}{6\omega_2^2} - \frac{A_1^2 A_2^2}{(\omega_1 - \omega_2)^2 - \omega_1^2} \right\} \frac{1}{(\omega_1 + 2\omega_2)^2 - \omega_1^2} + \right. \\
& \left. - \left\{ \frac{A_1^2 A_2^2}{6\omega_2^2} - \frac{A_1^2 A_2^2}{(\omega_1 - \omega_2)^2 - \omega_1^2} \right\} \frac{1}{(\omega_1 - 2\omega_2)^2 - \omega_1^2} + \right. \\
& \left. - \frac{A_1^2 A_2^2}{\{(\omega_1 + \omega_2)^2 - \omega_1^2\} \{(\omega_1 - \omega_2)^2 - \omega_1^2\}} \right] \frac{\cos 2\phi_2}{3\omega_2^2} + \\
& + \left[\frac{2A_1^2}{(2\omega_1)^2 - \omega_2^2} \left\{ \frac{A_2^2 - A_1^2}{\omega_2^2} + \frac{A_1^2/2}{(2\omega_1)^2 - \omega_2^2} + \frac{A_2^2}{(\omega_1 + \omega_2)^2 - \omega_1^2} + \right. \right. \\
& \left. \left. + \frac{A_2^2}{(\omega_1 - \omega_2)^2 - \omega_1^2} \right\} + \left\{ \frac{A_1^2 A_2^2/2}{(2\omega_1)^2 - \omega_2^2} - \frac{A_1^2 A_2^2}{(\omega_1 + \omega_2)^2 - \omega_1^2} \right\} \times \right. \\
& \times \frac{1}{(2\omega_1 + \omega_2)^2 - \omega_2^2} + \left\{ \frac{A_1^2 A_2^2/2}{(2\omega_1)^2 - \omega_2^2} - \frac{A_1^2 A_2^2}{(\omega_1 - \omega_2)^2 - \omega_1^2} \right\} \times \\
& \times \frac{1}{(2\omega_1 - \omega_2)^2 - \omega_2^2} - \frac{1}{2\omega_2^2} \frac{A_1^2(A_2^2 - A_1^2)}{(2\omega_1)^2 - \omega_2^2} + \frac{1}{16\omega_1^2} \frac{A_1^4}{(2\omega_1)^2 - \omega_2^2} \\
& \left. - \frac{A_1^2 A_2^2}{\{(\omega_1 + \omega_2)^2 - \omega_1^2\} \{(\omega_1 - \omega_2)^2 - \omega_1^2\}} \right] \frac{\cos 2\phi_1}{\omega_2^2 - (2\omega_1)^2} +
\end{aligned}$$

$$\begin{aligned}
& - \left[\frac{A_2^4}{48\omega_2^4} + \frac{A_2^4}{72\omega_2^4} \right] \frac{\cos 4\phi_2}{15\omega_2^2} + \\
& + \left[\left\{ \frac{A_1^2 A_2^2 / 2}{(2\omega_1)^2 - \omega_2^2} - \frac{A_1^2 A_2^2}{(\omega_1 + \omega_2)^2 - \omega_1^2} \right\} \frac{1}{(2\omega_1 + \omega_2)^2 - \omega_2^2} + \right. \\
& - \frac{1}{12\omega_2^2} \frac{A_1^2 A_2^2}{(2\omega_1)^2 - \omega_2^2} - \frac{A_1^2 A_2^2 / 2}{\{(\omega_1 + \omega_2)^2 - \omega_1^2\}^2} - \left\{ \frac{A_1^2 A_2^2}{6\omega_2^2} - \frac{A_1^2 A_2^2}{(\omega_1 + \omega_2)^2 - \omega_1^2} \right\} \times \\
& \times \left. \frac{1}{(\omega_1 + 2\omega_2)^2 - \omega_1^2} \right] \frac{\cos 2(\phi_1 + \phi_2)}{\omega_2^2 - 4(\omega_1 + \omega_2)^2} + \\
& + \left[\left\{ \frac{A_1^2 A_2^2 / 2}{(2\omega_1)^2 - \omega_2^2} - \frac{A_1^2 A_2^2}{(\omega_1 - \omega_2)^2 - \omega_1^2} \right\} \frac{1}{(2\omega_1 - \omega_2)^2 - \omega_2^2} + \right. \\
& - \frac{1}{12\omega_2^2} \frac{A_1^2 A_2^2}{(2\omega_1)^2 - \omega_2^2} - \frac{A_1^2 A_2^2 / 2}{\{(\omega_1 - \omega_2)^2 - \omega_1^2\}^2} + \\
& - \left. \left\{ \frac{A_1^2 A_2^2}{6\omega_2^2} - \frac{A_1^2 A_2^2}{(\omega_1 - \omega_2)^2 - \omega_1^2} \right\} \frac{1}{(\omega_1 - 2\omega_2)^2 - \omega_1^2} \right] \frac{\cos 2(\phi_1 - \phi_2)}{\omega_2^2 - 4(\omega_1 - \omega_2)^2} + \\
& + \frac{1}{\omega_2^2} \left[\frac{A_2^2 - A_1^2}{4\omega_2^4} + \frac{A_2^4}{72\omega_2^4} + \frac{A_1^4 / 8}{\{(2\omega_1)^2 - \omega_2^2\}^2} + \right. \\
& - \frac{A_1^2 A_2^2 / 2}{\{(\omega_1 + \omega_2)^2 - \omega_1^2\}^2} - \frac{A_1^2 A_2^2 / 2}{\{(\omega_1 - \omega_2)^2 - \omega_1^2\}^2} \left. \right] + \\
& + \left[\frac{A_1^4 / 8}{\{(2\omega_1)^2 - \omega_2^2\}} - \frac{1}{16\omega_1^2} \frac{A_1^4}{(2\omega_1)^2 - \omega_2^2} \right] \frac{\cos 4\phi_1}{\omega_2^2 - (4\omega_1)^2} \tag{A.32}
\end{aligned}$$

Inspection of (A.29) and (A.32) shows that in the $0(\varepsilon^3)$ problem, one has internal

Inspection of (A.29) and (A.32) shows that in the $O(\epsilon^3)$ problem, one has internal resonances at $\omega_2 = \frac{2}{3}\omega_1$ and $\omega_2 = 4\omega_1$.

These higher-order resonances, as is confirmed in the following, become weaker successively so that they do not lead to as much exchange of energy among the oscillators as the first-order resonance does. Let us first consider the latter case.

(i) First-Order Internal Resonance ($\omega_2 = 2\omega_1$):

Let us write the $O(\epsilon)$ terms on the right in equations (A.6) and (A.7) as follows:

$$\begin{aligned} -2A_1 A_2 \cos \phi_1 \cdot \cos \phi_2 &= -2A_1 A_2 \cos \phi_1 \cdot \cos[(\phi_2 - 2\phi_1) + 2\phi_1] \\ &= -A_1 A_2 \cos(\phi_2 - 2\phi_1) \cdot \cos \phi_1 + \\ &\quad - A_1 A_2 \cos(\phi_2 - 2\phi_1) \cdot \cos 3\phi_1 + \\ &\quad + A_1 A_2 \sin(\phi_2 - 2\phi_1) \cdot \sin \phi_1 + \\ &\quad + A_1 A_2 \sin(\phi_2 - 2\phi_1) \cdot \sin 3\phi_1 \\ -A_1^2 \cos^2 \phi_1 &= -\frac{A_1^2}{2} - \frac{A_1^2}{2} \cos(\phi_2 - 2\phi_1) \cdot \cos \phi_2 + \\ &\quad - \frac{A_1^2}{2} \sin(\phi_2 - 2\phi_1) \cdot \sin \phi_2 \end{aligned}$$

Using these expressions, equations (A.6) and (A.7) give

$$2\omega_1 A_1 \theta_{1_n} = -A_1 A_2 \cos(\phi_2 - 2\phi_1) \quad (\text{A.33})$$

$$-2\omega_1 A_{1_n} = A_1 A_2 \sin(\phi_2 - 2\phi_1) \quad (\text{A.34})$$

$$\begin{aligned} u_{1_n} + \omega_1^2 u_1 &= -A_1 A_2 \cos(\phi_2 - 2\phi_1) \cdot \cos 3\phi_1 + \\ &\quad + A_1 A_2 \sin(\phi_2 - 2\phi_1) \cdot \sin 3\phi_1 \end{aligned} \quad (\text{A.35})$$

$$2\omega_2 A_2 \theta_{2_n} = -\frac{A_1^2}{2} \cos(\phi_2 - 2\phi_1) \quad (\text{A.36})$$

$$-2\omega_2 A_{2_n} = -\frac{A_1^2}{2} \sin(\phi_2 - 2\phi_1) \quad (\text{A.37})$$

$$\nu_{1_n} + \omega_2^2 \nu_1 = \frac{1}{2} (A_2^2 - A_1^2) + \frac{1}{2} A_2^2 \cos 2\phi_2 \quad (\text{A.38})$$

Solving equations (A.35) and (A.38), one obtains

$$\begin{aligned} u_1 &= \frac{A_1 A_2}{8\omega_1^2} [\cos(\phi_2 - 2\phi_1) \cdot \cos 3\phi_1 - \sin(\phi_2 - 2\phi_1) \cdot \sin 3\phi_1] \\ \nu_1 &= \frac{A_2^2 - A_1^2}{2\omega_2^2} - \frac{A_2^2}{6\omega_2^2} \cos 2\phi_2 \end{aligned} \quad (\text{A.39})$$

Observe that (A.39) no longer exhibits any small divisors.
Also, one obtains from equations (A.34) and (A.37),

$$\omega_1 A_1 A_{1_n} + 2\omega_2 A_2 A_{2_n} = 0 \quad (\text{A.40a})$$

or

$$\frac{1}{2} \omega_1 A_1^2 + \omega_2 A_2^2 = \text{const} \quad (\text{A.40b})$$

which dictates the manner in which action is exchanged among the oscillators under an internal resonance. Note that (A.40) is only an approximate constant of motion, because it has been derived under conditions of weak nonlinearities in the coupled system, and this constant of motion will cease to exist when the nonlinearities become strong. If one introduces the action J_k by

$$J_k \equiv A_k^2 \omega_k \quad (\text{A.41})$$

then, (A.40)b becomes

$$J_1 \omega_1 + J_2 \omega_2 = \text{const} = E \quad (\text{A.42})$$

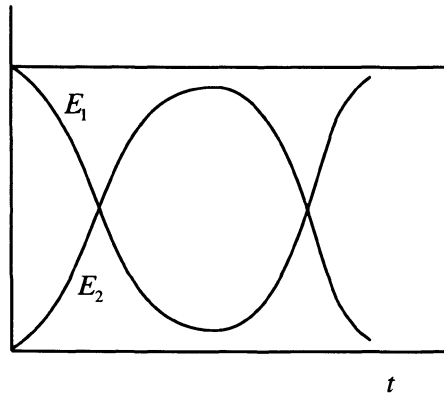


Figure 4.6. Variation of the individual actions with time during the first-order internal resonance (due to Ford and Waters (1963)). (By courtesy of the American Institute of Physics.)

This result was first given by Kabakow (1968) and van der Burgh (1976), and is similar to the “adelphic” integral discussed by Whittaker (1944). That the action exchange at the first-order resonance ($\omega_2 = 2\omega_1$) follows according to $E_1 + E_2 = \text{constant} = E$, where $E_k \equiv J_k \omega_k$, was demonstrated by the computer calculations of Ford and Waters (1963), as shown in Figure 4.6.

(ii) Second-Order Internal Resonance ($\omega_2 = \omega_1$):

Let us write

$$\begin{aligned}\cos(\phi_1 - 2\phi_2) &= \cos 2(\phi_1 - \phi_2) \cos \phi_1 + \sin 2(\phi_1 - \phi_2) \sin \phi_1 \\ \cos(2\phi_1 - \phi_2) &= \cos 2(\phi_1 - \phi_2) \cos \phi_2 - \sin 2(\phi_1 - \phi_2) \sin \phi_2\end{aligned}$$

on the right hand sides in equations (A.17) and (A.18); one obtains therefrom –

$$\begin{aligned}2\omega_1 A_1 \theta_{1_{12}} &= - \left[A_1 \frac{A_2^2 - A_1^2}{\omega_2^2} + \frac{A_1^3/2}{(2\omega_1)^2 - \omega_2^2} + \frac{A_1 A_2^2}{(\omega_1 + \omega_2)^2 - \omega_1^2} + \frac{A_1 A_2^2}{(\omega_1 - \omega_2)^2 - \omega_1^2} \right] + \\ &\quad - \left[\frac{A_1 A_2^2}{6\omega_2^2} - \frac{A_1 A_2^2}{(\omega_1 - \omega_2)^2 - \omega_1^2} \right] \cos 2(\phi_1 - \phi_2)\end{aligned} \tag{A.43}$$

$$-2\omega_1 A_{l_{12}} = -\left[\frac{A_1 A_2^2}{6\omega_2^2} - \frac{A_1 A_2^2}{(\omega_1 - \omega_2)^2 - \omega_1^2} \right] \sin 2(\phi_1 - \phi_2) \quad (\text{A.44})$$

$$u_{2_n} + \omega_1^2 u_2 = -\frac{A_1^3/2}{(2\omega_1)^2 - \omega_2^2} \cos 3\phi_1 - \left[\frac{A_1 A_2^2}{6\omega_2^2} - \frac{A_1 A_2^2}{(\omega_1 + \omega_2)^2 - \omega_1^2} \right] \cos(\phi_1 + 2\phi_2) \quad (\text{A.45})$$

$$\begin{aligned} 2\omega_2 A_2 \theta_{2_{12}} &= -\left[\frac{A_1^2 A_2}{\omega_2^2} - \frac{5}{6} \frac{A_2^3}{\omega_2^2} + \frac{A_1^2 A_2}{(\omega_1 + \omega_2)^2 - \omega_1^2} + \frac{A_1^2 A_2}{(\omega_1 - \omega_2)^2 - \omega_1^2} \right] + \\ &\quad - \left[\frac{A_1^2 A_2/2}{(2\omega_1)^2 - \omega_2^2} - \frac{A_1^2 A_2}{(\omega_1 - \omega_2)^2 - \omega_1^2} \right] \cos 2(\phi_1 - \phi_2) \end{aligned} \quad (\text{A.46})$$

$$-2\omega_2 A_{2_{12}} = \left[\frac{A_1^2 A_2/2}{(2\omega_1)^2 - \omega_2^2} - \frac{A_1^2 A_2}{(\omega_1 - \omega_2)^2 - \omega_1^2} \right] \sin 2(\phi_1 - \phi_2) \quad (\text{A.47})$$

$$v_{2_n} + \omega_2^2 v_2 = -\frac{A_2^3}{6\omega_2^2} \cos 3\phi_2 - \left[\frac{A_1^2 A_2/2}{(2\omega_1)^2 - \omega_2^2} - \frac{A_1^2 A_2}{(\omega_1 + \omega_2)^2 - \omega_1^2} \right] \cos(2\phi_1 + \phi_2) \quad (\text{A.48})$$

Solving equations (A.45) and (A.46), one obtains

$$\begin{aligned} u_2 &= \frac{A_1^3/16\omega_1^2}{(2\omega_1)^2 - \omega_2^2} \cos 3\phi_1 - \left[\frac{A_1 A_2^2}{6\omega_2^2} - \frac{A_1 A_2^2}{(\omega_1 + \omega_2)^2 - \omega_1^2} \right] \frac{\cos(\phi_1 + 2\phi_2)}{\omega_1^2 - (2\omega_1 + \omega_2)^2} \\ v_2 &= \frac{A_2^3}{48\omega_2^4} \cos 3\phi_2 - \left[\frac{A_1^2 A_2/2}{(2\omega_1)^2 - \omega_2^2} - \frac{A_1^2 A_2}{(\omega_1 + \omega_2)^2 - \omega_1^2} \right] \frac{\cos(2\phi_1 + \phi_2)}{\omega_2^2 - (2\omega_1 + \omega_2)^2} \end{aligned} \quad (\text{A.49})$$

Next, one obtains from equations (A.44) and (A.47),

$$2\omega_1 A_1 A_{l_{12}} + 2\omega_2 A_2 A_{2_{12}} = 0 \quad (\text{A.50a})$$

or

$$\omega_1 A_1^2 + \omega_2 A_2^2 = \text{const} \quad (\text{A.50b})$$

or

$$J_1 \omega_2 + J_2 \omega_2 = \text{const} \quad (\text{A.51})$$

which is the same as the one, namely (A.42), deduced for the first-order resonance. This integral was also found by Verhulst (1979) and Kevorkian (1980). The existence of this approximate constant of motion has already been confirmed by the numerical calculations of Ford and Waters (1963) – see Figure 4.7.

Comparison of (A.44) and (A.47) with (A.34) and (A.37) shows that the action exchange at the first-order resonance is much greater than that at the second-order resonance. The numerical calculations of Ford and Waters (1968), also showed that (see Figure 4.7) the action exchange at the second-order resonance was weaker than that at the first-order resonance.

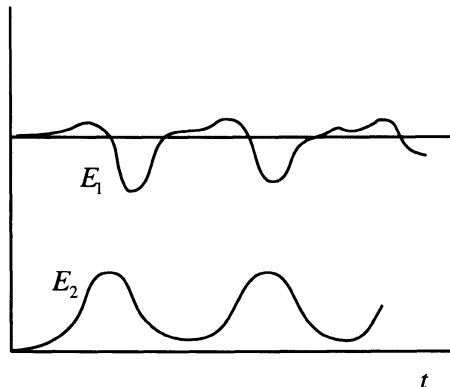


Figure 4.7. Variation of the individual actions with time during the second-order internal resonance (due to Ford and Waters, (1963)). (By courtesy of the American Institute of Physics.)

(iii) Third-Order Resonances $\left(\omega_2 = \frac{2}{3} \omega_1 \text{ and } \omega_2 = 4\omega_1 \right)$:

For the resonance $\omega_2 = \frac{2}{3} \omega_1$, let us write

$$\cos(\phi_1 - 3\phi_2) = \cos(3\phi_2 - 2\phi_1)\cos\phi_1 - \sin(3\phi_2 - 2\phi_1)\sin\phi_1$$

$$\cos(2\phi_1 - 2\phi_2) = \cos(3\phi_2 - 2\phi_1)\cos\phi_2 - \sin(3\phi_2 - 2\phi_1)\sin\phi_2$$

on the right hand sides of equations (A.25) and (A.26); one obtains therefrom –

$$2\omega_1 A_1 \theta_{I_3} = \left[-\frac{A_1 A_2^3}{48\omega_2^4} - \left\{ \frac{A_1 A_2^3}{6\omega_2^2} - \frac{A_1 A_2^3}{(\omega_1 - \omega_2)^2 - \omega_1^2} \right\} \frac{1}{(\omega_1 - 2\omega_2)^2 - \omega_1^2} + \right. \\ \left. + \frac{A_2^2}{6\omega_2^2} \frac{A_1 A_2}{(\omega_1 - \omega_2)^2 - \omega_1^2} \right] \cos(3\phi_2 - 2\phi_1) \quad (\text{A.52})$$

$$-2\omega_1 A_{I_3} = -\left[-\frac{A_1 A_2^3}{48\omega_2^4} - \left\{ \frac{A_1 A_2^3}{6\omega_2^2} - \frac{A_1 A_2^3}{(\omega_1 - \omega_2)^2 - \omega_1^2} \right\} \frac{1}{(\omega_1 - 2\omega_2)^2 - \omega_1^2} + \right. \\ \left. + \frac{A_2^2}{6\omega_2^2} \frac{A_1 A_2}{(\omega_1 - \omega_2)^2 - \omega_1^2} \right] \sin(3\phi_2 - 2\phi_1) \quad (\text{A.53})$$

$$2\omega_2 A_2 \theta_{I_3} = \left[\left\{ \frac{A_1^2 A_2^2 / 2}{(2\omega_1)^2 - \omega_2^2} - \frac{A_1^2 A_2^2}{(\omega_1 - \omega_2)^2 - \omega_1^2} \right\} \frac{1}{(2\omega_1 - \omega_2)^2 - \omega_2^2} + \right. \\ \left. - \frac{1}{12\omega_2^2} \frac{A_1^2 A_2^2}{(2\omega_1)^2 - \omega_2^2} - \frac{A_1^2 A_2^2 / 2}{\{(\omega_1 - \omega_2)^2 - \omega_1^2\}^2} + \right. \\ \left. - \left\{ \frac{A_1^2 A_2^2}{6\omega_2^2} - \frac{A_1^2 A_2^2}{(\omega_1 - \omega_2)^2 - \omega_1^2} \right\} \frac{1}{(\omega_1 - 2\omega_2)^2 - \omega_1^2} \right] \cos(3\phi_2 - 2\phi_1) \quad (\text{A.54})$$

$$\begin{aligned}
 -2\omega_2 A_{2_{n_3}} = & \left[\left\{ \frac{A_1^2 A_2^2 / 2}{(2\omega_1)^2 - \omega_2^2} - \frac{A_1^2 A_2^2}{(\omega_1 - \omega_2)^2 - \omega_1^2} \right\} \frac{1}{(2\omega_1 - \omega_2)^2 - \omega_2^2} + \right. \\
 & - \frac{1}{12\omega_2^2} \frac{A_1^2 A_2^2}{(2\omega_1)^2 - \omega_2^2} - \frac{A_1^2 A_2^2}{\{(\omega_1 - \omega_2)^2 - \omega_1^2\}^2} + \\
 & \left. - \left\{ \frac{A_1^2 A_2^2}{6\omega_2^2} - \frac{A_1^2 A_2^2}{(\omega_1 - \omega_2)^2 - \omega_1^2} \right\} \frac{1}{(\omega_1 - 2\omega_2)^2 - \omega_1^2} \right] \sin(3\phi_2 - 2\phi_1)
 \end{aligned} \tag{A.55}$$

One obtains from equations (A.53) and (A.55)

$$\omega_1 A_1 A_{1_{n_3}} + \frac{2}{3} \omega_2 A_2 A_{2_{n_3}} = 0 \tag{A.56a}$$

or

$$\omega_1 A_1^2 + \frac{2}{3} \omega_2 A_2^2 = \text{const} \tag{A.56b}$$

or

$$J_1 \omega_1 + J_2 \omega_2 = \text{const} \tag{A.57}$$

as before, in (A.42) and (A.51).

Next, for the resonance $\omega_2 = 4\omega_1$, let us write

$$\begin{aligned}
 \cos(3\phi_1 - \phi_2) &= \cos(\phi_2 - 4\phi_1) \cos \phi_1 - \sin(\phi_2 - 4\phi_1) \sin \phi_1 \\
 \cos 4\phi_1 &= \cos(\phi_2 - 4\phi_1) \cos \phi_2 + \sin(\phi_2 - 4\phi_1) \sin \phi_2
 \end{aligned}$$

on the right hand sides of equations (A.25) and (A.26); one obtains therefrom –

$$2\omega_1 A_1 \theta_{1_{i_3}} = - \left[\left\{ \frac{A_1^3 A_2 / 2}{(2\omega_1)^2 - \omega_2^2} - \frac{A_1^3 A_2}{(\omega_1 - \omega_2)^2 - \omega_1^2} \right\} \frac{1}{(2\omega_1 - \omega_2)^2 - \omega_2^2} + \frac{1}{16\omega_1^2} \frac{A_2 A_1^3}{(2\omega_1)^2 - \omega_2^2} + \frac{A_1^2}{(2\omega_1)^2 - \omega_2^2} \frac{A_1 A_2}{(\omega_1 - \omega_2)^2 - \omega_1^2} \right] \cos(\phi_2 - 4\phi_1) \quad (\text{A.58})$$

$$-2\omega_1 A_{1_{i_3}} = \left[\left\{ \frac{A_1^3 A_2 / 2}{(2\omega_1)^2 - \omega_2^2} - \frac{A_1^3 A_2}{(\omega_1 - \omega_2)^2 - \omega_1^2} \right\} \frac{1}{(2\omega_1 - \omega_2)^2 - \omega_2^2} + \frac{1}{16\omega_1^2} \frac{A_2 A_1^3}{(2\omega_1)^2 - \omega_2^2} + \frac{A_1^2 / 2}{(2\omega_1)^2 - \omega_2^2} \frac{A_1 A_2}{(\omega_1 - \omega_2)^2 - \omega_1^2} \right] \sin(\phi_2 - 4\phi_1) \quad (\text{A.59})$$

$$2\omega_2 A_2 \theta_{2_{i_3}} = \left[\frac{A_1^4 / 8}{\{(2\omega_1)^2 - \omega_2^2\}^2} - \frac{1}{16\omega_1^2} \frac{A_1^4}{(2\omega_1)^2 - \omega_2^2} \right] \cos(\phi_2 - 4\phi_1) \quad (\text{A.60})$$

$$-2\omega_2 A_{2_{i_3}} = \left[\frac{A_1^4 / 8}{\{(2\omega_1)^2 - \omega_2^2\}^2} - \frac{1}{16\omega_1^2} \frac{A_1^4}{(2\omega_1)^2 - \omega_2^2} \right] \sin(\phi_2 - 4\phi_1) \quad (\text{A.61})$$

One obtains from equations (A.59) and (A.61),

$$\omega_1 A_1 A_{1_{i_3}} + 4\omega_2 A_2 A_{2_{i_3}} = 0 \quad (\text{A.62a})$$

or

$$\omega_1 A_1^2 + 4\omega_2 A_2^2 = \text{const} \quad (\text{A.62b})$$

or

$$J_1 \omega_1 + J_2 \omega_2 = \text{const} \quad (\text{A.63})$$

as before, in (A.42), (A.51) and (A.57). It thus appears that this result remains valid for resonances of all order in the system (A.2).

CHAPTER 5

CHAOS IN CONSERVATIVE SYSTEMS

By Liouville's Theorem, the solution flow for a conservative Hamiltonian system preserves volumes in phase space. Poincaré's Recurrence Theorem then shows that most solution curves in phase space come back infinitely often arbitrarily close to the initial points. This implies that conservative systems can not asymptotically collapse onto any lower-dimensional attractors. However, conservative systems can exhibit a rich variety of structures with chaotic and regular orbits interspersed among each other, (Helleman, 1980). Chaotic motion appears via homoclinic intersections of unstable manifolds.

5.1. Phase-Space Dynamics of Conservative Systems

Consider a deterministic dynamical system governed by an evolution equation of the form

$$\frac{dx(t)}{dt} = F(x(t), \mu) \quad (1)$$

where x is a vector in R^n , and F may depend on a parameter μ .

Let us denote by $x(y, t)$ the solution of equation (1) with initial condition –

$$t = 0 : x = y \quad (2)$$

For conservative Hamiltonian systems, we have

$$\sum_{i=1}^n \frac{\partial F_i(x, \mu)}{\partial x_i} = 0 \quad (3)$$

so that the volumes in the phase space are preserved locally by the flow $x(t) = \Phi_t(y)$, (Liouville's Theorem).

If \bar{x} is an equilibrium point of equation (1) and λ_k are the eigenvalues of the Jacobian matrix $\left[\frac{\partial F_i(\bar{x}, \mu)}{\partial x_j} \right]$ at this equilibrium point, Liouville's Theorem shows that

$$\sum_{k=1}^N \operatorname{Re}(\lambda_k) = 0. \quad (4)$$

Thus, all fixed points of a conservative Hamiltonian system are either centers or saddles.

5.2. Poincaré's Surface of Section

Consider again the deterministic dynamical system given by equation (1), with the function F periodic in t with period, say T . In this case, though the system is deterministic, keeping track of the evolution continuously in time from every initial state leads to a complex tangle of trajectories that can hardly give any insight into the behavior of the system. For the latter purpose, it proves useful to convert the continuous flow $x = \phi_t(y)$ near a periodic orbit into the iterations of a discrete mapping, in the neighborhood of a fixed point, given by

$$x_{n+1} = \phi_T(x_n). \quad (5)$$

(5) implies a stroboscopic sampling of the state vectors x_0, x_1, x_2, \dots at times $t = 0, T, 2T, \dots$, respectively. This discrete mapping is also much less complicated than the continuous flow while still retaining useful information about the flow, and hence, provides a more efficient means to explore the evolution of the dynamical system¹.

Poincaré (1892) pointed out that this idea can be pursued further to give a general convenient technique for quantifying and rationalizing the breakdown of integrability and the motion in the gaps between destroyed invariant tori. This geometric approach, which considers the topological structure of dynamical trajectories in phase space, is based on Liouville's Theorem implying that the evolution of a conservative Hamiltonian system in the phase space can be considered as an area-preserving mapping of the energy surface onto itself. An area-preserving map is obtained by assigning to any orbit in a constant-energy surface a sequence of points in which the orbit intersects a given

¹ Indeed, a dynamical system may be defined as a transformation $f: X \rightarrow X$ on a metric space (see Footnote 1 in Chapter 6) X . The orbit of a point $x \in X$ is then the sequence $\{f^{[n]}(x)\}_{n=0}^{\infty}$.

hyperplane with the same orientation, i.e., if \hat{n} is the normal to the hyperplane, $\hat{n} \cdot \dot{x}$ must have the same sign. Given a periodic orbit on the $(2n-1)$ dimensional energy surface, one picks a point x_o on it and chooses an $2(n-1)$ dimensional manifold S called the Poincaré surface of section passing through x_o and transverse to the periodic orbit. Then, through a point x near x_o on S there passes an orbit which will come back and hit the section near x , but not necessarily at x because not every orbit near x_o need be periodic. Thus, the Hamiltonian flow defines an invertible mapping, ϕ , of a neighborhood of x_o on the section S onto itself, (see Figure 5.1), and this map can be determined by recording the position of the trajectory on successive crossings of a surface S . The Poincaré surface of section method, therefore, reduces a continuous time system of dimensionality n to a discrete map of dimensionality $(n-1)$, which can be a simpler situation to deal with.

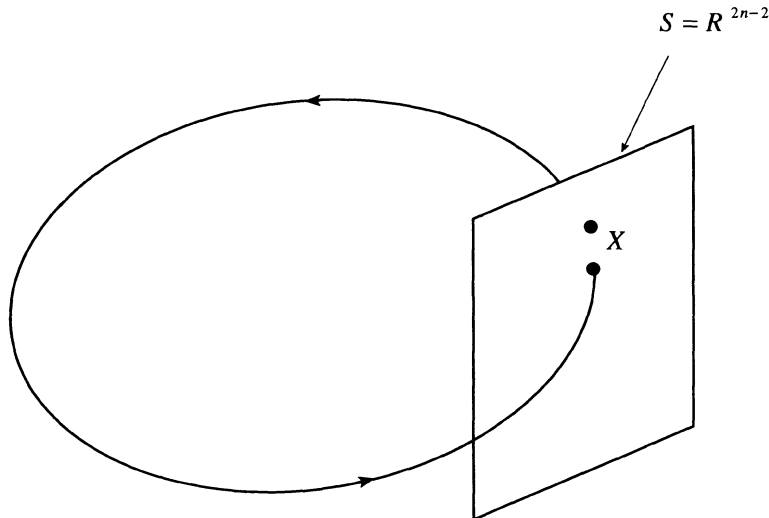


Figure 5.1. Poincaré return map $\phi: S \rightarrow S$.

DEFINITION: If $W \subset S$ is an open set containing x_o on W , the map associating points in W with the points of first return in S defines a diffeomorphism² $\phi: S \rightarrow S$ called the Poincaré return map. The point x_o is called a fixed point of this mapping, if $x_o = \phi(x_o)$.

² A diffeomorphism is a one-to-one map $y = F(x)$ where the function $F(x)$ and its inverse are both differentiable.

One can study the asymptotic behavior of orbits near the periodic orbit by studying the iterates $\phi^{[n]}(\mathbf{x})$ under the Poincaré mapping, (see Dowell (1984) for a good account of the details of the method of construction of Poincaré maps).

Consider a two-degree-of-freedom system with a four-dimensional phase space (x, y, p_x, p_y) , which has within it a three-dimensional energy surface $E(x, y, p_x)$. Let a surface of section S_x be the intersection of E with $y = 0$ and with (x, p_x) as coordinates. The system will then be represented by a point on S_x . Starting out from a point, say X_o , on S_x , the system trajectory will cross it repeatedly because, in a bounded system, y will repeatedly oscillate through zero, and at each new crossing the whole plane S_x is mapped onto itself because every point X_o maps onto some new point $X_1 = \phi(X_o)$. Since, the evolution from X_o to X_1 can be thought of as the unfolding of a canonical transformation (see Section 3.3) with the generator $S'''(\mathbf{q}_o, \mathbf{p}_1)$, the state X_1 can be obtained from the state X_o by a canonical transformation:

$$\mathbf{p}_o = \nabla_{\mathbf{q}_o} S''', \quad \mathbf{q}_1 = \nabla_{\mathbf{p}_1} S''' \quad (5a)$$

or

$$p_{x_o} = \frac{\partial S'''}{\partial x_o}, \quad x_1 = \frac{\partial S'''}{\partial p_{x_1}} \quad (5b)$$

so that

$$\frac{\partial p_{x_o}}{\partial p_{x_1}} - \frac{\partial x_1}{\partial x_o} = 0. \quad (6)$$

Therefore, we have

$$|dX_1| = |dx_1 dp_{x_1}| = |dX_o| = |dx_o dp_{x_o}| \quad (7)$$

which shows that the mapping of S_x is area-preserving, as expected.

The usefulness of these surfaces of section lies in the fact that the successive iterates X_1, X_2, \dots of an initial point X_o reveal whether or not the system is integrable and invariant tori exist. If they do, the trajectory lying on a torus will not intersect randomly some or all of S_x , but is constrained further to a one-dimensional smooth

closed curve C of intersection of the torus with S_x (see Figure 5.2). Conversely, one may determine if the system is integrable by determining if the trajectory intersects S_x in a closed curve C . If the torus in question is one with an irrational winding number, a single orbit never closes on itself and covers the torus ergodically. This will show up in the surface of section by the filling-up of the smooth closed curve C by the successive iterates X_j . On the other hand, if the torus has a rational winding number, namely,

$$\frac{\omega_1}{\omega_2} = \frac{m}{n}, \text{ where } \omega_1 \text{ and } \omega_2 \text{ are the frequencies of periodic motions about small circle}$$

and large circle of the torus, respectively, an orbit on the torus is periodic and closed, and there will only be a finite number of intersections X_j ($j = 0, \dots, n$) such that $X_0 = X_n$, and X_0 is a fixed point of the mapping $\phi^{[n]}$. In fact, so are all iterates X_j and the curve C is an invariant curve of the mapping because ϕ maps C onto itself: $\phi(C) = C$.

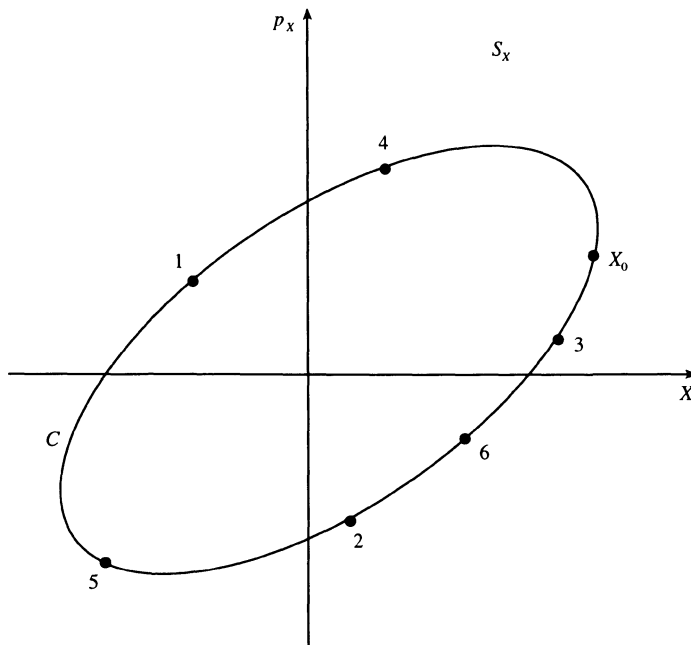


Figure 5.2. The successive iterates of an initial point X_0 on the surface of section for an integrable system.

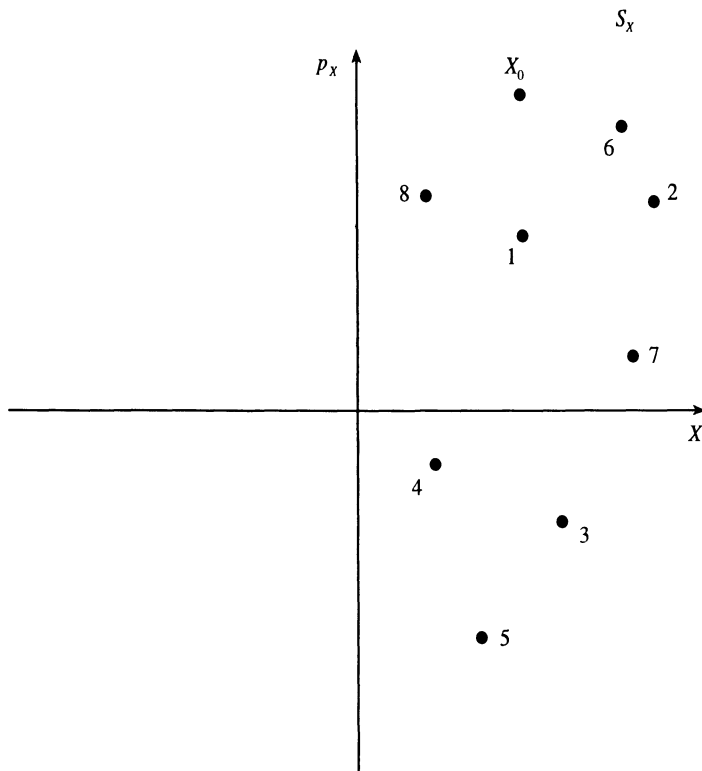


Figure 5.3. The successive iterates of an initial point X_0 on the surface of section for a non-integrable system.

Note that for a nonintegrable system, the crossings of the trajectory with S_x cover not a smooth closed curve C but constitute a set of randomly scattered points on S_x , (see Figure 5.3). When the sequence of numerically computed iterates turns out to be chaotic, a question naturally arises: Is the sequence truly chaotic, or is it periodic with a very large period, accompanied by very long-lived transients? This question has not found a definitive answer yet, although some facts support the idea of genuine chaos.

EXAMPLE 1

Hénon and Heiles (1964) studied the bounded motion of a system with Hamiltonian

$$H = \frac{1}{2}(\dot{x}^2 + \dot{y}^2) + U(x, y) \quad (8)$$

where,

$$U(x, y) = \frac{1}{2} \left(x^2 + y^2 + 2x^2 y - \frac{2}{3} y^3 \right).$$

The question now is whether or not a well-defined constant of motion exists for the Hamiltonian (8), in addition to the total energy $E = H$, and hence determine the tendency toward chaotic behavior in this system. For a given total energy H , the flow in the phase space for the system (8) is essentially three-dimensional. This enables one to construct a two-dimensional (local) transverse cross section and an associated Poincaré map in specific cases, and to study the dynamics (and the existence of the second integral of motion, in particular) in terms of this two-dimensional area-preserving map.

Note that the condition $\dot{x}^2 \geq 0$ defines, for a certain E , a bounded volume

$$\frac{1}{2} \dot{y}^2 + U(x, y) \leq E. \quad (9)$$

Now, if a second integral of motion does not exist, then any single trajectory evolving according to Hamilton's equations

$$\ddot{x} = -\frac{\partial U}{\partial x}, \quad \ddot{y} = -\frac{\partial U}{\partial y} \quad (10)$$

would permeate this volume in a random fashion, whereas the existence of a second integral would mean that the trajectory would lie on some two-dimensional surface. Consider, in particular, the bounded area defined by the intersection of the plane $x = 0$ with the bounded volume given by (9):

$$\frac{1}{2} \dot{y}^2 + U(0, y) \leq E. \quad (11)$$

The successive intersections of a given trajectory with the plane $x = 0$ will, in general, define an infinite sequence of mapping points P_i ; $i = 1, 2, \dots$, which lie in the y, \dot{y} -plane. If these points uniformly cover some or all of the whole area compatible with conservation of energy, then no second integral exists. If, however, the points P_i lie on a smooth curve, the second integral exists.

The trajectory from P_i to P_{i+1} defines a mapping which is completely determined by the potential $U(x, y)$ and the total energy E as follows: Suppose P_i is known; this defines y and \dot{y} . Further, x is zero; so \dot{x} is found from

$$E = \frac{1}{2}(\dot{x}^2 + \dot{y}^2) + U(x, y) \quad (12)$$

Using these values as the initial conditions, the equations of motion can be integrated forward, until $x = 0$ again. The values of y and \dot{y} at this time define P_{i+1} .

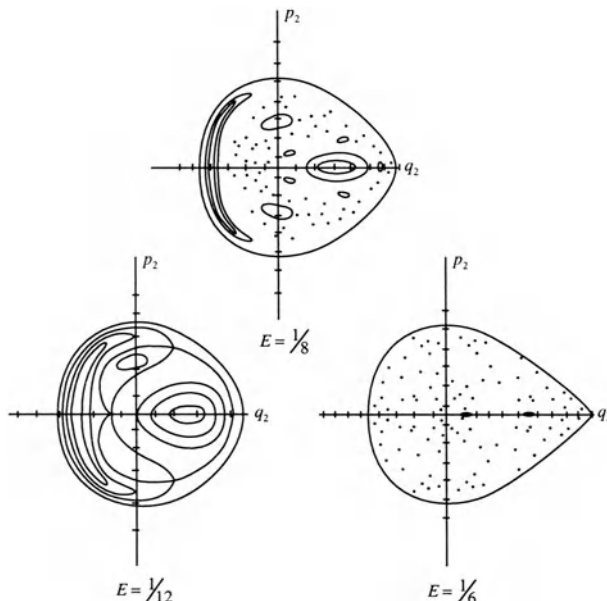


Figure 5.4. Surfaces of section for Hénon-Heiles Hamiltonian system (from Ford (1975)).
(By courtesy of Elsevier Science Publishers.)

The results of this numerical experiment suggested strongly that the existence of a second integral depends on the value of E . For $E \leq 1/8$, the points P_i lie on a smooth curve. The totality of trajectories formed a one-parameter family of curves which completely filled the available area defined by (11) (see Figure 5.4). The three self-intersection points of separatrix level curves represent distinct unstable periodic solutions, while the four invariant points at the center of each closed curve represent distinct stable periodic solutions. As E was increased past $1/8$, some of the closed curves near the hyperbolic points disappeared, and the area covered by them previously

was now covered by randomly scattered points of intersection P_i defined by a trajectory starting in this area. At $E = 1/6$, almost the entire area defined by (11) was covered by any single trajectory. This strongly suggested the nonexistence of the second integral, for values of E greater than about $1/8$.

5.3. Area-Preserving Mappings

In order to do a surface of section mapping by numerical integration of Hamilton's equations one determines the intersections of the trajectory with the surface of section by solving the equations of motion over time scales much shorter than the mapping period T . But, this approach can be very time-consuming. Area-preserving mappings offer advantages in this regard because direct iteration of an area-preserving mapping exhibits essentially the same behavior and can be easily carried out over hundreds of thousands of mapping periods. Consider a discrete map constructed from the flow generated by a continuous time system by sampling the flow at discrete times $t_n = t_o + n\tau (n = 0, 1, 2, \dots)$,

$$\mathbf{x}_{n+1} = \mathbf{T}(\mathbf{x}_n) \quad (13)$$

where,

$$\mathbf{x}_n \equiv \mathbf{x}(t_n).$$

The above map is area-preserving if the determinant of its Jacobian matrix of partial derivatives has unit magnitude,

$$\left| \det \left[\frac{\partial \mathbf{T}(\mathbf{x})}{\partial \mathbf{x}} \right] \right| = 1.$$

See MacKay (1985) for a good geometrical introduction to area-preserving maps.

EXAMPLE 2

Consider an area-preserving mapping, (Berry *et al.* (1979)),

$$\left. \begin{aligned} x_{n+1} &= x_n + y_n \\ y_{n+1} &= y_n - x_{n+1}^3 \end{aligned} \right\} \quad (14)a$$

where n may be thought of as the discrete time. The Jacobian of this transformation is, therefore, unity,

$$\left| \frac{\partial(x_{n+1}, y_{n+1})}{\partial(x_n, y_n)} \right| = 1. \quad (15)$$

Let us denote the mapping (13) by

$$(x_{n+1}, y_{n+1}) = T(x_n, y_n) = T^{[n]}(x_o, y_o). \quad (14)b$$

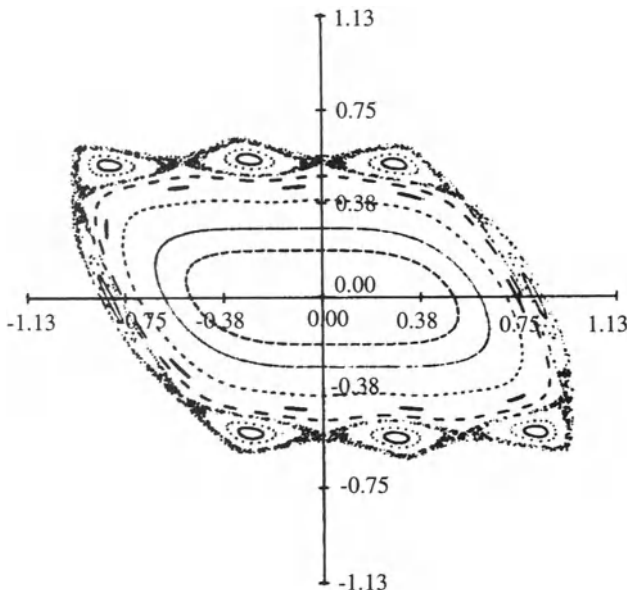


Figure 5.5. Phase plane of the area-preserving map of Berry *et al.* (1979) (from Berry *et al.* (1979)).
(By courtesy of Academic Press.)

Figure 5.5 shows a number of trajectories for this system in the (x, y) phase plane. Near the origin the orbits lie on smooth curves, which are the analogues of the invariant tori of integrable Hamiltonian systems. The outermost structure is remarkable with the set of eight small ellipses forming a set of islands. At the center of each island, there is an elliptic type fixed point of the mapping. These fixed points correspond to a closed

orbit; in this case, the orbit closes after eight iterations of the mapping, i.e., $T^{[8]}(x_o, y_o) = (x_o, y_o)$. This orbit is stable because, the corresponding fixed points are surrounded by smooth curves, so a nearby trajectory will stay close to it. The area in between the set of islands is covered by randomly-scattered points which are generated by an irregular trajectory filling up an area of the phase plane. At the center of this structure there is a hyperbolic type fixed point of the mapping. This set of eight fixed points corresponds to an unstable closed orbit. The island structure (with the concomitant alternating elliptic and hyperbolic fixed points) is a mark of the destroyed invariant tori of Hamiltonian systems under the action of resonant perturbations (see Section 5.6).

5.4. Twist Maps

We have seen that, for a two-degree-of-freedom system, the trace on the surface of section of a trajectory lying on a torus is a sequence of points X_o, X_1, \dots lying on a smooth curve, which corresponds to the intersection of that torus with the surface of section. If the frequency ratio ω_1/ω_2 is irrational, the sequence X_i fills up the curve densely, and the motion is quasi-periodic, while if ω_1/ω_2 is rational, the sequence of iterates is finite, and the trajectory starting from an initial point X_0 returns to X_0 after a time $T = m/\omega_1 = n/\omega_2$ where m and n are two integers such that $\omega_1/\omega_2 = m/n$. The corresponding trajectory on the torus is a closed orbit winding m times along the θ_1 -direction and n times along the θ_2 -direction at the same time. If we assume the system to be integrable and, furthermore, isoenergetic nondegenerate, we will have a family of nested tori with a frequency ratio varying smoothly, say increasing, from torus to torus. If we consider one of these tori, with actions J_1, J_2 (on the energy surface $E = H(J_1, J_2)$), the Hamiltonian flow on the torus is given by,

$$\left. \begin{aligned} \theta_1(t) &= \omega_1 t + \theta_1(0) \\ \theta_2(t) &= \omega_2 t + \theta_2(0) \end{aligned} \right\} \quad (16)$$

where,

$$\left. \begin{aligned} \omega_1 &= \omega_1(J_1, J_2) = \frac{\partial H}{\partial J_1} \\ \omega_2 &= \omega_2(J_1, J_2) = \frac{\partial H}{\partial J_2} \end{aligned} \right\}. \quad (17)$$

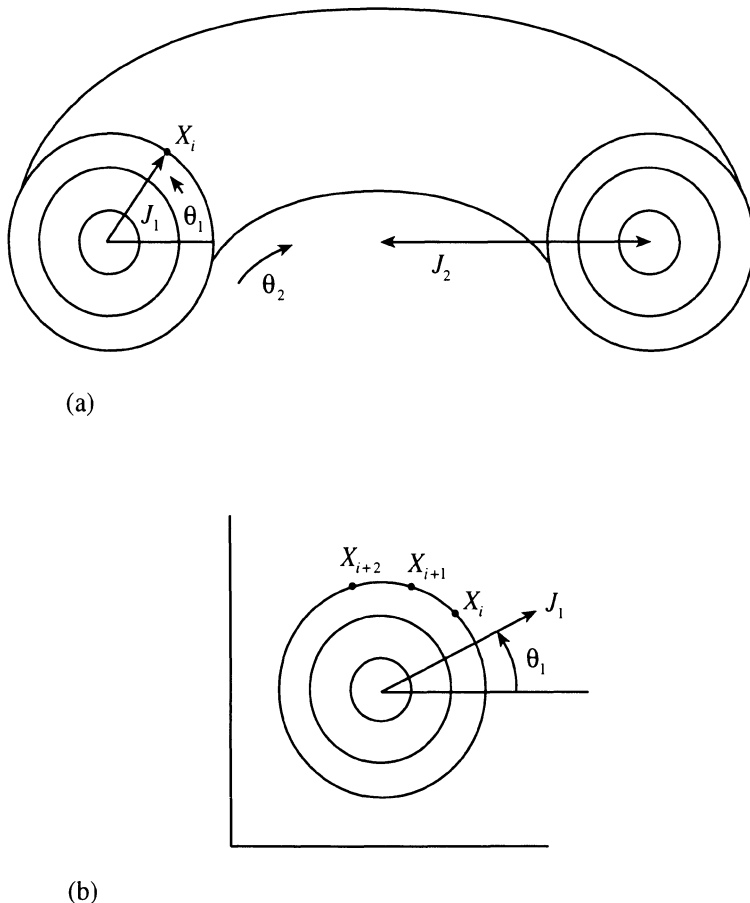


*Figure 5.6. (a) Point X_i on a torus in the action-angle representation J_1, θ_1 .
(b) Successive iterates X_i, X_{i+1}, X_{i+2} of corresponding twist map in a surface of section.*

The time, t_2 , taken by θ_2 to complete a 2π cycle is simply $t_2 = 2\pi/\omega_2$. In this period, the change in θ_1 is

$$\Delta\theta_1 = \omega_1 t_2 = 2\pi\omega_1/\omega_2 = 2\pi\alpha(J_1) \quad (18)$$

where α is the rotation number and J_2 has been expressed in terms of J_1 since, on a given energy surface, $E = H(J_1, J_2)$. If the (J_1, θ_1) -plane is taken to be a surface of section, the successive intersections of a trajectory on this torus with this plane are given by $X_i = (\theta_1(t + i t_2), J_1)$, see Figure 5.6. Denoting $\theta_i = \theta_1(t + i t_2)$ and $r = J_1$, the sequence of iterate points associated with the Hamiltonian flow on this torus can be represented by the area-preserving mapping of the (r, θ) -plane onto itself:

$$\left. \begin{array}{l} \theta_{i+1} = \theta_i + 2\pi\alpha(r_i) \\ T: \\ r_{i+1} = r_i \end{array} \right\} \quad (19)$$

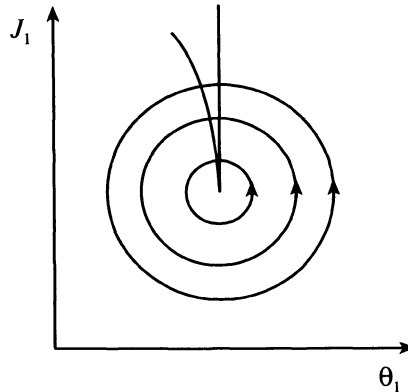


Figure 5.7. The twist map.

where the rotation number α is a smoothly varying function of r . (19) may be considered to be a mapping in a Poincaré section of the phase space of the given Hamiltonian system. Such a mapping is called a twist map because, due to the increase of the rotation number α with r , a radial line of points will bend under T (see Figure 5.7). Note that a twist map maps circles C onto circles C :

$$T(C) = C. \quad (20)$$

EXAMPLE 3

Consider the Chirikov (1979) map –

$$\left. \begin{array}{l} r_{n+1} = r_n + K \sin \theta_n \\ \theta_{n+1} = \theta_n + r_{n+1} \end{array} \right\}. \quad (21)a$$

This mapping is area-preserving because

$$\frac{\partial(r_{n+1}, \theta_{n+1})}{\partial(r_n, \theta_n)} = \begin{vmatrix} 1 & K \cos \theta_n \\ 1 & 1 + K \cos \theta_n \end{vmatrix} = 1. \quad (22)$$

When $K = 0$, this map becomes

$$\left. \begin{array}{l} r_{n+1} = r_n \\ \theta_{n+1} = \theta_n + r_n \end{array} \right\}. \quad (23)$$

Thus, under this map, the radius remains constant, while the larger circles rotate faster. This is an example of a twist map.

When $K \neq 0$, (21a) may be rewritten as

$$\theta_{n+1} = \theta_n + r_n + K \sin \theta_n \equiv f(\theta_n) \quad (21)b$$

which shows that

- * for the case $K < 1$, $f'(\theta) = 1 + K \cos \theta$ cannot vanish and the map (21) is invertible,
- * for the case $K > 1$, $f'(\theta) = 1 + K \cos \theta$ can vanish and the map is not invertible.

This mapping leads to periodic orbits, ergodic orbits and chaotic orbits, (see Figure 5.8). The periodic orbits are represented by the elliptic points at the centers of the islands. The ergodic orbits appear as a single curve going from one side to the other in Figure 5.8. Any orbit lying between two such ergodic orbits (representing tori) cannot cross them and is, therefore, trapped between the two orbits forever. Chaotic orbits, of course, appear as randomly scattered points.

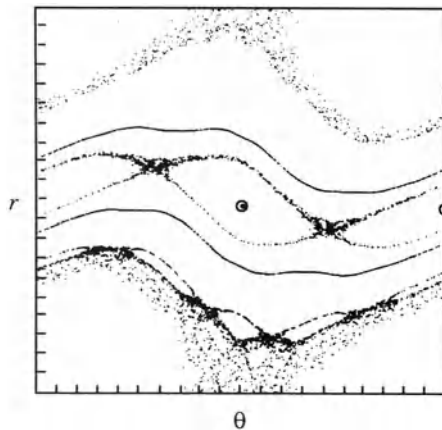


Figure 5.8. Phase plane of standard map for $k = 0.97$ (from Greene (1979)).
(By courtesy of the American Institute of Physics.)

Upon the addition of a "nonintegrable" perturbation, provided it is sufficiently small, Moser (1973) showed that circles with sufficiently irrational winding numbers are preserved, albeit as some smooth closed curves.

5.5. Tangent Maps

Consider a two-dimensional map T given by

$$\begin{bmatrix} x_{i+1} \\ y_{i+1} \end{bmatrix} = T \begin{bmatrix} x_i \\ y_i \end{bmatrix} = \begin{bmatrix} f(x_i, y_i) \\ g(x_i, y_i) \end{bmatrix}. \quad (24)$$

For simplicity, let us assume that there is a fixed point of T at the origin $(0, 0)$. The type of a fixed point is defined by the form of the nearby invariant curves. The latter can be determined by linearizing the mapping equations near the fixed point. Such a linear mapping is called the tangent map:

$$\begin{bmatrix} \delta x_{i+1} \\ \delta y_{i+1} \end{bmatrix} = \begin{bmatrix} T_{11} & T_{12} \\ T_{21} & T_{22} \end{bmatrix} \begin{bmatrix} \delta x_i \\ \delta y_i \end{bmatrix} \quad (25)$$

where,

$$\begin{aligned} T_{11} &\equiv \left(\frac{\partial f}{\partial x} \right)_{(0,0)}, & T_{12} &\equiv \left(\frac{\partial f}{\partial y} \right)_{(0,0)} \\ T_{21} &\equiv \left(\frac{\partial g}{\partial x} \right)_{(0,0)}, & T_{22} &\equiv \left(\frac{\partial g}{\partial y} \right)_{(0,0)} \end{aligned} \quad . \quad (26)$$

Note that $\det |T_{ij}| = 1$, since T is an area-preserving transformation.

The nature of the fixed point is determined by the eigenvalues of the matrix $[T_{ij}]$:

$$|T_{ij} - \lambda I| = 0 \quad (27)$$

from which,

$$\lambda_{1,2} = \frac{\text{tr } T \pm \sqrt{(\text{tr } T)^2 - 4}}{2}. \quad (28)$$

Using a similarity-transformation matrix P such that

$$P^{-1} \begin{bmatrix} \delta x_i \\ \delta y_i \end{bmatrix} = \begin{bmatrix} \xi_i \\ \eta_i \end{bmatrix} \quad (29)$$

and

$$P^{-1}[T]P = \begin{bmatrix} \lambda_1 & 0 \\ 0 & \lambda_2 \end{bmatrix}, \quad (30)$$

one may diagonalize the tangent map (25):

$$\begin{bmatrix} \xi_{i+1} \\ \eta_{i+1} \end{bmatrix} = \begin{bmatrix} \lambda_1 & 0 \\ 0 & \lambda_2 \end{bmatrix} \begin{bmatrix} \xi_i \\ \eta_i \end{bmatrix}. \quad (31)$$

We now have three cases:

- (i) $|tr T| < 2$: $\lambda_{1,2}$ are a complex conjugate pair lying on the unit circle,

$$\lambda_{1,2} = e^{\pm i\alpha}. \quad (32)$$

The tangent map (29) now corresponds to a rotation in the neighborhood of the fixed point $(0,0)$. The latter is a stable or elliptic fixed point, because an orbit near it remains near it after arbitrarily many iterations of T . Thus, in the neighborhood of $(0,0)$, one expects to find invariant curves.

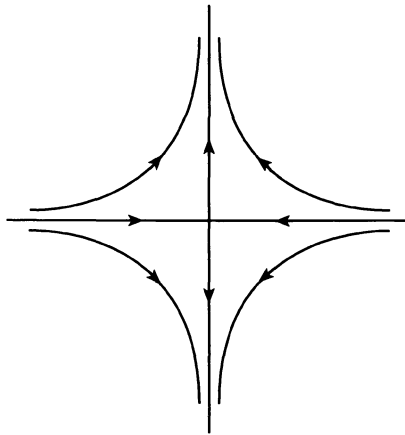


Figure 5.9. A hyperbolic fixed point.

- (ii) $|tr T| > 2$: $\lambda_{1,2}$ are real numbers such that $\lambda_1 \lambda_2 = 1$. The tangent map (25) now leads to a runaway motion in the neighborhood of $(0,0)$. The latter is an unstable or hyperbolic fixed point, because any orbit near it, but not going through it, will eventually map far away from it (Figure 5.9).

The special case $\lambda_1 = \lambda_2 = \pm 1$ corresponds, in the original variables, to the following map

$$\begin{bmatrix} \delta x_{i+1} \\ \delta y_{i+1} \end{bmatrix} = \begin{bmatrix} \pm 1 & C \\ 0 & \pm 1 \end{bmatrix} \begin{bmatrix} \delta x_i \\ \delta y_i \end{bmatrix} \quad (33)$$

where C is a constant. This map represents to a translation parallel to the x -axis. $(0,0)$ is now called a parabolic fixed point. If we choose $\delta y_o = 0$, then

every point on the x -axis will be a fixed point of the map (33). Such a situation arises for closed orbits, all points on which are fixed points.

As with differential equations (see Chapter 1), one may again define the linear eigenspaces E_s, E_c and E_u corresponding to eigenvalues with modulus less than 1, equal to 1, or greater than 1, respectively. Then, there exist manifolds W_s, W_c and W_u for the nonlinear map tangent to E_s, E_c and E_u , respectively, at the fixed point.

5.6. Poincaré-Birkhoff Fixed-Point Theorem

The Kolmogorov-Arnol'd-Moser Theorem says nothing about the fate of invariant tori whose winding numbers are not sufficiently incommensurable. Let us consider now the fate of tori with rational winding number, or equivalently, curves with rational rotation number, under small perturbation. The invariant tori are covered by families of closed orbits. Let us consider a surface of section by cutting an invariant torus transversely by a $(2n - 2)$ -dimensional cross section S lying in the $(2n - 1)$ -dimensional energy surface. In a surface of section, a single one of these orbits with winding number P/Q would generate a pattern of Q fixed points lying on a smooth closed curve. On perturbation this family of fixed points is broken up. The Poincaré-Birkhoff Fixed-point Theorem states that in its place kQ pairs of fixed points (k is an arbitrary integer) arise. Of these, kQ points are elliptic fixed points and kQ points are hyperbolic fixed points. (Recall that all fixed points of a conservative Hamiltonian system are either centers or saddles.)

Consider a twist map T on the two-dimensional torus:

$$\begin{bmatrix} \varphi' \\ J' \end{bmatrix} = \begin{bmatrix} \frac{\partial}{\partial J'} S'''(\varphi, J') \\ J \end{bmatrix} = T \begin{bmatrix} \varphi \\ J \end{bmatrix}. \quad (34)$$

Here, the unprimed and the primed variables denote, respectively, the i th and the $(i + 1)$ th iterates of the mapping, and $S'''(\varphi, J')$ is the transformation:

$$S'''(\varphi, J') = \varphi J' + S_1'''(\varphi, J'), \quad \frac{\partial S_1'''}{\partial J'} = 2\pi \frac{\omega_1}{\omega_2}. \quad (35)$$

According to the Kolmogorov-Arnol'd-Moser Theorem, for sufficiently small perturbation of (34), "most" invariant curves (excluding those with rational rotation

number $\alpha = \omega_1/\omega_2 = r/s$) will be preserved, provided the isoenergetic nondegeneracy condition

$$\det \left| \frac{\partial^2 S'''}{\partial J_i \partial J_j} \right| \neq 0 \quad (36)$$

is satisfied.

Let us now determine the images of the rational curves under the twist map (34). Consider two curves C^+ and C^- lying on either side of the rational curve C with $\alpha = r/s$ (Figure 5.10) and possessing irrational rotation numbers α . The latter is guaranteed by the fact that $\alpha = \alpha(J)$, according to (36), increases smoothly with J .

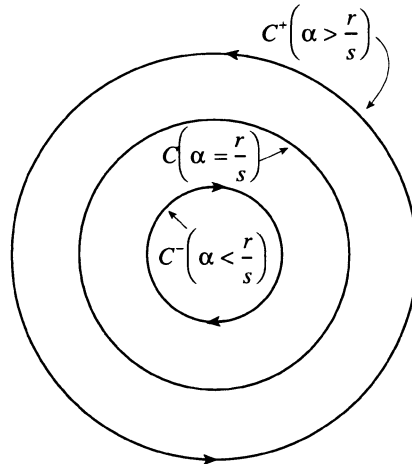


Figure 5.10. Invariant curves of unperturbed twist map T .

Now, every point on C will be a fixed point of $T^{[s]}$ since

$$T^{[s]} \begin{bmatrix} \varphi \\ J \end{bmatrix} = \begin{bmatrix} \varphi + s \frac{\partial S'''_1}{\partial J} \\ J \end{bmatrix} = \begin{bmatrix} \varphi + s \cdot 2\pi \frac{r}{s} \\ J \end{bmatrix} = \begin{bmatrix} \varphi + 2\pi r \\ J \end{bmatrix} = \begin{bmatrix} \varphi \\ J \end{bmatrix}. \quad (37)$$

Thus, under the mapping $T^{[s]}$, C^+ rotates counterclockwise and C^- rotates clockwise relative to C .

Next, consider the slightly perturbed mapping T_ϵ . By the Kolmogorov-Arnol'd-Moser Theorem, the curves C^+ and C^- , though slightly distorted, remain preserved, as C_ϵ^+ and C_ϵ^- (see Figure 5.11).

Now, if ϵ is sufficiently small, we may assume that the relative twists of C^+ and C^- are nearly preserved under the perturbed map $T_\epsilon^{[s]}$. Thus, along each radius from the center there must be one point between C^+ and C^- whose angular coordinate φ is preserved under $T_\epsilon^{[s]}$. These radially mapped points make up a curve D close to C . Figure 5.11 shows the curve D , and its image $T_\epsilon^{[s]}(D)$ which cuts D in an even number of points because the area enclosed by D and $T_\epsilon^{[s]}(D)$ must be the same. The points common to D and $T_\epsilon^{[s]}(D)$ are the fixed points of $T_\epsilon^{[s]}$, and these form an alternating sequence of elliptic and hyperbolic fixed points. This leads to the Poincaré-Birkhoff Fixed-point Theorem:

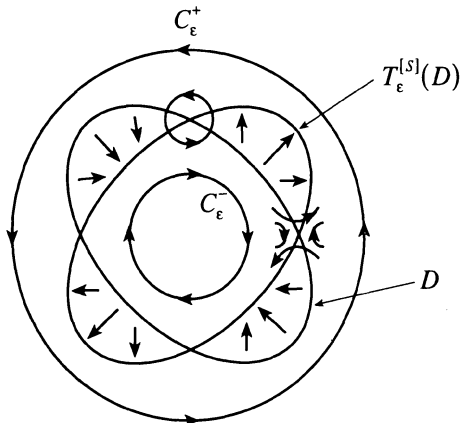


Figure 5.11. Effect of perturbed twist map on the curves of Figure 5.10.

THEOREM 5.1

Let T be a twist map, and T_ϵ be a slightly perturbed twist map. Consider a rational curve of an unperturbed system, with rotation number r/s (for which every point is a fixed point of $T^{[s]}$). Then, only an even number of fixed points $2ks$ ($k = 1, 2, \dots$) will survive the perturbation. These fixed points are alternately elliptic and hyperbolic.

In order to see that the number of fixed points is an even multiple of s , consider one of the even number of fixed points X determined by the intersection of D and $T_\epsilon^{[s]}(D)$. This fixed point maps, under T_ϵ , to $T_\epsilon X, T_\epsilon^{[2]}X, \dots, T_\epsilon^{[s-1]}X, T_\epsilon^{[s]}X = X$, each of which is also a fixed point of $T_\epsilon^{[s]}$. Therefore, there are s distinct fixed points associated with each point of intersection of D and $T_\epsilon^{[s]}(D)$ – so $2ks$ fixed points as a whole.

The elliptic fixed points correspond to stable closed orbits and each is surrounded by smooth invariant curves corresponding to higher order tori. On the other hand, the hyperbolic fixed points correspond to unstable closed orbits and exhibit an extremely complicated structure in their neighborhood: One finds chaotic orbits in these regions. Furthermore, by the Kolmogorov-Arnol'd-Moser Theorem, the rational members of the invariant-curve family around each elliptic fixed point will break up, and according to the Poincaré-Birkhoff Theorem, a new subsequence of elliptic and hyperbolic points appears. This decomposition process will repeat ad infinitum and will lead to a self-similar structure on all scales.

5.7. Homoclinic and Heteroclinic Points

An elliptic fixed point has a center manifold with invariant tori associated with it. A hyperbolic fixed point, on the other hand, is characterized by four invariant manifolds, (all solutions starting from initial conditions on an invariant manifold always remain on it under the evolution of the dynamical system). Out of these, two are incoming or stable manifolds, H^+ , and the other two are outgoing or unstable manifolds, H^- (Figure 5.12). The stable manifold of a hyperbolic fixed point P is the set of all those points which

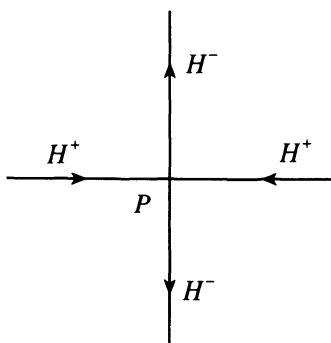


Figure 5.12. Stable manifolds H^+ and unstable manifolds H^- of a hyperbolic fixed point.

converge to P under the flow. The unstable manifold of a hyperbolic fixed point P is the set of all those points which diverge from P under the flow. Thus,

$$\lim_{s \rightarrow \infty} T^{[s]} x \rightarrow P, (x \in H^+) \quad (38)$$

$$\lim_{s \rightarrow -\infty} T^{-[s]} x \rightarrow P, (x \in H^-). \quad (39)$$

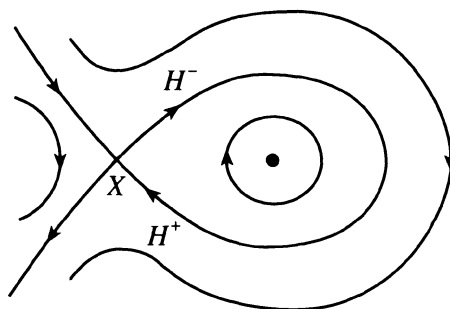


Figure 5.13a. Smooth joining of H^- to H^+ from same hyperbolic fixed point X leading to homoclinic orbit.

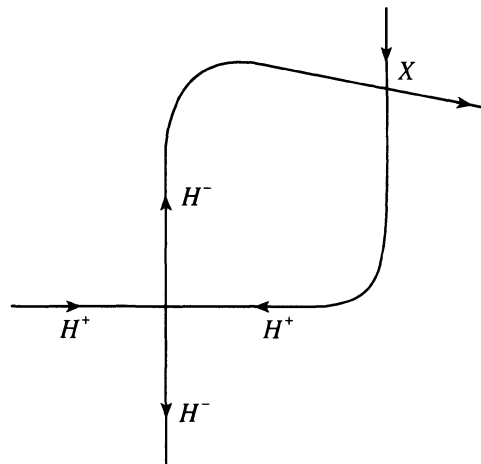


Figure 5.13b. Intersection of stable manifold H^+ and unstable manifold H^- , of the same hyperbolic fixed point leading to a homoclinic point X .

Thanks to deterministic nature of the flow, the manifolds H^+ and H^- cannot intersect themselves, but can intersect each other transversely, as shown in Figure 5.13a. If the manifolds H^+ and H^- from the same fixed point or from the fixed points of the same family, intersect at a point, that point is called a homoclinic point. (Note that these are the only points along the manifolds that tend to the fixed point both as $t \rightarrow \infty$ and $t \rightarrow -\infty$.) For integrable systems, like the simple pendulum, the stable and unstable manifolds H^+ and H^- emanating from a hyperbolic fixed point join smoothly to form a single loop called a homoclinic orbit (Figure 5.13b). It should be noted, however, that such a smooth joining of manifolds, that is typical of integrable systems, is only an exception. The generic flows, on the other hand, show a very complex behavior.

If the manifolds H^+ and H^- from the fixed points of different families, intersect at a point, that point is called a heteroclinic point. Figure 5.14 shows the case of an outgoing manifold and an incoming manifold from different hyperbolic fixed points intersecting to form a heteroclinic orbit. (Note that the curves drawn here do not represent a trajectory but correspond to curves joining the successive intersections of a trajectory with the plane.)

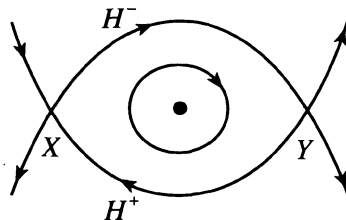


Figure 5.14. Intersection of H^- and H^+ from different hyperbolic fixed points leading to a heteroclinic orbit.

For integrable systems, the homoclinic intersections are isolated. But, for non-integrable systems, these intersections turn out to be quite complicated because one homoclinic point leads to an infinite number of homoclinic points! This follows from the fact that a homoclinic point lies on both stable and unstable invariant manifolds, so is asymptotic to the hyperbolic point in both directions of time. Consequently, each iterate of a homoclinic point will also be a homoclinic point. An analytic criterion for the occurrence of homoclinic intersections was given by Melnikov (1963), (see Lichtenberg and Lieberman, 1992, for a readable account of Melnikov's method).

Consider the homoclinic point X , as shown in Figure 5.15, and its two adjacent points X' and X'' , which map to TX' and TX'' , respectively (Tabor (1989)). Since X is "ahead" of both X' and X'' , due to the continuity of mapping, its image TX should be "ahead" of both TX' and TX'' . This becomes possible when the unstable manifold

H^- makes a loop, (Figure 5.15) so that TX is a homoclinic point. Repeating this argument, we see that TX must next map to a new homoclinic point $T^{[2]}X$ via a second loop, as shown in Figure 5.15. Now, since $T^{[2]}X$ is closer to the hyperbolic point than TX , $T^{[2]}X$ is closer to TX than TX is to X . Since the mapping is area-preserving, the area in the loop between X and TX , and the area in the loop between TX and $T^{[2]}X$ must be

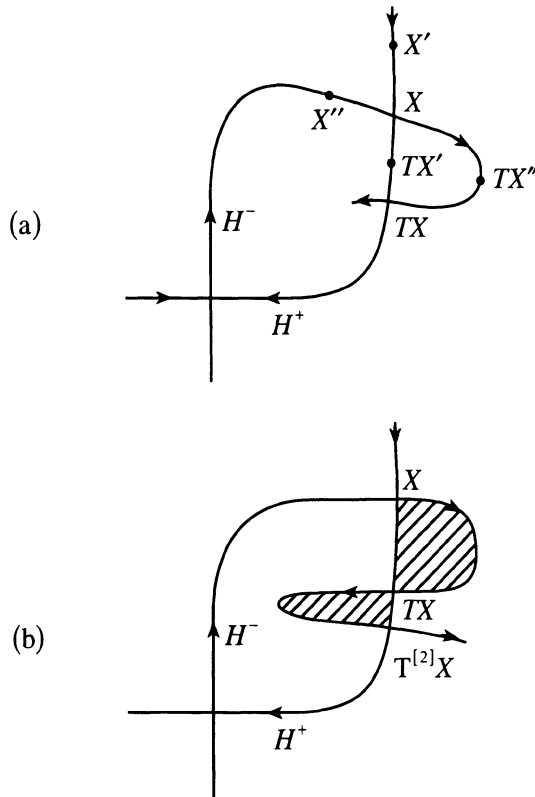


Figure 5.15. (a) Mapping of a homoclinic point X and neighboring points X' and X'' to TX, TX' and TX'' .

(b) Creation of a longer and thinner loop enclosing the same area by the image T^2X of TX , (from Tabor (1989)). (By courtesy of John Wiley & Sons, Inc.)

the same. This implies that the second loop must be longer and thinner than the first. Thus, these intersections get closer and closer without limit as the unstable manifold H^- starts oscillating unboundedly around the stable manifold H^+ , and as a result, we see

that the stable manifold H^+ becomes densely covered with homoclinic points accumulating on the hyperbolic point and the intervening loops become longer, thinner and more convoluted as one approaches the hyperbolic point. Thus, the orbit fills densely a region of the plane and its Hausdorff dimension (see Chapter 6) will be close to 2 rather than 1 as for the regular orbits (which are diffeomorphic to circles). The overall picture, called the homoclinic tangle is, therefore, one of enormous complexity, (see Figure 5.16)³. This structure repeats on all scales, and typically occurs when the stable and unstable manifolds of neighboring hyperbolic fixed points intersect one another transversely an infinite number of times. Thus, this structure may be taken to represent the emergence of chaotic regions around the hyperbolic fixed points. The strong bending of the manifolds near a homoclinic point, on the other hand, leads to stretching and folding of a rectangular element which can be described by Smale's horseshoe map (see Section 6.2).

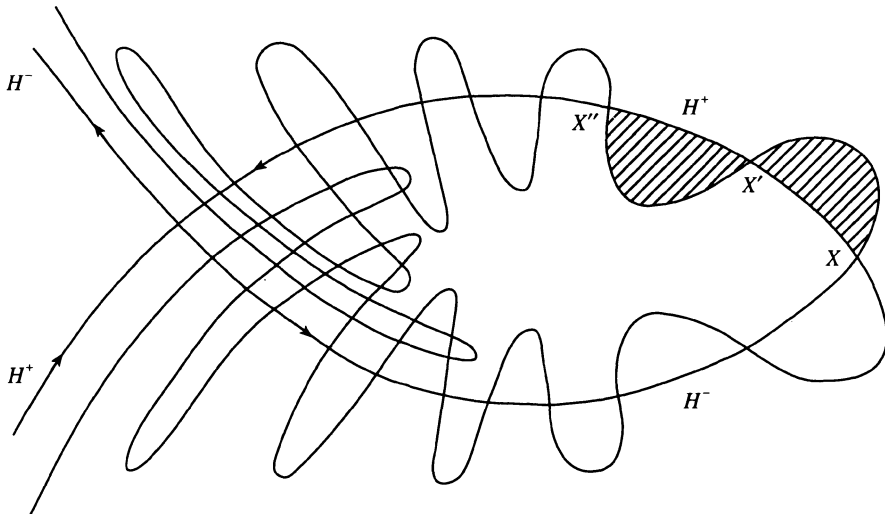


Figure 5.16. Successive intersections of H^+ and H^- leading to dense collection of homoclinic points and ever longer and thinner loops of the same area.

³ To quote Poincaré (1899) –

“...Each of the curves must never self-intersect, but it must fold itself in a very complex way, so as to return and cut the lattice an infinite number of times. The complexity of this figure is so astonishing that I cannot even attempt to draw it. Nothing is more appropriate to give us an idea of the complexity of the three-body problem and, in general, of all the problems in Dynamics where there is no uniform integral.”
(Translation due to Ozorio de Almeida, (1988).)

Now, the heteroclinic points correspond to the intersections of stable and unstable manifolds H^+ and H^- from different fixed-point families so that some intervening invariant torus will have to breakup before such an intersection can occur. Thus, the appearance of heteroclinic points would indicate the onset of fairly widespread chaos. A typical heteroclinic connection arises in a resonance-overlap setting (see Section 4.6).

There is a great deal of numerical evidence for this picture. One example is the results by Hénon and Heiles (1964) for the Hamiltonian

$$H = \frac{1}{2} \left(p_x^2 + p_y^2 + x^2 + y^2 \right) + x^2 y - \frac{1}{3} y^3. \quad (40)$$

For $E = 1/12$, there are three hyperbolic fixed points (see Figure 5.3). As E is raised to $1/8$, these have all disappeared, and their neighborhood is filled by an irregular trajectory. One of the invariant curves surrounding the rightmost elliptic point, in accord with the Poincaré-Birkhoff Theorem, has broken into a chain of five "islands", i.e., five elliptic points representing fixed points of $T^{[5]}$, each corresponding to periodic or quasi-periodic motion on invariant tori.

Another example is the Hénon map (Hénon, (1969)) given by⁴

$$\begin{bmatrix} x_{i+1} \\ y_{i+1} \end{bmatrix} = \begin{bmatrix} x_i \cos \alpha - y_i \sin \alpha + x_i^2 \sin \alpha \\ x_i \sin \alpha + y_i \cos \alpha - x_i^2 \cos \alpha \end{bmatrix} = T \begin{bmatrix} x_i \\ y_i \end{bmatrix} \quad (41)$$

the linearized version of which is just a simple rotation through the angle α . The nonlinear perturbation terms are small near the origin 0, which is therefore an elliptic fixed point of the unperturbed mapping. According to the Kolmogorov-Arnol'd-Moser Theorem, the perturbed mapping will also have closed invariant curves near 0. The perturbation becomes large far from 0, and it may be shown that all points (x_i, y_i) escape exponentially fast to infinity, under iterations of T .⁵ Figure 5.17 shows Hénon's

⁴ The Hénon map may be written as the product of two simpler maps –

$$T = RS$$

where S is a shearing-map parallel to the y -axis,

$$S: x'_n = x_n, y'_n = y_n - x_n^2$$

followed by a rotation about the origin,

$$R: \begin{cases} x_{n+1} = \cos \alpha \cdot x'_n - \sin \alpha \cdot y'_n \\ y_{n+1} = \sin \alpha \cdot x'_n + \cos \alpha \cdot y'_n \end{cases}$$

⁵ The fixed points of the map T are

calculation of the mapping plane for $\alpha = 0.2114$. At moderate distances from 0, there is a chain of 5 elliptic islands around 0, interlaced with 5 hyperbolic points, all these being fixed points of $T^{[5]}$, in accordance with the Poincaré-Birkhoff Theorem. The hyperbolic fixed points, which are expected to be the seeds of irregular motion, look a bit fuzzy. The halo which surrounds the picture on the outside is formed by a single trajectory which apparently wanders aimlessly. Figure 5.17 shows Hénon's magnification of the region near the right most hyperbolic point. Observe an "area-exploring" chaotic trajectory as well as several stages of the hierarchy of islands interspersed in a "sea" of chaos.

$$\left. \begin{array}{l} x^{(1)} = 0, \quad y^{(1)} = 0 \\ x^{(2)} = 2 \tan \frac{\alpha}{2}, \quad y^{(2)} = 2 \tan^2 \frac{\alpha}{2} \end{array} \right\}$$

The point $(x^{(1)}, y^{(1)})$ is an elliptic point while the point $(x^{(2)}, y^{(2)})$ is a hyperbolic point, because, at the point $(x^{(2)}, y^{(2)})$, the Jacobian matrix of the map T is given by

$$M = \begin{bmatrix} \cos \alpha + 4 \sin \alpha \cdot \tan \frac{\alpha}{2} & -\sin \alpha \\ \sin \alpha - 4 \cos \alpha \cdot \tan \frac{\alpha}{2} & \cos \alpha \end{bmatrix}.$$

If λ_1 and λ_2 are the eigenvalues of M , then

$$\lambda_1 + \lambda_2 = \text{tr } M = 2 + 4 \sin^2 \frac{\alpha}{2} > 2.$$

Further, since the map T is area-preserving,

$$\lambda_1 \lambda_2 = 1,$$

so that λ_1 and λ_2 are real, (otherwise, λ_1 and λ_2 would be complex conjugate and would lie on the unit circle in the complex plane so that $\lambda_1 + \lambda_2 < 2$, in violation of the previous condition).

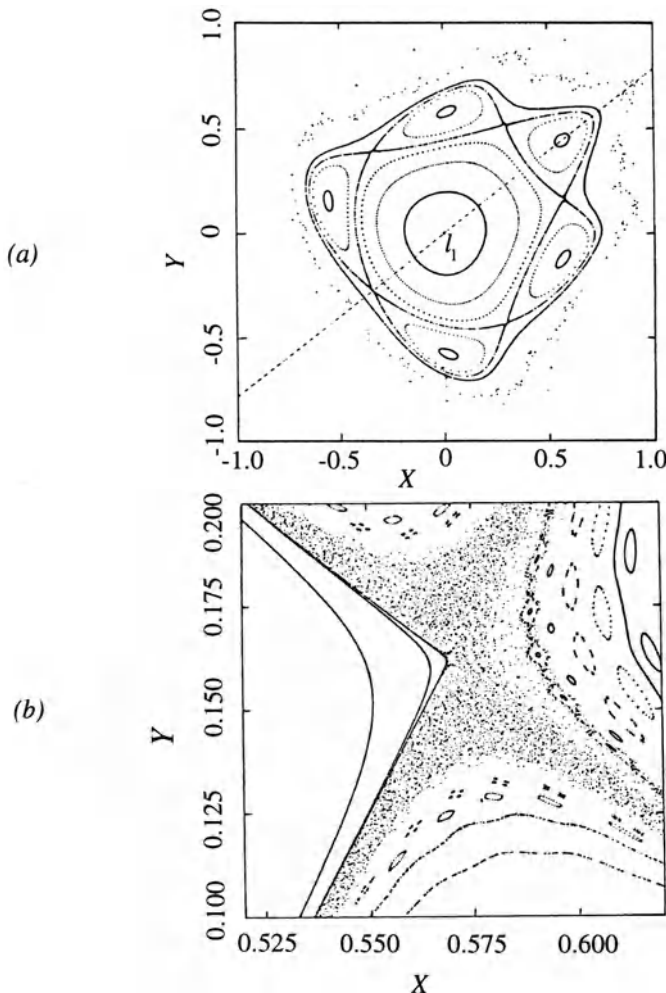


Figure 5.17. (a) Phase plane of Hénon map for $\alpha = 0.2114$. (b) Blowup of region around right-hand-most hyperbolic point (from Hénon (1969)). (By courtesy of the American Mathematical Society.)

5.8. Quantitative Measures of Chaos

Quantification of chaotic behavior proves to be helpful in –

- distinguishing chaotic behavior from quasi-periodic motion and noise,

- determining the number of variables needed to model the dynamics.

Some of the quantitative measures of chaos are –

- (i) Liapunov exponents,
- (ii) Kolmogorov entropy,
- (iii) autocorrelation function,
- (iv) power spectra.

We now discuss these measures.

(i) Liapunov Exponents

A characteristic feature of chaotic motion is the extreme sensitivity of the motion to small changes in initial conditions. For a chaotic motion, adjacent trajectories diverge exponentially, whereas for a regular motion trajectories are asymptotically stable (see Section 1.2) and separate only linearly in time.⁶ (Thus, for a regular motion, nearby states remain close to each other which implies predictability of such a motion far into the future.) The rate of divergence of adjacent trajectories can be quantified conveniently in terms of Liapunov exponents, which measure the mean rate of this exponential separation and describe the asymptotic stability properties of a trajectory. Thus, systems having a torus as their attractor exhibit the same Liapunov exponent spectrum $(0, 0, -)$ implying that the rate of divergence of adjacent trajectories is zero along two directions and negative along the third direction. This may be understood by noting that a torus is topologically equivalent to a plane and a plane is obtained by contracting a three-dimensional volume in only one direction.

Consider an autonomous system governed by the equations

$$\frac{dx_i}{dt} = F_i(x_1, \dots, x_n); \quad i = 1, 2, \dots, n. \quad (42)$$

Linearize these equations about a reference trajectory $\bar{x} = (\bar{x}_1, \dots, \bar{x}_n)$ to obtain a linear system

$$\frac{d\delta x_i}{dt} = \sum_{j=1}^n \delta x_j \left(\frac{\partial F_i}{\partial x_j} \right)_{x=\bar{x}}. \quad (43)$$

Then, the norm

⁶ The flow $\phi_t(x)$ with a metric $d(x', x)$ (see footnote 1, Chapter 6) has sensitive dependence on the invariant compact set Λ if there exists an $\varepsilon > 0$ such that, for any neighborhood U of x on Λ , there exists an $x' \in U$ with $d(\phi_t(x'), \phi_t(x)) > \varepsilon$ for $t > 0$.

$$d(t) = \sqrt{\sum_{i=1}^n \delta x_i^2(t)} \quad (44)$$

provides a measure of the divergence of two neighboring trajectories, i.e., the reference trajectory \bar{x} and its neighboring trajectory with initial conditions $\bar{x}(0) + \delta \bar{x}(0)$. The mean rate of exponential divergence, called the Liapunov exponent, is then defined as

$$\sigma = \lim_{\substack{t \rightarrow \infty \\ d(0) \rightarrow 0}} \left(\frac{1}{t} \right) \ln \frac{d(t)}{d(0)} \quad (45)$$

where,

$$d(0) \equiv \sqrt{\sum_{i=1}^n \delta x_i^2(0)}. \quad ^7$$

For a regular motion, this exponent is zero since $d(t)$ grows only linearly with time.

Consider now a one-dimensional map $f: I \rightarrow I$, where $I \subset \mathbb{R}$ is a bounded interval,

$$x_{i+1} = f(x_i) \quad (46)$$

the tangent map for which is

$$\delta x_{i+1} = f'(x_i) \delta x_i = \prod_{j=0}^i f'(x_j) \delta x_o. \quad (47)$$

The Liapunov exponent associated with the map (46) is defined to be

⁷ For a flow $\phi_t(x)$, the Liapunov exponent is alternatively defined as

$$\sigma = \lim_{t \rightarrow \infty} \sup_{x \in A(x)} \frac{1}{t} \ln \| D\phi_t(x)(x' - x) \|$$

if this limit exists for sufficiently small neighborhoods $A(x)$. Here, $D\phi_t(x)$ is the Jacobian matrix of ϕ_t at x . Osledec's Multiplicative Ergodic Theorem (Osledec, 1968) provides for the existence of this limit if the flow $\phi_t(x)$ generates an ergodic measure. Further, the value of this limit is the same for almost every x with respect to the ergodic measure.

$$\sigma = \lim_{N \rightarrow \infty} \frac{1}{N} \ln \left[\prod_{j=1}^{N-1} f'(x_j) \right] = \lim_{N \rightarrow \infty} \frac{1}{N} \sum_{j=0}^{N-1} \ln |f'(x_j)|^8. \quad (48)a$$

If f has a stable period- k cycle containing the point x_o , i.e.,

$$x_o = f^{[k]}(x_o)$$

then (48)a becomes

$$\sigma = \frac{1}{k} \sum_{j=0}^{k-1} \ln |f'(x_j)|.$$

Invoking the chain rule, this becomes

$$\sigma = \frac{1}{k} \ln \left| \left(f^{[k]} \right)' (x_o) \right| < 0.$$

⁸ This formula can be derived alternately as follows: Let us write, for the difference between two initially nearby states, after N iterations,

$$\varepsilon e^{N\sigma(x_o)} = \left| f^{[N]}(x_o + \varepsilon) - f^{[N]}(x_o) \right|$$

which in the limits $\varepsilon \rightarrow 0$ and $N \rightarrow \infty$, leads to

$$\begin{aligned} \sigma(x_o) &= \lim_{N \rightarrow \infty} \lim_{\varepsilon \rightarrow 0} \frac{1}{N} \ln \left| \frac{f^{[N]}(x_o + \varepsilon) - f^{[N]}(x_o)}{\varepsilon} \right| \\ &= \lim_{N \rightarrow \infty} \frac{1}{N} \ln \left| \frac{df^{[N]}(x_o)}{dx_o} \right|. \end{aligned}$$

This implies that $\sigma(x_o)$ is the average rate of divergence of two closely adjacent points over the whole evolution. Note that

$$\begin{aligned} \sigma(x_o) &= \lim_{N \rightarrow \infty} \frac{1}{N} \ln \left| \prod_{j=0}^{N-1} f'(x_j) \right| \\ &= \lim_{N \rightarrow \infty} \frac{1}{N} \sum_{j=0}^{N-1} \ln |f'(x_j)|. \end{aligned}$$

If the system is ergodic, then the long-time average of any continuous function of a state variable is essentially independent of the initial conditions. Thus, for a certain class of initial conditions, the distribution of iterates can be described by a stationary density $\rho(x)$ so that the above time average can be replaced by a phase-space average:

$$\sigma = \int dx \rho(x) \ln |f'(x)|. \quad (48b)$$

For an attractor, the Liapunov exponents may be defined with respect to the natural measure on the attractor so that they will be the same for all the initial conditions in the basin of attraction of the attractor (see Section 6.1).

In the case of an n -dimensional mapping

$$\mathbf{x}_{i+1} = \mathbf{F}(\mathbf{x}_i) \quad (49)$$

there will be a set of n Liapunov exponents corresponding to the n eigenvalues $|\lambda_k(N)|$, $k = 1, \dots, n$ of the associated tangent map $M(\mathbf{x}_N)$ at \mathbf{x}_N . Noting that

$$M(\mathbf{x}_N) = M(\mathbf{x}_{N-1}) M(\mathbf{x}_{N-2}) \dots M(\mathbf{x}_o)$$

where $M(\mathbf{x}_i)$ represents the tangent map at \mathbf{x}_i , the Liapunov exponents are defined as

$$\sigma_k = \lim_{N \rightarrow \infty} \frac{1}{N} \ln |\lambda_k(N)|; \quad k = 1, \dots, n. \quad (50)$$

Note that for area-preserving maps and Hamiltonian flows, the sum of the exponents must be zero so that the phase-space volume is preserved.⁹

One may also use the Liapunov exponent to estimate the "predictability horizon", i.e., the time for which the state of a chaotic system can be predicted reliably into the future. After this time, the uncertainty in the state of the system would have amplified to the size of the phase space of the system so that the system will then appear random.

⁹ An n -dimensional initial volume V_o evolves, on average, as

$$V = \begin{cases} V_o e^{(k_1 + k_2 + \dots + k_n)t}, & \text{for maps} \\ V_o e^{|(k_1 + k_2 + \dots + k_n)t|}, & \text{for continuous dynamical systems.} \end{cases}$$

Suppose the system is characterized by a positive Liapunov exponent σ , with an uncertainty of ε in defining its initial state. Then, corresponding to the predictability horizon T , this uncertainty amplifies to the size L of the attractor, in time T , so that

$$L \sim \varepsilon e^{\sigma T} \quad (51a)$$

from which,

$$T \sim \frac{1}{\sigma} \log \frac{L}{\varepsilon}. \quad (51b)$$

(51b) shows that the predictability horizon T increases only logarithmically with the precision in the specification of the initial state of the system, thus, making only a short-term prediction possible for chaotic systems.

(ii) Kolmogorov Entropy

In statistical mechanics, entropy is defined as the average of the logarithm of the coarse-grained probabilities:

$$S = -k \sum_{i=1}^N p_i \log p_i \quad (52)$$

where p_i is the probability of finding the system in the state i , i.e., S is a measure of the disorder of the system. According to Shannon's (1949) information theory, S is the amount of information needed to locate the system in the state i . If the states are equally probable so that $p_i = 1/N$ for all i , then (52) reduces to $S = \log N$, the maximum value. On the other hand, if the system is known to be in a particular state i , then (52) gives $S = 0$, the minimum value.

Kolmogorov (1958) pointed out that the same idea can be used to describe how chaotic a dynamical system is. The Kolmogorov entropy K is proportional to the rate at which information about the state of the dynamical system is lost as the system evolves in time and, therefore, allows one to quantify the rate at which an initial uncertainty about the state of the system increases.

In order to calculate K , consider a trajectory $x(t)$ of a dynamical system. Let us partition the d -dimensional phase space into boxes of size l , and measure the state of the system at regular time intervals τ . Let $P_{i_0 i_1 \dots i_n}$ be the joint probability that the system (or $x(t = k\tau)$) is in box i_k at time $t = k\tau$, $k = 0, 1, \dots, n$. The quantity

$$K_n = - \sum_{i_0 \dots i_n} P_{i_0 \dots i_n} \log P_{i_0 \dots i_n} \quad (53)$$

gives the coarse-grained information needed to locate the system. Note that, the difference $K_{n+1} - K_n$ represents the additional information needed to predict occupation of the box i_{n+1} provided that the boxes i_0, \dots, i_n had been occupied previously. Thus, $K_{n+1} - K_n$ is a measure of the information lost about the system from time $t = n\tau$ to time $t = (n+1)\tau$. The Kolmogorov entropy K is then defined as the average rate of this loss of information –

$$\begin{aligned} K &= \lim_{\tau \rightarrow 0} \lim_{l \rightarrow 0} \lim_{N \rightarrow \infty} \frac{1}{N\tau} \sum_{n=0}^{N-1} (K_{n+1} - K_n) \\ &= - \lim_{\tau \rightarrow 0} \lim_{l \rightarrow 0} \lim_{N \rightarrow \infty} \frac{1}{N\tau} \sum_{i_0 \dots i_N} P_{i_0 \dots i_N} \log P_{i_0 \dots i_N} \end{aligned} \quad (54)$$

where the limit $l \rightarrow 0$ is needed to make the Kolmogorov entropy K independent of the particular partition used to calculate it. In dealing with maps with discrete time steps $\tau = 1$, say, the limit $\tau \rightarrow 0$ is omitted.

The Kolmogorov entropy provides a useful measure to distinguish the regular motion, random motion and chaotic motion from each other (Schuster (1989)).

Consider a regular motion, for which initially adjacent points remain adjacent, so that

$$P_{i_0} = l, \quad P_{i_0 i_1} = l \cdot 1, \text{ etc.} \quad (55)$$

Approximating the telescopic sum in (54) by the first term, (55) leads to

$$K = 0, \quad (56)$$

implying that there is no loss of information, as to be expected.

Consider a random motion, for which initially adjacent points get distributed with equal probability over all newly created boxes, so that

$$P_{i_0} = l, \quad P_{i_0 i_1} = l^2, \text{ etc.} \quad (57)$$

which leads to

$$K \sim -\log l \rightarrow \infty \quad (58)$$

implying that the rate of loss of information is now infinite!

Consider next a chaotic motion, for which initially adjacent points become exponentially separated, so that

$$P_{i_o} = l, \quad P_{i_o i_1} = le^{-\lambda}, \text{ etc.} \quad (59)$$

which, on assuming equal probability of occupation over all newly created boxes, leads to

$$K = \lambda > 0 \quad (60)$$

implying that a positive but finite Kolmogorov entropy corresponds to a chaotic behavior.

(60) shows that for one-dimensional maps, K is just the positive Liapunov exponent. In higher-dimensional systems, the loss of information about the system is due only to the positive Liapunov exponents because the box-occupation of the system spreads in phase space at a rate determined by the positive Liapunov exponents. Pesin (1977), in fact, showed that K is equal to the averaged sum of positive Liapunov exponents –

$$K = \int d^d x \rho(x) \sum_i \lambda_i^+(x) \quad (61)$$

where $\rho(x)$ is the invariant density of the system, (see Benettin *et al.* 1976, for a readable discussion).

The Kolmogorov entropy is generally harder to determine than the Liapunov exponents, and so, is less useful in practice.

(iii) Autocorrelation Function

This also provides a useful device to distinguish a true chaotic motion from a quasi-periodic motion as well as a random motion.

If $q(t)$ is a relevant variable, the autocorrelation function $C(\tau)$ is defined by

$$C(\tau) = \lim_{T \rightarrow \infty} \left[\frac{1}{T} \int_0^T q(t + \tau) q(t) dt \right]. \quad (62)$$

If $q(t)$ is periodic or quasi-periodic, then so is the autocorrelation function $C(\tau)$. On the other hand, if $q(t)$ is chaotic and has zero mean, the autocorrelation function $C(\tau)$

decays rapidly with t due to the linear independence¹⁰ of q with itself at a later time. The latter, in turn, is caused by the sensitive dependence of $q(t)$ on initial conditions and the loss of information by the orbit about its past history. If $q(t)$ is purely random possessing no “memory” of the past at any t , the auto-correlation function $C(\tau)$ fluctuates randomly about zero.

(iv) Power Spectra

The Fourier transform or power spectrum of trajectories provides another valuable characterization of chaotic behavior. The power spectrum gives the frequency content of the time variation of the dynamical variables and also helps in distinguishing between quasi-periodic behavior and chaos.

Consider first the case of regular motion. Since the trajectories are confined to tori, they can be represented by the Fourier series

$$\mathbf{q}(t) = \sum_m \mathbf{q}_m e^{im \cdot (\omega t + \delta)} \quad (63)$$

where $\boldsymbol{\omega} = (\omega_1, \dots, \omega_n)$ are the frequencies of the associated torus.¹¹ Clearly, the Fourier transform of $q(t)$,

$$\mathbf{q}(\boldsymbol{\omega}) = \frac{1}{\sqrt{2\pi}} \int_{-\infty}^{\infty} e^{i\omega t} \mathbf{q}(t) dt \quad (64)$$

¹⁰ Linear independence of two random variables implies statistical independence only if the process is a Gaussian random process.

¹¹ Alternatively, if a flow $\phi_t(x)$ is sampled at equally spaced times $j\Delta t$ over a period $T = N\Delta t$, then one has, in place of (63), the following discrete Fourier transform decomposition:

$$q_j = \frac{1}{\sqrt{N}} \sum_{k=0}^{N-1} \hat{q}_k e^{2\pi k j / N}; \quad j = 0, 1, 2, \dots, N-1.$$

The *Sampling Theorem* guarantees that the entire information content of the signal $q(t)$ is contained in the finite set of sampled values $\{\hat{q}_k\}$ if the frequency content of $q(t)$ is limited to frequencies below the *Nyquist critical frequency* $v_c = 1/2\Delta t$, i.e., the sampling rate is sufficiently high. Low sampling rates lead to aliasing problems, seen well in movies in the apparent backward rotation of the wheels of a stagecoach even when the horses are running at full speed!

will be a set of δ -functions at ω_i 's and various overtones, (with frequencies corresponding to all the possible sum and difference frequencies for all the harmonics present), and its power spectrum¹²

$$P(\omega) \equiv |q(\omega)|^2 \quad (65)$$

will consist only of discrete lines of the corresponding frequencies and the various overtones.

In contrast, a chaotic motion, which is completely aperiodic, is indicated by broad noise in $P(\omega)$ (or a broad continuous power spectrum). However, for a complicated quasi-periodic motion, when a signal has very many periodic components, the peaks may blend together and the spectrum may almost look like a broad continuum.

5.9. Ergodicity and Mixing

(i) Ergodicity

Consider a differential equation

$$\frac{dx}{dt} = f(x) \quad (66)$$

on an open subset B of R^n and $f : B \rightarrow B$. Let us examine long-time average behavior along a trajectory $x(t, x_o)$ originating from a point $x_o \in R^n$. If $g(x)$ is some continuous function of the state x , $g : B \rightarrow R^n$, the long-time average is given by,

$$\langle g(x) \rangle = \lim_{\tau \rightarrow \infty} \frac{1}{\tau} \int_0^\tau g[x(t, x_o)] dt. \quad (67)$$

Similarly, consider a discrete map –

$$x_{n+1} = F(x_n) \quad (68)$$

¹² The power spectrum is actually the Fourier transform of the autocorrelation function $C(\tau)$ via the Wiener-Khinchin Theorem.

on an open subset $B \in R^n$ and $F: B \rightarrow B$. For each continuous $g: B \rightarrow R^n$, the long-time average is given by

$$\langle g \rangle = \lim_{N \rightarrow \infty} \frac{1}{N} \sum_{n=1}^N g[F^{[n]}(x_o)]. \quad (69)$$

The dynamical system or the discrete map above are then said to be ergodic if $\langle g \rangle$ is essentially independent of the choice of x_o for every continuous $g: B \rightarrow R^n$. This property implies that every invariant subset B given by

$$F(B) = B$$

is either the null set or R^n .

An example of an ergodic system is one associated with the flow on a torus with incommensurate frequencies. Consider a two-dimensional torus, for which the flow is

$$\left. \begin{aligned} \phi_1 &= \frac{\omega_1 t}{2\pi} + \phi_1(0), \quad \text{mod } \phi_1 = 1 \\ \phi_2 &= \frac{\omega_2 t}{2\pi} + \phi_2(0), \quad \text{mod } \phi_2 = 1 \end{aligned} \right\} \quad (70)$$

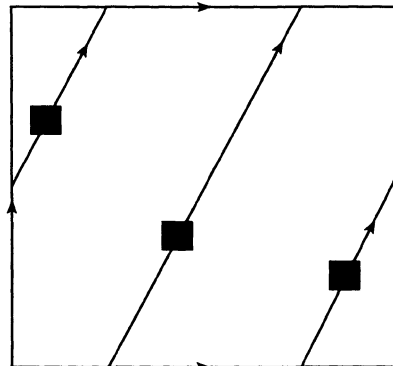


Figure 5.18. Ergodicity on the torus by uniform translation.

where we have introduced the variables $\phi_i = \frac{\theta_i}{2\pi}$ having period 1. This two-dimensional torus is topologically equivalent to the unit square (Figure 5.18) and the flow is ergodic because any orbit densely covers the torus. However, a small area element under this continuous mapping only explores the torus by uniform translation without undergoing any distortion so that neighboring elements map together. Thus, ergodicity does not imply mixing (see below).

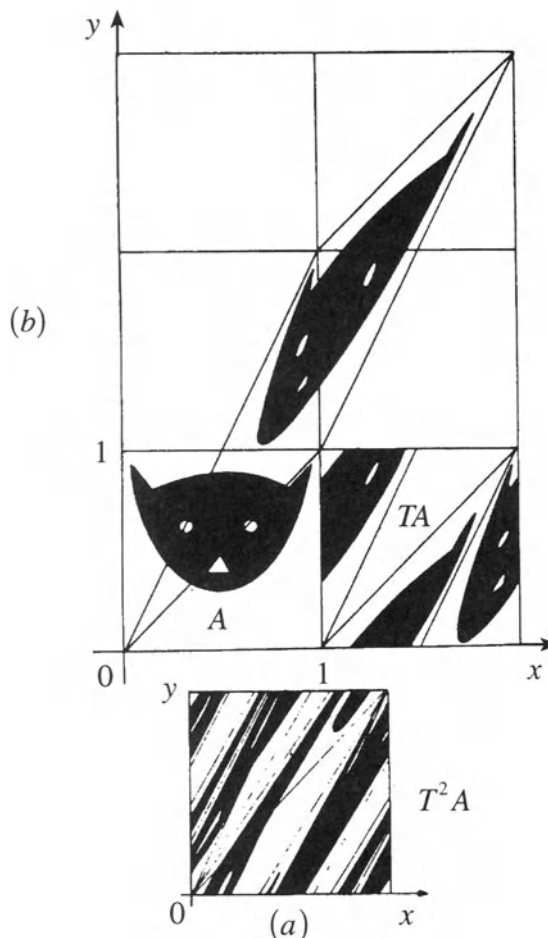


Figure 5.19. (a) Two iterations of the Arnol'd cat map . (b) Mixing on the torus by translation and stretching. (from Arnol'd and Avez (1989)).

(ii) Mixing

We have traced the origin of irregular motion in dynamical systems to hyperbolic fixed points of associated area-preserving mappings. If, therefore, we want models for strongly irregular motion, it is obviously appropriate to try to find mappings all of whose fixed points are hyperbolic. Now, chaotic behavior has been traced to the exponential divergence of nearby trajectories and hence positive Liapunov exponents. Therefore, in a chaotic evolution, a small area element will undergo considerable distortion – this is the basis of the concept of mixing. A simple system which exhibits mixing is the "cat map" of Arnol'd; this is a linear, area-preserving mapping of the unit torus onto itself

$$T: \begin{bmatrix} x_{n+1} \\ y_{n+1} \end{bmatrix} = \begin{bmatrix} 1 & 1 \\ 1 & 2 \end{bmatrix} \begin{bmatrix} x_n \\ y_n \end{bmatrix}, \quad \text{mod } x_n = 1 \quad \text{mod } y_n = 1. \quad (71)$$

As shown in Figure 5.19, an area element undergoes considerable distortion, after merely two iterations of the map (71). The map (71) differs from the ergodic map (70) by possessing a shearing component with stretching. Further, the periodicity of the torus implies that the iterates are modded back onto the unit square, as stated in (71), which, in turn, implies folding the total stretched interval and intermingling previously separated points. Under this combination of stretching and folding, leading to mixing, a small area element is distorted into ever finer and finer filaments and is eventually wrapped densely over the whole torus, just as a drop of ink is homogeneously distributed throughout a glass of water after it has been stirred. Clearly, mixing implies ergodicity, but ergodicity does not imply mixing¹³, (see Lebowitz and Penrose, (1973), for an excellent review).

¹³ A system is said to be mixing over an invariant set S , if the measures associated with a pair of subsets A and B satisfy the following relation (Arnol'd and Avez (1989)) –

$$\lim_{n \rightarrow \infty} \mu(T^{[n]} A \cap B) = \mu(A)\mu(B).$$

(A measure, $\mu(A)$, of a set A in R^n is a set function giving a real number for any set, $\mu: A \rightarrow R$ with the properties: (a) $0 \leq \mu(A) \leq \infty$, (b) $\mu(A \cup B) = \mu(A) + \mu(B)$ for any two disjoint sets A and B .) The term on the left hand side describes the extent to which the subset A is mixed with the subset B under the map T . Mixing occurs when the probability that two points picked at random on S (so they are in the intersection of A and B) is the same as the probability that one point is in A and the other in B . In other words, mixing renders the statistical properties of an ensemble independent of initial conditions.

In order to see that mixing implies ergodicity assume A to be an invariant set so that

$$T^{[n]} A \cap A = A$$

and let $B = A$. The mixing property then implies

$$\mu(A) = [\mu(A)]^2$$

The eigenvalues of T , defined in (71), are

$$\lambda_{\pm} = \frac{3 \pm \sqrt{5}}{2} \quad (72)$$

so that the fixed points of $T^{[n]}$ are of hyperbolic type. Note that $\lambda_+ \lambda_- = 1$ since the transformation (71) is area-preserving. This map therefore leads to stretching and contracting in the direction of the eigenvectors ξ_+ and ξ_- , respectively, where

$$\xi_{\pm} = \begin{bmatrix} 1 \\ \frac{1 \pm \sqrt{5}}{2} \end{bmatrix}. \quad (73)$$

The hyperbolic nature of the fixed points of T causes initially close points to move far apart. The Liapunov exponent for this map is $\sigma = \ln \left(\frac{3 + \sqrt{5}}{2} \right)$.

The mapping $T^{[n]}$ has many fixed points. Any point on the torus for which x_o and y_o are rational fractions is a fixed point of $T^{[n]}$, for some n – the n 's becoming larger with the denominators of the fraction – and these rationals are the only fixed points of $T^{[n]}$ because T has integer coefficients. (Note that these fixed points are dense on the torus because the rational numbers are dense among the reals.) However, all such fixed points are unstable in the sense that nearby points diverge away exponentially. Chaotic behavior then follows from the fact that the points are "scattered" off the dense set of unstable fixed points. These fixed points are given by

$$\begin{bmatrix} x \\ y \end{bmatrix} = T^{[n]} \begin{bmatrix} x \\ y \end{bmatrix} - \begin{bmatrix} k \\ l \end{bmatrix} \quad \begin{array}{l} \text{mod } x_n = 1 \\ \text{mod } y_n = 1 \end{array}. \quad (74)$$

from which,

$$\mu(A) = 0 \text{ or } 1.$$

Thus, an invariant set must be an empty set or the entire system. So, the system is ergodic (i.e., it cannot have two or more disjoint sets with positive measure). Note that ergodicity, on the other hand, does not imply mixing because the measures of the intersections of $T^{[n]}A$ with B can alternate between zero and one, as in the case of quasi-periodic motions on a torus, considered in (i), without any mixing!

Note that, the only fixed point of T is $(0,0)$. The fixed points of $T^{[2]}_1$ ¹⁴ are $(\frac{1}{5}, \frac{3}{5}), (\frac{2}{5}, \frac{1}{5}), (\frac{3}{5}, \frac{4}{5}),$ and $(\frac{4}{5}, \frac{2}{5})$ which are all hyperbolic with eigenvalues $\lambda_{\pm} = (\frac{7 \pm 3\sqrt{5}}{2})/2$. One may locate the homoclinic and heteroclinic points of $T^{[2]}$ as follows: Stable and unstable manifolds H^{\pm} emanate from the fixed point $(0,0)$ of T and wrap around the torus in irrational directions, given by ξ_{\pm} , respectively. Therefore, H^{\pm} intersect each other infinitely often. The stable and unstable manifolds of the fixed points of $T^{[2]}$ also behave similarly, but they also intersect the manifolds H^{\pm} of the fixed point of T , and hence producing an infinity of heteroclinic points (see Figure 5.20).

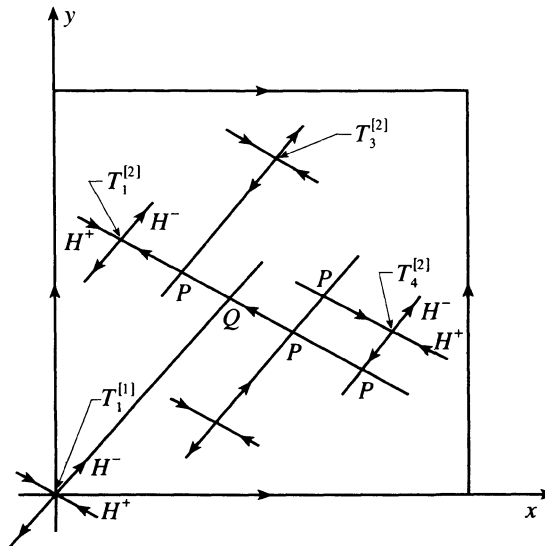


Figure 5.20. Homoclinic (P) and heteroclinic (Q) points of the cat map ($T_i^{[2]}$ ($i = 1, 4$) are the four fixed points of $T^{[2]}$, and $T_1^{[1]}$ is the fixed point of T , (from Tabor (1989)).

(By courtesy of John Wiley and Sons, Inc.)

$$14 \quad T^{[2]} : \begin{bmatrix} x_{n+1} \\ y_{n+1} \end{bmatrix} = \begin{bmatrix} 2 & 3 \\ 3 & 5 \end{bmatrix} \begin{bmatrix} x_n \\ y_n \end{bmatrix}, \text{ mod } x_n = 1$$

(iii) Baker's Transformation

We now understand, at least qualitatively, how ergodicity, mixing and loss of determinacy arise. We have yet to consider the approach to equilibrium and randomness. As a model for these two kinds of behavior, we now discuss the Baker's transformation, which occupies a central phase in chaos dynamics because it provides a paradigm to describe deterministic chaos. (In fact, the Baker's transformation mimics a large number of deterministic systems, at some level of abstraction.) The Baker's transformation can be written as the following area-preserving mapping on the unit square:

$$T : \begin{bmatrix} x_{n+1} \\ y_{n+1} \end{bmatrix} = \begin{cases} \begin{bmatrix} 2x_n \\ \frac{y_n}{2} \end{bmatrix}, & 0 \leq x_n < \frac{1}{2} \\ \begin{bmatrix} 2x_n - 1 \\ \frac{y_n + 1}{2} \end{bmatrix}, & \frac{1}{2} \leq x_n < 1. \end{cases} \quad (75)$$

This map is equivalent to a stretching in the x -direction and a contraction in the y -direction, followed by a cutting and stacking in the y -direction. This process is then repeated, again and again. As can be seen in Figure 5.21, this transformation, therefore, resembles a baker rolling out dough, then cutting and stacking it. Observe that a few iterations of this mapping will lead to rapid mixing, and hence ergodicity, because any area element will ultimately stretch into a long horizontal filament crossing the square many times¹⁵. (However, the rate at which the area elements are stretched is not exponential.)

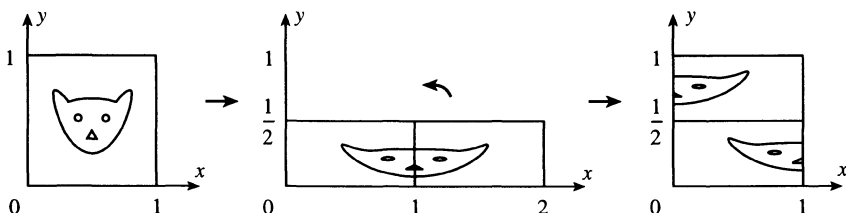


Figure 5.21. Baker's transformation.

¹⁵ Mathematically, the existence of a limiting set A under the transformation T is guaranteed (Strogatz, 1994) by noting that A is the countable intersection of a nested family of compact sets, and is hence, a non-empty compact set, (the successive images of the unit square under T being nested inside each other and compact sets).

The strongly random nature of this transformation may be seen by considering the symbolic dynamics of the binary sequences. For this purpose, let us represent the iterates (x_n, y_n) in binary notation, i.e.,

$$\begin{aligned} x_n &= \sum_{\gamma=1}^N \hat{a}_\gamma 2^{-\gamma} = 0 \cdot \hat{a}_1 \hat{a}_2 \hat{a}_3 \dots \\ y_n &= \sum_{\gamma=1}^N \hat{b}_\gamma 2^{-\gamma} = 0 \cdot \hat{b}_1 \hat{b}_2 \hat{b}_3 \dots \end{aligned} \tag{76}$$

where the \hat{a}_γ 's and the \hat{b}_γ 's are either 0 or 1.

EXAMPLE 4

Note that

$$\begin{aligned} \frac{1}{4} &= 0.0100\dots \\ \frac{1}{8} &= 0.00100\dots \\ \frac{1}{16} &= 0.000100\dots \end{aligned}$$

Note that doubling of a number corresponds to moving the decimal point one place to the right and halving a number corresponds to moving it one place to the left. This feature is, of course, very suitable for representing the Baker's transformation. Let the initial condition $X_o = (x_o, y_o)$ be represented by the strings

$$\left. \begin{aligned} x_o &= \cdot a_1 a_2 a_3 \dots \\ y_o &= \cdot b_1 b_2 b_3 \dots \end{aligned} \right\} \tag{77}$$

where the a 's and the b 's are all either 0 or 1. This suggests that one may represent the position of (x_o, y_o) in the unit square conveniently by putting these two strings back to back, i.e.,

$$X_o = (x_o, y_o) \equiv \dots b_3 b_2 b_1 \cdot a_1 a_2 a_3 \dots \quad (78)$$

Now, a forward iteration of the map corresponds to a doubling of x and a halving of y , so that X_1 is obtained by simply moving the decimal point one place to the right, i.e.,

$$X_1 = \dots b_3 b_2 b_1 a_1 \cdot a_2 a_3 \dots \quad (79)$$

which is repeated to obtain the successive X_i . This process is known as a Bernoulli shift.¹⁶

¹⁶ The Bernoulli shift is a map which corresponds to taking for θ_{n+1} the fractional part of $2\theta_n$ for $n = 0, 1, \dots$ (Note that this is not a one-to-one mapping because each θ_{n+1} is the image of two points θ_n .) Thus,

$$\theta_{n+1} = 2\theta_n \pmod{1}$$

which implies

$$\theta_{n+1} = \begin{cases} 2\theta_n, & \text{if } 0 \leq \theta_n < \frac{1}{2} \\ 2\theta_n - 1, & \text{if } \frac{1}{2} \leq \theta_n < 1 \end{cases}.$$

If we represent θ_o using a binary expression

$$\theta_o = c_1 c_2 c_3 \dots$$

then an iteration of the map corresponds to moving the decimal place one place to the right. If θ_o has a binary representation of finite length, say, $\theta_o = a/2^m$ for some positive integers m and a (a odd), then $\theta_n = 0$ for all $n > m$. (Ex: $\theta_o = \frac{1}{4}$ leads to $\theta_n = \frac{1}{4}, \frac{1}{2}, 0, 0, \dots$, with a fixed point at 0.) If θ_o is a rational number and has a binary representation of infinite length, say, $\theta_o = a/2^m r$ for some integers $a, m \geq 0, r \geq 3$ (r odd), then $\theta_{n+p} = \theta_n$ ($1 \leq p \leq r$) for all $n \geq m$. (Ex: $\theta_o = \frac{1}{3}$ leads to $\theta_n = \frac{1}{3}, \frac{2}{3}, \frac{1}{3}, \frac{2}{3}, \dots$ which is a two-cycle with $\theta_o = 0.01010 \dots = 1/3$, $\theta_1 = 0.1010 \dots = 2/3$.) On the other hand, $\theta_o = \frac{1}{7}$ leads to $\frac{1}{7}, \frac{2}{7}, \frac{4}{7}, \frac{1}{7}, \dots$ which is a three-cycle with $\theta_o = 0.001001 \dots$, $\theta_1 = 0.01001 \dots$) If θ_o is an irrational number, then θ_n will be an aperiodic sequence which wanders arbitrarily close to each point of the interval $[0, 1]$. The sensitivity to initial conditions can be demonstrated by shifting the initial point slightly, i.e., putting $\theta'_o = \theta_o + \varepsilon$, so that

$$\theta'_n - \theta_n = 2^n \varepsilon = \varepsilon e^{n \ln 2}.$$

One may adopt a more "coarse-grained" description of the motion and identify an orbit by 0 if $0 \leq x_n < \frac{1}{2}$ and by 1 if $\frac{1}{2} \leq x_n < 1$. (This implies recognizing just the first digit in the full binary representation of the x_n .) Thus, the coarse-grained history of the motion when the map is run from $n = -\infty$ to $n = +\infty$, will be the doubly infinite sequence (called the symbolic description of the orbit)

$$\dots b_3 b_2 b_1 a_1 a_2 a_3 \dots \quad (80)$$

(Note that in the reverse direction $n \leq 0$, x and y deformations are interchanged.) The binary representations (77) associated with typical, irrational initial coordinates (x_o, y_o) are infinite nonrepeating sequences of zeros and ones so that this motion is isomorphic to a coin toss (1 for heads, 0 for tails) and is random. (It may be noted that each orbit has a unique symbolic sequence.)

In order to predict the sequence X_k for all k one needs to specify the initial condition X_o with an infinite number of digits, i.e., with zero error, which, of course, is impossible. On the other hand, any uncertainty, however small, in specifying the initial condition X_o , leads to an error having any magnitude between zero and one for sufficiently large n . This sensitive dependence of the motion on initial conditions signifies the presence of chaos in the motion generated by this completely deterministic system.

This system is also ergodic because the trajectory starting from any initial condition, with the exception of a set of measure zero (the rationals), passes arbitrarily close to any point (x, y) in the unit square.

As this mixing system approaches an equilibrium state, a "coarse-grained" observable function approaches a limit that is uniform, independent of initial conditions. In order to demonstrate the approach to this equilibrium state, it proves convenient to define a distribution function $f^{[n]}(x, y)$ after n iterations (Berry, (1978)). The Master equation for $f^{[n]}(x, y)$ is (McCauley, (1993)),

$$f^{[n]}(x, y) = \int_0^1 \int_0^1 dx' dy' f^{[n-1]}(x', y') \delta(x - g(x')) \delta(y - h(y')) \quad (81)$$

where,

Thus, two initially very close orbits exponentially separate with Liapunov exponent $\sigma = \ln 2 > 0$. (This may, of course, be appreciated by noting that there exists an irrational number close to every rational number.)

$$g(x) = \begin{cases} 2x, & 0 \leq x \leq 1/2 \\ 2x - 1, & 1/2 \leq x \leq 1 \end{cases}$$

$$h(y) = \begin{cases} y/2, & 0 \leq y \leq 1/2 \\ (y + 1)/2, & 1/2 \leq y \leq 1. \end{cases}$$

Equation (81) merely states that the point (x', y') is mapped onto the point (x, y) after one iteration of the map (75), and represents a Markov process with a deterministic transition rate $\delta[x - g(x')] \delta[y - h(y')]$.

On noting that

$$\delta(x - g(x')) = \frac{1}{|g'(x')|} \delta(x' - g^{-1}(x))$$

$$\delta(y - h(y')) = \frac{1}{|h'(y')|} \delta(y' - h^{-1}(y))$$

equation (81) becomes

$$f^{[n]}(x, y) = \int_0^{1/2} \int_0^{1/2} dx' dy' f^{[n-1]}(x', y') \delta\left(x' - \frac{x}{2}\right) \delta\left(y' - 2y\right) \quad (82)$$

$$+ \int_{1/2}^1 \int_0^1 dx' dy' f^{[n-1]}(x', y') \delta\left(x' - \frac{x+1}{2}\right) \delta\left(y' - (2y-1)\right)$$

from which, we obtain the “Liouville Equation of Motion” for $f^{[n]}(x, y) -$

$$f^{[n]}(x, y) = \begin{cases} f^{[n-1]}\left(\frac{x}{2}, 2y\right), & 0 \leq y < 1/2 \\ f^{[n-1]}\left(\frac{x+1}{2}, 2y-1\right), & 1/2 \leq y \leq 1. \end{cases} \quad (83)$$

Next, let us "coarse-grain" $f^{[n]}$ to remove some of its fine-scale variations. This may be done by defining the invariant measure (which does not change during the course of evolution of the iterates under the map (83)¹⁷⁾ $W_n(x)$ –

$$W_n(x) \equiv \int_0^1 f^{[n]}(x, y) dy \quad (84)$$

which serves as a measure of how the iterates become distributed over the unit interval. (Note that for an ergodic system, $W_n(x)$ does not depend on x .) We then obtain an equation of motion for the W_n :

$$W_n(x) = \int_0^{\frac{1}{2}} f^{[n-1]}\left(\frac{x}{2}, 2y\right) dy + \int_{\frac{1}{2}}^1 f^{[n-1]}\left(\frac{x+1}{2}, 2y-1\right) dy \quad (85)a$$

or

$$W_n(x) = \frac{1}{2} \left[W_{n-1}\left(\frac{x}{2}\right) + W_{n-1}\left(\frac{x+1}{2}\right) \right]. \quad (85)b$$

Equation (85) resembles the "rate equation" for a random-walk process (with steps to x from $\frac{x}{2}$ and $\frac{x+1}{2}$). Note that the map (85) continually averages $f^{[n]}$ in each half of the mapping. Therefore, in the limit $n \rightarrow \infty$, this process must lead to a $f^{[n]}$ that is uniform in x , corresponding to equilibrium. Note that the "equilibrium" state given by

¹⁷ More precisely, a measure μ is invariant under the map ϕ if, for any set S in the support of μ , we have

$$\mu(S) = \mu(\phi(S)).$$

Further, an invariant measure μ is ergodic provided μ cannot be decomposed into two other invariant measures, i.e.,

$$\mu \neq \alpha \mu_1 + (1-\alpha) \mu_2$$

with $\alpha \neq 0$ and 1, and $\mu_1 \neq \mu_2$.

$W_n(x) = 1$ is actually a fixed-point solution of equation (85)b! In fact, since each iteration replaces the value of W at x by the mean of its values at the points $\left(\frac{x}{2} \text{ and } \frac{x+1}{2}\right)$ surrounding x , any initial $W_o(x)$ will tend to unity after an infinity of iterations¹⁸. (This smoothing effect of the mapping may also be seen by noting that the iterations destroy all Fourier components $e^{2\pi i \ell x}$ ($\ell = 1, 2, \dots$) describing the variation of $W_o(x)$ (see Exercise 3).)

¹⁸ In order to see more clearly that an arbitrary smooth initial density $W_o(x)$ evolves to the “equilibrium” solution $W(x) = 1$, note first that direct iteration of the equation of motion (85)b gives (McCauley, (1993))

$$\begin{aligned} W_1(x) &= \frac{1}{2} \left[W_o\left(\frac{x}{2}\right) + W_o\left(\frac{x+1}{2}\right) \right] \\ W_2(x) &= \frac{1}{2^2} \left[W_o\left(\frac{x}{2^2}\right) + W_o\left(\frac{x+1}{2^2}\right) + W_o\left(\frac{x+2}{2^2}\right) + W_o\left(\frac{x+3}{2^2}\right) \right] \\ &\vdots \\ W_n(x) &= \sum_{j=0}^{2^n-1} \frac{1}{2^n} W_o\left(\frac{x+j}{2^n}\right). \end{aligned}$$

Thus, in the limit $n \rightarrow \infty$, $W_n(x)$ is the average of the values of $W_o(x)$ over the interval $(0,1)$. In fact, in the limit $n \rightarrow \infty$, the sum on the right hand side becomes the Riemann sum

$$\sum_{j=0}^{2^n-1} \Delta x_j W_o(x_j)$$

with,

$$x_j \equiv \frac{x+j}{2^n}, \quad \Delta x_j \equiv \frac{\Delta j}{2^n} = \frac{1}{2^n}$$

for the integral

$$\int_0^1 W_o(x) dx.$$

Therefore,

$$\lim_{n \rightarrow \infty} W_n(x) = \int_0^1 W_o(x) dx = 1$$

as expected!

CHAPTER 6

CHAOS IN DISSIPATIVE SYSTEMS

A crucial distinction exists between the dissipative systems and conservative Hamiltonian systems. By Liouville's Theorem, the solution flow for a Hamiltonian system preserves volumes in phase space. Dissipative systems, by contrast, usually give rise to solution flows which contract volumes in phase space. Though this volume contraction is a local property in phase space, it produces global effects by giving rise to a bounded set in the phase space, which ultimately contains the solution flow. Indeed, dissipative systems of dimensions equal to and greater than three can have bounded trajectories, which may be attracted not by a fixed point nor by a periodic/quasi-periodic orbit, but by an object of complicated infinitely many-layered structure called a strange attractor. The trajectories on this attractor diverge continually from each other locally, but remain bounded globally. Besides, the evolution on the attractor is essentially aperiodic. Strange attractors are sometimes modeled by fractals which are geometric objects that have the same shape at all scales. Lack of differentiability is also a hallmark of fractal sets, so fractals always appear jagged. Adoption of fractal geometry releases one from bondage to smooth surfaces and smooth curves and enables one to come to terms with nature, for as Mandelbrot (1983) put it – “clouds are not spheres, mountains are not (cones), and bark is not smooth, nor does lightning travel in a straight line”.

6.1. Phase-Space Dynamics of Dissipative Systems

Consider a deterministic dynamical system governed by an evolution equation of the form

$$\frac{d\mathbf{x}(t)}{dt} = \mathbf{F}(\mathbf{x}(t), \mu) \quad (1)$$

where \mathbf{x} is a vector in R^n , and \mathbf{F} may depend on a parameter μ .

Let $\mathbf{x}(\mathbf{y}, t)$ be the solution of equation (1) with initial condition –

$$t = 0 : \mathbf{x} = \mathbf{y} \quad (2)$$

For dissipative systems, the phase flow $\phi_t(y) = x(y, t)$ contracts volumes, i.e.,

$$\sum_{i=1}^n \frac{\partial F_i}{\partial x_i}(x, \mu) < 0. \quad (3)$$

This then implies that, for a finite volume V in phase space R^n , the sets $\phi_t(V)$ decrease, as $t \rightarrow \infty$, to a set

$$X = \bigcap_{t>0} \phi_t(V) \quad (4)$$

(of zero volume). Thus, every solution curve starting at some $y \in V$ approaches X as $t \rightarrow \infty$. (By contrast, for conservative bounded systems, thanks to Poincaré's Recurrence Theorem, almost all curves $\phi_t(y)$ return infinitely often, arbitrarily close to their initial state y .) X is called an attractor.

DEFINITION: An attractor, for the flow ϕ_t , is a compact set X , satisfying the following properties:

- (i) X is invariant under $\phi_t : \phi_t(X) = X$;
- (ii) X has a shrinking neighborhood, i.e., there is an open neighborhood U of X , $U \supset X$, such that $\phi_t(U) \subset U$ for $t > 0$, and $X = \bigcap_{t>0} \phi_t(U)$,¹

¹ The existence of an attractor is therefore associated with a contractive mapping on a complete metric space:

$$a_{n+1} = f(a_n)$$

where a_0, a_1, a_2, \dots is a bounded, monotone sequence of elements from a complete metric space X (which possesses a metric $d: X \times X \rightarrow R$ with the properties: $d(x, y) \geq 0$, $d(x, y) = 0$ if and only if $x = y$, $d(x, y) = d(y, x)$, and $d(x, y) \leq d(x, z) + d(z, y)$ – the triangle inequality $\forall (x, y, z) \in X$) so that

$$d(f(x), f(y)) \leq cd(x, y), \quad 0 \leq c < 1, \quad \forall (x, y) \in X,$$

(Peitgen *et al.* (1992)). A sequence $\{a_n\}_{n=1}^\infty$ of elements in a metric space X is said to converge to a point $a \in X$ if, for a given number $\varepsilon > 0$, there is an integer $N > 0$ such that $d(a_n, a) < \varepsilon$, $\forall n > N$. The point $a \in X$ is called the limit of the sequence, $a = \lim_{n \rightarrow \infty} a_n$. A metric space X is compact if every infinite sequence $\{a_n\}_{n=1}^\infty$ in X contains a subsequence having a limit $a \in X$. A metric space X is complete if every converging sequence $\{a_n\}_{n=1}^\infty$ in X has a limit $a \in X$. The uniqueness and invariance of the attractor (or the fixed point of the above contractive mapping) then implies

- (iii) The motion on X is recurrent: ϕ_t has an orbit which is dense in X , i.e., there is a point x_0 of X such that every x in X can be approximated arbitrarily closely by points of the form $\phi_t(x_0)$ with $t \geq 0$.

Thus, an attractor is an invariant set that attracts nearby states. Note that an attractor results due to local repulsion and global attraction of the flow and can be considered to be the closure of unstable manifolds of a system executing globally bounded motions. One may define an invariant measure on the attractor, which may then be used to characterize the statistical properties of the motion on the attractor.

DEFINITION: If X is an attractor, its basin of attraction $B(X)$ is defined to be the closure of the set of initial points y such that $\phi_t(y)$ approaches X as $t \rightarrow \infty$, i.e.,

$$B(X) = \left\{ y \left| y = \lim_{t \rightarrow \infty} \phi_t(x) \text{ for } x \in X \right. \right\}.$$

$$a = \lim_{n \rightarrow \infty} a_n, \quad f(a) = a.$$

The contractive nature of the map also implies that

$$\frac{d(b, a)}{d(b, f(b))} \geq 1 \quad \forall b \in X.$$

However, it turns out that this ratio is also bounded from above (Barnsley (1988)). Because, by noting that the function $d(x, y)$ for fixed $x \in X$ is continuous in $y \in X$, we have

$$\begin{aligned} d(b, a) &= d\left(b, \lim_{n \rightarrow \infty} f^{[n]}(b)\right) \\ &= \lim_{n \rightarrow \infty} d\left(b, f^{[n]}(b)\right) \\ &\leq \lim_{n \rightarrow \infty} \sum_{m=1}^n d\left(f^{[m-1]}(b), f^{[m]}(b)\right), \text{ by the triangle inequality} \\ &\leq \lim_{n \rightarrow \infty} d(b, f(b)) \left(1 + c + c^2 + \cdots + c^{n-1}\right) \\ &= (1 - c)^{-1} d(b, f(b)). \end{aligned}$$

So,

$$\frac{d(b, a)}{d(b, f(b))} \leq (1 - c)^{-1}, \quad 0 \leq c < 1.$$

Thus, the basin of attraction B is the union of all the neighborhoods U discussed above. A given dynamical system may have many attractors, each with its own distinct basin of attraction. The boundaries separating the basins of attraction is usually a fractal (see Section 6.3).²

EXAMPLE 1

Consider a map $x_{n+1} = F(x_n) = x_n^2$ (Gulick (1992)). The fixed points of this map are at $\bar{x} = 0$ and 1. The basin of attraction for $\bar{x} = 0$ is

$$B(\bar{x} = 0) = \left\{ x \mid \lim_{n \rightarrow \infty} F^{[n]}(x) = x^{2^n} \rightarrow 0 \right\}$$

or

$$B(\bar{x} = 0) = \{ x \mid |x| < 1 \}.$$

Thus, after a transient, a dissipative system usually evolves in the neighborhood of the attractor. This implies that dissipative flows, which initially occupy higher-dimensional manifolds, eventually end up on very low-dimensional manifolds.

An attractor may be a regular attractor (which is a smooth Euclidean manifold with regular trajectories) or a strange attractor (which may be a topologically complex fractal with chaotic trajectories). Further, since an attractor must have zero volume, it must be a fixed point or a limit cycle in the regular case, or a strange attractor in the chaotic case (see Section 6.2).

In a two-dimensional phase space, the only possible attractors are asymptotically stable fixed points and limit cycles.

² The well known Newton's method for finding zeros of a polynomial $g(x)$ can be viewed as a dynamical system with attracting fixed points corresponding to the zeros of $g(x)$:

$$a_{k+1} = N(a_k); \quad k = 0, 1, 2, \dots$$

where,

$$N(a) \equiv a - \frac{g(a)}{g'(a)}$$

implying that if the sequence a_0, a_1, a_2, \dots converges to some number, then the limit is a zero of $g(x)$. Thus, trajectories from an arbitrary starting point lead to one of these fixed points. From this point of view, the usefulness of Newton's method is determined by the size of the basins of attraction of the fixed points (a_0 being taken from inside one of these basins of attraction) (Eubank and Farmer (1989)).

THEOREM 6.1 (Poincaré-Bendixson Theorem)

Consider the system

$$\left. \begin{aligned} \frac{dx}{dt} &= f(x, y) \\ \frac{dy}{dt} &= g(x, y) \end{aligned} \right\}$$

where f and g are continuous functions in R^2 . If a trajectory remains bounded as t increases indefinitely, then the trajectory is a fixed point or a limit cycle, or approaches a fixed point or limit cycle.

6.2. Strange Attractors:

The idea of chaos in a dissipative system, at first sight, might appear to be somewhat paradoxical since sensitivity to initial conditions implies divergence of nearby trajectories, whereas dissipation implies convergence of trajectories. For flows on the plane, at any rate, it is topologically impossible to reconcile these two opposing tendencies. (Actually, since two trajectories cannot intersect in phase space, according to the Poincaré-Bendixson Theorem, one cannot have anything more than a simple closed curve in two dimensions!) However, if the phase space is three (or higher) dimensional, the above paradox can be resolved by the following scenario: Trajectories diverge within a plane by spiralling out. Then, they emerge from the plane and "fold over" and return back to the center of the spiral (see Figure 6.1). This process is repeated ad infinitum. Observe that this process involves two operations –

- (i) stretching, which leads to local exponential separation of trajectories and hence the sensitive dependence on initial conditions,
- (ii) folding, which leads to global convergence of trajectories and keeps the phase-space volume covered by the trajectories still bounded, (note that stretching can occur in a bounded domain only if there is folding of the orbits!)

This process leads to an object of great topological complexity called the "strange attractor". Strange attractors have zero volume because, for a dissipative system, the phase-space volumes must contract to zero for large times. Thus, a strange attractor would have to be a surface, a curve or a point! However, none of these objects allows a chaotic motion. So, a strange attractor must be an object of folds within folds ad infinitum with a noninteger dimension – the intersection of a strange attractor with a

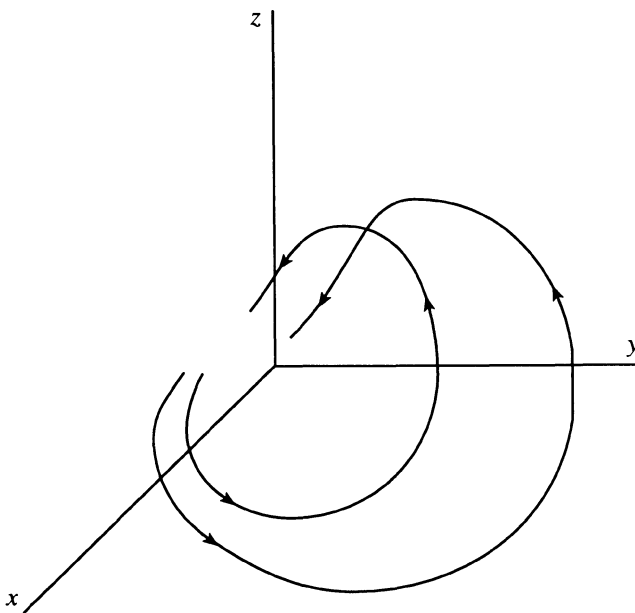


Figure 6.1. The stretching and folding process.

straight line is a Cantor set (see Section 6.3). (Note that a fractional dimension of the attractor is only a necessary condition for chaos, a positive Liapunov exponent being the sufficient condition.) Strange attractors provide a mechanism by which the motion of deterministic dissipative dynamical systems can display intrinsically chaotic behavior.

For an n -dimensional map, the local volume $\Delta\tau$ contracts by a factor $|\det M(x)|$ for each iteration, where M is the Jacobian matrix of the map. This factor represents a rate of volume contraction, which is also given in terms of the Liapunov exponents

$$\sum_{i=1}^n \sigma_i = \ln |\det M(x)| \quad (5)$$

where $|\det M(x)| < 1$ so that the sum of the Liapunov exponents is less than zero. However, at least one of these exponents must be positive to allow sensitive dependence on initial conditions, necessary for chaos.

As an example of a strange attractor, let us consider Smale's horse-shoe map.

EXAMPLE 2

Smale's horseshoe map.

Smale's horseshoe mapping (Smale, 1967) is a mapping of a rectangular phase space onto itself and consists of a sequence of stretching and folding operations as follows: Take some initial rectangle $ABCD$ (call it the region R) and stretch it out into a long thin one of reduced area $A_1B_1C_1D_1$ on account of dissipation in the system (call this operation S). This new rectangle is then folded over into the shape of a horseshoe and fitted back into the original rectangle $ABCD$ (call this operation F). Upon repeating this sequence of operations an infinite number of times $SFSF\dots$ on the horseshoe, a highly complex layered-structure ensues. This structure is a strange attractor because while neighboring points are pulled apart by each stretching, distant points are brought together by the successive foldings. Letting $s = F \circ S$ denote the composite map on R , i.e., $s: R \rightarrow R$, the attracting set X is given by the intersection of all the sets produced by iterations of s on R , i.e.,

$$X = \bigcap_{n=0}^{\infty} s^{[n]}(R).$$

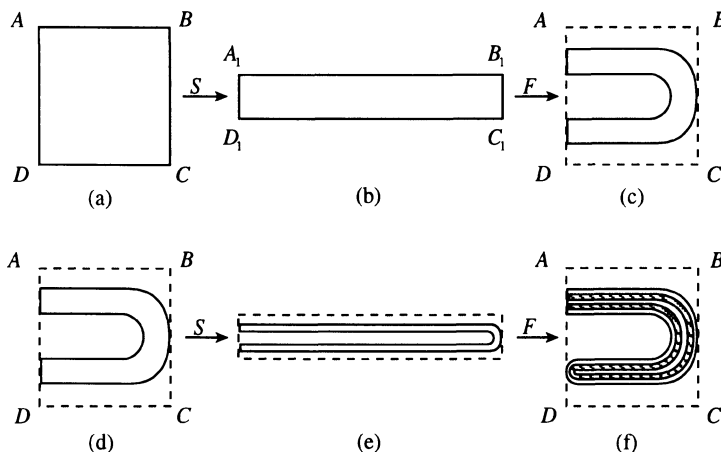


Figure 6.2. Two iterations of the Smale horseshoe mapping.

Now, a look at a cross section OO' of successive images of the transformation, reveals a sequence of segments doubling in number with each iteration (Figure 6.3). This structure corresponds to a Cantor set (see Section 6.3).

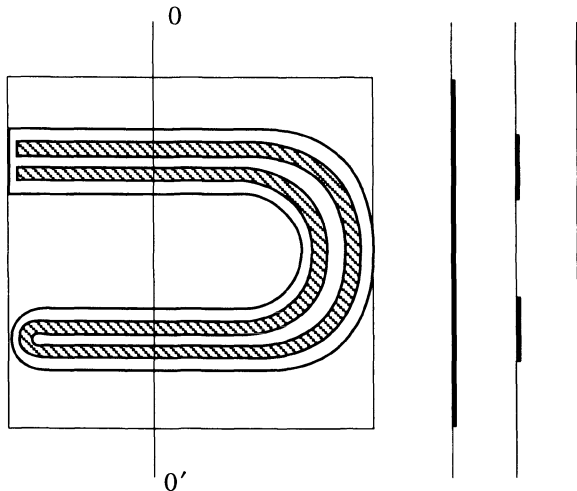


Figure 6.3. Successive cross sections of Smale's horseshoe.

Smale's horseshoe map provides a paradigm to describe the strong bending of the manifolds near a homoclinic point leading to stretching and folding of a rectangular element. So, horseshoe-type constructions are extensively used to describe chaotic motion in dynamical systems.

6.3. Fractals

Mandelbrot associated many physical processes and mathematical constructions with fractal behavior. The unifying feature of fractal distributions is the absence of a characteristic length or scale invariance³. Fractals are self-similar objects possessing a

³ A structure is said to be scale-invariant if its characteristic measures have the following property:

$$f(br) = b^{-\alpha} f(r).$$

It can be shown that the only function which does not introduce a characteristic scale in the problem and satisfies this property is the one possessing a power-law behavior

recursive structure, i.e., apart from the scaling factor, they look the same on different scales of observation so that each part, however small, has a shape similar to that of the whole. Despite their geometrical complexity, fractals can be generated by the application of simple transformations on simple spaces like a compact metric space (see Footnote 1). The fractal dimension of a set describes how densely the set occupies the embedding metric space. One may calculate the fractal dimension by using a coarse-graining of the structure, i.e., covering the set with unit volumes and regarding the volume as a function of the size of the measuring unit. Let S be a bounded subset of an Euclidean space R^p and $N(l)$ be the number of p -dimensional cubes of side l needed to cover the subset S . The fractal dimension of S is then defined as a "capacity measure" in the limit

$$D = \lim_{l \rightarrow 0} \frac{\ln N(l)}{\ln(1/l)} \quad (6)$$

provided this limit exists. (6) implies that $N(l) \sim l^{-D}$, for small l , expressing the fact that the number $N(l)$ (and hence the volume measured) increases as l diminishes. Sets for which $D \sim p-1$ will be "very sparse" while sets for which $D \sim p$ "almost fill" the embedding space. Note that the capacity measure of the fractal dimension considers the length l as the measure, so depends on the metric properties of the space R^p . The capacity dimension turns out to be merely a specialized version of the Hausdorff dimension (see Appendix 6.1) with the restriction that the length of the cubes are the same.

The fractal dimension of a set may also be defined as a self-similarity dimension. In order to appreciate this definition, consider a single object of linear size L . Divide this object into N identical pieces of size l , each of which is a reduced version of the original object by the same factor $r = l/L < 1$. This procedure is then repeated again so that N of the newly created pieces of size Lr^2 are arranged inside a piece of size Lr in exactly the same way as these parts were arranged inside the original object. The fractal is then obtained by repeating this procedure an infinite number of times.

Consequently, the fractal can be divided into N identical parts, each of which is a rescaled version (by a factor r) of the whole set. Let $N_1(\varepsilon)$ denote the number of boxes on a grid of size ε needed to cover one such part. Then, the number of boxes needed to cover the complete fractal is

$$N(\varepsilon) = N(l)N_1(\varepsilon). \quad (7a)$$

$$f(r) \sim r^{-\alpha}.$$

Due to the self-similarity, $N_1(\varepsilon)$ is the same as the number of boxes needed to cover the complete set with boxes of size ε/r :

$$N_1(\varepsilon) = N(\varepsilon/r) = N\left(\frac{\varepsilon}{l}L\right). \quad (8)$$

Using (8), (7)a leads to

$$N(ab) = N(a)N(b) \quad (7b)$$

which implies a power-law behavior

$$N(l) \sim l^{-D} \quad (9a)$$

or

$$D = \frac{\ln N(l)}{\ln(1/l)} \text{ for small } l. \quad (9b)$$

where D is the self-similarity dimension⁴. According to (9), the fractal dimension D is independent of the scale size l , and depends only on the scaling under changes in

⁴ For non-uniform fractals, for which the reduction factor r is not identical for all of the N offsprings at a given stage of the fragmentation process, the formula (9)a can be generalized as follows: The number of boxes needed to cover the complete fractal now is

$$N(\varepsilon) = \sum_{i=1}^{N(l)} N_i(\varepsilon)$$

where, by self-similarity of the structure, the number of boxes on a grid of size ε needed to cover the i th part is given by

$$N_i(\varepsilon) = N\left(\varepsilon/r_i\right).$$

If $N(l)$ scales according to

$$N(l) \sim l^{-D}$$

we then have

$$\sum_{i=1}^N r_i^D = 1,$$

resolution or size so that the fractal dimension of a fractal is the same no matter what part of the fractal one considers for the calculation of D . Thus, the fractal dimension D is a global invariant of the motion on a chaotic attractor, (see Farmer *et al.* (1983) for an excellent review).

Note that the number of segments of size l needed to cover a line goes as l^{-1} , and thus its dimension is 1. (If the line is so contorted that it seems to fill an area rather than a line, its dimension is close to 2. Therefore, a non-integer value of D between 1 and 2 would be a useful measure of the non-smoothness of a line.) The number of squares with side l necessary to cover a surface goes as l^{-2} , and its dimension is 2 (a non-integer value of D between 2 and 3 would similarly be a measure of the non-smoothness of a surface); the number of cubes of side l necessary to cover a solid object goes as l^{-3} , and its dimension is 3. For a fractal object, D is, in general, a non-integer. The fractal dimension of an object is always larger than the topological dimension of the object, but is, however, less than the dimension of the space where the object is embedded. Further, the dimension of the natural measure on an object may be different from that of its support which gives rise to the concept of a multi-fractal (Mandelbrot, 1974); see Section 6.4.

EXAMPLE 3

Cantor Set.

Divide a unit interval into thirds, remove the central third and repeat the process on each remaining segment, so that at each generation the number of intervals increases by a factor of 2, while the length of each subinterval decreases by a factor of 3. In the limit of infinite iterations, this process leads to the Cantor set S . S is defined in terms of a nested sequence of closed subsets

$$S_o \supset S_1 \supset S_2, \dots$$

of $[0,1]$ (see Figure 6.4), where

which, for a uniform fractal (with $r_i = r \sim l$, $i = 1, 2, \dots, N$), reduces to (9)! Observe that the fractal dimension D now appears as a kind of statistical average.

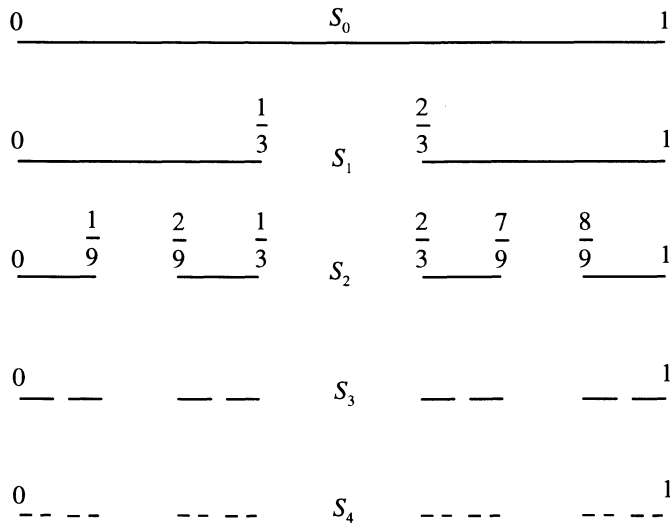


Figure 6.4. Construction of Cantor's middle-thirds set $S = \cap_{n=0}^{\infty} S_n$.

$$S_o = [0, 1]$$

$$S_1 = \left[0, \frac{1}{3}\right] \cup \left[\frac{2}{3}, 1\right]$$

$$S_2 = \left[0, \frac{1}{9}\right] \cup \left[\frac{2}{9}, \frac{1}{3}\right] \cup \left[\frac{2}{3}, \frac{7}{9}\right] \cup \left[\frac{8}{9}, 1\right]$$

etc.

S is the set of all points common to S_o, S_1, S_2, \dots so that

$$S = \bigcap_{n=0}^{\infty} S_n$$

where S_n is the union of 2^n closed subintervals of length $1/3^n$ of $[0, 1]$ of the form $\left[\frac{k}{3^n}, \frac{(k+1)}{3^n}\right]$ for an integer k , $0 \leq k < 3^n - 1$. The fractal dimension of the Cantor set S is

$$D = \lim_{n \rightarrow \infty} \frac{\ln(2^n)}{\ln\left(\frac{1}{1/3^n}\right)} = \frac{\ln 2}{\ln 3} = 0.6309\dots$$

which is an irrational number less than 1. However, since the Cantor set is merely a discrete set of points, its topological dimension is zero. Thus, the Cantor set is a fractal set.

Note that the Cantor set S is nowhere dense in $[0,1]$, because, in any interval, there is a subinterval which does not contain a point of S . In fact, what is left, after infinite iterations, is a set that has zero Lebesgue measure with zero net length L and an uncountable number of elements because

$$L = 1 - \frac{1}{3} - \frac{2}{9} - \frac{4}{27} - \dots = 1 - \frac{1}{3} \sum_{n=0}^{\infty} \left(\frac{2}{3}\right)^n = 0.$$

Thus, the Cantor set contains no non-empty open intervals and hence an infinite set of disconnected pieces which lie in a zero length space, yet they have a one-to-one correspondence with the set of all real values which fill the interval $[0,1]$. The Cantor set S contains no isolated points because every point in S has a neighboring point arbitrarily closeby. Further, the Cantor set is closed because every point of the set is a limit point for the set. Note that the Cantor set constructed above has the property of scalar invariance: the set between 0 and 1 will look precisely the same as that part of it between 0 and $1/3$, if the latter is magnified by a factor of 3.

EXAMPLE 4

Koch's Snowflake.

Consider a line segment of unit length. Then, the central third of this line is extracted and replaced by two lines of length $1/3$. This process is continued, the central

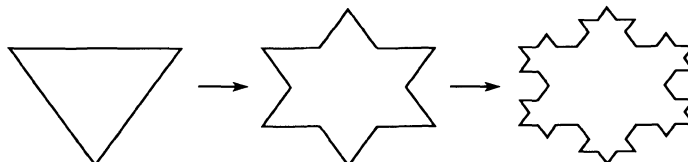


Figure 6.5. The first steps of constructing a Koch snowflake.

third of any line segment being replaced at each stage by two line segments of length one third of the original line segment. The protrusion of the replacement is always on the same side of the curve (Figure 6.5). This iteration leads to a curve whose length diverges with resolution⁵ but which encloses a finite area⁶. (The perimeter of the usual objects also depends on the resolution, but it converges very fast to a finite limiting value.) Thus, the fractal dimension D of this curve is between 1 and 2. In order to find D , note that after n iterations, the resulting set will have $N = 2^{2n}$ pieces of length $1/3^n$ so that

$$D = \lim_{n \rightarrow \infty} \frac{\ln(2^{2n})}{\ln\left(\frac{1}{1/3^n}\right)} = \frac{\ln 4}{\ln 3} = 1.2618\dots$$

which is an irrational number between 1 and 2.

EXAMPLE 5

Sierpinski Triangle.

To construct a Sierpinski triangle, extract from an original triangle the inverted half-scale copy of itself formed by joining the midpoints of the three sides. Three half-scale triangles now remain, so one-fourth of the area A of the original triangle has been removed (Figure 6.6). The process is now repeated for each triangle remaining in the object. At the second stage, three triangles are removed, of area $(1/4)^2$ of the area of the

⁵ The Koch curve is an example of a continuous curve which is generated by a non-differentiable function, i.e., it does not possess a tangent at any point on it (a situation contemplated by Karl Weierstrass already in 1872!).

⁶ Suppose the initial equilateral triangle has sides of length a . Then, the area of this triangle is $A_1 = \frac{\sqrt{3}}{4}a^2$. At

the first step, $n_1 = 3$ triangles of area $\frac{1}{3^2}A_1$ are added. At the k th step, $n_k = 3 \cdot 4^{k-1}$ triangles of area $(1/3)^{2k} A_1$ are added. Thus,

$$A_{k+1} = A_k + 3 \cdot 4^{k-1} \left(\frac{1}{3}\right)^{2k} A_1.$$

On iterating this relation, we obtain

$$A_\infty = A_1 + \frac{1}{3} \left(1 + \frac{4}{9} + \frac{4^2}{9^2} + \dots\right) A_1 = A_1 + \frac{3}{5} A_1 = \frac{2\sqrt{3}}{5} a^2.$$

original triangle; at the third stage, there are nine triangles removed, of area $(1/4)^3$ of the area of the original triangle. The area removed by this process gives a geometric progression –

$$A \left[\frac{1}{4} + 3\left(\frac{1}{4}\right)^2 + 3^2\left(\frac{1}{4}\right)^3 + \dots \right] = \frac{A}{4} \left[1 + \left(\frac{3}{4}\right) + \left(\frac{3}{4}\right)^2 + \dots \right] = A.$$

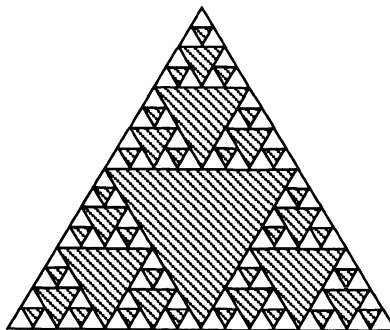


Figure 6.6. The sierpinski triangle.

As in the Cantor set, we have extracted a region of the same size as the whole of the original space, but we still have points left in the Sierpinski triangle. These points which exist in an area of magnitude zero are disconnected, forming a dust. In order to find the fractal dimension D of the Sierpinski triangle, note that after n iterations, the resulting set will have $N = 3^n$ pieces of length $1/2^n$ so that

$$D = \lim_{n \rightarrow \infty} \frac{\ln(3^n)}{\ln\left(\frac{1}{1/2^n}\right)} = 1.5850\dots$$

which is an irrational number less than 2.

BOX-COUNTING METHOD:

To calculate the fractal dimension of generic attracting sets, analytic procedures like the ones discussed in the foregoing do not prove helpful. One then needs to use

numerical methods. For the direct numerical calculation of the fractal dimension D of an attractor by the box-counting method (Grassberger and Proccacia, (1983)), one divides the space into boxes of size ε , and iterates the map until the initial transients have died away (and the motion is on the attractor). We assume that the dynamical system/map is ergodic and mixing so that it is possible to extract the statistical properties of the system by a time average on a single orbit. For subsequent iterations, one counts those boxes containing at least one point on the attractor. Each newly generated box is checked to see if it contains a point of the set; if it does, it is counted. Let $N(\varepsilon)$ be the number of such boxes, after many iterations. One then determines the fractal dimension D by fitting a straight line to the graph of $\ln N(\varepsilon)$ vs. $\ln(1/\varepsilon)$ (see Figure 6.7) for several small values of ε , and extrapolating the result to $\varepsilon \rightarrow 0$. This method, however, becomes

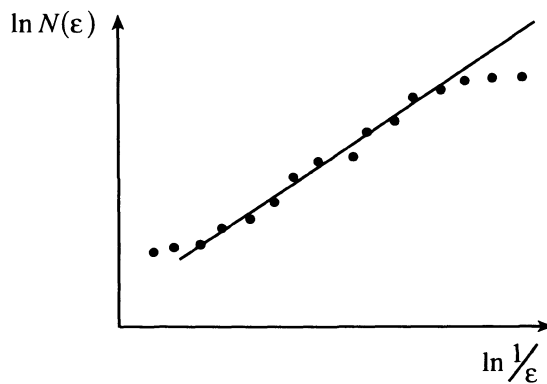


Figure 6.7. A schematic plot of $\ln N(\varepsilon)$ vs. $\ln(1/\varepsilon)$.

very time-consuming and becomes impractical in three and higher dimensions because an enormous number of points on the attractor is required to make sure that a given area in the phase space is empty and not just visited seldom (thus, creating excessive storage requirements). Further, this method does not keep track of any inhomogeneities in the attractor because a given box is counted at most once and only once no matter how many times the orbit visits it. In order to remedy this shortcoming, it is apparent that it is necessary to assign a weight to each box according to how frequently the orbit visits it. If the dynamical system/map is ergodic and mixing, the frequencies with which a typical orbit visits the various boxes covering the attractor will be natural measures of the boxes, because these frequencies would be the same for all initial conditions in the basin of attraction in question. This leads us now to consider methods of characterizing objects with different natural measures for different covering boxes – multi-fractals.

6.4. Multi-Fractals

There exist many fractals whose structure varies from one scale to another. Although some structures show a perfect self-similarity like the Koch snowflake, there are some others which show a self-similarity only in a statistical sense that, upon magnification, segments of these fragments look alike, but are never exactly alike, at different scales.

The multi-fractal model was therefore introduced to simulate such structures which exhibit a scale invariance instead. As Mandelbrot (1989) clarified, a multi-fractal is a probabilistic concept and tool, generalizing the notion of self-similarity from sets to measures (a measure specifies a method of distributing probability over a supporting set). In a multi-fractal model a fractal measure is represented in terms of interwoven fractal subsets having a continuous spectrum of scaling exponents. Multi-fractal distributions are also suitable for structures exhibiting scale invariance and are described by the scaling properties of coarse-grained measures.

Since a singular measure (here the word ‘singular’ refers to a power-law divergent behavior) defined on a multi-fractal has different fractal dimensions in different regions of the multi-fractal, Mandelbrot (1974) pointed out that infinitely many generalized fractal dimensions D_q ’s are needed to give a statistical characterization of the diversity of scaling in a multi-fractal. For one thing, the fractal dimension D does not keep track of the distribution of points from an orbit on the attractor reflecting the fact that the orbit may visit some areas of the attractor more frequently than others. This can be accounted for by weighing the various areas according to how many times an orbit visits them. In order to determine the generalized fractal dimension D_q , let us cover the support of a given measure with $N(l)$ boxes of size l (which amounts to coarse graining of resolution l). Let us generate an arbitrarily long orbit on the attractor, and determine the fraction of time (or the probability) p_i that the orbit spends in the i th box, so the probability distribution $\{p_i\}_{i=1}^{N(l)}$ describes the coarse-grained distribution of iterates. Let $S(\alpha)$ be the support of singularities in the measure $\{p_i\}_{i=1}^{N(l)}$ of strength α , i.e.,

$$p_i(l) \sim l^\alpha. \quad (10)$$

Thus, the fractal measure $\{p_i\}_{i=1}^{N(l)}$ is modeled by interwoven sets $S(\alpha)$.

If $f(\alpha)$ are the different fractal dimensions of the iso- α sets $S(\alpha)$, then the number of boxes $dN_\alpha(l)$ needed to cover $S(\alpha)$ should scale as follows –

$$dN_\alpha(l) = d\mu(\alpha)l^{-f(\alpha)} \quad (11)$$

which also means that the exponent $f(\alpha)$ characterizes the scaling properties of the distribution of the local exponent α (Halsey *et al.* (1986))⁷. Here, the measure $d\mu(\alpha)$ gives the weight of the different scaling exponents α .

Consider the moments of p_i –

$$\chi_q(l) = \sum_{i=1}^{N(l)} p_i^q(l) \quad (12)$$

which may be interpreted as the probability that q points drawn randomly from the multi-fractal fall into one box of size l . (12) enables one to bring out the effect of correlations among different parts of the multi-fractal, and hence, describe the degree of inhomogeneity of the multi-fractal. Note that, according to (12),

$$\chi_o(l) = N(l)$$

$N(l)$ being the number of boxes of size l needed to cover the fractal support – the region where $p_i \neq 0$, and

$$\chi_1(l) = 1$$

so that this multi-fractal distribution satisfies the normalization condition.

Note further that, as q is varied in (12), different iso- α sets $S(\alpha)$, become dominant. In particular, for large q , boxes with high p_i 's (or boxes which are frequented highly) contribute dominantly, and for small q ($q < 0$), boxes with low p_i 's (or boxes which are frequented least often) contribute dominantly. We have from (10) and (11),

$$\chi_q(l) \sim \int d\mu(\alpha) l^{\alpha q - f(\alpha)}. \quad (13)$$

One introduces now the generalized fractal dimension D_q as follows (Hentschel and Procaccia, (1983)) –

$$\chi_q(l) \sim l^{(q-1)D_q} \quad (14)$$

⁷ $f(\alpha)$ attains practical significance because it can be determined directly in physical experiments (see Chapter 7). However, $f(\alpha)$ can only be determined approximately, because experiments allow a finite number of observed scales while numerical computations allow a finite resolution.

Note that the factor $(q-1)$ is introduced so as to preserve the normalization condition $\chi_1 = 1$. (13) and (14) enable one to determine the function $f(\alpha)$, for the measure in question, by relating it to observable properties, like the generalized fractal dimension D_q , of the measure.

It is of interest to note that the function $\chi_q(l)$ is formally analogous to the partition function $Z(\beta)$ in thermodynamics so that q is like $\beta = 1/kT$, T being the temperature, and $-(q-1)D_q$ is like the free energy (Stanley and Meakin, (1988)). The Legendre transform $f(\alpha)$ is thus the analogue of the entropy, with α being the analogue of the energy E . Indeed, the characteristic shape of plots of $f(\alpha)$ vs. q and $f(\alpha)$ vs. α are reminiscent of plots of the dependence on T and E of the entropy for a thermodynamic system!

Since l is small, the integral in (13) will be dominated by those values of α which minimize the exponent $\alpha q - f(\alpha)$, so that the integral can be evaluated for small l by the saddle point method –

$$D_q = \frac{1}{(q-1)} [\bar{\alpha}q - f(\bar{\alpha})] \quad (15)$$

where,

$$\alpha = \bar{\alpha} : \frac{d}{d\alpha} [\alpha q - f(\alpha)] = 0$$

with

$$\left. \frac{d^2}{d\alpha^2} [\alpha q - f(\alpha)] \right|_{\alpha=\bar{\alpha}} > 0$$

or

$$\left. \begin{aligned} \frac{df}{d\alpha} \Big|_{\alpha=\bar{\alpha}} &= q(\bar{\alpha}) \\ \frac{d^2 f}{d\alpha^2} \Big|_{\alpha=\bar{\alpha}} &< 0 \end{aligned} \right\}. \quad (16)$$

Thus, for any measure, the curve $f(\alpha)$ vs. α will be convex, with a single maximum at $q=0$, and with infinite slope at $q=\pm\infty$. Further, (15) shows that $(q-1)D_q$ and $f(\alpha)$ are Legendre transforms of each other.

A homogeneous fractal corresponds to equally probable partitioning $p_i = N_\alpha^{-1}$ so that we have from (10) and (11), $\alpha = f(\alpha)$, and (15) then gives $D_q = f(\alpha) = D_o$ for all q . In general, we have $f(\alpha) \leq D_o$ because $N_\alpha(l) \leq N(l)$. Fractals on which a measure is distributed with a constant density form an interesting class, since in such cases multi-fractality can manifest itself only through geometrical properties like the support of the set (Vicsek, (1992)). On the other hand, note that the multi-fractal is approximated for fixed q by a uniform fractal whose dimension is $f(\alpha(q))$ and each of whose $l^{-f(\alpha(q))}$ intervals is visited with frequency $p_i \sim l^{\alpha(q)}$ by the map.

Thus, given the singularity spectrum $f(\alpha)$, one can determine the generalized fractal dimension D_q . Alternatively, given D_q , one may find α from the relation (which follows from (15)),

$$\bar{\alpha} = \frac{d}{dq} [(q-1)D_q] \quad (17)$$

from which, since D_q is finite, we have

$$q \rightarrow \pm\infty : \bar{\alpha} = D_q. \quad (18)$$

In order to evaluate D_q from experimental data, one first determines the set of values p_i by using a suitable normalization. One then determines D_q from the formula –

$$D_q = \lim_{l \rightarrow 0} \left[\frac{\frac{1}{q-1} - \frac{\ln \sum_{i=1}^{N(l)} p_i^q}{\ln l}}{\ln \sum_{i=1}^{N(l)} p_i^q} \right]$$

via a log-log plot.

Let us now consider the geometric interpretations of D_q . For $q=0$, we have, from (16), $f'(\alpha)=0$ so that, from (15), $D_o = f(\alpha(0))$ lies at the maximum of the curve $f(\alpha)$ vs. α . Note that, since D_o is a measure of the number of boxes needed to cover

the attractor and pays no attention to the measure distribution among these boxes, so D_o is the fractal dimension of the support of the measure having singularities of strength α and is called the capacity (or Hausdorff) dimension. It should be noted that one can have a multi-fractal distribution even if the support of the measure is not a fractal.

Next, in order to interpret D_1 , set $q = 1 + \delta q$, and let $\alpha(1) = \alpha$, $\alpha'(1) = \alpha'$ when $q = 1$. Then, we have from (15),

$$D_1 \approx \frac{1}{\delta q} [(1 + \delta q)(\alpha + \delta q \alpha') - f(\alpha) - \delta q \alpha' f'(\alpha)]$$

or

$$D_1 \approx \alpha + \alpha' [1 - f'(\alpha)] + \frac{1}{\delta q} [\alpha - f(\alpha)] \quad (19)$$

which shows that $\alpha(1) = f(\alpha(1))$ so that D_1 is finite. Further, when $q = 1$, we have from (16),

$$f'(\alpha(1)) = 1 \quad (20)$$

so that (19) becomes

$$D_1 = \alpha(1) = f(\alpha(1)). \quad (21)$$

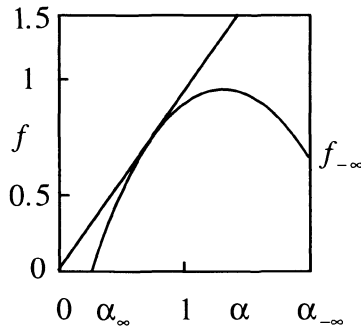


Figure 6.8. The $f(\alpha)$ vs. α curve for the multi-fractal. (The line is the diagonal $f = \alpha$.) (From Tél, (1988)).

(By courtesy of the Verlag der Zeitschrift für Naturforschung).

Thus, D_1 lies on the curve $f(\alpha)$ vs. α at the point where $\alpha = f(\alpha)$ and $f'(\alpha) = 1$, (see Figure 6.8).

Further, note, as $q \rightarrow 1$, that

$$p_i^q = p_i p_i^{q-1} = p_i e^{(q-1)\ln p_i} \approx p_i [1 + (q-1)\ln p_i]. \quad (22)$$

Then, we have, from (12), (14), and (22),

$$D_1 = \lim_{l \rightarrow 0} \frac{\sum_{i=1}^{N(l)} p_i \ln p_i}{\ln l}. \quad (23)$$

(23) shows that D_1 describes the scaling behavior of the entropy

$$S(l) = - \sum_{i=1}^{N(l)} p_i \ln p_i \quad (24)$$

of the partition of the measure $P = \{p_i\}_{i=1}^{N(l)}$ distributed over boxes of size l on the set $\xi = \bigcup_{\alpha} S(\alpha)$. Note that $S(l)$ represents the amount of information needed to specify the distribution of the measure P , so D_1 is the information dimension.

Thus, D_1 is the fractal dimension of the set on which the measure is concentrated⁸. If the points are uniformly distributed in d -dimensional space, $p_i(l)$ is simply proportional to the size of the boxes, so $p_i(l) \sim l^d$, and $D_1 = d$, as to be expected! On

⁸ Kaplan and Yorke (1979) have conjectured that there is a relationship between the information dimension D_1 and the Liapunov exponents σ_j for a typical chaotic attractor:

$$D_1 = k + \frac{1}{|\sigma_{k+1}|} \sum_{j=1}^k \sigma_j$$

where k is the largest integer such that

$$\sum_{j=1}^k \sigma_j \geq 0$$

with the ordering

$$\sigma_1 \geq \sigma_2 \geq \dots$$

The Kaplan-Yorke formula implies that $k \leq D_1 \leq k + 1$.

the other hand, if the probability $p_i(l)$ for each box is the same, then $S(l) = -N(l)p \ln p$ and $p = 1/N(l)$, so $S(l) = \ln N(l)$ and we have $D_1 = D_o$! For this case of equi-probable events, the amount of information needed to specify the distribution of the measure P is maximum. In general, $S(l) < \ln N(l)$ ⁹, so $D_1 \leq D_o$. Further, as D_1 gets smaller, the distribution becomes more localized. When $D_1 \approx 0$, the distribution is almost concentrated at one point – the system in question is then well-ordered and structured.

Next, in order to interpret D_2 ,

$$D_2 = \lim_{l \rightarrow 0} \frac{\ln \sum_{i=1}^{N(l)} p_i^2(l)}{\ln l}. \quad (25)$$

Consider a data consisting of n points x_1, \dots, x_N on the attractor generated by sampling an orbit at some constant time interval εt . Then, the correlation sum $C(l)$ (Grassberger and Proccacia (1983)) is, given by

$$C(l) = \lim_{N \rightarrow \infty} \frac{1}{N^2} \sum_{i=1}^{N(l)} \sum_{j=1}^{N(l)} \theta(l - |x_i - x_j|) \quad (26)$$

where θ is the Heaviside step function, provides a natural measure of the attractor for small l . (The Heaviside step function counts the number of pairs of points within a

⁹ In order to prove this, note that for a set of positive numbers a_1, \dots, a_N , we have

$$\prod_{i=1}^{N(l)} a_i^{p_i} \leq \sum_{i=1}^{N(l)} p_i a_i.$$

Putting $a_i = 1/p_i$, we obtain

$$\prod_{i=1}^{N(l)} \left(\frac{1}{p_i} \right)^{p_i} \leq \sum_{i=1}^{N(l)} p_i \frac{1}{p_i} = N(l).$$

On taking the logarithm on both sides, we obtain

$$S(l) = \sum_{i=1}^{N(l)} p_i \ln \left(\frac{1}{p_i} \right) \leq \ln N(l).$$

radius l of the point x_i while the correlation $C(l)$ gives the average fraction of such points.) Now, $\sum_i p_i^2$ is the probability that two points of the attractor are in the same box which is the same as the probability that two points are separated by a distance smaller than l as described by $C(l)$ in (26)! Thus,

$$\ln C(l) = D_2 \ln l$$

or

$$C(l) \sim l^{D_2} \quad (27)$$

so that D_2 is the correlation dimension describing the scaling law of the number of pairwise correlations in a ball of radius l on the attractor. Note that the correlation dimension D_2 , like the information dimension D_1 depends on the distribution of the measure on the attractor. Grassberger and Proccacia (1983) have shown that $D_2 \leq D_1$. In fact, D_q can be shown to be monotonically decreasing with q .

One may obtain an implicit equation for the generalized fractal dimension D_q , similar to the one derived in Footnote 4 for a non-uniform fractal, as follows (Hentschel and Proccacia (1983) and Halsey *et al.* (1986)). For this purpose, one generalizes the procedure for non-uniform fractals to vary also the measure associated with an offspring. Consider a fragmentation process whereby the fractal, on which the measure is defined, is divided into N parts of size l . If, $p_{j,i}$ is the probability associated with the i th box, of size lr_j ($0 < r_j < 1$), in the j th part, consider the moments of $p_{j,i}$ –

$$\chi_{q,j}(lr_j) = \sum_i p_{j,i}^q = P_j^q \chi_q(l) \quad (28)$$

where P_j is the total measure associated with the j th part. We have for the complete set,

$$\chi_q(l) = \sum_{j=1}^{N(l)} \chi_{q,j}(l). \quad (29)$$

Using (14) and (28), (29) gives an implicit equation for D_q –

$$\sum_{j=1}^{N(l)} P_j^q r_j^{-(q-1)D_q} = 1. \quad (30)$$

Note that, for the case $q = 0$, (30) reduces to the one derived before in Footnote 4 for a non-uniform fractal!

If, $r_j \equiv r \sim l, j = 1, \dots, N$, (30) can be solved for D_q –

$$D_q = \frac{1}{q-1} \frac{\ln \left(\sum_{j=1}^N P_j^q \right)}{\ln l} = \frac{1}{q-1} \frac{\ln \chi_q(l)}{\ln l} \quad (31)$$

in agreement with (14).

EXAMPLE 6

Consider a multi-fractal distribution generated by dividing the unit interval into three equal parts at length $1/3$, the probabilities associated with them being P_1, P_2 and P_3 , with $P_2 > P_1$. This process is then repeated on each of these three parts with the probability redistributed within the q new parts according to the proportions used in the first step. The probability distributions for the first few steps of this process are shown in Figure 6.9. In the limit of infinite iterations, the probability distribution function becomes a single-valued, everywhere discontinuous function.

Using (31), we have for this multi-fractal distribution –

$$D_q = \frac{1}{(q-1) \ln(1/3)} \ln \left(2P_1^q + P_2^q \right).$$

Using this formula, we have from (17) and (15),

$$\alpha(q) = \frac{1}{\ln(1/3)} \frac{2P_1^q \ln P_1 + P_2^q \ln P_2}{2P_1^q + P_2^q}$$

$$f(\alpha(q)) = \frac{1}{\ln(1/3)} \left[q \frac{2P_1^q \ln P_1^q + P_2^q \ln P_2^q}{2P_1^q + P_2^q} - \ln \left(2P_1^q + P_2^q \right) \right].$$

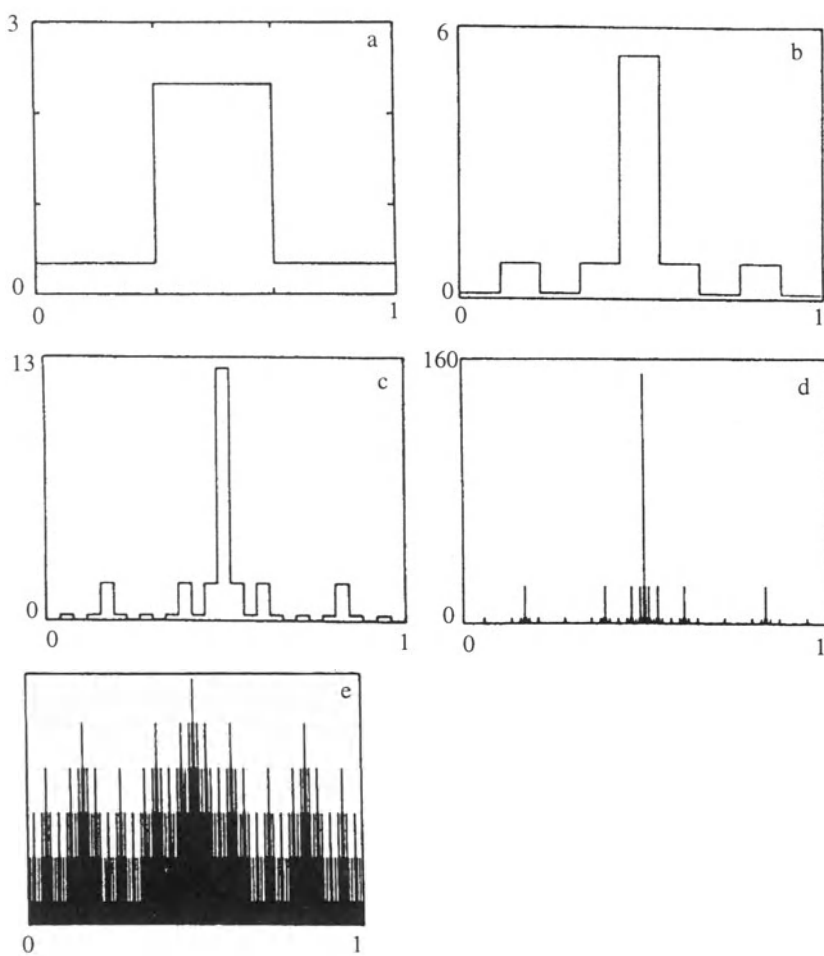


*Figure 6.9. The first steps of constructing a fractal measure on the unit interval (Farmer (1982)).
(By courtesy of the Verlag der Zeitschrift für Naturforschung.)*

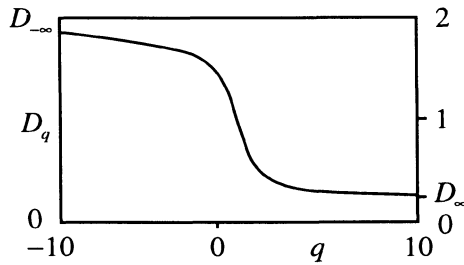


Figure 6.10. The D_q vs. q curve, for the multifractal. (From Tél, (1988)). (By courtesy of the Verlag der Zeitschrift für Naturforschung).

In Figures 6.8, 6.10 and 6.11, we have plotted f , α and D_q vs. q and $f(\alpha)$ vs. α for this multi-fractal. Observe that $f(\alpha(0)) > f(\alpha(q))$ for $q \neq 0$ since the multi-fractal is the union of all subfractals with dimension $f(\alpha(q))$. Further, $f(\alpha) \leq \alpha$, because the measure carried by any subset of boxes with the exponent between α and $\alpha + d\alpha$ goes like $l^{-f(\alpha)+\alpha}$; thus, the curve $f(\alpha)$ vs. α must lie below the bisector $f(\alpha) = \alpha$ (see

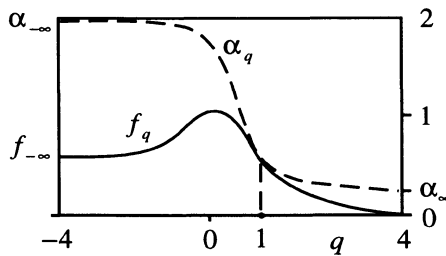


Figure 6.11. The $\alpha(q)$ vs. q and $f(\alpha(q))$ vs. q curves, for the multifractal, (from Tél, (1988)). (By courtesy of the Verlag der Zeitschrift für Naturforschung).

Figure 6.8). The function $f(\alpha(q))$ vs. q increases until it reaches its maximum D_o and then decreases. As higher powers q select denser regions, $\alpha(q)$ vs. q is monotonically decreasing. Small α implies large intensity of the measure, but such sets occupy small volume because they have $f \approx 0$. On the other hand, sets corresponding to larger α occupy larger volumes but possess low-intensity measure. (Thus, D_∞ corresponds to the region in the set where the measure is most concentrated, while $D_{-\infty}$ corresponds to the region where the measure is most rarefied.) (20) and (21) show that the curves $f(\alpha(q))$

vs. q and $\alpha(q)$ vs. q touch each other at $q = 1$ and the curve $f(\alpha)$ vs. α is tangent to the line $f(\alpha) = \alpha$ at the point $f(\alpha) = D_1$, as is apparent in Figures 6.8 and 6.11.

6.5. Analysis of Time-Series Data

One of the problems associated with the measured data is how to determine the underlying deterministic dynamics, if one exists (if not, the measured data could be just noise without any structure). The inverse problem of the determination of a dynamical system of a given trajectory is beset with the following difficulties:

- the information available is incomplete,
- there are inevitable measurement errors,
- there is usually some external noise present,
- the physical processes determining the evolution are not known.

Takens (1981) showed, based on a suggestion of D. Ruelle, that the time-series¹⁰ data of a single variable of a system contains the essential details of the evolution of the system, like the number of state variables needed to specify the state of the system. Takens (1981) further proposed a time-delay embedding technique to reconstruct the underlying phase space and obtain some characterizations of the attractor, assuming that one exists and is low-dimensional. In this technique, a trajectory describing the evolution of a dynamical system in its phase space is constructed and the correlations between different parts of it that intersect a region of the phase space are used to compute the correlation dimension. However, the dimension of the attractor is not known a priori so one varies the embedding dimension until one converges to a structure.

Given the time-series measurements of a variable $x(t)$, the time-delay embedding technique consists of constructing an m -component "state" vector x_i at time $t = t_i$ as

$$x_i = \{x_1(t_i), x_2(t_i), \dots, x_m(t_i)\}$$

where m is called the embedding dimension, and

$$x_k(t_i) \equiv x(t_i + (k-1)\tau)$$

and τ is an appropriate time delay large enough to overcome the autocorrelation effect (otherwise, correlated variables would bias our estimations) and small enough to preserve the causal link between consecutive signals and resolve the physical processes

¹⁰ Time series data refers to sequences of data representing the time evolution of a variable of a system, sampled at fixed finite time intervals.

of interest, (otherwise, the trajectory would appear to wander all over the phase space making it difficult to detect any structure.) If the underlying attractor has dimension D , then, in order to capture the attractor, one requires $m \geq D$. One may obtain some characterizations, like the correlation dimension ν , of the attractor, in this reconstructed phase space via correlation sums (whose scaling behavior leads to the correlation dimension ν of the system (Grassberger and Proccacia (1983))). One defines the correlation sum for N vectors distributed in an m -dimensional space, as a function of distance l , as in (26):

$$C(l; m) = \lim_{N \rightarrow \infty} \frac{1}{N^2} \sum_{i=1}^N \sum_{j=1}^N \theta(l - |x_i - x_j|) \quad (26)$$

where θ is the Heaviside step function. If the number of points is large enough, as assumed above, this distribution will obey a power-law scaling with l , for small l :

$$C(l; m) \sim l^\nu$$

where ν is the correlation dimension¹¹, defined as

$$\nu = \lim_{l \rightarrow 0} \frac{\ln C(l; m)}{\ln l}.$$

Such a scaling region exists between a depopulation (for small l) and saturation (for large l) for every m .

As one increases the control parameter m , ν first varies with m , and, if the time series has some structure and possesses an attractor, ν converges to its true value (Vassiliadis *et al.* (1990)), see Figure 6.12¹². Thus, phase-space reconstruction preserves geometrical invariants of the dynamics (when there is a limit set).

However, interpretation of the results of the phase-space reconstruction from time series is often hampered by the limitations of the algorithms, data requirements and other problems (see Tsonis (1992) and Abarbanel *et al.* (1993) for details).

¹¹ Grassberger and Proccacia (1983) have shown that the correlation dimension ν represents a lower limit for both the information dimension D_1 and the capacity dimension D_0 , i.e.,

$$\nu \leq D_1 \leq D_0.$$

¹² This property can also serve to distinguish a chaotic dynamics from noise, since, for the latter case, ν will continue to increase indefinitely as m increases without any saturation. The latter is due to the fact that a noise of infinite sample size embedded in an m -dimensional space always fills that space.

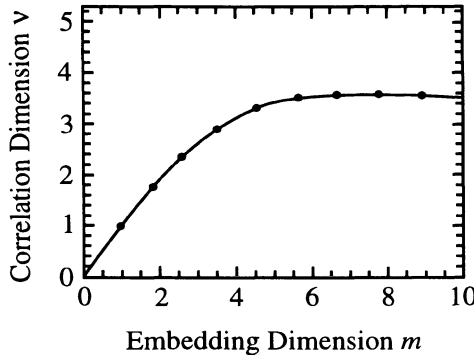


Figure 6.12. Saturation of the attractor dimension v with increasing dimension m of the embedding space.
(Due to Vassiliadis *et al.*, (1990)). (By courtesy of the American Geophysical Union).

6.6. The Lorenz Attractor

The Lorenz equations are obtained from a truncated modal expansion of the Navier-Stokes equations governing the two-dimensional roll pattern due to convection in a fluid layer heated from below.¹³ Consider two rigid plane parallel walls at $z = 0, L$ with the space in between occupied by a fluid. Gravity acts in the negative z -direction, and the plate at $z = 0$ is maintained at a higher temperature T_o than T_L for the plate at $z = L$. One possible equilibrium state of this system is one in which the fluid is at rest and heat is transferred across the fluid through thermal conduction. Rayleigh (1916) studied the linear stability of this equilibrium and found that if $(T_o - T_L)$ exceeds a certain critical value, this equilibrium state becomes unstable and convective circulatory flow sets in.¹⁴

Once instability sets in, the linear analysis cannot be used, however, to specify the ensuing convective dynamical development of the fluid. By considering variations only in two dimensions, Saltzman (1962) derived a set of nonlinear ordinary differential equations by expanding the stream function and the temperature perturbations in double Fourier series in space, with the Fourier coefficients depending on t only. By substituting the series into the original Navier-Stokes equations and truncating the infinite sum to a finite number of terms, Saltzman (1962) obtained a set of ordinary differential equations.

¹³ Thermal convection is the main cause for the circulations of atmosphere and oceans. The latter, in turn, determine the weather changes as well as the continental drift.

¹⁴ In order to avoid the appearance of complex spatial structures, experiments are usually performed in a small cell. The boundary conditions limit the number of rolls. The observed dynamical behavior depends sensitively on the liquid chosen and on the linear dimensions of the box.

Lorenz (1963) examined the problem further and considered the truncation to only three Fourier modes, for which the governing equations become (see Appendix 6.2) –

$$\frac{dX}{dt} = \sigma(Y - X) \equiv F_1 \quad (32)$$

$$\frac{dY}{dt} = -XZ + rX - Y \equiv F_2 \quad (33)$$

$$\frac{dZ}{dt} = XY - bZ \equiv F_3 \quad (34)$$

Here, X is proportional to the circulatory fluid flow velocity, Y denotes the horizontal temperature difference across a convective roll, and Z denotes the horizontally averaged distortion of temperature profile from that of the conduction state. The three parameters σ , r , and b are, respectively, proportional to the Prandtl number, the Rayleigh number (proportional to the temperature difference across the fluid layer), and some physical dimension of the region under consideration; consequently, all three are taken to be positive. Lorenz (1963) solved equations (32)-(34) numerically and found that, under certain circumstances, this set of deterministic equations (which determine a unique flow valid for all time) gives rise to complicated non-periodic behavior whose form is very sensitive to initial conditions. The Lorenz equations have been object of much study because they provide a relatively simple example of a "strange attractor". (It should be noted, however, that the Lorenz model describes the Rayleigh-Bénard convection only in the proximity of the transition from thermal conduction to convection, when only simple rolls occur. Therefore, equations (32)-(34) have nothing to do with the chaotic behavior observed in experiments, for high Rayleigh numbers.)

We will discuss below the various equilibrium solutions of the Lorenz model, their stability and bifurcation aspects, and then comment on the chaotic behavior of the nonlinear solutions as well as the nature of the strange attractor in question.

(i) Equilibrium Solutions and Their Stability:

Equations (32)-(34) have a static equilibrium solution for $r < 1$:

$$X_o = Y_o = Z_o = 0 \quad (35)$$

and a stationary convective-flow solution for $r > 1$:

$$X_o = Y_o = \pm\sqrt{b(r-1)}, \quad Z_o = r-1. \quad (36)$$

One of the two solutions in (36) corresponds to clockwise rotation, while the other corresponds to counterclockwise rotation.

The equilibrium described by $X_o = Y_o = Z_o = 0$ is stable with respect to infinitesimal disturbances for $0 < r < 1$ and unstable for $r > 1$. This follows by looking at the matrix of partial derivatives of the right hand sides of equations (32)-(34) at the point $X_o = 0, Y_o = 0, Z_o = 0$:

$$\left. \frac{\partial F_i}{\partial X_j} \right|_{X_{1o}=X_{2o}=X_{3o}=0} = \begin{pmatrix} -\sigma & \sigma & 0 \\ r & -1 & 0 \\ 0 & 0 & -b \end{pmatrix}. \quad (37)$$

Here, $i, j = 1, 2, 3$ and $X_1 = X, X_2 = Y$ and $X_3 = Z$. The eigenvalues of this matrix are given by

$$\lambda = -b, \frac{-(\sigma+1) \pm \sqrt{(\sigma+1)^2 - \sigma(1-r)}}{2} \quad (38)$$

which have negative real part for $r < 1$ and positive real part for $r > 1$. Thus, for $0 < r < 1$, (35) is a globally attracting stationary solution, and all trajectories (corresponding to all different initial conditions) eventually spiral into it. For $r > 1$, (35) becomes unstable and bifurcates via pitch-fork bifurcation into a pair of locally attracting stationary solutions (36), which exist only when $r > 1$, (see subsection (ii) below).

The equilibria (36) are stable until some $r = r^* > 1$. For $r > r^*$, the equilibria (36) become unstable with respect to infinitesimal disturbances. This follows from a look at the matrix $(\partial F_i / \partial X_j)$ at the point $(\pm\sqrt{b(r-1)}, \pm\sqrt{b(r-1)}, r-1)$: the eigenvalues, at first, are real and negative, then one pair becomes complex conjugate. However, if $r > r^*$, then the complex-conjugate pair has now a positive real part. In order to see this, putting

$$\begin{aligned} X &= \sqrt{b(r-1)} + X_1 \\ Y &= \sqrt{b(r-1)} + Y_1 \\ Z &= (r-1) + Z_1. \end{aligned} \quad (39)$$

and linearizing in X_1, Y_1 and Z_1 , we obtain from equations (32)-(34):

$$\begin{aligned}\dot{X}_1 &= -\sigma(X_1 - Y_1) \\ \dot{Y}_1 &= X_1 - Y_1 - \sqrt{b(r-1)}Z_1 \\ \dot{Z}_1 &= \sqrt{b(r-1)}X_1 + \sqrt{b(r-1)}Y_1 - bZ_1.\end{aligned}\tag{40}$$

Looking for solutions of the form

$$X_1, Y_1, Z_1 \sim e^{\lambda t}\tag{41}$$

we obtain from (40),

$$\lambda^3 + (\sigma + b + 1)\lambda^2 + b(r + \sigma)\lambda + 2\sigma b(r - 1) = 0.\tag{42}$$

Equations (42) has one real negative root and two complex-conjugate roots when $r > 1$. The two complex-conjugate roots have a negative real part when $r < r^*$ and vice versa. The value of r^* is determined by demanding that the complex-conjugate roots be pure imaginary:

$$(\lambda + i\lambda_o)(\lambda - i\lambda_o)(\lambda - \lambda_1) = \lambda^3 - \lambda_1\lambda^2 + \lambda_o^2\lambda - \lambda_1\lambda_o^2 = 0\tag{43}$$

from which, on comparison with equation (42), we obtain

$$(\sigma + b + 1)b(r^* + \sigma) = 2\sigma b(r^* - 1)$$

or

$$r^* = \frac{\sigma(\sigma + b + 3)}{\sigma - b - 1}.\tag{44}$$

Let us now see how the convective-flow equilibria described by $X_0 = Y_0 = \pm\sqrt{b(r-1)}$, $Z_0 = (r-1)$ arise as a supercritical bifurcation from the solution $X_0 = Y_0 = Z_0 = 0$, as r exceeds 1.

(ii) Slightly Supercritical Case:

Let us consider a slightly supercritical case so that r is slightly greater than 1 and use the method of multiple scales to construct an approximate solution to equations (32)-(34), describing the dynamics on the center manifold, of the form –

$$\begin{aligned} X(t; \varepsilon) &= \varepsilon X_1(t_1, t_2) + \varepsilon^2 X_2(t_1, t_2) + \varepsilon^3 X_3(t_1, t_2) + O(\varepsilon^4) \\ Y(t; \varepsilon) &= \varepsilon Y_1(t_1, t_2) + \varepsilon^2 Y_2(t_1, t_2) + \varepsilon^3 Y_3(t_1, t_2) + O(\varepsilon^4) \\ Z(t; \varepsilon) &= \varepsilon Z_1(t_1, t_2) + \varepsilon^2 Z_2(t_1, t_2) + \varepsilon^3 Z_3(t_1, t_2) + O(\varepsilon^4) \\ r(\varepsilon) &= 1 + \varepsilon r_1 + \varepsilon^2 r_2 + O(\varepsilon^3) \end{aligned} \quad (45)$$

where,

$$t_1 = \varepsilon t, \quad t_2 = \varepsilon^2 t, \quad \varepsilon \ll 1. \quad (46)$$

The small parameter ε may be taken to characterize the closeness of r to 1. The slow time scales t_1 and t_2 characterize the slow variations with time of the system (32)-(34), for r slightly greater than 1.

Substituting (45) in equations (32)-(34), we obtain

$$0(\varepsilon): \quad 0 = \sigma(Y_1 - X_1) \quad (47)$$

$$0 = -Y_1 + X_1 \quad (48)$$

$$0 = -bZ_1 \quad (49)$$

$$0(\varepsilon^2): \quad \frac{\partial X_1}{\partial t_1} = \sigma(Y_2 - X_2) \quad (50)$$

$$\frac{\partial Y_1}{\partial t_1} = -Y_2 + X_2 + r_1 X_1 - X_1 Z_1 \quad (51)$$

$$\frac{\partial Z_1}{\partial t_1} = -bZ_2 + X_1 Y_1 \quad (52)$$

$$0(\epsilon^3): \quad \frac{\partial X_2}{\partial t_1} = \sigma(Y_3 - X_3) - \frac{\partial X_1}{\partial t_2} \quad (53)$$

$$\frac{\partial Y_2}{\partial t_1} = -Y_3 + X_3 + r_1 X_2 + r_2 X_1 - X_1 Z_2 - X_2 Z_1 - \frac{\partial Y_1}{\partial t_2} \quad (54)$$

$$\frac{\partial Z_2}{\partial t_1} = -b Z_3 + X_1 Y_2 + X_2 Y_1 - \frac{\partial Z_1}{\partial t_2}. \quad (55)$$

We obtain from equations (47)-(49):

$$\left. \begin{array}{l} X_1 = Y_1 = A_1(t_1, t_2) \\ Z_1 = 0 \end{array} \right\} \quad (56)$$

Using (56), equations (50)-(52) become

$$\frac{\partial A_1}{\partial t_1} = \sigma(Y_2 - X_2) \quad (57)$$

$$\frac{\partial A_1}{\partial t_1} = -Y_2 + X_2 + r_1 A_1 \quad (58)$$

$$0 = -b Z_2 + A_1^2. \quad (59)$$

In order to obtain bounded solutions, equations (57) and (58) require

$$\left. \begin{array}{l} A_1 = A_1(t_2), \quad r_1 = 0 \\ X_2 = Y_2 \end{array} \right\} \quad (60)$$

while equation (59) gives

$$Z_2 = \frac{A_1^2}{b}. \quad (61)$$

Using (56), (60), and (61), equations (53)-(55) become

$$X_{2t_1} + A_{1t_2} = \sigma(Y_3 - X_3) \quad (62)$$

$$A_{1t_2} + X_{2t_1} = -Y_3 + X_3 + r_2 A_1 - \frac{A_1^3}{b} \quad (63)$$

$$0 = -bZ_3 + 2A_1 X_2. \quad (64)$$

We obtain from equations (62) and (63),

$$\left(1 + \frac{1}{\sigma}\right)X_{2t_1} = -\left(1 + \frac{1}{\sigma}\right)A_{1t_2} + r_2 A_1 - \frac{A_1^3}{b}. \quad (65)$$

In order to have bounded solutions, equation (65) requires

$$\left(1 + \frac{1}{\sigma}\right)A_{1t_2} - r_2 A_1 + \frac{A_1^3}{b} = 0 \quad (66)$$

which is the Landau equation (Landau (1944)) and describes the dynamics on the center manifold at $r = 1$. The solution of equation (66) is given by

$$A_1(t_2) = \frac{\pm\sqrt{br_2}}{\left[1 - \left(1 - \frac{br_2}{A_{1o}^2}\right)e^{-\frac{2r_2}{1+\sqrt{\sigma}}t_2}\right]^{\frac{1}{2}}} \quad (67)$$

where,

$$A_{1o} \equiv A_1(0).$$

In terms of the original variables, (67) becomes

$$X(t) = Y(t) = \frac{\pm A_1^*}{\left[1 - \left(1 - \frac{A_1^{*2}}{X_0^2} \right) e^{-\frac{2(r-1)}{1+\sigma} t} \right]^{1/2}} \quad (68)$$

where,

$$A_1^* \equiv \sqrt{b(r-1)} \text{ and } X_0 \equiv X(0) = Y(0).$$

(68) shows that the nonlinear effects bring an exponentially-growing linear solution to the steady supercritical convective-flow equilibria given by

$$X = Y = \pm A_1^*, \quad Z = \frac{A_1^{*2}}{b}. \quad (69)$$

Note that corresponding to the case $r_2 = 0$, equation (66) becomes

$$\left(1 + \frac{1}{\sigma} \right) A_{1r_2} + \frac{A_1^3}{b} = 0 \quad (70)$$

from which,

$$A_1(t_2) = \frac{A_{1o}}{\sqrt{\frac{2A_{1o}}{b} \left(1 + \frac{1}{\sigma} \right) t_2 + 1}}. \quad (71)$$

(71) shows the nonlinear approach to the pure conduction state (35).

McLaughlin and Martin (1975) used a similar approach to construct an approximate analytical solution to equations (32)-(34) for r slightly greater than r^* and showed that the solutions of equations (32)-(34) show a subcritical Hopf bifurcation for $r \approx r^*$, i.e., there exists a one-parameter family of limit cycles for $r < r^*$. Thus, the convective-flow equilibria (69) lose stability at $r = r^*$ by absorbing an unstable limit cycle. As r decreases below r^* , the unstable limit cycle expands, and at $r \approx 13.926$, touches the saddle point at the origin and becomes a homoclinic orbit (see Section 5.7). This is called a homoclinic bifurcation.

(iii) Existence of an Attractor:

When all the equilibria (35) and (36) become unstable with respect to infinitesimal disturbances the question arises as to whether the motion will remain unbounded or not (when an attractor exists). In order to answer this, we consider a region of phase space enclosing all three fixed points (corresponding to the equilibria (35) and (36)) and large enough so that no trajectory leaves the region. If we find that the solutions corresponding to all initial conditions outside this region evolve into the region and remain trapped inside for all subsequent times, then all final motions would be bounded in phase space. Indeed, we obtain from equations (32)-(34), for the divergence of the phase-flow velocity:

$$\frac{\partial}{\partial X} \left(\frac{dX}{dt} \right) + \frac{\partial}{\partial Y} \left(\frac{dY}{dt} \right) + \frac{\partial}{\partial Z} \left(\frac{dZ}{dt} \right) = -(\sigma + b + 1) < 0, \quad (72)$$

because σ and b are both positive. The system (32)-(34) is therefore dissipative, and phase-space volumes always decrease. This need not, however, imply that phase-space volumes shrink to a point because, as we saw in Section 6.2, they may approach an infinitely-many sheeted fractal set having zero volume like a Cantor set (Mandelbrot (1983)).

(iv) Chaotic Behavior of the Nonlinear Solutions:

Numerical solutions of equations (32)-(34) for $r > r^*$ (Lorenz (1963)) show that, due to the nonlinear effects, the solution spirals out about each of the two unstable equilibrium points (36) until its amplitude is sufficiently large when due to the three-dimensionality of the phase space it is attracted to the other equilibrium point about which it then spirals. Thus, as r increases past r^* , a stable equilibrium form appears around each of the two unstable equilibrium points behaving like limiting cycles. These stable equilibrium forms become larger as r increases, and at one point they combine to form a single stable surface surrounding both unstable equilibrium points. This process exhibits the stretching and folding features necessary for a chaotic behavior in this system. The jumping of the solution trajectory from the vicinity of one unstable equilibrium point to that of the other seems to take place in a random fashion, much like balls in a pinball machine.

In Figure 6.13, a two-dimensional cut of the phase-plane trajectory is shown for $r = 28$, $\sigma = 10$ and $b = 8/3$ ($r^* = 24.74$ for these values) in terms of Z vs. Y , obtained from numerical integration of equations (32)-(34). The phase-plane trajectories spiral in a chaotic manner about the two stationary convective flow (and unstable) equilibria (36). Note that the trajectory shown does not intersect itself if we consider the full three-

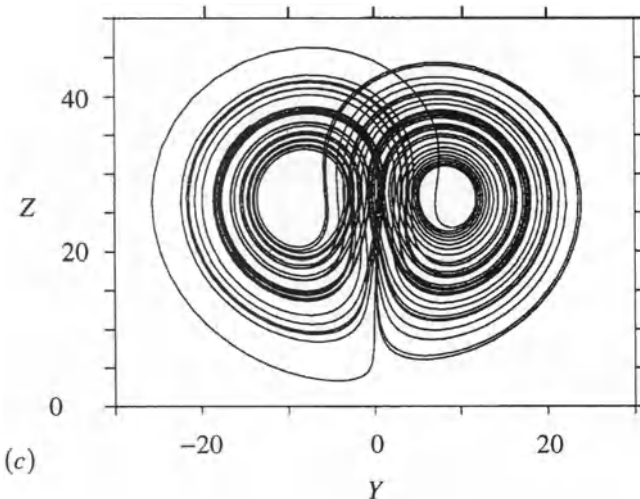


Figure 6.13. Projections of part of an orbit of the Lorenz system (for $30 \leq t \leq 70$ for $r = 28, \sigma = 10, b = \frac{8}{3}$ in the (Y, Z) -plane, (from Drazin (1992)). (By courtesy of the Cambridge University Press.)

dimensional picture. The crossings in Figure 6.13 are the result of projection onto two dimensions. The Lorenz attractor is, however, an exquisitely thin set of zero volume with a fractal dimension 2.06 (for the above parameter values)! (See Sparrow (1982), for further details of the Lorenz attractor.)

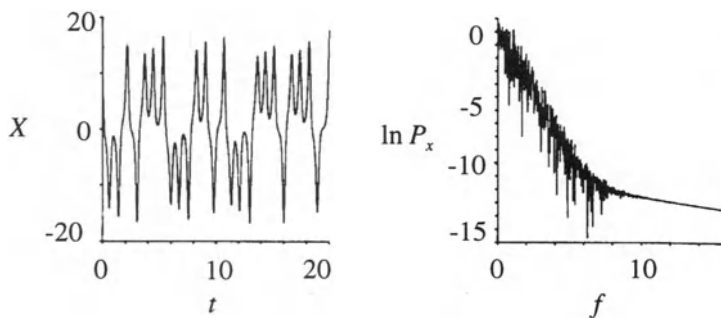


Figure 6.14. The time series $X(t)$ and the logarithm of its power spectrum vs. frequency, $\ln P_x(f)$ for the Lorenz system for $r = 28, \sigma = 10, b = \frac{8}{3}$, (from Drazin (1992)).
(By courtesy of the Cambridge University Press.)

In Figure 6.14, the time series and the Fourier spectrum for X are shown for the same values of the parameters r , σ and b , as above. The time series shows the chaotic motion about the two unstable equilibria (37). This then leads to the broad-band power spectrum with a large number of closely packed peaks which fall off rapidly as their frequency increases.

Lorenz (1963) followed the values of the successive maxima of $Z(t)$, say Z_n , as it spiralled about one of the stationary convective flow equilibria before jumping over to the other equilibrium and attaining its next maximum value Z_{n+1} , and so on. Based on the premise that Z_n predicts Z_{n+1} , Lorenz (1963) made a plot of Z_{n+1} vs. Z_n , shown in Figure 6.15, which is a one-dimensional “mapping”.¹⁵ Furthermore, since $|dZ_{n+1}/dZ_n| > 1$, this one-dimensional “map” cannot possess a stable periodic orbit and can be expected to generate a chaotic sequence.

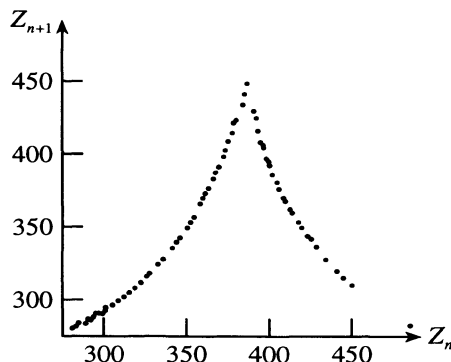


Figure 6.15. Maxima Z_{n+1} vs. previous maxima Z_n for Lorenz equations corresponding to $r = 28 > r^*$, (from Lorenz (1963)). (By courtesy of the American Meteorological Society).

6.7. Period-Doubling Bifurcations

(i) Difference Equations:

Consider first a linear difference equation

$$\phi_{n+1} + a\phi_n + b\phi_{n-1} = 0 \quad (73)$$

¹⁵ Such a dimensionality reduction is produced by disparate time scales present in the system (Nicolis, 1995). Fast processes eliminate evolution in certain directions while a slow evolution along the most unstable direction persists as time goes on.

where a and b are constants and n takes integer values.

Look for solutions of the form

$$\phi_n = \mu^n = A e^{n\lambda} \quad (74)$$

which, on substitution in equation (73), gives

$$\mu^2 + a\mu + b = 0, \quad (75a)$$

the roots of which are

$$\mu_+ = \frac{-a + \sqrt{a^2 - 4b}}{2}, \quad \mu_- = \frac{-a - \sqrt{a^2 - 4b}}{2}. \quad (75b)$$

Thus, the general solution is

$$\phi_n = A\mu_+^n + B\mu_-^n = A e^{n\lambda_+} + B e^{n\lambda_-}. \quad (76)$$

Though n takes only integer values, if n is large, one may view ϕ_n as a continuous function of n . Thus, one may write $\phi_n = \phi(\tau)$, where $\tau = n\Delta$ and Δ is a constant step length, and approximate $\phi_{n+1} \equiv \phi(n\Delta + \Delta) = \phi(\tau + \Delta)$ by the first two terms in a Taylor series. The difference equation (73) then reduces to a second-order differential equation

$$\frac{b}{2} \frac{d^2\phi}{d\tau^2} - \frac{b}{\Delta} \frac{d\phi}{d\tau} + \frac{(a+b)}{\Delta^2} \phi = 0. \quad (77)$$

EXAMPLE 7

Consider the difference equation (Rowlands, 1988)

$$\phi_{n+1} = a_n \phi_n, \quad a_n > 0 \text{ for all } n.$$

The solution of which is

$$\phi_{n+1} = \phi_o \prod_{j=0}^n a_j = \phi_o e^{\sum_{j=0}^n s_j}$$

where ϕ_o is the initial value and $S_j = \ln a_j$. Note that this equation shows quite distinct behavior depending on the values of a_j 's. Thus, $\phi_n \rightarrow 0$ as $n \rightarrow \infty$, if

$$\lim_{n \rightarrow \infty} \sum_{j=0}^n S_j > 0$$

while, $\phi_n \rightarrow 0$ for $n \rightarrow \infty$, if

$$\lim_{n \rightarrow \infty} \sum_{j=0}^n S_j < 0.$$

Observe that these limits do not, however, depend on the initial condition ϕ_o .

Let us consider next nonlinear difference equations.

EXAMPLE 8

Consider the difference equation (May, 1976)

$$x_{n+1} = 4\lambda x_n (1 - x_n).$$

If n is large, this difference equation may be approximated by the following differential equation –

$$\frac{dx}{d\tau} = \left(\frac{4\lambda - 1}{\Delta} \right) x - \left(\frac{4\lambda}{\Delta} \right) x^2,$$

where $\tau = n\Delta$ and Δ is a constant step length. This equation has the solution –

$$x = \frac{x_o(4\lambda - 1)}{4\lambda x_o \left[1 - e^{-\frac{(4\lambda - 1)\tau}{\Delta}} \right] + (4\lambda - 1)e^{-\frac{(4\lambda - 1)\tau}{\Delta}}},$$

where $x_o \equiv x(\tau = 0)$. This solution shows the following asymptotic behavior –

$$4\lambda < 1 : \lim_{t \rightarrow \infty} x = 0,$$

$$4\lambda > 1 : \lim_{t \rightarrow \infty} x = \frac{4\lambda - 1}{4\lambda},$$

which are again independent of the initial condition x_0 . Now, the above differential equation approximates the given difference equation for large n so that the latter may also be expected to display these features.

For an excellent account of further details of difference equations, see Devaney (1989).

(ii) The Logistic Map:

One dimensional non-invertible maps can exhibit a chaotic behavior (whereas invertible maps display the latter only when the dimensionality is greater than or equal to 2).

Consider one-dimensional mappings of the form

$$x_{n+1} = f_\lambda(x_n) \quad (78)$$

where $f_\lambda(x)$ satisfies the following conditions:

- $f_\lambda(x)$ is continuous and differentiable,
- $f_\lambda(x)$ has an extremum (this requires that $f(x)$ be a nonlinear function),
- $f_\lambda(x)$ has a negative Schwarzian derivative (this implies that f is concave), i.e.,

$$\frac{f_\lambda'''(x)}{f_\lambda'(x)} - \frac{3}{2} \left(\frac{f_\lambda''(x)}{f_\lambda'(x)} \right)^2 < 0 \text{ } 16. \quad (79)$$

¹⁶ In order to see this, as we will see below, note that the period-1 cycle bifurcates into a period-2 cycle when

$$\left. \frac{df_\lambda}{dx} \right|_{x=x^*} = -1, \quad \left. \frac{df_\lambda^{(2)}}{dx} \right|_{x=x^*} = 1$$

and

$$\left. \frac{d}{dx} \left(\frac{df_\lambda^{(2)}}{dx} \right) \right|_{x=x^*} = 0 \text{ and } \left. \frac{d^2}{dx^2} \left(\frac{df_\lambda^{(2)}}{dx} \right) \right|_{x=x^*} < 0$$

Collet and Eckmann (1980) have shown that such maps exhibit an infinite sequence of period-doubling pitchfork bifurcations, (see also Eckmann, 1981, and Shaw, 1981). As an example, consider the logistic map (May, (1976)),

$$x_{n+1} = 4\lambda x_n(1 - x_n), \quad 0 \leq x_n \leq 1 \quad (80)$$

which maps the unit interval onto itself (i.e., it is an *endomorphism*), if $\lambda \leq 1$. This mapping is non-invertible (i.e., it is not a *diffeomorphism*) because it results in the mapping of two different values of x_n to the same x_{n+1} . This mapping shows a stable fixed point bifurcating into a periodic orbit which then evolves via an infinite cascade of period doublings to a strange attractor. For $0 < \lambda < 3/4$, one finds that all iterates of $x_0 \neq 0$ converge onto a single limit point. As λ increases past $3/4$, this single fixed point bifurcates into a pair of fixed points or a period-2 limit cycle. As λ increases further, the period-2 limit cycle bifurcates into a period-4 limit cycle, which then bifurcates into a period-8 limit cycle, etc. The values of λ at which these pitchfork bifurcations occur ($\lambda_1, \lambda_2, \dots$) become closer and closer, converging geometrically to a critical value $\lambda_\infty (\approx 0.892)^{17}$, at which the orbit becomes aperiodic. For $\lambda_\infty < \lambda < 1$,

where $x = x^* \neq 0$ is a fixed point of f_λ .

Noting that,

$$\frac{d^3 f_\lambda^{[2]}}{dx^3} = f_\lambda'''(x) f_\lambda'(f_\lambda(x)) + 3 f_\lambda''(x) f_\lambda''(f_\lambda(x)) f_\lambda'(x) + f_\lambda'''(f_\lambda(x))(f_\lambda'(x))^3$$

we see that

$$\begin{aligned} \left. \frac{d^2}{dx^2} \left(\frac{df_\lambda^{[2]}}{dx} \right) \right|_{x=x^*} \\ = -2(f_\lambda'(x^*))^3 \left[-\left(\frac{1 + (f_\lambda'(x^*))^2}{2f_\lambda'(x^*)} \right) \frac{f_\lambda'''(x^*)}{f_\lambda'(x^*)} - \frac{3}{2} \left(\frac{f_\lambda''(x^*)}{f_\lambda'(x^*)} \right)^2 \right] < 0 \end{aligned}$$

implies, since $f_\lambda'(x^*) = -1$, that (Singer, 1978)

$$\frac{f_\lambda'''(x^*)}{f_\lambda'(x^*)} - \frac{3}{2} \left(\frac{f_\lambda''(x^*)}{f_\lambda'(x^*)} \right)^2 < 0.$$

¹⁷ Feigenbaum (1978) noticed that the sequence $(\lambda_1, \lambda_2, \dots)$ rapidly approaches geometric progression (a geometric progression is a sequence of numbers which converge to a limit point in such a way that the ratio of successive intervals is a constant) such that

both chaotic orbits and odd-period limit cycles appear. At $\lambda = 1$, the motion is uniformly chaotic on the unit interval $[0,1]$, i.e., the iterates x_n for each x_0 are densely and uniformly distributed on the interval $[0,1]$. For $\lambda > 1$, the map (76) does not map the interval $[0,1]$ onto itself and all orbits escape to infinity.

For the logistic map (80), with

$$f_\lambda(x) = 4\lambda x(1-x) \quad (81)$$

the successive iterates x_i , starting from x_0 , can be followed by plotting $y = f_\lambda(x)$ and the line $y = x$ on the same graph and moving successively vertically to the intersection with the curve $x_{n+1} = 4\lambda x_n(1-x_n)$, and horizontally to the intersection with the line $x_{n+1} = x_n$, between these two curves (Figure 6.16). Note that the points at which these two curves intersect (i.e., $y = f_\lambda(x) = x$) correspond to fixed points of the map (80)¹⁸. These fixed points are given by

$$x^* = 4\lambda x^*(1-x^*) \quad (82)$$

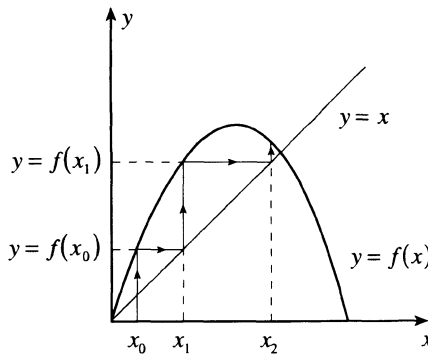


Figure 6.16. Graphical procedure for calculating successive iterates x_i of logistic map.

$$\lim_{n \rightarrow \infty} \frac{\lambda_{n+1} - \lambda_n}{\lambda_{n+2} - \lambda_{n+1}} = \delta = 4.6692016\dots$$

Feigenbaum (1978) also discovered that all nonlinear maps having a quadratic maximum as the logistic map had this same convergence rate.

¹⁸ This is provided for by the Fixed-Point Theorem: "If $f_\lambda : R \rightarrow R$ is continuous and there exists a closed interval I such that $I \subset f_\lambda(I)$, then there exists at least one point $x \in I$ such that $f_\lambda(x) = x$."

from which,

$$x^* = 0 \text{ and } 1 - \frac{1}{4\lambda}. \quad (83)$$

For $\lambda < 1/4$, only the fixed point $x^* = 0$ lies in the unit interval; but for $1/4 < \lambda < 1$, both fixed points become accessible. These fixed points will be stable (attracting) or unstable (repelling) depending on the slope of $f_\lambda(x)$. In order to see this, set $x_n = x^* + \varepsilon_n$, so that we have from (78),

$$x_{n+1} = f_\lambda(x^* + \varepsilon_n) \approx f_\lambda(x^*) + \varepsilon_n f'_\lambda(x^*) = x^* + \varepsilon_n f'_\lambda(x^*). \quad (84)$$

Putting $x_{n+1} = x^* + \varepsilon_{n+1}$, we obtain from (84),

$$\frac{\varepsilon_{n+1}}{\varepsilon_n} = f'_\lambda(x^*). \quad (85)$$

(85) implies that

$$\begin{aligned} |f'_\lambda(x^*)| &< 1 : x^* \text{ stable} \\ |f'_\lambda(x^*)| &= 1 : x^* \text{ neutrally stable} \\ |f'_\lambda(x^*)| &> 1 : x^* \text{ unstable.} \end{aligned} \quad (86)$$

For the logistic map (80), we have $f_\lambda(x) = 4\lambda x(1-x)$, so that

$$\left. \begin{aligned} f'_\lambda(0) &= 4\lambda \\ f'_\lambda\left(1 - \frac{1}{4\lambda}\right) &= 2 - 4\lambda \end{aligned} \right\}. \quad (87)$$

(87) implies that

$$\begin{aligned}
 \lambda &\leq \frac{1}{4} : x^* = 0 \text{ stable / unstable} \\
 \frac{1}{4} < \lambda < \frac{3}{4} &: x^* = 1 - \frac{1}{4\lambda} \text{ stable} \\
 \lambda < \frac{1}{4} \text{ and } \lambda > \frac{3}{4} &: x^* = 1 - \frac{1}{4\lambda} \text{ unstable.}
 \end{aligned} \tag{88}$$

Thus, for $\lambda < \frac{1}{4}$, all iterates in the unit interval converge to $x^* = 0$ ¹⁹; and for $\frac{1}{4} < \lambda < \frac{3}{4}$, all iterates converge to $x^* = 1 - \frac{1}{4\lambda}$ ²⁰. At $\lambda = \frac{3}{4}$, the fixed point $x^* = 1 - \frac{1}{4\lambda}$ becomes unstable and bifurcates into a stable 2-cycle. The two fixed points $x_{1,2}^*$ which make up the 2-cycle are, for $\lambda > \frac{3}{4}$, the stable fixed points of the composite function

$$f_\lambda^{[2]} = f_\lambda(f_\lambda(x)) \tag{89}$$

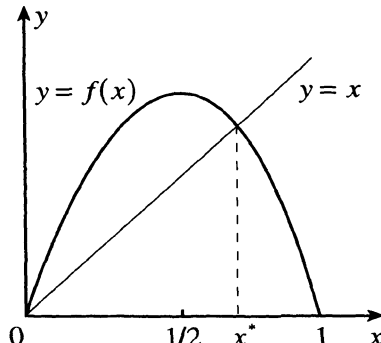
and are given by

$$x_{1,2}^* = \frac{(4\lambda+1) \pm \sqrt{(4\lambda-3)(4\lambda+1)}}{8\lambda}. \tag{90}$$

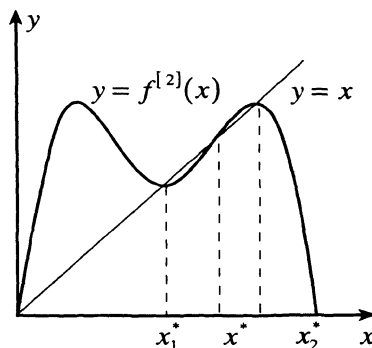
One may appreciate the appearance of these fixed points by looking at the graphs of f_λ and $f_\lambda^{[2]}$ (see Figure 6.17). While the function f_λ is a symmetric single-humped

¹⁹ For $\lambda < \frac{1}{4}$, it can readily be shown that $\left\{f_\lambda^{[n]}(x)\right\}_{n=0}^\infty$ forms a bounded decreasing sequence converging to the fixed point $x^* = 0$.

²⁰ For $\frac{1}{4} < \lambda < \frac{3}{4}$, it can readily be shown that $\left\{f_\lambda^{[n]}(x)\right\}_{n=0}^\infty$ forms a bounded increasing sequence if $0 < x < x^*$ and a bounded decreasing sequence if $x^* < x < 1$, both of which converge to the fixed point $x^* = 1 - \frac{1}{4\lambda}$.



(a)



(b)

Figure 6.17. The fixed point of (a) $f_\lambda(x)$ and (b) $f_\lambda^{[2]}(x)$.

function, the function $f_\lambda^{[2]}$ is a symmetric double-humped function. x^* is a fixed point of both f_λ and $f_\lambda^{[2]}$. (In fact, x^* is the only stable fixed point of f_λ and $f_\lambda^{[2]}$, if $\lambda < \frac{3}{4}$.)

For $\lambda > \frac{3}{4}$, x_1^* and x_2^* are fixed points of $f_\lambda^{[2]}$. However, they are not fixed points of f_λ so that they are mapped into each other under f_λ , i.e.,

$$x_1^* = f_\lambda(x_2^*) \text{ and } x_2^* = f_\lambda(x_1^*). \quad (91)$$

In the 2-cycle the iterates change from one fixed point to the other in perpetuity. Note that the slopes of $f_\lambda^{[2]}$ at x_1^* and x_2^* are the same, i.e.,

$$f_\lambda^{[2]'}(x_1^*) = \frac{d}{dx} f_\lambda(f_\lambda(x_1^*)) \Bigg|_{x=x_2^*} = \left[\frac{d}{dx} f_\lambda(x) \right]_{x=x_2^*} f_\lambda'(x_1^*) = f_\lambda'(x_2^*) f_\lambda'(x_1^*) \quad (92)$$

and

$$f_\lambda^{[2]'}(x_2^*) = f_\lambda'(x_1^*) f_\lambda'(x_2^*). \quad (93)$$

It may be shown that (see Exercise 5)

$$f_\lambda^{[2]'}(x_{1,2}^*) = (4\lambda)^2 (1 - 2x_1)(1 - 2x_2) = 1 - (4\lambda + 1)(4\lambda - 3).$$

Thus, the two fixed points x_1^* and x_2^* are both stable for $\lambda > \frac{3}{4}$ and then become both unstable at $\lambda = \frac{1+\sqrt{6}}{4}$. At this value of λ , x_1^* and x_2^* bifurcate into two new fixed points each and give rise to a stable 4-cycle corresponding to the fixed points of $f_\lambda^{[4]} = f_\lambda^{[2]}(f_\lambda^{[2]}(x))$.

In the 4-cycle, the iterates of (80) move to each fixed point of (89), in turn, in a periodic manner. This period-doubling or subharmonic sequence continues (as shown in Figure 6.18) via the mechanism of pitch-fork bifurcation to bring about the successive doublings of fixed points. (Observe that, at the bifurcation point $\lambda_1 = 3/4$, a single branch splits into two branches representing a stable period-2 cycle that emerges at $\lambda = \lambda_1$; these two branches then split into four branches representing the period-4 cycle at $\lambda = \lambda_2 = \frac{1+\sqrt{6}}{4}$ and so on.) Feigenbaum (1978) found that the band of values of λ over which a given period- 2^k cycle is stable decreases geometrically with k such that

$$\delta = \lim_{k \rightarrow \infty} \frac{\lambda_k - \lambda_{k-1}}{\lambda_{k+1} - \lambda_k} = 4.6692016\dots \quad (94)$$

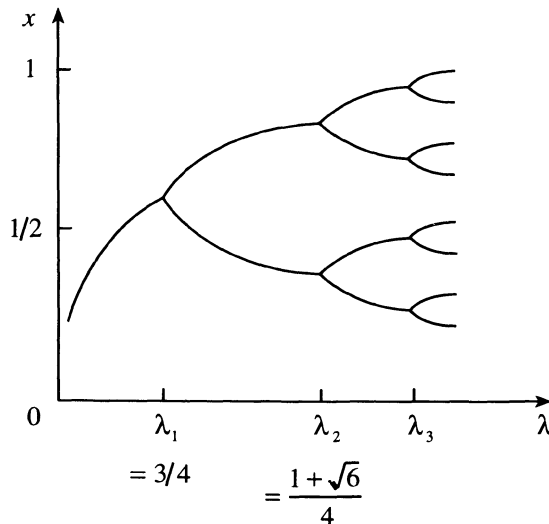


Figure 6.18. Period-doubling sequences via pitchfork bifurcation for the logistic map.

where λ_k is the value of λ at the point where the period- 2^k cycle bifurcates into the period- 2^{k+1} cycle. Thus, the values of λ_k get closer together as k increases, and this sequence of bifurcations terminates as $k \rightarrow \infty$ with

$$\lim_{k \rightarrow \infty} \lambda_k = \lambda_\infty = 0.892\ldots \quad (95)$$

i.e., there is an accumulation point of an infinite number of bifurcations at $\lambda_\infty = 0.892\ldots$ ²¹. Feigenbaum (1978) found that this terminating period-doubling

²¹ In order to give an approximate analytical evaluation of this result, let us shift (Hu (1982), Landau and Lifshitz (1987)),

$$x \Rightarrow \frac{x}{2}(2\lambda - 1) + \frac{1}{2} \quad (I)$$

so that the map (81) transforms to

$$x_{n+1} = 1 - \Lambda x_n^2 \quad (II)$$

where,

$$\Lambda \equiv 2\lambda(2\lambda - 1).$$

bifurcating sequence is universal, i.e., δ is the same for all iterated maps $x_{n+1} = f_\lambda(x_n)$, provided that $f_\lambda(x)$ has a single, locally quadratic maximum. (See Appendix 6.3 for an intuitive derivation of this universality.) λ_∞ , however, was found to be not universal but to depend on the detailed form of $f_\lambda(x)$.

The map (II) leads to $-1 < x < 1$ if $0 < \Lambda < 2$. Further, the map (II) has a fixed point x^* given by

$$x^* = 1 - \Lambda x^{*2} \quad (\text{III})$$

which becomes unstable and leads to the first bifurcation, when

$$2\Lambda x^* = 1 \quad (\text{IV})$$

i.e., when $\Lambda = 3/4$ with $x^* = \frac{2}{3}$.

Next, iterating the map (II), we have

$$x_{n+2} = 1 - \Lambda + 2\Lambda^2 x_n^2 - \Lambda^3 x_n^4. \quad (\text{V})$$

Neglecting the quartic term and rescaling x_n , according to $x_n \Rightarrow x_n(1 - \Lambda)$, (V) becomes

$$x_{n+2} = 1 - \Lambda_1 x_n^2 \quad (\text{VI})$$

where,

$$\Lambda_1 = 2\Lambda^2(\Lambda - 1) = \psi(\Lambda), \text{ say.}$$

Observe that (VI) is of the same form as (II), so becomes unstable and leads to the next bifurcation, when $\Lambda_1 = 3/4$. The succeeding bifurcations occur at $\Lambda_2 = \psi(\Lambda_1) = 1.2428$, $\Lambda_3 = \psi(\Lambda_2) = 1.3440$, $\Lambda_4 = \psi(\Lambda_3) = 1.3622, \dots$ finally accumulating at

$$\Lambda_\infty = \psi(\Lambda_\infty) \quad (\text{VII})$$

giving

$$\Lambda_\infty = \frac{1 + \sqrt{3}}{2} = 1.3660 \quad (\text{VIIIa})$$

or

$$\Lambda_\infty = 0.8856 \quad (\text{VIIIb})$$

which is quite close to the exact value $\Lambda_\infty = 0.8924$.

Further, observe that after each bifurcation, the mapping interval, which is initially $[-1, 1]$, shrinks by a factor $(1 - \Lambda)$. Therefore, after several bifurcation, the iterated map is sensitive only to the properties of the original map near its maximum, thus indicating a universality in the bifurcating sequence!

Such a universality implies that there are basic properties of the system (like critical exponents near the transition to chaos) that depend only on some global properties of the system. So, renormalization group considerations based on the scale invariance (Ma, 1976) would be in order (Feigenbaum, 1978; see also Greene *et al.*, 1981).

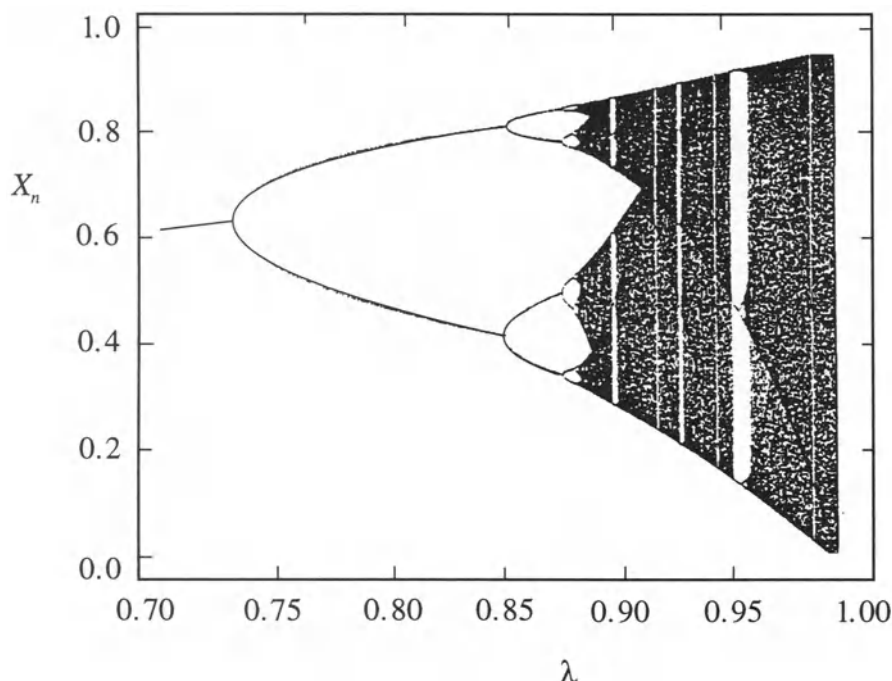


Figure 6.19. Bifurcation diagram of the logistic map. The map bifurcates from a fixed point to a two-cycle at the extreme left, and then period-doubles until it becomes chaotic. The chaotic region is interlaced with stable periodic orbits. (From Nayfeh and Balachandran (1995)). (By courtesy of John Wiley & Sons.)

If one iterates the map (80), for each value of λ , until all transients have died out and the orbit has settled onto the asymptotic state comprising the 2-cycle, 4-cycle, ... infinite-cycle or aperiodic attractor, one obtains a bifurcation diagram shown in Figure 6.19. This diagram shows the following basic features:

- the successive bifurcations of period- 2^k cycles appear for $\lambda = \lambda_{k-1}, k = 1, 2, \dots$, which become more and more compressed as λ increases;
- chaotic bands separated by odd cycles (eg. 3-cycle) appear beyond λ_∞ ; (here, no matter how many times this equation is iterated, it never repeats itself and the iterates spread out over a subinterval or a collection of subintervals of $[0, 1]$)²²; this behavior though apparently random is deterministic, i.e., once the initial value x_0 is given, x_n is uniquely determined by equation (80));
- uniformly chaotic behavior occurs at $\lambda = 1$; (for $\lambda > 1$, most of the trajectories escape to $x = -\infty$);
- the thick lines running through the chaotic region represent heavy concentrations of points corresponding to trajectories passing near the critical point $x = \frac{1}{2}$; here, the slope of the map function (80) is zero so that all trajectories passing near this point stay close to each other for several subsequent iterations.

An important feature of this scenario is that it is universal, being independent of the details of the mapping.

Thus, a typical scenario for chaos is as follows: An attracting stable fixed point bifurcates into a periodic orbit, which then evolves via an infinite cascade of period-doubling bifurcations to a chaotic attractor. It may be mentioned that even though the explicit reduction of the equations governing a fluid system to a one-dimensional map with a single quadratic maximum has still not been demonstrated, experiments of thermal convection for mercury in a magnetic field (Libchaber *et al.* (1983)) have shown at least four period doublings with a universal scaling that agrees to within 5% of the theoretical value for one-dimensional maps. It should be noted, however, that because of the relatively large value of the limiting ratio, all but the first few λ_n 's are very close to each other so that the observation of successive period doublings is extremely difficult. One typically observes three or four period doublings and then a chaotic behavior.

The chaotic behavior of the solutions for $\lambda > \lambda_\infty$ can be characterized by the Liapunov exponents. In order to determine these, note the tangent map near the point \bar{x}_n :

$$\delta x_{n+1} = 4\lambda(1 - 2\bar{x}_n)\delta x_n \quad (96)$$

from which, we have

²² It should be noted that the computer cannot resolve whether the iterates describe a stable cycle of very high period or they are in fact dense on the interval $[0, 1]$.

$$\delta x_{n+1} = \delta x_o e^{\sum_{j=0}^n S_j} \quad (97)$$

where,

$$S_j = \ln \left[4\lambda \left| (1 - 2\bar{x}_j) \right| \right]. \quad (98)$$

If the values of x_j do in fact attain an asymptotic state x^* , then, for sufficiently large n , the above summation is dominated by the contribution from the asymptotic state x^* . For example, if $\frac{1}{4} < \lambda < \frac{3}{4}$, we have $x^* = 1 - \frac{1}{4\lambda}$ and then

$$\delta x_{n+1} = \delta x_o e^{n \ln |(2-4\lambda)|}. \quad (99)$$

Observe that δx_n has an exponential growth if $\lambda > \frac{3}{4}$. Similarly, if $\lambda > \frac{3}{4}$, we have

$$x_{1,2}^* = \frac{(4\lambda + 1) \pm \sqrt{(4\lambda - 3)(4\lambda + 1)}}{8\lambda} \text{ and then}$$

$$\delta x_{n+1} = \delta \hat{x}_o e^{\frac{n}{2} \ln |1 - (4\lambda + 1)(4\lambda - 3)|} \quad (100)$$

which shows an exponential growth if $\lambda > \frac{1 + \sqrt{6}}{4}$. Thus, for sufficiently large n , we can

write for a periodic solution, $\sum_{j=0}^n S_j = n\sigma$, where σ is some constant and is a simple

measure of the rate of exponential growth of the distance between two neighboring orbits. One may therefore define the Liapunov exponent σ for any solution, periodic or otherwise, as an average taken over the iterates of the map, as follows:

$$\sigma = \lim_{n \rightarrow \infty} \frac{1}{n} \sum_{j=0}^n \ln \left[\left| 4\lambda \left(1 - 2\bar{x}_j \right) \right| \right]. \quad (101)$$

For periodic solutions, σ reduces to the constant values given by,

$$\sigma = \begin{cases} \ln(|2 - 4\lambda|), & \frac{1}{4} < \lambda < \frac{3}{4} \\ \frac{1}{2} \ln(|1 - (4\lambda + 1)(4\lambda - 3)|), & \frac{3}{4} < \lambda < \frac{1+\sqrt{6}}{4} \end{cases}. \quad (102)$$

(102) shows that, $\sigma \leq 0$ for the stable period-one and period-two orbits. This means that for large enough n 's, $\delta x_n \rightarrow 0$, which simply implies the stability of the state \bar{x}_n . When λ goes outside a given range, σ becomes positive. However, σ for the new bifurcated stable state, for this value of λ , is again negative. For $\lambda > \lambda_\infty$, σ is positive so that $\delta x_n \rightarrow \infty$, as $n \rightarrow \infty$, no matter how small δx_0 is, implying the sensitivity of the solution \bar{x}_n to initial conditions. Thus, one may use a positive σ to distinguish a truly chaotic sequence from a periodic one of large period.

In order to calculate σ for values of $\lambda > \lambda_\infty$ when chaotic solutions appear, one needs to introduce the concept of a probability distribution function which, of course, appears to be perfectly reasonable for a statistical description of the chaotic solution.

Thus, we define $P(x, n) dx$ as the probability of finding the n th iterate of the logistic map, in the interval between x and $x + dx$, for all equally probable initial conditions. This gives us the functional equation, called the Master equation,

$$P(x, n+1) = \int_0^1 P(x', n) \delta[x - 4\lambda x'(1-x')] dx' \quad (103)$$

which merely states that the point x' is mapped onto the point x after one iteration of the map (80), and represents a Markov process with a deterministic transition rate $\delta[x - 4\lambda x'(1-x')]$.

If $P(x, n)$ settles down to the "equilibrium" value $P(x)$ independent of n for large n (which is therefore a fixed point of the Master equation (103)), we have from equation (103),

$$P(x) = \int_0^1 P(x') \delta[x - 4\lambda x'(1-x')] dx'. \quad (104)$$

For the case, $\frac{1}{4} < \lambda < \frac{3}{4}$, for which the final state of the system is the asymptotic value $x^* = 1 - \frac{1}{4\lambda}$, we have

$$P(x) = \delta[x - x^*] \quad (105)$$

which is a solution of the Master equation (104). Similarly, for the case, $\frac{3}{4} < \lambda < \frac{1+\sqrt{6}}{4}$, the final states are $x_{1,2}^* = \frac{(4\lambda+1) \pm \sqrt{(4\lambda-3)(4\lambda+1)}}{8\lambda}$ so that

$$P(x) = \frac{1}{2} [\delta(x - x_1^*) + \delta(x - x_2^*)]. \quad (106)$$

We have, from the Master equation (104),

$$P(x) = \frac{P\left(\frac{1+\sqrt{1-x/\lambda}}{2}\right) + P\left(\frac{1-\sqrt{1-x/\lambda}}{2}\right)}{4\lambda\sqrt{1-x/\lambda}} \quad (107)$$

which may be re-expressed as a Frobenius-Perron equation:

$$P(4\lambda x(1-x)) = \frac{P(x) + P(1-x)}{4\lambda(|1-2x|)}. \quad (108)$$

In general, analytic solutions of the functional equation (108) are not known. An exception arises for the chaotic solution corresponding $\lambda = 1$ ²³. Putting $x = \sin^2\left(\frac{\theta}{2}\right)$, $0 \leq \theta \leq \pi$, and defining

$$\bar{P}(\theta) d\theta = P(x) dx \quad (109)$$

equation (108) reduces to

²³ In fact, for $\lambda = 1$, the logistic map is equivalent to the Bernoulli shift map (see Exercise 4).

$$\bar{P}(2\theta) = \frac{\bar{P}(\theta) + \bar{P}(\pi - \theta)}{2}. \quad (110)$$

One solution of equation (110) is the invariant density function –

$$\bar{P}(\theta) = \text{const} \quad (111)$$

which implies that the iterates are found uniformly over the interval $0 \leq \theta \leq \pi$, as is expected for a chaotic behavior, and corresponds to the invariant probability density function (because it represents properties of the map (81) that are independent of initial data)

$$P(x) = \frac{1}{\sqrt{\pi x(1-x)}} \quad (112)$$

where the factor $1/\sqrt{\pi}$ arises from the normalization condition, (Figure 6.20). (It is of interest to note that this solution was derived by von Neumann (1951) well before the concept of deterministic chaos emerged!) (112) shows that the iterates are found more often near the ends than at the middle of the interval $[0,1]$. The infinity in the probability density function (112), at $x = 0$ and 1, is caused by the critical point of $x = 1/2$, where the logistic map (80) has zero slope (Eubank and Farmer, 1989). Under a linear approximation of the map, a small interval around $x = 1/2$ is mapped to $x = 1$, which

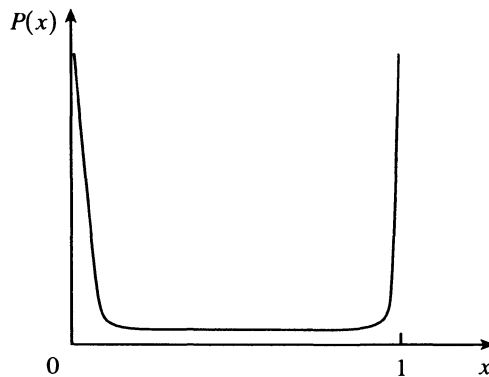


Figure 6.20. The probability density function for the logistic map for $\frac{3}{4} < \lambda < \frac{1+\sqrt{6}}{4}$.

produces an infinite probability density function. The point $x = 1$ is then mapped to $x = 0$, which also produces an infinite probability density function. This infinity cannot propagate further to any other point on $[0,1]$, because the point $x = 0$ is unstable for $\lambda = 1$!

In terms of the probability density function $P(x)$, one may now define the Liapunov exponent alternatively via the ergodic hypothesis as follows:

$$\sigma = \int_0^1 P(x) \ln(4\lambda|1-2x|) dx. \quad (113)$$

Note that for a periodic solution of period N , with the individual iterates taking the values, $x_j, i = 1, 2, \dots, N$, we have

$$P(x) = \frac{1}{N} \sum_{j=0}^N \delta(x - x_j) \quad (114)$$

which leads, from (113), to

$$\sigma = \frac{1}{N} \sum_{j=0}^N \ln(4\lambda|1-2x_j|). \quad (115)$$

This, in turn, gives, for instance,

$$\sigma = \begin{cases} \ln(|2-4\lambda|), & \frac{1}{4} < \lambda < \frac{3}{4} \\ \frac{1}{2} \ln(|1-(4\lambda+1)(4\lambda-3)|), & \frac{3}{4} < \lambda < \frac{1+\sqrt{6}}{4} \end{cases} \quad (116)$$

as in (102).

For the chaotic solution (112) corresponding to $\lambda = 1$, we have from (113),

$$\sigma = \frac{1}{\sqrt{\pi}} \int_0^1 \frac{\ln(4|1-2x|)}{\sqrt{x(1-x)}} dx = \ln 2 \quad (117)$$

which confirms the fact that, for $\lambda = 1$, the logistic map is equivalent to the Bernoulli shift map. Also, observe that (117) is exactly the same as that for the unstable period-one and period-two orbits, given by (102)!

In order to obtain further information from (113), one resorts to numerical computation. Figure 6.21 shows the variation of the Liapunov exponent σ for points on the unit interval mapped under the logistic map (80) as a function of the parameter λ . For $\lambda < \lambda_\infty$, $\sigma < 0$, indicating that nearby orbits converge to some stable cycle. For $\lambda > \lambda_\infty$, σ is largely positive, indicating that nearby orbits diverge asymptotically. Observe that the sign of σ agrees very well with the behavior of the logistic map (80) as represented by the bifurcation diagram (Figure 6.19); a bifurcation occurs every time σ goes through zero. Note, however, that there are nevertheless sharp negative dips which correspond to stable orbits ("windows") in the chaotic region (see below). The most pronounced stable window is the one associated with a period-3 solution which occurs for $\lambda = .95$.

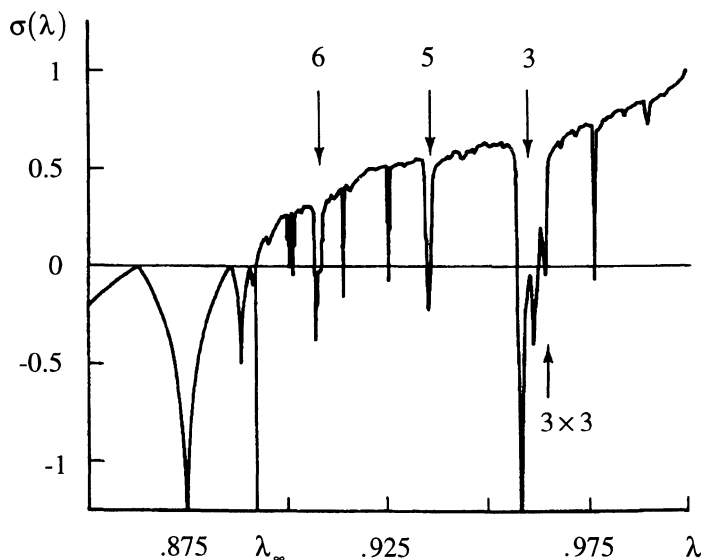


Figure 6.21. Variation of the Liapunov exponent σ , with the parameter λ , for the logistic map. (Due to Jackson (1989)). (By courtesy of the Cambridge University Press.)

The fact that orbits beyond λ_∞ are chaotic implies that they show sensitive dependence to initial conditions. The latter property would require the presence of some stretching and folding mechanism in the map (80). The folding property of the map

arises from its noninvertibility (recall that for each value of x_{n+1} there are two values of x_n). In order to see these features, consider the case $\lambda = 1$, for which the map involves two steps (see Figure 6.22) –

- a uniform stretching of the interval $[0,1]$ to twice its original length;
- a folding in half of the stretched interval so that it now has its original length.

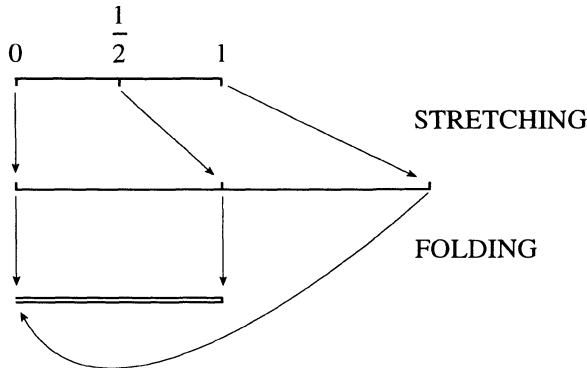


Figure 6.22. The stretching and folding properties of the logistic map for $\lambda = 1$.

The stretching property leads to exponential separation of nearby points, and hence, sensitive dependence on initial conditions due to the loss of information about the initial conditions as the iteration number increases. The folding property, which is due to the non-invertibility of the map (80), implies a loss of memory in the mapping process and keeps the generated sequence bounded.

On the other hand, for the case $\frac{1}{2} < \lambda < 1$, after one application of f_λ , there are no

points on $\lambda < x < 1$ (see Figure 6.23b). Further, the interval 0 to $4\lambda^2(1-\lambda)$ is stretched but no points are folded back onto it. Thus, the generated sequence is eventually trapped in $4\lambda^2(1-\lambda) < x < \lambda$, where any initial x_0 will wander chaotically when $\lambda_\infty \leq \lambda < 1$. (Any point in $0 < x < 4\lambda^2(1-\lambda)$ will eventually leave that interval and never return, see Ott (1981) for further details.)

Another important feature of the motion, for $\lambda > \lambda_\infty$, is the existence of an infinite number of narrow windows in λ for $\lambda_\infty < \lambda < 1$ for which the generated sequences are odd cycles. These windows are believed to be dense (Ott (1993)) throughout the region $\lambda > \lambda_\infty$. The appearance of period-3 cycle may be understood by considering the map

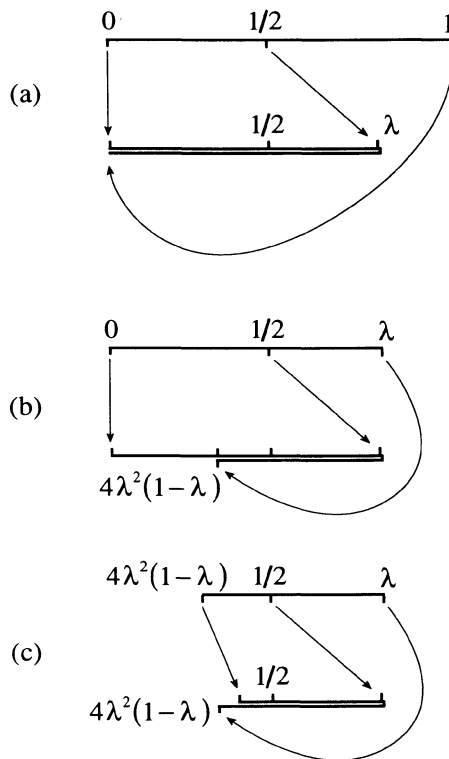


Figure 6.23. The logistic map for $\lambda = 0.8$; (a) mapping of the interval 0 to 1, (b) 0 to λ , and (c) $4\lambda^2(1-\lambda)$ to λ .

$f_\lambda^{[3]}(x)$. For small λ , the only fixed points of $f_\lambda^{[3]}(x)$ are the fixed points of $f_\lambda(x)$. As λ increases, for $\lambda = \lambda_*(= \frac{1}{4}(1 + \sqrt{8})) > \lambda_\infty$, $f_\lambda^{[3]}(x)$ becomes exactly tangent to the line $y = x$ (see Figure 6.24), and a 3-cycle appears through a tangent bifurcation (Myrberg (1958)). Tangent bifurcation corresponds to the merging of two fixed points (a stable and an unstable one), as shown in Figure 6.25a. This leads to the appearance of a periodic orbit after a region of chaotic motion. For $\lambda > \lambda_*$, each fixed point of the 3-cycle bifurcates into a pair of fixed points – one stable and one unstable via a saddle-node bifurcation. (In contrast, in a period-doubling bifurcation an unstable fixed point goes into a pair of stable fixed points via a pitch-fork bifurcation.) As λ increases further, these bifurcations accumulate at an aperiodic state ending the 3-cycle window

for $\lambda = 0.9624$. As λ increases still further, other periodic windows, with their entourage of bifurcations leading to chaos, appear but are exceedingly narrow in λ , and most of the range $\lambda_* < \lambda < 1$ appears to be chaotic.

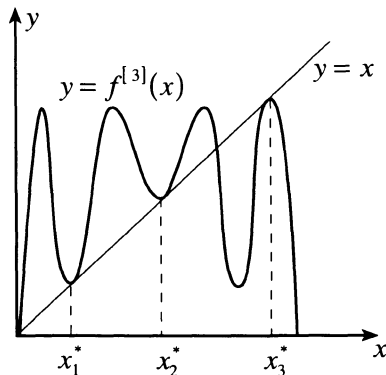


Figure 6.24. Birth of a period-3 orbit.

For λ just below λ_* , $f_\lambda^{[3]}(x)$ is not quite tangent to the line $y = x$ so that the iterates will spend a long time nearly trapped in the resulting narrow tunnel and then go around freely in the plane (Figure 6.25b) until they get trapped again in another narrow gap. Further, the narrower the tunnel, the longer time the iterates spend to pass through the tunnel. Thus, if the logistic map is viewed as a Poincaré surface of section for some continuous dynamical system, then the above scenario would correspond to a physical variable showing a nearly periodic evolution with occasional irregular bursts. Therefore, tangent bifurcation was invoked by Manneville and Pomeau (1979) to explain the phenomenon of intermittency²⁴ wherein the long phases of regular behavior are interrupted at seemingly random times by short irregular bursts.

In order to determine the average time spent by the system in the periodic region, let us approximate the mapping function $f_\lambda^{[3]}(x)$ in this region by a quadratic polynomial

$$x_{n+1} = \epsilon + x_n + ax_n^2 \quad (118)$$

where,

²⁴ The phenomenon of intermittency appears to be a common feature in chaotic systems because there are infinitely many periodic windows arising from tangent bifurcations in the chaotic regions. Besides, it is one of the characteristic features of fully-developed turbulence (see Chapter 7).

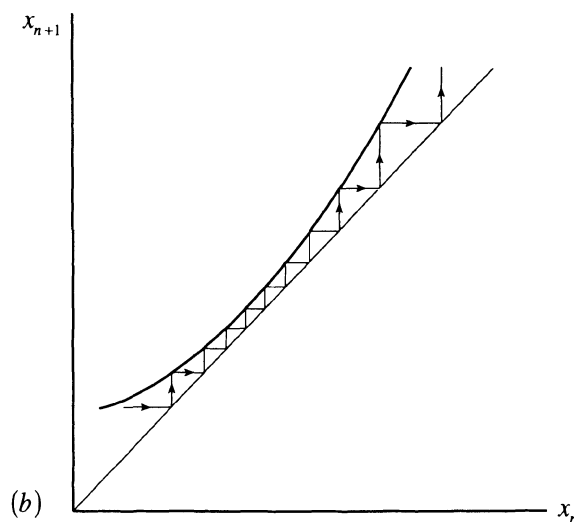
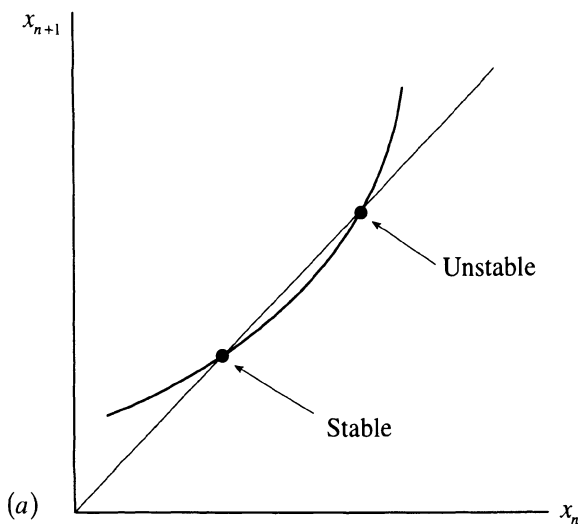


Figure 6.25. The logistic map for (a) $\varepsilon = \lambda_* - \lambda < 0$ and (b) $\varepsilon = \lambda_* - \lambda > 0$, in the vicinity of the stable ($\varepsilon < 0$) orbit.

$$\varepsilon \equiv \lambda_* - \lambda > 0$$

and a is a positive constant that may be scaled away.

For λ just below λ_* , the tunnel of periodic or regular behavior is very narrow so that x_n changes very little after each iteration. The discrete map (118) may then be replaced by the continuous flow:

$$x_{n+1} - x_n = \frac{\Delta x}{\Delta n} \Big|_{\Delta n=1} \approx \frac{dx}{dt} = \varepsilon + x^2. \quad (119)$$

Equation (119) has the solution –

$$t = \frac{1}{\sqrt{\varepsilon}} \tan^{-1} \left[\frac{x(t) - x_*}{\sqrt{\varepsilon}} \right] \quad (120)$$

where x_* refers to the value at the center of the tunnel which is also taken to be $x(t=0)$.

If ε is very small, the average time taken by the iterates to go from one end of the tunnel to the other end is given, from (120), by

$$\langle t \rangle \sim \frac{\pi}{\sqrt{\varepsilon}} = \frac{\pi}{\sqrt{\lambda_* - \lambda}} \quad (121)$$

showing the behavior to be almost regular as $\lambda \rightarrow \lambda_*$ (Pomeau and Manneville (1980)); see also Berge *et al.* (1984) for a detailed account).

APPENDIX 6.1

The Hausdorff-Besicovitch Dimension:

In order to give a measure of the size of a set of points, S , in space, corresponding to a resolution of the measurement δ , we take a function $h(\delta) = \gamma(d)\delta^d$, which may represent a line, square, disk, ball or cube, and cover the set S to form the measure:

$$M_d(S) = \sum h(\delta) = \sum \gamma(d)\delta^d. \quad (\text{A1.1})$$

Here, the geometrical factor $\gamma(d) = 1$ for lines, squares and cubes; $\gamma = \pi/4$ for disks and $\gamma = \pi/6$ for spheres. In the limit $\delta \rightarrow 0$, the measure $M_d(S)$ turns out to be zero or infinite depending on the choice of d – the dimension of $M_d(S)$. (Note that for the Koch curve, the 1-dimensional measure, namely, the length, is diverging, while the 2-dimensional measure, namely, the area is 0.) The Hausdorff-Besicovitch dimension $D(S)$ of the set S is the critical dimension for which the measure $M_d(S)$ jumps from zero to infinity:

$$M_d(S) = \sum \gamma(d) \delta^d = \gamma(d) N(\delta) \delta^d \rightarrow \begin{cases} 0, & d > D(S) \\ \infty, & d < D(S) \end{cases} \text{ as } \delta \rightarrow 0 \quad (\text{A1.2})$$

or

$$D(S) = \inf \{d \mid M_d(S) = 0\} = \sup \{d \mid M_d(S) = \infty\}$$

which implies $N(\delta) \sim \delta^{-D(S)}$, or that the measure is finite when $d = D(S)$. Note that this definition makes the Hausdorff-Besicovitch dimension a local property in the sense that it measures properties of sets of points in the limit of a vanishing parameter or size δ of the test function used to cover the set.

Some fundamental properties of the Hausdorff-Besicovitch dimension may be noted:

- (i) if $S \subset R^n$, then $D(S) \leq n$;
- (ii) if $S \subset U$, then $D(S) \leq D(U)$;
- (iii) if $S \subset R^n$ and $D(S) < 1$, then S is totally disconnected.

(A1.2) also implies that an object may be called a fractal if it is not possible to obtain a finite measure for its volume, surface or length when measuring with d , $d-1, \dots$ dimensional hyper cubes of size ε and changing ε over several orders of magnitude.

EXAMPLE A.1

The Cantor Set.

Let A be the cover of the Cantor set consisting of 2^n intervals of length $1/3^n$ each, for $n = 1, 2, \dots$. Then, we have from (A1.2),

$$2^n \cdot \left(\frac{1}{3^n} \right)^D = 1$$

from which the Hausdorff-Besicovitch dimension D is

$$D = \frac{\ln 2}{\ln 3} = 0.69$$

in agreement with the capacity dimension derived in EXAMPLE 2.

Note that, for a given set, the Hausdorff-Besicovitch dimension need not be the same as the capacity dimension, because the latter does not distinguish between a set and its closure (Falconer, (1990)). For example, the set of rational numbers is a countable union of points so that its Hausdorff-Besicovitch dimension is 0 while its capacity dimension is 1 because its closure is \mathbb{R} . In general, the Hausdorff-Besicovitch dimension is smaller than (or equal to) the capacity dimension.

APPENDIX 6.2

The Derivation of Lorenz's Equations:

Consider a fluid layer of depth H , with the lower surface maintained at a higher temperature $T_o + \Delta T$ than the temperature T_o of the upper surface. The equation governing the evolution of vorticity in this layer, with the inclusion of buoyancy effects is

$$\frac{\partial}{\partial t} \nabla^2 \psi + \left(\frac{\partial \psi}{\partial x} \frac{\partial}{\partial z} - \frac{\partial \psi}{\partial z} \frac{\partial}{\partial x} \right) \nabla^2 \psi - v \nabla^4 \psi - g \alpha \frac{\partial \theta}{\partial x} = 0 \quad (\text{A2.1})$$

where, the flow has been assumed to depend only on x (the horizontal direction), z (the vertical direction) and t . If (u, v) is the fluid velocity, the stream function ψ is defined by

$$u = -\frac{\partial \psi}{\partial z}, \quad v = \frac{\partial \psi}{\partial x}. \quad (\text{A2.2})$$

θ is the departure of the temperature profile from the conduction situation in the fluid,

$$\theta = T - T_o - \Delta T \left(1 - \frac{z}{H} \right). \quad (\text{A2.3})$$

g is the acceleration due to gravity, α is the coefficient of thermal expansion and v is the kinematic viscosity of the fluid.

The equation governing the evolution of temperature in the fluid layer is

$$\frac{\partial \theta}{\partial t} + \left(\frac{\partial \psi}{\partial x} \frac{\partial}{\partial z} - \frac{\partial \psi}{\partial z} \frac{\partial}{\partial x} \right) \theta - \frac{\Delta T}{H} \frac{\partial \psi}{\partial x} - \kappa \nabla^2 \theta = 0 \quad (\text{A2.4})$$

where κ is the thermal conductivity of the fluid.

As the temperature difference across the fluid layer ΔT is increased, the heat transport process via the conduction mechanism becomes unstable and gives way to the transport process via the convection mechanism involving a steady cellular flow. (The latter arises due to the fact that the fluid near the warmer lower surface expands and rises because of the buoyancy, while the cooler and heavier fluid near the upper surface descends under gravity.) If ΔT is increased further, the convection process shows a time-dependent behavior. In this regime, taking clues from the previous numerical work of Saltzman (1962), Lorenz (1963) considered the dynamics to be primarily described by three Fourier modes –

$$\begin{aligned} \psi &= X(t) \frac{2^{1/2}(1+a^2)}{a^2} \sin \frac{\pi ax}{H} \sin \frac{\pi z}{H} \\ \theta &= Y(t) \frac{2^{1/2} R_c}{\pi R} \cos \frac{\pi ax}{H} \sin \frac{\pi z}{H} - Z(t) \frac{R_c}{\pi R} \sin \frac{2\pi z}{H} \end{aligned} \quad (\text{A2.5})$$

where R is the Rayleigh number,

$$R = \frac{g\alpha H^3 \Delta T}{\nu \kappa}$$

and R_c is the value of R for which conduction gives way to convection. Upon substituting (A2.5), equations (A2.1) and (A2.4) give Lorenz's equations –

$$\begin{aligned} \dot{X} &= -\sigma(X - Y) \\ \dot{Y} &= rX - Y - XZ \\ \dot{Z} &= -bZ + XY \end{aligned} \quad (\text{A2.6})$$

where the dot denotes derivative with respect to a non-dimensionalized time $\tau = \frac{\pi^2(1+a^2)\kappa t}{H^2}$, and

$$r \equiv \frac{R}{R_c}, \sigma = \frac{v}{\kappa} \text{ and } b = \frac{4}{1+a^2}.$$

APPENDIX 6.3

The Derivation of Universality for One-Dimensional Maps:

We will give here an intuitive derivation of universality for one-dimensional maps which have a single, locally quadratic maximum (the following formulation is adapted from Holton and May (1993)).

Consider the composite map

$$x_{n+k} = f_\lambda^{[k]}(x_n). \quad (\text{A3.1})$$

Let $x^{*(k)}$ be the fixed point of this map; $x^{*(k)}$ is, therefore, a period- k cycle. Let,

$$\mu^{(k)}(\lambda) \equiv \left. \frac{\partial f_\lambda^{[k]}}{\partial x} \right|_{x=x^{*(k)}}. \quad (\text{A3.2})$$

So, a stable period- k cycle appears at $\mu^{(k)} = 1$, which becomes unstable, giving birth to a period-doubled period- $2k$ cycle at $\mu^{(k)} = -1,25$ with $\mu^{(2k)} = 1$. The latter then becomes unstable when $\mu^{(2k)} = -1$ and $\mu^{(k)}$ takes some negative value $\mu_c^{(k)}$, say.

Let $\lambda_o^{(k)}$ be the value of the parameter λ at which the period- k cycle appears, i.e.,

$$\mu^{(k)}(\lambda_o^{(k)}) = 1. \quad (\text{A3.3})$$

Writing,

$$\lambda = \lambda_o^{(k)} + \varepsilon \quad (\text{A3.4})$$

a Taylor expansion then gives

²⁵ $\mu^{(k)} = -1$ corresponds to the linearized flow $x_{n+1} = -x_n$ which represents a period- $2k$ cycle because $x_{n+2} = x_n$.

$$\mu^{(k)}(\lambda) = 1 + \varepsilon M_o^{(k)} + O(\varepsilon^2), \quad \lambda \approx \lambda_o^{(k)} \quad (\text{A3.5})$$

where,

$$M_o^{(k)} \equiv \left. \frac{d\mu^{(k)}}{d\lambda} \right|_{\lambda=\lambda_o^{(k)}}.$$

Similarly, let $\lambda_o^{(2k)}$ be the value of λ at which the period-k cycle disappears, (and period- 2k cycle appears), i.e.,

$$\mu^{(k)}(\lambda_o^{2k}) = -1. \quad (\text{A3.6})$$

Writing,

$$\lambda = \lambda_o^{(2k)} + \varepsilon \quad (\text{A3.7})$$

a Taylor expansion then gives

$$\mu^{(k)}(\lambda) = -1 + \varepsilon M_o^{(2k)} + O(\varepsilon^2), \quad \lambda \approx \lambda_o^{(2k)} \quad (\text{A3.8})$$

where,

$$M_o^{(2k)} \equiv \left. \frac{d\mu^{(k)}}{d\lambda} \right|_{\lambda=\lambda_o^{(2k)}}.$$

If $\Delta\lambda(k)$ denotes the change in λ as $\mu^{(k)}$ varies from 1 to -1, then we have from (A3.5),

$$\Delta\lambda(k) = -\frac{2}{M_o^{(k)}}. \quad (\text{A3.9})$$

Similarly, if $\Delta\lambda(2k)$ denotes the change in λ as $\mu^{(2k)}$ varies from 1 to -1 or $\mu^{(k)}$ varies from -1 to $\mu_c^{(k)}$, then we have from (A3.8),

$$\Delta\lambda(2k) = \frac{\mu_c^{(k)} + 1}{M_o^{(2k)}}. \quad (\text{A3.10})$$

Using (A3.9) and (A3.10), the Feigenbaum number δ (see (94)) is given by

$$\delta = \lim_{k \rightarrow \infty} \frac{\Delta\lambda(k)}{\Delta\lambda(2k)} = \lim_{k \rightarrow \infty} \frac{-2}{\mu_c^{(k)} + 1} \quad (\text{A3.11})$$

In order to determine $\mu_c^{(k)}$, we need an asymptotic relation between $\mu^{(2k)}$ and $\mu^{(k)}$. For this purpose, we approximate the map $f_\lambda^{[2k]}$ by using a cubic:

$$f_\lambda^{[2k]}(x^{*(k)} + \xi) \approx x^{*(k)} + A\xi + \frac{1}{2}B\xi^2 + \frac{1}{6}C\xi^3 + O(\xi^4). \quad (\text{A3.12})$$

The cubic approximation is necessary to enable $f_\lambda^{[2k]}$ to exhibit a bifurcation into a pair of points (corresponding to a period- $2k$ cycle) as the period- k cycle becomes unstable.

Noting that

$$f_\lambda^{[2k]}(x^{*(k)} + \xi) = f_\lambda^{[k]}(f_\lambda^{[k]}(x^{*(k)} + \xi)) = f_\lambda^{[k]}(x^{*(k)} + \mu^{(k)}\xi + \frac{1}{2}\sigma^{(k)}\xi^2 + \dots) \quad (\text{A3.13})$$

we have, on comparison with (A3.12),

$$A = (\mu^{(k)})^2, \quad B = \mu^{(k)}(1 + \mu^{(k)})\sigma^{(k)} \quad (\text{A3.14})$$

where,

$$\sigma^{(k)} \equiv \left. \frac{\partial^2 f_\lambda^{[k]}}{\partial x^2} \right|_{x=x^{*(k)}}.$$

If we write for the fixed point $x^{*(2k)}$ of the map $f_\lambda^{[2k]}$,

$$x^{*(2k)} = x^{*(k)} + \xi^* \quad (\text{A3.15})$$

then we have

$$f^{[2k]}(x^{*(2k)}) = f^{[2k]}(x^{*(k)} + \xi^*) = x^{*(k)} + A\xi^* + \frac{1}{2}B\xi^{*2} + \frac{1}{6}C\xi^{*3} + \dots = x^{*(k)} + \xi^*$$

or

$$\xi^* \approx A\xi^* + \frac{1}{2}B\xi^{*2} + \frac{1}{6}C\xi^{*3}. \quad (\text{A3.16})$$

On discarding the degenerate period-k solution ($\xi^* = 0$), (A3.16) yields

$$0 \approx (A - 1) + \frac{1}{2}B\xi^* + \frac{1}{6}C\xi^{*2}. \quad (\text{A3.17})$$

Next, we have from (A3.12),

$$\mu^{(2k)} = \left[\frac{df_\lambda^{[2k]}}{d\xi} \right]_{\xi=\xi^*} \approx A + B\xi^* + \frac{1}{2}C\xi^{*2}. \quad (\text{A3.18})$$

Using (A3.17), (A3.18) becomes

$$\mu^{(2k)} \approx (3 - 2A) - \frac{1}{2}B\xi^*. \quad (\text{A3.19})$$

Dropping the second term on the right hand side in (A3.19) in comparison with the first, we have corresponding to $\mu^{(2k)} = -1$ or $\mu^{(k)} = \mu_c^{(k)}$,

$$-1 \approx 3 - 2A$$

or

$$A \approx 2. \quad (\text{A3.20})$$

Using (A3.20), we have from (A3.14),

$$\mu_c^{(k)} \approx -\sqrt{2}. \quad (\text{A3.21})$$

Using (A3.21), we have from (A3.11),

$$\delta \approx \frac{-2}{-\sqrt{2} + 1} = 4.828\dots \quad (\text{A3.22})$$

which differs from the exact numerical result (94) by about 3%!

CHAPTER 7

FRACTALS AND MULTI-FRACTALS IN TURBULENCE

Turbulent flows refer to situations in which the flow properties at any point vary in a statistically random manner. Fourier analysis shows that wave fluctuations in a range of frequencies and wavenumbers are present, the width of the range changing with certain flow parameters like the Reynolds number. The various component motions interact through the nonlinear terms in the equations of motion, and the observed properties of the turbulence are thought of as being the statistical result of such interactions.

Mathematically, the description of these interactions should center on invariant measures. Although, there is no rigorous theory about the existence of strictly invariant measures in turbulence, experimental observations strongly support the idea that turbulence at small scales organizes itself into a statistically stationary universal state. Apparently, as the Reynolds number of the flow becomes infinite, all the invariance properties of the Navier-Stokes equations, possibly broken by the mechanisms producing the turbulence, are recovered asymptotically at small scales in a statistical sense (Frisch, (1985)).

According to the Kolmogorov (1941) theory of local similarity in turbulence, the small-scale structure has a scale-invariant and universal character in turbulence at high Reynolds numbers of the flow. This implies that there exists, for large wavenumbers, an inertial range where the statistical properties of the small-scale components are isotropic, uniquely determined by the average energy dissipation rate ε and the kinematic viscosity ν , and are independent of the detailed form of the large-scale features of the flow.

However, early measurements of the velocity field and its derivatives in a grid turbulence by Batchelor and Townsend (1949) showed that the turbulent activity at small scales was not distributed uniformly throughout space. Instead, one observed some regions which were active and some others which were relatively quiescent. This spatially spotty pattern¹ (which is called intermittency, Section 6.6) became more

¹ Note that a spatially varying boundary separating the laminar and turbulent flow regions will show temporal intermittency because the flow velocity measured at a given point near this boundary will show alternating laminar or turbulent behavior as the boundary moves causing the point to move into or out of the laminar flow region.

marked with increasing order of the derivative. The velocity field (denoted by u) measurements showed a flatness factor

$$F = \frac{\langle [u(x+r) - u(x)]^4 \rangle}{\langle [u(x+r) - u(x)]^2 \rangle^2} \quad (1)$$

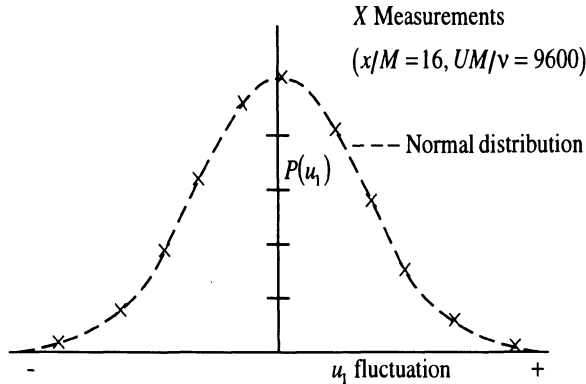


Figure 7.1. Probability density function of the velocity component u_1 in the direction of the stream for the turbulence generated by a square-mesh grid in a wind tunnel measured by Townsend (1947). (By courtesy of the Cambridge University Press).

of about 3, in agreement with the well-known result that the distribution of turbulent velocities at a point is approximately Gaussian (see Figure 7.1). However, the measurements of the velocity derivatives gave values for the flatness factor significantly greater than 3.² Numerical simulations (Vincent and Meneguzzi, (1991)) also showed

² The effect of intermittency on the measured flatness factor can be understood by the following simple example. Consider a velocity field $u(x, t)$ which has a Gaussian probability distribution in its active state. The velocity field is intermittent between this and a completely inactive state when u and all its derivatives are zero. If we denote the global average by $\langle \cdot \rangle$, the local average over the statistically active state by $[\cdot]$, and the fraction of time a variable u is found to be in its active state by $\gamma(\gamma < 1)$, then we have for the moments of u

$$\langle u^n \rangle = \gamma[u^n], \text{ for all } n.$$

The globally averaged flatness factor is then given by

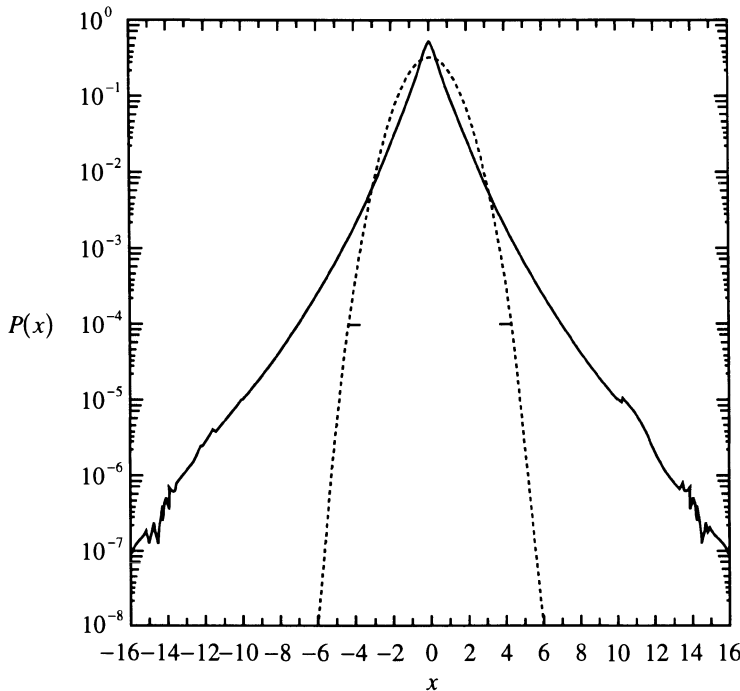


Figure 7.2. Probability density functions, normalized by standard deviation for $\partial u_1 / \partial x_2$ from a simulation at $R_\lambda \approx 150$ (solid line), and the Gaussian distribution (dashed line). (Due to Vincent and Meneguzzi, (1991)).

(By courtesy of the Cambridge University Press).

that the probability distribution functions of velocity gradients are far from Gaussian and exhibit long and exponential tails (see Figure 7.2). Further, these probability distribution functions do not have universal forms, independent of the Reynolds number. The measurements of Stewart *et al.* (1970), on the other hand, showed that (see Figure 7.3) the probability distribution function of $\log \left| \frac{\partial u}{\partial x} \right|$ is asymmetric with respect to the mean

$$F = \frac{3}{\gamma}$$

which is greater than 3!

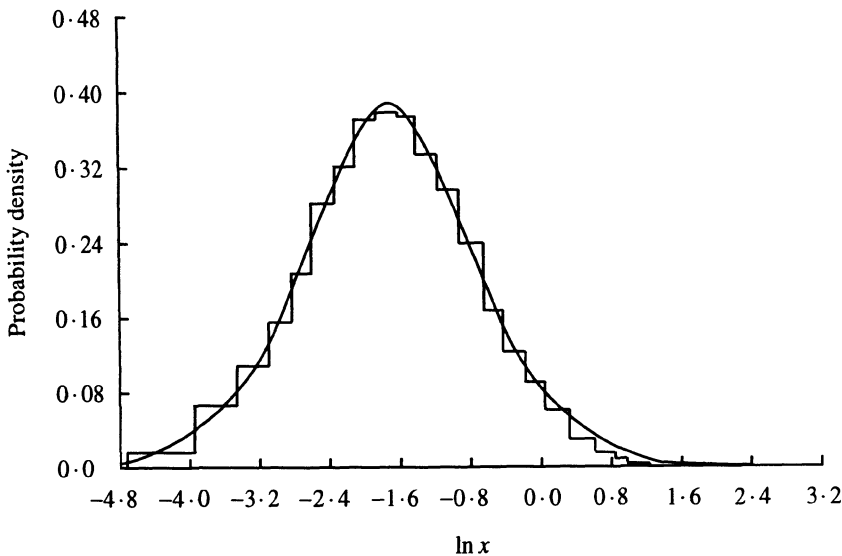


Figure 7.3. The probability density function for the $\ln|\partial u/\partial x|$ (the bar graph) measured by Stewart *et al.* (1970). (By courtesy of the Cambridge University Press).

value: it has a longer tail for very small values of $\log\left|\frac{\partial u}{\partial x}\right|$ than for very large values so that the skewness for the velocity derivative

$$S = \frac{\langle [q(x+r) - q(x)]^3 \rangle}{\langle [q(x+r) - q(x)]^2 \rangle^{3/2}} \quad (2)$$

is negative. Numerical simulations of Chen *et al.* (1993) showed that this trend gets accentuated with increasing order of the derivative of the velocity, (see Figure 7.4).

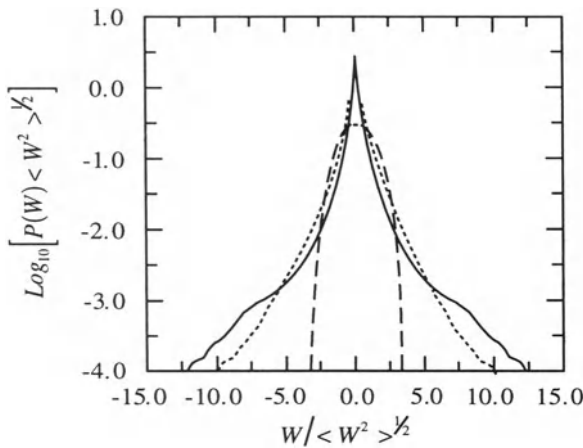


Figure 7.4. Probability density function $P(\omega)$ of the field $\omega = (-\nabla^2)^m u_i$ for $m = 0$ (dashed), $m = 2$ (dotted), and $m = 4$ (solid), averaged over $i = 1, 2, 3$. (Due to Chen *et al.* (1993)). (By courtesy of the American Physical Society.)

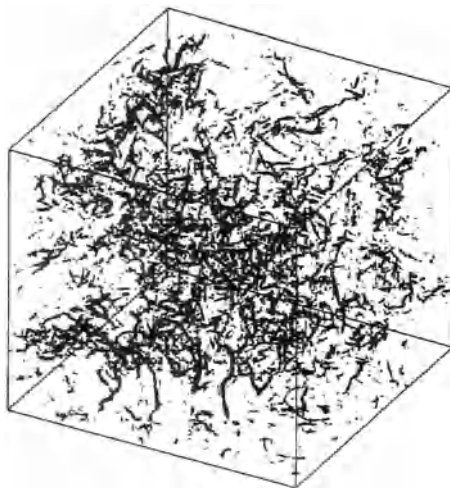


Figure 7.5. View of the vorticity field, represented by a vector of length proportional to the vorticity amplitude at each grid point. Only vectors larger than a given threshold value are shown (from Vincent and Meneguzzi, (1991)). (By courtesy of the Cambridge University Press.)

The velocity field structure is found to become increasingly intermittent as the scale size r decreases, in accord with an intuitive picture of the smallest scales as very stretched out shear layers or filaments of vorticity showing concentrated activity in localized regions in space. Numerical simulations (Kerr, (1985); Vincent and Meneguzzi, (1991)) have shown that the vorticity field is organized in very long and thin tubes (Figure 7.5). Laboratory experiments of Douady *et al.* (1991) on flow in a cylinder with counter-rotating disks at opposite ends provided visualizations of vortex filaments in a turbulent flow (Figure 7.6). (Douady *et al.* (1991) made use of the fact that high-vorticity concentrations are low-pressure regions where cavitation can occur, and therefore, seeded the flow with tiny bubbles which tend to concentrate in low-pressure regions and hence making the high-vorticity concentrations visible.)

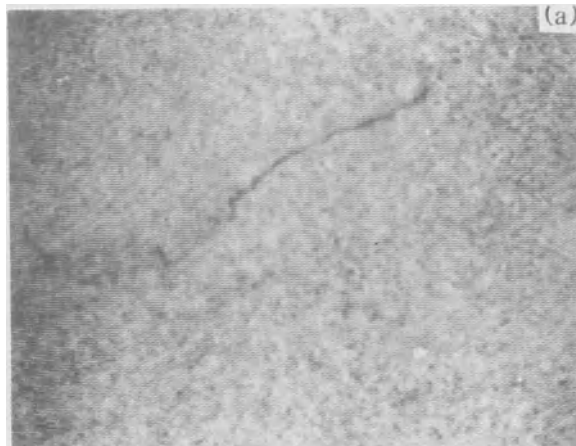


Figure 7.6. Video image showing a sideview of a vortex filament observed in a turbulent flow at a Reynolds number 80,000. (Due to Douady *et al.*, (1991)). (By courtesy of the American Physical Society.)

The viscous dissipation of turbulent kinetic energy is mainly associated with regions where the velocity gradients are large. Thus, the fine-structure intermittency observed above also implies that the energy dissipation ε may be distributed in a rather spotty way, at every scale of motion. One may expect that the energy dissipation also becomes more nonuniform in space as the range of scales of the turbulence (or the Reynolds number) increases. Figure 7.7 shows experimental signals of a representative component of ε obtained in a laboratory boundary layer and in the atmospheric surface layer. Observe the intermittent nature of ε and note that it becomes increasingly conspicuous with increasing Reynolds number.

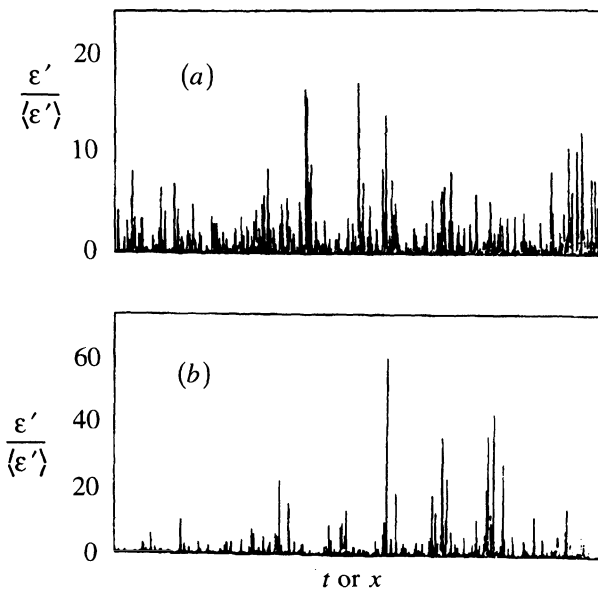


Figure 7.7. Typical signals of a representative component of ε , namely $\varepsilon' \sim (du_1/dt)^2$ normalized by the mean: (a) was obtained in a laboratory boundary layer at a moderate Reynolds number, and (b) in the atmospheric surface layer at a high Reynolds number. (Due to Meneveau and Sreenivasan, (1991).
(By courtesy of the Cambridge University Press.)

Landau (1944) actually pointed out long ago that Kolmogorov (1941) theory did not take into account the intermittency in the flow that leads to the spatial randomness of the energy dissipation rate. Landau (see Landau and Lifshitz, 1987) even argued that the latter aspect would depend on the Reynolds number and cause systematic departures from the Kolmogorov (1941) scaling laws which used a mean energy dissipation value.

Global statistical scaling invariance assumed by the Kolmogorov (1941) theory is therefore broken by the small-scale intermittency. However, one may venture to assume that the scaling invariance remains valid, nonetheless, locally. Thus, Obukhov (1962) and Kolmogorov (1962) reformulated the ideas in the Kolmogorov (1941) theory by introducing a local mean energy dissipation, determined by averaging the latter quantity over a suitably small region in space³. Obukhov (1962) assumed that this was a random

³ This could be a sphere of radius a centered at the point r , so that the local mean energy dissipation is given by

variable following a logarithmic normal distribution, and showed how some of the original local similarity arguments applied to velocity structure functions would change under the new interpretation involving a fluctuating energy dissipation⁴.

The lognormal distribution gives good agreement with experimental measurements for low-order moments but discrepancies appear for high-order moments (Anselmet *et al.* (1984)). The latter are determined by the rare and strong events⁵ related to the characteristic maximum and minimum level of fluctuations in the energy transfer rate which are associated with the tails of the distribution functions of the energy dissipation. The lognormal model keeps good track of only the weak and frequent events and underestimates the strong and rare events.

One may make use of an alternative approach involving marginal gamma distribution to describe the local kinetic energy dissipation (Andrews *et al.* (1989)). In this model, the velocity derivative is assumed to be conditionally Gaussian distributed with zero mean and with variance gamma-distributed. This model gave excellent agreement with the experimental measurements for even high-order moments⁶.

The dynamical processes leading to fully developed turbulence are believed to consist of stretching and folding of the sheet-like structures in physical space in a manner qualitatively similar to what happens in establishing a strange attractor in phase space. Thus, Mandelbrot (1976) argued that the deviations from the Kolmogorov (1941) scaling laws are related to the fractal aspects of the geometry of turbulence. The underlying idea is that the dissipative structures (which are regions in which the energy dissipation is concentrated) are so extremely convoluted that they are not completely space-filling. In fact, as experiments have indicated, they become less and less space-

$$\varepsilon_a(r) = \frac{1}{4\pi a^3/3} \int_{|r-r'| < a} dr' \frac{1}{2} \sum_{i,j} (\nabla v_i + \nabla v_j^T) : (\nabla v_i + \nabla v_j^T).$$

⁴ If the moments of local mean energy dissipation $\varepsilon_a(x)$ show a scaling behavior –

$$\langle (\varepsilon_r(x))^p \rangle \sim r^{\mu(p)}$$

the exponents $\mu(p)$ are obtained as follows: Experiments derive a squared velocity gradient component, which is considered as a measure of the local energy dissipation rate, from measurements at fixed position via Taylor's frozen flow hypothesis (see Footnote 13). The power law exponents $\mu(p)$ then follow from a log-log plot of $\langle \varepsilon_r^p \rangle$ vs. r .

⁵ This aspect poses difficulties with signal-recording in experiments since one then has to process very long records of the turbulent signal to ensure convergence of the statistics.

⁶ As Kraichnan (1974) pointed out, all the intermittency theories suffer from a kind of logical inconsistency. Because, they are concerned with prediction of scaling laws in the inertial range, yet they work with the energy dissipation, which is not an inertial-range quantity!

filling as the scale size decreases! This fact can be represented by assuming that the mean energy dissipation rate is concentrated on a Cantor set like fractal with non-integer Hausdorff dimension, which is a measure of the extent to which the dissipative structures fill space. A characteristic feature of a multi-fractal, as we saw in Section 6.4 is that a "measure" defined on the object has a different fractal dimension on different regions of the object in consonance with the fact that at each step of the cascade the measure sets distributed randomly according to a certain probability distribution. In the multi-fractal model, one assumes that the velocity increment over a length l scales as $\delta v(l) \sim l^{\alpha/3}$ with the local scaling exponent α taking a continuous range of values. For any α in this range, there is a set $S(\alpha) \in R^3$ of Hausdorff dimension $D(\alpha)$ (Frisch and Parisi, 1985).

The uniform fractal model (also called the β -model (Frisch *et al.* (1978))) corresponds to only a single value for the exponent α ; this is due to the imposition of global scale-invariance and is equivalent to assuming that the flux of energy occurs to only a fixed fraction β of the eddies downstream in the cascade. However, measurements of the scaling properties of high-order velocity structure function (Gibson *et al.* (1970), Tennekes and Wyngaard (1972), Van Atta and Antonia (1980), and Anselmet *et al.* (1984)) revealed that the β -model is not adequate in describing the intermittency. In an effort to achieve better agreement with experiments, a multi-fractal model may be considered wherein one may dilute the global scale-invariance constraint into a local scale-invariance constraint so that the exponent α is allowed to vary continuously in some range, each value of α having a fractal set of dimension $D(\alpha)$ and a scaling law with exponent α . A multi-fractal version of the β -model was advanced by Benzi *et al.* (1984) in which the contraction factors β 's are considered as independent random variables which can take different values at each scale i in the n th step of the cascade.

Hentschel and Procaccia (1983) introduced a characterization of multi-fractals in terms of the so-called generalized dimensions D_q which corresponds to scaling exponents for the q th moments of the measure (see Section 6.4). Halsey *et al.* (1986) introduced the so-called singularity spectrum $f(\alpha)$ and proposed that a multi-fractal measure be modeled by interwoven sets of singularities of strength α each characterized by its own dimension $f(\alpha)$, called the singularity spectrum. The multi-fractal formalism was thus developed to describe the statistical properties of the singular measures in terms of their singularity spectrum or their generalized dimensions. Experiments of Meneveau and Sreenivasan (1987 and 1991) have shown that the statistical properties of the mean energy dissipation field are universal and well described by the multi-fractal formalism. In Section 7.3, a nested-singularity set model for the energy dissipation field

velocity structure function in terms of the generalized fractal dimension of the velocity field.

It should be noted that the introduction of the multi-fractal measures does not presume anything about the underlying dynamical scenarios leading to such measures; these scenarios are considered by their consequences only. Actually, most of the intermittency models considered to date are not based on the Navier-Stokes equations, but rather on phenomenological self-similar processes that are believed to mimic turbulence dynamics, at least qualitatively.

7.1. Scale Invariance of the Navier-Stokes Equations and the Kolmogorov (1941) Theory:

Consider the flow of an incompressible fluid. The velocity \mathbf{v} of the fluid then satisfies the Navier-Stokes equations –

$$\frac{\partial \mathbf{v}}{\partial t} + (\mathbf{v} \cdot \nabla) \mathbf{v} = -\nabla \left(\frac{p}{\rho} \right) + \nu \nabla^2 \mathbf{v} \quad (3)$$

$$\nabla \cdot \mathbf{v} = 0 \quad (4)$$

where p is the pressure and ρ is the mass density of the fluid.

Let us now make a scaling transformation given by,

$$\mathbf{r}' = \frac{\mathbf{r}}{\lambda}, \quad t' = t \lambda^{\frac{\alpha}{3}-1} \quad (5)$$

α being a scaling index. Equations (3) and (4) then are scale-invariant, i.e., they are

$$\frac{\partial \mathbf{v}'}{\partial t'} + (\mathbf{v}' \cdot \nabla') \mathbf{v}' = -\nabla' \left(\frac{p'}{\rho} \right) + \nu' \nabla'^2 \mathbf{v}' \quad (6)$$

$$\nabla' \cdot \mathbf{v}' = 0 \quad (7)$$

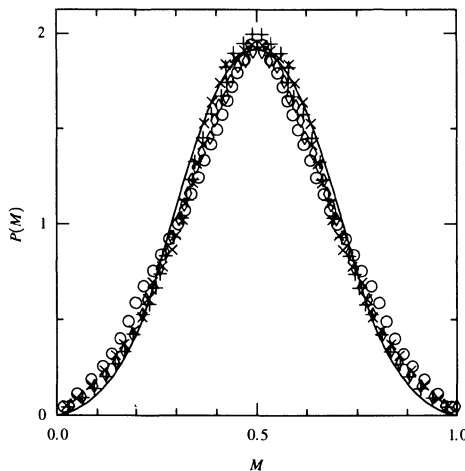
if we choose

$$\left(\frac{p}{\rho} \right)' = \lambda^{\frac{2\alpha}{3}} \left(\frac{p}{\rho} \right), \quad \mathbf{v}' = \lambda^{\frac{\alpha}{3}+1} \mathbf{v}. \quad (8)$$

Observe that the scaling transformation given by (5) and (8) leaves the Reynolds number UL/v invariant, where U is a characteristic velocity and L is a characteristic dimension of the flow. Note that the exponent α is so far arbitrary. This simply reflects the fact that equations (3) and (4) are formally scale-invariant with an arbitrary scaling index α . Such a scale invariance implies that features at one scale are related to those at another by means of one or many scaling factors or functions.

Even in a statistically stationary turbulence, the scale invariance, discussed above, is broken because the turbulent field singles out a large length scale l_o at which energy is fed into the fluid. (This energy, following an early proposition of Richardson (1922), is then believed to cascade through successively smaller length scales via the mechanism of vortex-stretching⁷ and is finally dissipated at a length scale l_d by viscous effects.)

⁷ Turbulence cascade is believed to be a multiplicative process whereby a large piece fragments into smaller pieces and each new piece receives a fraction of the "measure" of the larger piece. The size and measure of a small piece at a certain stage j may be taken to be products of multipliers l_j and M_j ($M_j \geq 0$ and $l_j \leq 1$) associated with the pieces at all previous stages. The quantities l_j and M_j may be considered to be random variables with a certain probability distribution. When these distribution functions are scale-invariant, i.e., they are the same for all stages j (this has been confirmed by the experiments of Sreenivasan and Stolovitzky (1995), see figure below), one has a self-similar process and the moments and distribution function of the total energy dissipation ε_r in a piece of size r then show a power-law behavior. Experiments of Sreenivasan and Stolovitzky (1995), on the other hand, showed that the multiplier distribution at any stage j is not independent of those at previous stages. However, this was shown not to have any effect on the scaling behavior of turbulence except for negative moments below a certain order.



Probability distribution function for the multipliers M . Different symbols correspond to different levels in the inertial range. Diamonds correspond to a starting level of 384η , where η is the Kolmogorov scale, pluses to

However, the scale invariance may be assumed to hold asymptotically at length scale $l \ll l_0$ in a statistical sense, i.e., the average quantities are assumed to be scale invariant, whereas detailed structures need not be⁸. Even this statistical scale-invariance may be destroyed by the intermittency effects that tend to be present more strongly in small scales.

The Kolmogorov (1941) theory assumes that the mean rate of energy dissipation

$$\varepsilon = v \left\langle \frac{1}{2} (\nabla v + \nabla v^T) : (\nabla v + \nabla v^T) \right\rangle \quad (9)$$

768η , crosses to 1536η , and circles to 3072η . (Due to Sreenivasan and Stolovitzky (1995)). (By courtesy of the Plenum Publishing Corp.)

⁸ The length of the inertial range where this scale-invariance holds can be estimated as follows: We have from (11), see below, for the characteristic velocity –

$$v_l \sim \varepsilon^{1/3} l^{1/3}.$$

The characteristic time is thus

$$t_l \sim \frac{l}{v_l} \sim \varepsilon^{-1/3} l^{2/3}.$$

the viscous diffusion time is, on the other hand, given by

$$t_d \sim \frac{l^2}{v}.$$

The dissipation length then corresponds to

$$l_d \sim t_d$$

from which

$$l_d \sim (v^3 / \varepsilon)^{1/4}.$$

Therefore,

$$\frac{l_o}{l_d} \sim \left(\frac{v_o l_o}{v} \right)^{3/4} = R_{l_o}^{3/4}$$

so that the length of the inertial range goes like the $3/4$ power of the Reynolds number R_{l_o} and can be very large when $R_{l_o} \gg 1$.

depends only on flow quantities local to the scale l ; in particular, on l and the velocity $v(l)$ of eddies of size l . In (9), $\langle \rangle$ denotes some ensemble average. Now, observe that ε , considered as a measure distributed over the real axis, changes under the scaling transformation (5) and (8), according to

$$\varepsilon = \varepsilon' \lambda^{1-\alpha} \quad (10)$$

where,

$$\varepsilon' \equiv v' \left\langle \frac{1}{2} (\nabla' v' + \nabla' v'^T) : (\nabla' v' + \nabla' v'^T) \right\rangle.$$

Kolmogorov's (1941) theory assumes that the locally averaged energy dissipation rate is independent of the extent of the averaging domain. This implies the invariance of ε under the scaling transformation (5) and (8), and, from (10), corresponds to⁹

$$\alpha = 1. \quad (11)$$

This implies that, in the inviscid limit (which, from (8), corresponds to $\lambda \rightarrow 0$), the mean rate of energy dissipation is finite and non-vanishing, and hence the result – *the inviscid dissipation of energy* in three-dimensional turbulence. (11) further implies that the structure function of order p , defined as the average of the p th power of velocity increments $\delta v(l)$ measured over distances l , parallel to the velocity, scales as

$$[\delta v(l)]^p \sim \varepsilon^{p/3} l^{p/3} \sim l^{\alpha p/3}. \quad (12)$$

(5) and (11) also indicate that the velocity field v exhibits singularities of order $1/3$. The development of such singularities is believed to be caused by the mechanism of vortex stretching that generates strongly localized features in the small-scale structure¹⁰.

The Kolmogorov (1941) theory assumes that the distribution of these singularities is space filling. However, thanks to the small-scale intermittency revealed by

⁹ The β -model (see Section 7.3) assumes that the energy dissipation is confined to a homogeneous fractal of dimension D_o , so that $\alpha = D_o - 2$. The multi-fractal model (see Section 6.4) assumes that α takes on different values on different interwoven fractal subsets containing the energy dissipation field, the fractal dimension of the subset corresponding to the scaling exponent α being denoted by $f(\alpha)$.

¹⁰ It may be mentioned, however, that there is no conclusive numerical evidence (Brachet *et al.* (1983, 1992)) that ideal-flow solutions, starting from regular initial conditions, will spontaneously develop a singularity in finite time. Apparently, due to some mechanism not yet understood, there is a weakening of the nonlinear effects in the vortex dynamics! However, this aspect is likely to remain unsettled until the regularity and uniqueness of the solutions of the three-dimensional Navier-Stokes equations are established.

experiments, the distribution of these singularities is not space filling (the scale invariance associated with (11) is broken as well). Physically, this implies that the dissipative structures are so extremely convoluted that they are never space-filling (actually, they become less and less space-filling as the scale-size decreases). Mandelbrot (1976) proposed that this aspect be represented by a fractal whose fractal dimension is a measure of the extent to which the dissipative structures fill space.

7.2. The β -Model for Turbulence

Fractals, as we saw in Chapter 6, are invariant to dilation and, one may therefore expect that they will naturally preserve the scale-invariance of the Navier-Stokes equations. Mandelbrot (1976) therefore proposed to model intermittency by assuming that the mean energy dissipation field is concentrated on a Cantor set like fractal with a non-integer Hausdorff dimension.

These ideas may be formulated in a simpler manner through the so-called β -model (Frisch *et al.* (1978)) which assumes that the fractal set in question is homogeneous with Hausdorff dimension D_o (which is equivalent to assuming that the flux of kinetic energy is transferred to only a fixed fraction β of the eddies downstream in the cascade¹¹). Homogeneous fractals are generated by a set of rules which relate its statistical properties over a certain scale of lengths to those of a larger scale of lengths. Inhomogeneous fractals are, on the other hand, generated by rules that are not fixed for a given scale of length but are given at random according to a certain probability distribution.

In order to understand the geometry of the β -model, it proves convenient to consider the two-dimensional Sierpinski carpet (EXAMPLE 1).

EXAMPLE 1

A two-dimensional Sierpinski carpet.

A two-dimensional Sierpinski carpet is obtained by iterating a fragmentation process (see Figure 7.8). At each step j , a square of scale l_j leads to n^2 squares of scale

¹¹ In the β -model, the multipliers M_j (see footnote 7) are nonzero and equal on a fraction β of the new offsprings but zero on the fraction $(1-\beta)$ of the new offsprings. One assumes that there is no mixing between these functions which is valid if the time scale of this spatial mixing is much larger than the time scale characterizing the fragmentation of eddies. If the value of β is the same for all stages j , the scaling properties are again restored.

$l_{j+1} = \frac{l_j}{n}$ of which, only a fraction β are "full". Note that Figure 7.8 corresponds to $n = 2$.

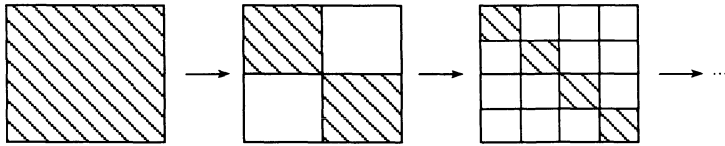


Figure 7.8. A uniform Sierpinski carpet.

The carpet is called homogeneous if β is the same for each step j and is given by $\beta n^2 = n^{D_s}$ or $\beta = n^{D_s - 2}$. The carpet is inhomogeneous if β is a random variable depending on the particular square and the step j .

Let us now formulate the β -model. Consider a discrete sequence of scales –

$$l_n = l_o 2^{-n}; \quad n = 0, 1, 2, \dots \quad (13)$$

and a discrete sequence of wavenumbers $k_n = l_n^{-1}$. Here, the number of offsprings produced at each step of the cascade is 2. The kinetic energy per unit mass in the n th scale is defined by

$$E_n = \int_{k_n}^{k_{n+1}} E(k) dk. \quad (14)$$

Let us assume that we have a statistically stationary turbulence where energy is introduced into the fluid at scales $\sim l_o$ and is then transferred by nonlinear interactions successively to scales $\sim l_1, l_2, \dots$, until some scale l_d is reached where viscous dissipation is able to compete with nonlinear energy transfer. We now make the assumption that, at the n th step, only a fraction β^n of the total space has an appreciable excitation.

The kinetic energy per unit mass in the n th scale is then given by

$$E_n \sim \beta^n v_n^2 \quad (15)$$

where v_n is a characteristic velocity of the n th scale (which is a typical velocity difference across a distance l_n). We have

$$\beta = \frac{2^{D_o}}{2^3} = 2^{D_o - 3} \quad (16)$$

so that

$$\beta^n = 2^{n(D_o - 3)} = \left(\frac{l_n}{l_o} \right)^{3-D_o}. \quad (17)$$

D_o being the Hausdorff dimension of the region in which the energy dissipation is concentrated. (17) shows that intermittency increases with decrease of scale size, as expected.

The rate of transfer of energy per unit mass from the n th scale to $(n+1)$ th scale is given by

$$\varepsilon_n \sim \frac{E_n}{t_n} \sim \frac{\beta^n v_n^3}{l_n} \quad (18)$$

where t_n is a characteristic time of the n th scale (also called the eddy turnover time). This energy flux is the actual energy dissipation rate when $l_n \sim \eta$, η being the Kolmogorov length scale $\eta \sim (v^3/\varepsilon)^{1/4}$.

In the inertial range, we assume a stationary process in which energy is introduced at scales $\sim l_o$ and removed at scales $\sim l_d$; conservation of energy requires that

$$\varepsilon_n = \bar{\varepsilon}, \quad l_d \leq l_n \leq l_o \quad (19)$$

where $\bar{\varepsilon}$ is the rate of energy dissipation.

Using (17) and (19), we have from (18),

$$\begin{aligned}
 v_n &\sim \bar{\epsilon}^{1/3} l_n^{1/3} \left(\frac{l_n}{l_o} \right)^{-\frac{3-D_o}{3}} \\
 t_n &\sim \bar{\epsilon}^{-1/3} l_n^{2/3} \left(\frac{l_n}{l_o} \right)^{\frac{3-D_o}{3}} \\
 E_n &\sim \bar{\epsilon}^{2/3} l_n^{2/3} \left(\frac{l_n}{l_o} \right)^{\frac{3-D_o}{3}}.
 \end{aligned} \tag{20a,b,c}$$

(20)c leads to the energy spectrum

$$E(k) \sim \bar{\epsilon}^{2/3} k^{-5/3} (kl_o)^{-\frac{3-D_o}{3}}. \tag{21}$$

Observe that, since $D_o < 3$, (21) implies that the intermittency effects make the energy spectrum steeper. This may be understood by recalling that intermittency increases as scale size l_n decreases, and if the Kolmogorov (1941) theory holds in local regions, then the cascade should become more efficient as r decreases. This would imply that the energy spectrum $E(k)$ must fall off more rapidly than $k^{-5/3}$ if the overall cascade rate is independent of l_n as required by the conservation of energy.

(20)a also implies that, according to the β -model, the velocity field has singularities (or Hölder exponents) of order $\alpha/3$, i.e.,

$$\delta v \sim l^{\alpha/3} \quad \text{as } l \rightarrow 0 \tag{22}$$

where,

$$\alpha = 1 - (3 - D_o). \tag{23}$$

These singularities are distributed over a homogeneous fractal set with Hausdorff dimension $D_o < 3$ so that the latter has a measure zero in order to keep the total energy dissipation finite. The velocity structure function of order p , $S_p(l)$, behaves as

$$S_p(l) \equiv \langle |\delta v(l)|^p \rangle \sim N(l) l^3 l^{\frac{\alpha p}{3}} \tag{24}$$

where the number $N(l)$ of boxes of size l that contain values of α within a band $d\alpha$ around α scales according to

$$N(l) \sim l^{-D_o}. \quad (25)$$

Using (25), (24) gives

$$S_p(l) \sim l^{\zeta_p} \quad (26)$$

where the characteristic exponent ζ_p is given by

$$\zeta_p = \frac{\alpha p}{3} + 3 - D_o. \quad (27)$$

(27) may be rewritten as

$$\zeta_p = \frac{p}{3} + \left(1 - \frac{p}{3}\right)(3 - D_o). \quad (28)$$

Using (16), (28) may be rewritten as

$$\zeta_p = \frac{p}{3} - \log_2 \beta^{\left(\frac{1-p}{3}\right)}. \quad (29)$$

(28) or (29) is compared with the experimental data of Anselmet *et al.* (1984), see Figure 7.10. Observe that the β -model cannot account for the nonlinear behavior of the characteristic exponents ζ_p of high-order velocity structure functions. Frisch and Parisi (1985) introduced the multi-fractal idea in order to resolve this discrepancy.

7.3. The Multi-Fractal Models

Multi-fractal models are based on the idea that a singular measure resulting from a multiplicative fragmentation process has a limiting scale-invariant distribution and the relevant variable is a local exponent α characterizing the strength of the singularities whose distribution is given in terms of the so-called singularity spectrum $f(\alpha)$: $f(\alpha)$ can often be interpreted geometrically as a Hausdorff dimension (Section

6.4). We now generalize the formulation of Section 7.2 to describe the possibility that the energy dissipation is concentrated on a multi-fractal.

We assume that the velocity increment over a distance l has singularities of order $\alpha/3$ distributed on a set $S(\alpha)$, i.e.,

$$\lim_{l \rightarrow 0} \delta v \sim l^{\alpha/3}. \quad (30)$$

Further, the fractal over which these singularities are distributed is non-uniform with Hausdorff dimension $f(\alpha)$ and is embedded in R^3 . This implies that there is a continuous spectrum of scaling exponents α in a certain range $I = (\alpha_{\min}, \alpha_{\max})$, and when $\alpha \in I$, the number $N_l(\alpha)d\mu(\alpha)$ of boxes of size l that contain values of α within a band $d\alpha$ around α scales according to

$$N_l(\alpha)d\mu(\alpha) \sim l^{-f(\alpha)}d\mu(\alpha) \quad (31)$$

where the measure $d\mu(\alpha)$ gives the weight of the different scaling exponents α . The sets $S(\alpha)$ are nested so that $S(\alpha') \subset S(\alpha)$ for $\alpha' \leq \alpha$.

The velocity structure function of order p , $S_p(l)$, is now obtained by space averaging $[\delta v(l)]^p$ over the entire volume. Noting that the total number of boxes of size l in the entire three-dimensional space is proportional to l^{-3} , the probability to belong to the set $S(\alpha)$ at scale l is proportional to $l^{3-f(\alpha)}d\mu(\alpha)$. Thus,

$$S_p(l) \equiv \langle |\delta v(l)|^p \rangle \sim \int d\mu(\alpha) l^{3-f(\alpha)+\frac{\alpha p}{3}} \sim l^{\zeta_p} \quad (32)$$

where ζ_p is the characteristic exponent of the velocity structure function of order p . Note that for large p , the structure functions are dominated by the strongest singularities which have the smallest Holder exponent α_{\min} .

Now, for $l \rightarrow 0$, the contribution from the smallest exponent dominates so that one may apply the method of steepest descent to extract the dominant term from the integral in (32) to obtain

$$\zeta_p = \inf_{\alpha} \left(3 - f(\alpha) + \frac{\alpha p}{3} \right) = 3 - f(\alpha^*) + \frac{\alpha^* p}{3} \quad (33)$$

where,

$$\frac{df(\alpha^*)}{d\alpha} = \frac{p}{3}.$$

If $f(\alpha)$ is assumed to be convex, i.e., $f''(\alpha) < 0$, there is a single exponent $\alpha_*(p)$ which minimizes the exponent ζ_p . (33) shows that the scaling exponent ζ_p is the Legendre transform of the co-dimension $3 - f(\alpha_*)$.

In order to relate the singularity spectrum $f(\alpha)$ to the generalized fractal dimension D_q one needs to assume that the scaling laws of the local energy dissipation

averaged over a domain of size l and the quantity $\frac{[\delta v(l)]^3}{l}$ are the same – *Kolmogorov's*

Refined Similarity Hypothesis.

Consider a coarse-grained probability measure given by the total energy dissipation occurring in a three-dimensional box of size l –

$$E(l) \sim \varepsilon(l) l^3 \sim l^{\alpha+2}. \quad (34)$$

We then divide the three-dimensional space into boxes of size l and sum the moments of the total energy dissipation $[E(l)]^q$ over all boxes. (Such a moment sum enables one to accentuate the relative importance of the active regions of the energy dissipation.) If the energy dissipation field is a multi-fractal, one may expect such sums to scale with the box size l according to some power law

$$\sum [E(l)]^q \sim l^{(q-1)D_q}{}^{12}. \quad (35)$$

Upon approximating the sum on the left-hand side in (35) by an integral over all possible values of α , we have

$$\int d\mu(\alpha) l^{(\alpha+2)q-f(\alpha)} \sim l^{(q-1)D_q} \quad (36)$$

¹² Note that high positive values of q emphasize regions of strong energy dissipation while negative values of q emphasize regions of weak energy dissipation.

where we have assumed that the number of iso- α boxes for which α takes on values between α and $\alpha + d\alpha$ is proportional to $d\mu(\alpha)l^{-f(\alpha)}$.

One may again use the method of steepest descent to extract the dominant terms from the integral in (36), in the limit $l \rightarrow 0$. This gives

$$(\hat{\alpha} + 2)q - f(\hat{\alpha}) = (q - 1)D_q \quad (37)$$

where,

$$\frac{df(\hat{\alpha})}{d\alpha} = q.$$

Eliminating $f(\alpha)$ from (33) and (37), and putting $q = p/3$, we have

$$\zeta_p = \frac{p}{3} - \frac{1}{3}(p-3)(3-D_{p/3}). \quad (38)$$

For a homogeneous fractal, $D_q = \text{constant} = D_0$, which is just the fractal dimension of the support of the measure $\varepsilon(l)$. (38) then agrees with the corresponding result (28) for the β -model. Observe that the intermittency effects are described by the departures of $D_{p/3}$ from 3 (the value it takes in the Kolmogorov (1941) theory). It should be noted, however, that the characteristic exponent ζ_p is of limited use because it provides a quantitative information only relative to the point $\zeta_3 = 1$.

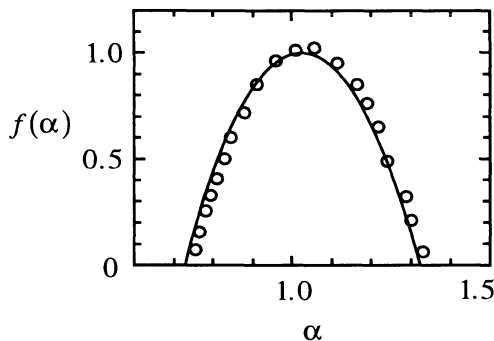


Figure 7.9. The singularity spectrum for the energy dissipation field measured by Meneveau and Sreenivasan (1991). (By courtesy of the American Physical Society.)

Experiments of Meneveau and Sreenivasan (1991) have shown that the statistical properties of the mean energy dissipation field are well described by the multi-fractal formalism. In view of the difficulties involved in measuring the local energy dissipation field directly, Meneveau and Sreenivasan (1991) made measurements along a straight line cutting through the support of the energy dissipation field embedded in three-dimensional space¹³. Figure 7.9 shows the singularity spectrum for the energy dissipation field which has been found to be universal for a variety of fully turbulent flows. Observe that the log-normal approximation (for which the α -distributions obey Gaussian statistics, and $f(\alpha) \sim \alpha^2$) is adequate only for the central portion of the curve¹⁴.

Note that the maximum of the spectrum curve occurs at $\alpha_o = 3.117$ (or 1.117 for a one-dimensional cut) and corresponds to $f(\alpha_o) = 3$; thus, the metric support of the energy dissipation field is the embedding space itself! This implies that there is at least "some" energy dissipation everywhere, even at high Reynolds numbers, which, of course, supports the concept of inviscid dissipation of energy in three-dimensional turbulence (Section 7.1).

7.4. The Random- β Model

In the foregoing formalism, the multi-fractal properties were attributed to an unsigned function like the velocity field. We will now consider an alternative approach wherein the multi-fractal properties are attributed to a positive measure of the dynamical system in question, namely, the local mean energy dissipation.

Fully developed turbulence may be considered to be a probabilistic cascading process where each interval fragments into smaller pieces and the total measure of the energy dissipation rate is divided among them according to a certain probability distribution. We will now consider a probabilistic extension of the β -model called the

¹³ It may be noted that the record of measurements in these experiments consists of a time-series at a fixed point in the flow. A hot-wire probe at this point measures the fluctuating velocity and Taylor's sweeping hypothesis (which states that the changes in the flow quantities with time at the fixed measuring point are due to the passage of a frozen pattern of turbulent flow past the point, and hence, the spatial statistics of quantities like $(q(x+r,t) - q(x,t))$ may be inferred from the temporal statistics of quantities like $(q(x,t+\tau) - q(x,t))$, where the time delay τ is related to the spatial interval $|r|$ via $\tau = |r|/v$, v being the convection velocity of the fluid) is used to derive the fluctuating shear, and hence the energy dissipation rate, from these measurements. If the flow is approximately stationary for the duration of these measurements, one may regard this record as Eulerian, representing a spatial "cut" through the flow at a single instant in time. Thus, the small scale structure of the flow is obtained by analyzing the high-frequent components of the measured signal.

¹⁴ It may be noted that the singularity spectrum obtained from one-dimensional cuts can go negative (Meneveau and Sreenivasan (1991)), which is purely an artifact of the one-dimensional nature of the cut.

random- β model, due to Benzi *et al.* (1984). This model simulates a multi-fractal where the contraction factors $\beta_n(l_i)$ are independent random variables which take different values in each scale i at the n th step of the cascade and are distributed according to a given probability distribution $P(\beta_1, \beta_2, \dots, \beta_n)$.

Consider a discrete sequence of scales, as in Section 7.3,

$$l_n = l_o 2^{-n}, \quad n = 0, 1, 2, \dots \quad (39)$$

and a discrete sequence of wavenumbers $k_n = l_n^{-1}$. The kinetic energy per unit mass in the n th scale is defined by

$$E_n = \int_{k_n}^{k_{n+1}} E(k) dk. \quad (40)$$

Let us assume again that we have a statistically stationary turbulence where the kinetic energy is introduced into the fluid at scales $\sim l_o$ and is then transferred by nonlinear interactions successively to scales l_1, l_2, \dots until some scale l_d where viscous dissipation is able to compete with nonlinear energy transfer.

At the n th step of fragmentation, if there are N_n active eddies with contraction factors $\beta_n(j)$, they will cover fractions

$$B_n = \sum_{j=1}^{N_n} \frac{\beta_n(j)}{N_n} \quad (41)$$

of the volumes occupied by their mother eddies (where the standard Kolmogorov (1941) phenomenology holds), and are given by

$$N_n \sim 2^{3n} \prod_{i=1}^n B_i. \quad (42)$$

(42) reflects the fact that intermittency becomes more acute as the scale size l_n decreases (or n increases).

Averaging N_n over the probability distributions of the β 's, we have

$$\langle N_n \rangle \sim 2^{3n} \prod_{i=1}^n \langle B_i \rangle. \quad (43)$$

If the dissipative structures cover sets with Hausdorff dimension D_o , we have

$$\langle N_n \rangle \sim l_n^{-D_o}. \quad (44)$$

Combining (39), (41), (43) and (44), we obtain

$$D_o = 3 + \log_2 \{\beta\} \quad (45)$$

where,

$$\log_2 \{\beta\} \equiv \frac{\ln \left\langle \prod_{i=1}^n B_i \right\rangle}{n \ln 2}.$$

Let $v_n(i_n)$ be the velocity difference in the active eddies between two pairs of points at distance $l_n(i_n)$; $\beta_{n+1}(i_{n+1})$ be the percentage of volume occupied by the active eddies of scale $l_{n+1}(i_{n+1})$ generated by the eddies of scale $l_n(i_n)$. In the inertial range, we assume a stationary process in which the constancy of the energy transfer rate among eddies of scale l_n , namely,

$$\varepsilon_n = \varepsilon_{n+1} \quad (46)$$

gives

$$\frac{v_n^3(i_n)}{l_n(i_n)} = \beta_{n+1}(i_{n+1}) \frac{v_{n+1}^3(i_{n+1})}{l_{n+1}(i_{n+1})} \quad (47)$$

where $i_n = 1, 2, \dots, N_n$. Solving (47) iteratively, we obtain for the velocity difference $v_n(i_n)$ in an eddy generated by a particular set of fragmentation

$$v_n(i_n) \sim l_n^{1/3}(i_n) \prod_{j=1}^n \beta_j^{-1/3}(i_j). \quad (48)$$

The velocity structure function is defined by

$$\langle |\delta v(l_n)|^p \rangle \sim \int \prod_{i=1}^n d\beta_i P(\beta_1, \dots, \beta_n) \beta_i |v_n|^p. \quad (49)$$

Following Benzi *et al.* (1984), one may now assume that the turbulent cascade is a statistically independent Bernoullian fragmentation process so that the β 's are uncorrelated with each other as well, and that the probability distributions are the same for all i , i.e.,

$$P(\beta_1, \dots, \beta_n) = \prod_{i=1}^n P(\beta_i). \quad (50)$$

Using (50), (49) becomes

$$\langle |\delta v(l_n)|^p \rangle \sim l_n^{p/3} \left(\int d\beta P(\beta) \beta \beta^{-p/3} \right)^n \sim l_n^{p/3} \left\{ \beta^{\frac{1-p}{3}} \right\}^n \sim l_n^{\zeta_p} \quad (51)$$

where,

$$\zeta_p = \frac{p}{3} - \log_2 \left\{ \beta^{\frac{1-p}{3}} \right\}. \quad (52)$$

Observe that the similarity between (29) and (52) is as to be expected.

For a homogeneous fractal, $\beta_i = \text{constant} = \beta = 2^{D_0-3}$ for all i ; (52) now reduces to

$$\zeta_p = \frac{p}{3} + \frac{1}{3}(3-p)(3-D_0) \quad (53)$$

in agreement with the result (28) for the β -model.

Let us consider a two-parameter random- β model, as follows –

$$P(\beta) = x\delta(\beta - 2^{-2}) + (1-x)\delta(\beta - 1). \quad (54)$$

(54) assumes that filament-like structures are created with probability x (Benzi *et al.* (1984), on the other hand, considered sheet-like structures) while space-filling eddies are created with probability $(1-x)$. This model is based on a simple phenomenological idea, in accord with the numerical simulation results (Vincent and Meneguzzi, 1991), that an active eddy can generate either filament-like dissipative structures ($\beta = 2^{-2}$) or space-filling Kolmogorov-like eddies ($\beta = 1$).

Using (54), (52) becomes

$$\zeta_p = \frac{p}{3} - \frac{\ln \left[x 4^{\frac{p}{3}-1} + (1-x) \right]}{\ln 2}. \quad (55)$$

(55) gives, for $p=0$,

$$\zeta_o = -\frac{\ln \left(1 - \frac{3x}{4} \right)}{\ln 2} = 3 - D_o. \quad (56)$$

Further, for small p , (55) gives, on using (56),

$$\zeta_p \approx 3 - D_o + \frac{p}{3} \begin{pmatrix} 1 - \frac{5x}{4} \\ \frac{4}{1 - \frac{3x}{4}} \end{pmatrix} \quad (57)$$

which shows a linear dependence on p , like the β -model.

On the other hand, for large p , (55) gives

$$\zeta_p \approx -\frac{p}{3} + 2 - \frac{\ln x}{\ln 2}. \quad (58)$$

Figure 7.10 gives a comparison of (55), for the choice $x = \frac{1}{8}$, with the experimental data of Anselmet *et al.* (1984). The agreement is seen to be very good¹⁵.

¹⁵ However, the random- β idea for the turbulent velocity field runs into difficulties on application of Novikov's (1971) inequality. This may be seen by assuming that there are only two different fragmentation processes characterized by values β_1 and β_2 , say $\beta_1 \geq \beta_2$, occurring with probabilities x and $1-x$, respectively, so that, we have in place of (54),

$$P(\beta) = x\delta(\beta - \beta_1) + (1-x)\delta(\beta - \beta_2). \quad (I)$$

Thus,

$$\left\{ \beta^{1-\frac{p}{3}} \right\} = x \beta_1^{1-\frac{p}{3}} + (1-x) \beta_2^{1-\frac{p}{3}}$$

so,

$$\left\{ \beta^{1-\frac{p}{3}} \right\} \approx (1-x) \beta_2^{1-\frac{p}{3}}, \quad \text{for } p \gg 1. \quad (\text{II})$$

We then have, from (51),

$$\zeta_p \approx p \left(\frac{1}{3} - c \right) \quad (\text{III})$$

where,

$$c \equiv -\frac{1}{3} \log_2 \beta_2.$$

If one assumes the moments of the local mean dissipation to scale according to

$$\langle [\varepsilon_a(r)]^q \rangle \sim \langle \varepsilon_a \rangle^q \left(\frac{L}{r} \right)^{\mu}, \quad (\text{IV})$$

then Novikov (1973) showed that μ_q should increase at most linearly, i.e.,

$$\mu_q \leq q + 3(\mu - 2), \quad \text{for } q > 2 \quad (\text{V})$$

where,

$$\langle \varepsilon_a(x) \varepsilon_a(x+r) \rangle \sim r^{-\mu}.$$

(III) and (V) imply that

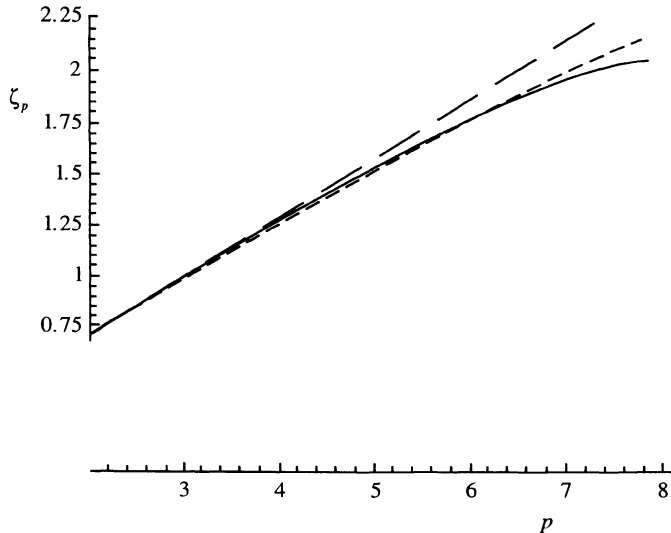


Figure 7.10. Velocity structure function exponent versus moment index p . Short dashed line represents the recent experimental data of Benzi *et al.* (1993) while the long dashed line represents the uniform- β model.

The full lines corresponds to the random β -model with $x = 1/20$.

In order to calculate the generalized fractal dimension D_q for the random- β model, let us first rewrite (38) as follows –

$$\zeta_{3q} = q - \mu_{3q} \quad (59)$$

where,

$$\mu_{3q} \equiv (q - 1)(3 - D_q). \quad (60)$$

$$-\frac{p}{3} \log_2 \beta_2 \leq \frac{p}{3} + 3(\mu - 2)$$

from which,

$$\beta_2 \geq 2^{-1}. \quad (\text{VI})$$

(VI), therefore, dictates that the fragmentation process in question cannot generate any structures more sparse than sheet-like structures. But, it is now a well-established fact that the dissipation field is localized in quasi-one-dimensional tube-like structures!

We have from (60),

$$D_q = 3 - \frac{\mu_{3q}}{q-1}. \quad (61)$$

Comparison of (52) and (59) gives

$$\mu_{3q} = \log_2^{\{\beta^{1-q}\}}. \quad (62)$$

Using (62), (61) becomes

$$D_q = 3 - \frac{\log_2^{\{\beta^{1-q}\}}}{q-1}. \quad (63)$$

On using the two-parameter model (54), (63) becomes

$$D_q = 3 - \frac{\ln[x \cdot 4^{q-1} + (1-x)]}{(q-1)\ln 2}. \quad (64)$$

For small q , (64) may be approximated by

$$D_q \approx \left[3 + \frac{\ln(1-3x/4)}{\ln 2} \right] + q \left[\frac{\ln(1-3x/4)}{\ln 2} + \frac{x/2}{1-3x/4} \right] \quad (65)$$

which shows a linear dependence on q .

Figure 7.11 gives a comparison of (64) for the choice $x=2/3$ with the experimental data of Meneveau and Sreenivasan (1987). The agreement is seen to be better than that given by the log-normal model and the β -model.

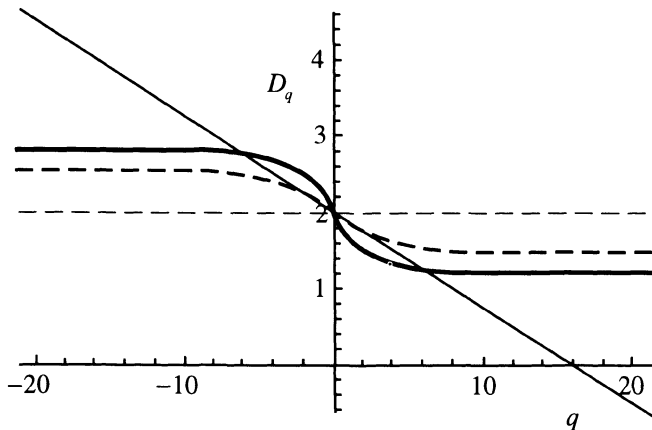


Figure 7.11. Comparison of the theory with the experimental data (represented by the thick dashed line) of Meneveau and Sreenivasan (1987) for the generalized fractal dimension D_q for the energy dissipation field –

- (i) log-normal model (thin full line)
- (ii) uniform- β model (thin dashed line)
- (iii) random- β model (thick full line) with $x = 2/3$.

5. The Intermediate Dissipation Range

When dissipative effects arise, the power-law behavior described by (32) breaks down for very small l and the cut-offs are determined by external parameters like the Reynolds number. In such cases, Wu *et al.* (1990) and Frisch and Vergassola (1991) pointed out that the multifractal in question would exhibit a multiscaling behavior with

certain universal features, following a suitable rescaling: thus, $\frac{\ln[S_p(l)/S_o]}{\ln[R/R_o]}$ would be a

universal function of $\frac{\ln[l/l_o]}{\ln[R/R_o]}$, (here, S_o, l_o and R_o (the Reynolds number) are

normalizing constants). This implies that the structure function data for different values of R would fall onto a single curve.

The dissipative effects materialize when typically the eddy turn-over time exceeds the viscous diffusion time, i.e.,

$$\frac{l}{\delta v} \geq \frac{l^2}{v}$$

or

$$\delta v < \frac{v}{l} = \delta \equiv l^{-\bar{\alpha}/3}. \quad (66)$$

(66) implies the presence of a viscous cut-off δ so that the boxes with measures $\delta v < \delta$ or indices $\alpha > \bar{\alpha}$, where

$$\frac{\bar{\alpha}}{3} = \frac{\ln \delta}{\ln l} = -1 - \frac{\ln v}{\ln(1/l)} \quad (67)$$

would be empty and would not therefore be present in the integral for S_p in (32). Thus,

$$S_p(l, \delta) = \int_{\alpha_{\min}}^{\bar{\alpha}} l^{-\frac{\alpha p + 3 - f(\alpha)}{3}} d\mu(\alpha) \quad (68)$$

signifying the existence of a continuous range of viscous cut-offs in the multi-fractal model for the inertial range.

If $l > \eta \sim (v^3/\epsilon)^{1/4}$, then $\bar{\alpha} > 1 > \alpha_*$, and one has the usual single-scaling multi-fractal regime in the inertial range. *This regime also includes length scales smaller than the Kolmogorov microscale, $l < \eta$, so long as $1 > \bar{\alpha} > \alpha_*$.* But, when length scales fall well below η so that $\bar{\alpha} < \alpha_* < 1$, the minimum of ζ_p is attained for $\alpha = \bar{\alpha}$ (see Figure 7.12). One now has a multi-scaling behavior (Jensen *et al.*, (1991)) (different moments scale differently) that is pseudo-algebraic, since the power law in question has a slowly-varying exponent proportional to $\ln l$. However, if the probe size is much longer than the viscous cutoff the measurements can be spurious (Frisch and Vergassola, 1991).

Thus, in the limit of small l , (68) leads to

$$S_p(l, \delta) \sim \begin{cases} l^{\zeta_p}, & \text{if } \bar{\alpha} > \alpha_* \\ l^{-\frac{\bar{\alpha} p + 3 - f(\bar{\alpha})}{3}}, & \text{if } \bar{\alpha} \leq \alpha_* \end{cases}. \quad (69)$$

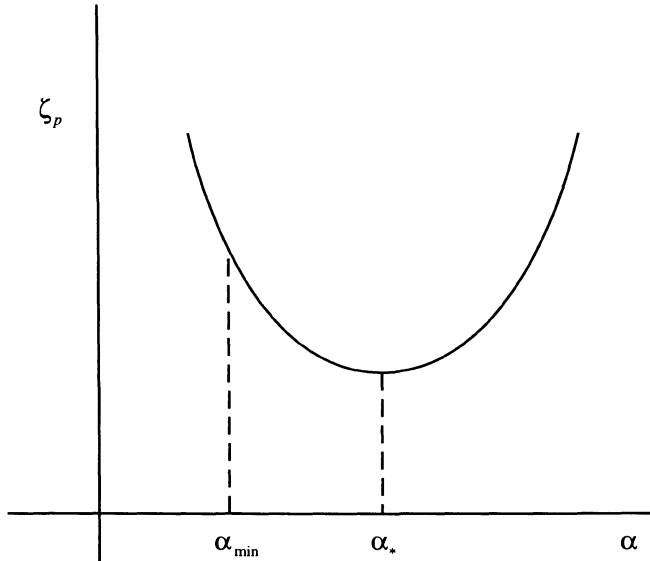


Figure 7.12. Schematic graph of the structure function exponent ζ_p vs. the singularity strength α .

In order to see if this multi-scaling behavior shows any universal features, let us rescale the variables as follows –

$$F_p(\theta) = \frac{\ln S_p}{\ln \delta}, \quad \theta = \frac{\ln l}{\ln \delta} = \frac{3}{\alpha}. \quad (70)$$

(69) then implies

$$F_p(\theta) = \begin{cases} \theta \zeta_p, & \text{if } \theta < 3/\alpha_* \\ p + \theta[3 - f(3/\theta)], & \text{if } \theta \geq 3/\alpha_* \end{cases}. \quad (71)$$

According to (71), the graph of $F_p(\theta)$ vs. θ is a straightline with slope ζ_p in the single-scaling regime $\theta < 3/\alpha_*$, which then bends around in the multi-scaling regime $\theta \geq 3/\alpha_*$. Thus, the structure function data for different Reynolds numbers would fall onto a single curve in the neighborhood of the viscous regime – multifractal universality. This would enable one to use the low Reynolds number data from laboratory measurements and

numerical simulations, for which no inertial range exists, in a more physically significant way.

Note that, in the limit $\bar{\alpha} \rightarrow \alpha_{\min}$, one obtains a homogenous fractal,

$$S_p(l, \delta) \sim l^{\frac{\alpha_{\min} p}{3} + 3 - f(\alpha_{\min})} \quad (72)$$

which is, of course, the β -model result (28).

CHAPTER 8

SINGULARITY ANALYSIS AND THE PAINLEVE' PROPERTY OF DYNAMICAL SYSTEMS

Recent studies have shown that (see Ablowitz and Segur, 1981; Tabor, 1984 and 1989; Ramani *et al.* 1989; and Lakshmanan and Sahadevan, 1993 for excellent reviews) there are certain connections between the global real-time motion of a dynamical system and the local structure of singularities of this system extended into the complex-time domain. The precise nature of these connections, however, remains unclear yet. Chaotic motion is described by functions having complicated singularity structure in the complex t -plane. On the other hand, regular motion is usually described by functions which are analytic everywhere, except perhaps for some poles in the complex t -plane. Based on these observations, Ablowitz *et al.* (1980) proposed a valuable tool for the identification of integrable systems. They conjectured and subsequently verified by integration via inverse-scattering methods that a dynamical system described by a differential equation is integrable whenever the solutions have the Painlevé property, namely, that their only movable singularities (see Section 8.1) are poles, and therefore, they live on a single Riemann sheet. In practice, this property can be exhibited by demonstrating that the solution can be expanded in "formal" Laurent series ("formal" since the convergence of the series is not obvious), near every one of its movable singularities. It is now believed that (Ramani *et al.* 1984 and Dorizzi *et al.* 1984) the Painlevé property is a *sufficient* condition so that some equations violating this property may still be integrable.¹ Therefore, a reliable route to test for integrability appears to be the dual approach – singularity analysis and direct search for integrals of the dynamics for each case of predicted integrability.

8.1. The Painlevé Property

Let us first recapitulate some facts about linear ordinary differential equations (Ince, 1956). Consider a linear second order ordinary differential equation

¹ It turns out that some systems, which have branch points with rational exponents, are integrable and are said to possess "weak Painlevé" property (Ramani *et al.* 1984, Dorizzi *et al.* 1984). However, integrable "weak Painlevé" cases may not be transformed to full Painlevé cases by some reasonably simple global transformations of the dependent variables.

$$\frac{d^2w}{dz^2} + P_1(z) \frac{dw}{dz} + P_o(z)w = 0 \quad (1)$$

If the coefficients are all analytic at a point z_o in the complex plane, then z_o is a regular point of the ordinary differential equation. If one or both coefficients are singular at a point z_o , then z_o is a singular point of the ordinary differential equation, since the solutions of which now exhibit singularities at z_o . These singularities are called *fixed*, because their locations do not depend on the constants of integration. The linear differential equations have a general property that their solutions possess singularities of only fixed type. For example, consider,

$$\frac{dw}{dz} + \frac{w}{z - c} = 0 \quad (2)$$

has the solution

$$w = \frac{w_o}{c - z}, \quad w_o \equiv w(0). \quad (3)$$

which shows a singularity at a fixed point c (that does not depend on the initial conditions).

Nonlinear ordinary differential equations do not have this property. Consider, for example,

$$\frac{dw}{dz} + w^2 = 0 \quad (4)$$

which has a general solution

$$w = \frac{1}{z - z_o} \quad (5)$$

showing a *movable* type singularity (namely, a pole) at z_o , because z_o is a constant of integration.

Consider another example,

$$\frac{dw}{dz} - e^{-w} = 0 \quad (6)$$

which has a general solution

$$w = \log(z - z_o) \quad (7)$$

showing a movable branch point at z_o .

Consider a third example,

$$\frac{dw}{dz} + w(\log w)^2 = 0 \quad (8)$$

which has a general solution

$$w = e^{\frac{1}{z-z_o}} \quad (9)$$

showing a movable essential singularity at z_o .

Thus, nonlinear ordinary differential equations have solutions that exhibit both fixed and movable type singularities.

It became a problem of interest in the last century to classify ordinary differential equations based on whether or not their general solutions have movable singularities. Fuchs (1884) showed that out of all first order ordinary differential equations of the form

$$\frac{dw}{dz} = F(w, z)$$

where F is rational in w and analytic in z , the only equation that is free from movable singularities is the generalized Riccati equation

$$\frac{dw}{dz} = P_0(z) + P_1(z)w + P_2(z)w^2. \quad (10)$$

Kovalevskaya (1888) made an application of these ideas, interestingly, for the physical problem of the motion of a top under gravity. She found that the equations of motion can be integrated explicitly in terms of elliptic functions whenever the equations admitted only movable poles as singularities (depending on the parameters of the problem taking certain values). (See Golubov (1953) for an account of Kovalevskaya's work.)

The generalization of Fuchs' characterization of first-order ordinary differential equations to second-order ordinary differential equations was carried out by Painlevé

(1900) and his co-workers. They considered second-order ordinary differential equations of the form

$$\frac{d^2 w}{dz^2} = F\left(\frac{dw}{dz}, w, z\right)$$

where F is rational in w and $\frac{dw}{dz}$ and analytic in z , and showed that out of all equations

of this form, there are only 50 canonical equations which admitted only movable poles as singularities – Painlevé property. 44 of these canonical equations are soluble in terms of known functions such as elliptic functions. The remaining six equations, called the Painlevé transcendent, have transcendental meromorphic² solutions for which convergent expansions are explicitly known. They are

$$\frac{d^2 w}{dz^2} = 6w^2 + z \quad (11)$$

$$\frac{d^2 w}{dz^2} = zw + 2w^3 + \alpha \quad (12)$$

$$\frac{d^2 w}{dz^2} = \frac{1}{w} \left(\frac{dw}{dz} \right)^2 - \frac{1}{z} \frac{dw}{dz} + \frac{1}{z} (\alpha w^2 + \beta) + \gamma w^3 + \frac{\delta}{w} \quad (13)$$

$$\frac{d^2 w}{dz^2} = \frac{1}{2w} \left(\frac{dw}{dz} \right)^2 + \frac{3w^3}{2} + 4zw^3 + 2(z^2 - \alpha) + \frac{\beta}{w} \quad (14)$$

$$\frac{d^2 w}{dz^2} = \left(\frac{1}{2w} + \frac{1}{w-1} \right) \left(\frac{dw}{dz} \right)^2 - \frac{1}{z} \frac{dw}{dz} + \frac{(w-1)^2}{z^2} \left(\alpha w + \frac{\beta}{w} \right) + \frac{\gamma w}{z} + \frac{\delta w(w+1)}{w-1} \quad (15)$$

$$\begin{aligned} \frac{d^2 w}{dz^2} &= \frac{1}{2} \left(\frac{1}{w} + \frac{1}{w-1} + \frac{1}{w-z} \right) \left(\frac{dw}{dz} \right)^2 - \left(\frac{1}{z} + \frac{1}{z-1} + \frac{1}{w-z} \right) \frac{dw}{dz} \\ &\quad + \frac{w(w-1)(w-z)}{z^2(z-1)^2} \left[\alpha + \frac{\beta z}{w^2} + \frac{\gamma(z-1)}{(w-1)^2} + \frac{\delta z(z-1)}{(w-z)^2} \right] \end{aligned} \quad (16)$$

² Meromorphic functions are analytic functions except for movable poles.

8.2. Singularity Analysis

The nature of movable singularities of nonlinear ordinary differential equations can be determined by considering the local properties of the solutions. The Painlevé property can be reformulated as follows.

THEOREM 8.1

A necessary condition that an n th order ordinary differential equation of the form

$$\frac{d^n w}{dz^n} = F\left(\frac{d^{n-1}w}{dz^{n-1}}, \dots, \frac{dw}{dz}, w, z\right) \quad (17)$$

where F is rational in w , $\frac{dw}{dz}, \dots, \frac{d^{n-1}w}{dz^{n-1}}$ and analytic in z , has the Painlevé property is that there is a formal Laurent expansion about an arbitrary pole position z_o –

$$w(z) = (z - z_o)^m \sum_{j=0}^{\infty} a_j (z - z_o)^j \quad (18)$$

with $(n-1)$ arbitrary expansion coefficients a_j , besides the pole position z_o which is arbitrary (in order that the expansion (18) is a local representation of the general solution).

The Painlevé analysis thus consists of implementation of the following program:

- expansion of the solution as a Laurent series in the neighborhood of a movable singular point z_o ;
- determination of the leading-order behavior of the Laurent series in the neighborhood of z_o ; for this purpose, one substitutes

$$w(z) = a(z - z_o)^\alpha$$

into equation (17) and balances the most singular terms to determine a and α ;

- determination of resonances, i.e., the powers at which arbitrary constants of the solution can enter into the Laurent series;
- verification that a sufficient number of arbitrary constants exist to cover the entire solution manifold of equation (17) without the introduction of movable critical points.

EXAMPLE 1

Consider the equation

$$\frac{d^2 w}{dz^2} = 6w^2 + Aw \quad (19)$$

which is actually the first Painlevé transcendent (11).

In order to determine the leading-order behavior of the solutions of equation (19) at a movable singularity z_o , substitute

$$w(z) \sim a(z - z_o)^\alpha \quad (20)$$

into equation (19), we then obtain

$$a\alpha(\alpha - 1)(z - z_o)^{\alpha-2} = 6a^2(z - z_o)^{2\alpha} + Aa(z - z_o)^\alpha$$

Balancing the most singular terms, this leads to

$$\left. \begin{array}{l} \alpha - 2 = 2\alpha \text{ or } \alpha = -2 \\ \text{and} \\ a\alpha(\alpha - 1) = 6a^2 \text{ or } a = 1 \end{array} \right\}. \quad (21)$$

Thus, at z_o , the solution behaves as

$$w(z) \sim (z - z_o)^{-2} \quad (22)$$

In order to determine the behavior of $w(z)$ in the neighborhood of the singularity, a local expansion, with the leading behavior (22) as the first term, must be constructed. If the singularity is indeed a movable pole, then this expansion will be a simple Laurent series. In order to find the resonances, namely, the powers of $(z - z_o)$ at which the arbitrary coefficients appear in this series, one substitutes

$$w(z) = (z - z_o)^{-2} + \beta(z - z_o)^{r-2} \quad (23)$$

in equation (19), and finds a linear equation in β by balancing the most singular terms again,

$$\beta[(r-2)(r-3)-12]=0.$$

So, β is arbitrary, provided

$$r = -1 \text{ or } 6. \quad (24)$$

This implies that the coefficient a_6 of the term $(z-z_o)^{6-2}$ in the Laurent series is arbitrary. The other root, namely, $r = -1$, should be discarded, since it corresponds to the arbitrariness of the location of the pole $(z-z_o)$.

The resonance analysis only indicates which coefficients in the series should be arbitrary. This needs to be verified by examining the full recursion relations. This sometimes leads to a compatibility condition that has to be satisfied in order to ensure the arbitrariness of the coefficient at such a resonance. This is usually found to be possible only for certain values of the system parameters.

Consider then the expansion

$$w(z) = \xi^{-2} + a_1 \xi^{-1} + a_2 + a_3 \xi + a_4 \xi^2 + a_5 \xi^3 + a_6 \xi^4 + \dots \quad (25)$$

where,

$$\xi = z - z_o.$$

Substituting (25) into equation (19) and collecting terms of equal powers of ξ , we obtain

$$\xi^{-3} : 2a_1 = 12a_1 \quad (26)$$

$$\xi^{-2} : 0 = 6(a_1^2 + 2a_2) + A \quad (27)$$

$$\xi^{-1} : 0 = 6(2a_3 + 2a_1 a_2) + A a_1 \quad (28)$$

$$\xi^0 : 2a_4 = 6(2a_2^2 + 2a_4 + 2a_1 a_3) + a_2 A \quad (29)$$

$$\xi^1 : 6a_5 = 6(2a_5 + 2a_1a_4 + 2a_2a_3) + Aa_3 \quad (30)$$

$$\xi^2 : 12a_6 = 6(2a_3^2 + 2a_6 + 2a_1a_5 + 2a_2a_4) + Aa_4 \quad (31)$$

Equations (26) - (30) lead to

$$a_1 = 0, a_2 = -\frac{A}{12}, a_3 = 0, a_4 = -\frac{A^2}{240},$$

$$a_5 = 0 \quad (32)$$

Using (32), equation (31) becomes

$$0 \cdot a_6 = 0 \quad (33)$$

so that a_6 is arbitrary.

Thus, the Laurent series (25) has two arbitrary constants a_6 and z_o which are *just* sufficient to make (25) a valid local representation of the general solution of equation (19). Therefore, the general solution has only a movable pole at $z = z_o$. Consequently, equation (19) possesses the Painlevé property, as expected!

EXAMPLE 2

Consider the equation (Ablowitz and Segur, 1981)

$$\frac{d^2w}{dz^2} = z^m w + 2w^3 \quad (34)$$

The leading-order behavior of the solutions of equation (34) at a movable singularity z_o is determined by proceeding as before,

$$w \sim \xi^{-1}, \quad \xi \equiv z = z_o. \quad (35)$$

The resonances are determined by setting

$$w = \xi^{-1} + \beta \xi'^{-1} \quad (36)$$

and balancing the most singular terms in equation (34),

$$\beta[(r-1)(r-2)-6]=0$$

or

$$r = -1 \text{ or } 4. \quad (37)$$

The root $r = -1$ is discarded as before, while the coefficient of the term ξ^{4-1} in the Laurent series can be arbitrary.

Consider then the expansion,

$$w(z) = \xi^{-1} + a_o + a_1\xi + a_2\xi^2 + a_3\xi^3 + \dots \quad (38)$$

Substituting (38) into equation (34) and collecting terms of equal powers of ξ , as before, we obtain

$$\xi^{-2} : 6a_o = 0 \quad (39)$$

$$\xi^{-1} : z_o^m + 6a_o^2 + 6a_1 = 0 \quad (40)$$

$$\xi^0 : 2a_2 = z_o a_o + m z_o^{m-1} + 2a_o^3 + 6a_2 \quad (41)$$

$$\xi^1 : 6a_3 = z_o a_1 + m(m-1)z_o^{m-2} + a_o m z_o^{m-1} + 6a_1^2(a_o^2 + 1) + 6a_3. \quad (42)$$

Equations (39) - (41) lead to

$$a_0 = 0, \quad a_1 = -\frac{1}{6}z_o^m, \quad a_2 = -\frac{m}{4}z_o^{m-1}. \quad (43)$$

Using (43), equation (42) becomes

$$0 \cdot a_3 = m(m-1)z_o^{m-2} \quad (44)$$

so that a_3 is arbitrary if $m = 0$ or 1 . Therefore, the general solution of equation (34) has only a movable pole at $z = z_o$ if the parameter m is either 0 or 1 .

EXAMPLE 3

Consider the equation (Ramani *et al.* 1989)

$$\frac{d^2w}{dz^2} + 4w \frac{dw}{dz} + 2w^3 = 0. \quad (45)$$

The leading-order behavior of the solutions of equation (45) at a movable singularity z_o is given by

$$w \sim \xi^{-1}, \quad \xi \equiv z - z_o. \quad (46)$$

The resonances are determined by setting

$$w \sim \xi^{-1} + \beta \xi^{r-1} \quad (47)$$

and proceeding as before, to find

$$r = -1 \text{ or } 0 \quad (48)$$

The root $r = 0$ implies that the coefficient of the leading term ξ^{-1} is arbitrary, but it is not (as seen in (46)). Therefore, the solution of equation (45) will not be a Laurent series and the expansion in question now needs to be augmented by logarithmic terms so that the general solution now has a movable critical point:

$$w(z) = \frac{1}{\xi} \left(a_o + \frac{a_1}{\log \xi} + \dots \right). \quad (49)$$

Substituting (49) into equation (45), we find

$$a_o = 1, \quad a_1 = \frac{1}{2}, \quad \text{etc.} \quad (50)$$

EXAMPLE 4

Consider the generalized Hénon-Heiles system (Bountis *et al.* 1982)

$$\left. \begin{array}{l} \ddot{x} + Ax = 2xy \\ \ddot{y} + By = \varepsilon y^2 + x^2 \end{array} \right\} \quad (51)$$

In order to determine the leading-order behavior of the solutions of equations (51) at a movable singularity t_o , substitute

$$x \sim a\tau^p, \quad y \sim b\tau^q, \quad \tau \equiv t - t_o \quad (52)$$

into equations (51) and balance the most singular terms; this gives

$$\left. \begin{array}{l} p(p-1)a\tau^{p-2} = 2ab\tau^{p+q} \\ q(q-1)b\tau^{q-2} = \varepsilon b^2\tau^{2q} + a^2\tau^{2p} \end{array} \right\} \quad (53)$$

(53) has two distinct sets of solutions –

$$\left. \begin{array}{l} (i) \quad \begin{array}{l} p = -2, \quad q = -2 \\ a = \pm 3\sqrt{2-\varepsilon}, \quad b = 3 \end{array} \\ (ii) \quad \begin{array}{l} p = \frac{1}{2}\left(1 \pm \sqrt{1 + \frac{48}{\varepsilon}}\right), \quad q = -2 \\ a \text{ arbitrary}, \quad b = \frac{6}{\varepsilon} \end{array} \end{array} \right\}. \quad (54)$$

Next, in order to determine the resonances, substitute

$$x = a\tau^{-p} + \alpha\tau^{r-p}, \quad y = b\tau^{-q} + \beta\tau^{r-q} \quad (55)$$

into equations (51) and balance the most singular terms again; this gives

$$\left. \begin{array}{l} (i) \quad r = -1, 6, \frac{1}{2}\left(5 \pm \sqrt{1 - 24(1-\varepsilon)}\right) \\ (ii) \quad r = -1, 0, 6 \pm \sqrt{1 + \frac{48}{\varepsilon}} \end{array} \right\}. \quad (56)$$

These expressions yield integer values for r , for the following values of ε :

- (a) $\varepsilon = 1$: (i) $r = -1, 6, 2, 3$
(ii) $r = -1, 0, 6, \pm 7$
- (b) $\varepsilon = 2$: (i) $r = -1, 0, 6, 5$
(ii) $r = -1, 0, 6, \pm 5$
- (c) $\varepsilon = 6$: (i) $r = -1, 6, 8, -3$
(ii) $r = -1, 0, 6, \pm 3$
- (d) $\varepsilon = 16$: (i) $r = -1, 6, 12, -7$
(ii) $r = -1, 0, 6, \pm 2$. (57)

Let us now consider expansions of the solution, near the singularity $t = t_o$, for these various cases separately.

- (a) $\varepsilon = 1$: Let,

$$\left. \begin{aligned} x &= a\tau^{-2} + a_1\tau^{-1} + a_2 + \dots \\ y &= b\tau^{-2} + b_1\tau^{-1} + b_2 + \dots \end{aligned} \right\}. \quad (58)$$

Substituting (58) into equations (51) and collecting terms of equal powers of τ , we obtain

$$\left. \begin{aligned} \tau^{-4}: 6a &= 2ab \\ 6b &= b^2 + a^2 \end{aligned} \right\} \quad (59)$$

$$\left. \begin{aligned} \tau^{-3}: 2a_1 &= 2ab_1 + 2ba_1 \\ 2b_1 &= 2bb_1 + 2aa_1 \end{aligned} \right\} \quad (60)$$

$$\left. \begin{aligned} \tau^{-2}: 0 &= -Aa + 2ab_2 + 2ba_2 \\ 0 &= -Bb + 2bb_2 + 2aa_2 \end{aligned} \right\}. \quad (61)$$

Equations (59) and (60) give

$$a = b = 3, \quad a_1 = b_1 = 0 \quad (62)$$

in agreement with (54). Using (62), equations (61) demand that

$$A = B. \quad (63)$$

Proceeding further, it may be verified that, for this case, the general solution of equations (51) has only a movable pole at $\tau = \tau_o$. Indeed, for this case, equations (51) become separable in the variables $(x + y)$ and $(x - y)$. Putting,

$$m = x - y, \quad n = x + y \quad (64)$$

equations (51) lead to

$$\left. \begin{aligned} \ddot{m} + m &= -m^2 \\ \ddot{n} + n &= n^2 \end{aligned} \right\}. \quad (65)$$

(b) $\varepsilon = 2$: Following the previous procedure, it may be verified that, for this case, the expansions do not contain sufficient number of arbitrary constants to cover the entire solution manifold of equations (51). So, the general solution of equations (51) admits movable critical points.

(c) $\varepsilon = 6$: Let

$$\left. \begin{aligned} x &= a\tau^{-1} + a_1 + a_2\tau + \dots \\ y &= b\tau^{-2} + b_1\tau^{-1} + b_2 + b_3\tau + \dots \end{aligned} \right\}. \quad (66)$$

Substituting (66) into equations (51) and collecting terms of equal powers of τ , we obtain

$$\tau^{-4} : \quad 6b = 6b^2 \quad (67)$$

$$\left. \begin{aligned} \tau^{-3} : \quad 2a &= 2ab \\ 2b_1 &= 12bb_1 \end{aligned} \right\} \quad (68)$$

$$\left. \begin{aligned} \tau^{-2} : 0 &= 2ab_1 + 2a_1b \\ 0 &= -Bb + 6b_1^2 + 12bb_2 + a^2 \end{aligned} \right\} \quad (69)$$

$$\tau^{-1} : 0 = -Aa + 2ab_2 + 2a_1b_1 + 2a_2b \quad (70)$$

$$\left. \begin{aligned} \tau^0 : 2a_3 &= -a_1A + 2ab_3 + 2a_1b_2 + 2a_2b_1 + 2a_3b \\ 2b_4 &= -Bb_2 + 6b_2^2 + 12bb_4 + 12b_1b_3 + a_1^2 + 2aa_2 \end{aligned} \right\}. \quad (71)$$

Equations (67) - (70) lead to

$$\left. \begin{aligned} b &= 1, \\ b_1 &= 0, \quad a_1 = 0 \\ b_2 &= \frac{B}{12} - \frac{a^2}{12}, \quad a_2 = \frac{Aa}{2} + \frac{Ba}{12} - \frac{a^3}{12} \end{aligned} \right\}. \quad (72)$$

Using (72), equation (71) give

$$b_3 = 0, \quad a_3 \text{ arbitrary.} \quad (73)$$

Proceeding further, it may be verified that, for this case, the general solution of equations (51) has only a movable pole at $t = t_o$. Indeed, Greene (1982) gave a second integral for this case –

$$x^4 + 4x^2y^2 + 4\dot{x}(xy - x\dot{y}) - 4Ax^2y + (4A - B)(\dot{x}^2 + Ax^2) = \text{const.}$$

(d) $\epsilon = 16$: Following the previous procedure, it may be verified, for this case, that the general solution of equations (51) has only a movable pole at $t = t_o$, provided $B = 16A$. Hall (1983) gave a second integral for this case –

$$3\dot{x}^4 + 6(A - 2y)x^2\dot{x}^2 + 4x^3\dot{x}\dot{y} + 4x^4(Ay - y + 3A^2x^4) - \frac{2}{3}x^6 = \text{const.}$$

8.3. The Painlevé Property for Partial Differential Equations

Ablowitz *et al.* (1980) suggested that a nonlinear partial differential equation is integrable if *all* its exact reductions to ordinary differential equations have the Painlevé property. This approach poses obvious operational difficulties. Weiss *et al.* (1983) and Ward (1984) showed a way to circumvent this difficulty by introducing the Painlevé property directly for the partial differential equations. Ward's proposition was as follows: If S is an analytic non-characteristic hyper surface in the complex space \mathcal{C}^n (n being the number of independent variables), then every solution of the partial differential equation which is analytic on \mathcal{C}^n/S , is meromorphic on \mathcal{C}^n . A weaker version of this Painlevé property was proposed by Weiss *et al.* (1983). According to Weiss *et al.* (1983), a partial differential equation possesses the Painlevé property if its solutions are single-valued about a singular manifold $\phi(x, t) = 0$ ³.

The Painlevé analysis of partial differential equations proposed by Weiss *et al.* (1983) involves (in analogy with that for ordinary differential equations) –

- determination of the leading-order behaviors;
- identification of the powers at which arbitrary functions can enter into the Laurent series called resonances;
- verifying that, at the resonance values, sufficient number of arbitrary functions exist without the introduction of movable critical manifolds; this leads to the determination of certain compatibility conditions which take the form of an auxiliary partial differential equation that the manifold function $\phi = \phi(x, t)$ must satisfy.

EXAMPLE 5

Consider Burgers equation (Weiss *et al.* 1983),

$$u_t + uu_x = u_{xx} \quad (74)$$

The behavior of solutions of equation (74) at a movable singular manifold

$$\phi(x, t) = 0 \quad (75)$$

is determined by a leading-order analysis whereby one makes the ansatz

$$u(x, t) = u_o(x, t)[\phi(x, t)]^\alpha \quad (76)$$

³ The singularities of a function of several complex variables cannot be isolated.

Substituting (76) into equation (74) and balancing the most singular terms uu_x and u_{xx} , we obtain

$$\begin{aligned} u_o \phi^\alpha \left(\alpha u_o \phi^{\alpha-1} \phi_x + u_{ox} \phi^\alpha \right) &\sim \alpha(\alpha-1) u_o \phi^{\alpha-2} \phi_x^2 + \\ &+ \alpha u_o \phi^{\alpha-1} \phi_{xx} + 2\alpha u_{ox} \phi^{\alpha-1} \phi_x + u_{ox} \phi^\alpha \end{aligned}$$

from which,

$$\left. \begin{aligned} 2\alpha - 1 &= \alpha - 2 \text{ or } \alpha = -1 \\ \text{and} \\ u_o &= -2\phi_x \end{aligned} \right\}. \quad (77)$$

The behavior of solutions of equation (74) in the neighborhood of the singular manifold (75) is then determined by constructing a local expansion with (76) as the leading term. Equation (74) is taken to exhibit the Painlevé property if this expansion yields single-valued solutions about the movable singular manifold (75). The powers of ϕ at which the arbitrary coefficient functions appear in the series, i.e., the resonances, are determined by setting

$$u = u_o \phi^{-1} + p \phi^{r-1} \quad (78)$$

and balancing again the most singular terms in equation (74); thus,

$$p \left[-u_o \phi^{r-3} \phi_x + (r-1)u_o \phi^{r-3} \phi_x - (r-1)(r-2)\phi^{r-3} \phi_x^2 - (r-1)\phi^{r-2} \phi_{xx} \right] = 0. \quad (79)$$

Using (77), (79) yields

$$r = -1 \text{ or } 2 \quad (80)$$

The first root $r = -1$ simply corresponds to the arbitrariness of the singular manifold ϕ .

We thus consider a generalized Laurent expansion of the form

$$u = u_o \phi^{-1} + u_1 + u_2 \phi + u_3 \phi^2 + \dots \quad (81)$$

where the u_j 's and ϕ are analytic functions of x and t in the neighborhood of the singular manifold (75). Substitution of (81) into equation (74) then leads to the recursion

relations for the u_j 's which will now take the form of coupled partial differential equations.

Substituting (81) into equation (74) and collecting terms of equal powers of ϕ , we obtain

$$\phi^{-3} : -u_o^2 = 2u_o\phi_x \quad (82)$$

$$\phi^{-2} : -u_o\phi_t + u_ou_{ox} - u_1u_o\phi_x = -2u_{ox}\phi_x - u_o\phi_{xx} \quad (83)$$

$$\phi^{-1} : u_{ot} + u_ou_{1x} + u_ou_2\phi_x + u_1u_{ox} - u_ou_2\phi_x = u_{oxx} \quad (84)$$

$$\phi^0 : u_{1t} + u_1u_{1x} = u_{1xx} + 2u_ou_3\phi_x. \quad (85)$$

Equations (82) and (83) give

$$u_o = -2\phi_x \quad (77)$$

$$\phi_t + u_1\phi_x = \phi_{xx} \quad (86)$$

Using (77) and (86), equation (84) becomes

$$\frac{\partial}{\partial t}(\phi_t + u_1\phi_x - \phi_{xx}) = 0 = 0 \cdot u_2 \quad (87)$$

so that u_2 is arbitrary.

This implies that the generalized Laurent series is a valid "local" representation of the general solution to equation (74) in the neighborhood of a movable singular manifold (75). Therefore, we can say that equation (74) possesses the Painlevé property.

It is of interest to note that further examination of the expansion (81) reveals a non-trivial auto-Backlund transformation (see Ablowitz and Segur (1981) for a detailed account of such transformations) with the equations involving ϕ being transformable into the associated Lax pair (see above reference again).

If we set the arbitrary function u_2 equal to zero, and require that u_1 satisfies the original equation (74),

$$u_{1t} + u_1u_{1x} = u_{1xx} \quad (88)$$

then equation (85) and similar relations corresponding to higher powers of ϕ show that

$$u_j = 0, \quad j \geq 2. \quad (89)$$

Using (89), the expansion (81) leads to the following auto-Backlund transformation for equation (74):

$$u = -2 \frac{\phi_x}{\phi} + u_1 \quad (90)$$

where u and u_1 satisfy equation (74) and ϕ satisfies

$$\phi_t + u_1 \phi_x = \phi_{xx}. \quad (86)$$

The auto-Backlund transformation provides a vehicle to generate new solutions to equation (74) from old solutions.

When $u_1 = 0$, (90) leads to the Cole-Hopf transformation:

$$u = -2 \frac{\phi_x}{\phi} \quad (91)$$

with ϕ satisfying now, from equation (86), the heat equation:

$$\phi_t = \phi_{xx}. \quad (92)$$

On the other hand, when $u_1 = \phi$, (90) yields,

$$u = -2 \frac{\phi_x}{\phi} + \phi \quad (93)$$

with ϕ satisfying, from equation (86), the original equation (74)!

EXAMPLE 6

Consider the Korteweg-deVries equation (Weiss *et al.* 1983),

$$u_t + 6uu_x + u_{xxx} = 0. \quad (94)$$

The leading-order behavior of the solutions of equation (94) at a movable singular manifold

$$\phi(x, t) = 0 \quad (95)$$

is determined by proceeding as before,

$$u \sim -2 \frac{\phi_x^2}{\phi^2}. \quad (96)$$

The resonances are determined by setting

$$u = -2 \frac{\phi_x^2}{\phi^2} + p \phi^{r-2} \quad (97)$$

and balancing the most singular terms in equation (94),

$$p[24\phi^{r-5}\phi_x^3 - 12(r-2)\phi^{r-5}\phi_x^3 + (r-2)(r-3)(r-4)\phi^{r-5}\phi_x^3] = 0$$

or

$$r = -1, 4 \text{ or } 6. \quad (98)$$

The root $r = -1$ is discarded as before.

Consider then a generalized Laurent expansion,

$$u = u_o \phi^{-2} + u_1 \phi^{-1} + u_2 + u_3 \phi + u_4 \phi^2 + u_5 \phi^3 + u_6 \phi^4 + \dots \quad (99)$$

where the u_j 's and ϕ are analytic functions of x and t .

Substituting (99) into equation (94) and collecting terms of equal powers of ϕ , we obtain (Weiss *et al.* 1983),

$$\phi^{-5} : u_o = -2\phi_x^2 \quad (100)$$

$$\phi^{-4} : u_1 = 2\phi_{xx} \quad (101)$$

$$\phi^{-3} : \phi_x \phi_t + 4\phi_x \phi_{xxx} - 3\phi_{xx}^2 + 6\phi_x^2 u_2 = 0 \quad (102)$$

$$\phi^{-2} : \phi_{xt} + 6\phi_{xx} u_2 + \phi_{xxxx} - 6\phi_x^2 u_3 = 0 \quad (103)$$

$$\phi^{-1} : \frac{\partial}{\partial x} (\phi_{xt} + 6\phi_{xx}u_2 + \phi_{xxx} - 6\phi_x^2 u_3) = 0 = 0 \cdot u_4 \quad (104)$$

$$\phi^0 : u_{2t} + u_{2xxx} + 6u_2u_{2x} - 6u_5\phi_x^3 = 0. \quad (105)$$

Equation (104) shows that u_4 is arbitrary, and it may be verified that u_6 is also arbitrary.

If we now,

- set the arbitrary functions u_4 and u_6 equal to zero,
- require that u_2 satisfies the original equation (94),
- set u_3 also equal to zero,

then equation (105) and similar relations corresponding to higher powers of ϕ show that

$$u_j = 0, \quad j \geq 3. \quad (106)$$

Using (106), the expansion (99) leads to the following auto-Backlund transformation for equation (94):

$$u = 2 \frac{\partial^2}{\partial x^2} \log \phi + u_2 \quad (107)$$

where u and u_2 satisfy equation (94) and ϕ satisfies

$$\phi_x \phi_t + 4\phi_x \phi_{xxx} - 3\phi_{xx}^2 + 6u_2\phi_x^2 = 0 \quad (102)$$

and

$$\phi_{xt} + \phi_{xxx} + 6u_2\phi_{xx} = 0. \quad (103)$$

On substituting

$$\phi_x = \psi^2 \quad (104)$$

equations (102) and (103) transform into the Lax pair for equation (94):

$$\psi_{xx} + (\lambda + u_2)\psi = 0 \quad (108)$$

$$\psi_t + 4\psi_{xx} + 6u_2\psi_x + 3u_x\psi = 0. \quad (109)$$

EXERCISES

Chapter 1

1. Locate equilibria, determine their nature and find the phase-plane portrait for the system (Bender and Orszag, (1978)):

$$\left. \begin{array}{l} \dot{x} = x^2 - xy - x \\ \dot{y} = y^2 + xy - 2y \end{array} \right\}.$$

2. Find the limit cycle for the system

$$\begin{aligned} \frac{dx}{dt} &= -y + \frac{x(1-x^2-y^2)}{\sqrt{x^2+y^2}} \\ \frac{dy}{dt} &= x + \frac{y(1-x^2-y^2)}{\sqrt{x^2+y^2}}. \end{aligned}$$

3. A damped vertical pendulum has the following equation of motion –

$$\ddot{\psi} + k\dot{\psi} + \omega^2 \sin \psi = 0, \quad (k > 0)$$

where ψ is the angle between the pendulum and the downward vertical. Determine the position and nature of the fixed points. Sketch the phase-plane curves to show all the qualitative features of the motion. Describe what happens to the motion and fixed points as $k \rightarrow 0$ and when $k = 0$.

4. Determine the flow on the local center manifold near the origin for the following system (Guckenheimer and Holmes, (1986)) –

$$\begin{aligned} \dot{x} &= \alpha x^2 - y^2 \\ \dot{y} &= -y + x^2 + xy. \end{aligned}$$

5. Consider a van der Pol's oscillator under external excitation –

$$\ddot{x} + x = \varepsilon(1-x^2)\dot{x} + \varepsilon F \cos \lambda t, \quad \varepsilon \ll 1.$$

Study the forced oscillations for the cases $\lambda \neq 1$ and $\lambda \approx 1$. For the latter case, determine the equilibrium points and their stability. Represent this information on the $|x|^2, \left(\frac{1-\lambda}{\varepsilon}\right)$ -plane, for the case $\lambda \approx 1$.

Chapter 2

1. Consider the differential equation

$$\dot{u} = u(\mu - u) + \varepsilon$$

where ε is a real number. If $\varepsilon = 0$, there are two bifurcating solutions. Show that if $\varepsilon > 0$, the bifurcation is broken.

2. Consider the differential equation

$$\frac{du}{dt} = r\left(1 - \frac{u}{k}\right)u - \mu, \quad r \text{ and } k > 0.$$

Investigate the stability of equilibrium solutions as μ passes through the value $rk/4$, and identify the type of bifurcation involved (Logan, (1987)).

3. For the following differential equation determine the equilibrium solutions and sketch a branching diagram. Identify the bifurcation points and bifurcating solutions. Investigate the stability of equilibrium solutions, and identify the type of bifurcation involved (Logan, (1987)):

$$\frac{du}{dt} = (u - \mu)(u^2 - \mu).$$

4. For the following system of equations show that there is a Hopf bifurcation from the zero solution $x = 0, y = 0$ at $\mu = 0$ (Grimshaw, (1990)):

$$\begin{cases} \frac{dx}{dt} = \mu x + y - xy^2 \\ \frac{dy}{dt} = -x + \mu y \end{cases}.$$

Chapter 3

1. Consider a plane vertical pendulum made of a mass m attached to one end of a light rod of length l , with the other end moving horizontally in the plane of the motion, so that its distance from a fixed point is given by a known function, $\gamma(t)$, of time. Show that the Hamiltonian is given by

$$H = \frac{p_\psi^2}{2ml^2} + ml[\ddot{\gamma}(t)\sin\psi - g\cos\psi]$$

where ψ is the angle between the pendulum and the downward vertical. For the particular case $\dot{\gamma}(t) = \text{constant}$, determine the fixed points, discuss their stability, and find the period of small oscillations about any elliptic fixed points, (Percival and Richards, (1982)).

2. Consider the time-dependent Hamiltonian

$$H = \frac{1}{2}\left(p^2 + \omega^2 q^2\right) - \frac{A}{2\omega}(p\cos\Omega t + \omega q\sin\Omega t).$$

In terms of the action-angle variables (J, θ) of free oscillator, show that

$$\bar{H}(J, \theta, t) = \omega J - A\sqrt{\frac{J}{2\omega}} \cos(\theta - \Omega t).$$

Find the canonical transformation which reduces \bar{H} to a time-independent Hamiltonian $\bar{\bar{H}}$

$$\bar{\bar{H}}(\phi, \hat{J}) = (\omega - \Omega)\hat{J} - A\sqrt{\frac{\hat{J}}{2\omega}} \cos\phi$$

where $\hat{J} = J$, (Percival and Richards, (1982)).

3. If F_1 and F_2 are two constants of motion, then show that so is the Poisson Bracket $[F_1, F_2]$. (Repeated application of this result can in principle lead to a complete sequence of constants of the motion.)

Chapter 4

1. Consider the motion of a vertical pendulum which is rotating fast enough for the gravitational forces to be considered as a small perturbation. For this problem, the unperturbed Hamiltonian is

$$H_o = \frac{1}{2} p^2$$

and the perturbation is

$$H_1 = -\omega_o^2 \cos q.$$

Use the perturbation theory to show that the energy and frequency of rotation are

$$\left. \begin{aligned} \bar{H}(\hat{J}) &= \frac{1}{2} \hat{J}^2 + \frac{1}{4} \varepsilon^2 \frac{\omega_o^4}{\hat{J}^2} + O(\varepsilon^3) \\ \omega(\hat{J}) &= \hat{J} - \frac{1}{2} \varepsilon^2 \frac{\omega_o^4}{\hat{J}^3} + O(\varepsilon^3) \end{aligned} \right\}$$

(Percival and Richards (1982)).

2. A linear harmonic oscillator has its mass suddenly increased by a fractional amount ε . Using the canonical perturbation theory find the resultant shift in the frequency to first order in ε . Show that, to the same order in ε , your result agrees with the rigorous prediction for the shift.
3. To lowest order in correction terms, the relativistic Hamiltonian for the one-dimensional harmonic oscillator has the form

$$H = \frac{1}{2m} (p^2 + m^2 \omega^2 q^2) - \frac{1}{8} \frac{p^4}{m^3 c^2}.$$

Using the canonical perturbation theory calculate the lowest order relativistic correction to the frequency of the harmonic oscillator.

Chapter 5

1. For the following area-preserving mapping of the unit torus on itself,

$$T: \begin{bmatrix} x_{n+1} \\ y_{n+1} \end{bmatrix} = \begin{bmatrix} 1 & 1 \\ 1 & 2 \end{bmatrix} \begin{bmatrix} x_n \\ y_n \end{bmatrix}, \quad \begin{array}{l} \text{mod } x = 1 \\ \text{mod } y = 1 \end{array}$$

find the fixed points, eigenvalues and eigenvectors and Liapunov exponents of T and $T^{[2]}$.

2. For the following area-preserving mapping of the unit torus on itself,

$$T: \begin{bmatrix} x_{i+1} \\ y_{i+1} \end{bmatrix} = \begin{bmatrix} x_i + y_{i+1} \\ y_i + \frac{k}{2\pi} \sin 2\pi x_i \end{bmatrix}, \quad \begin{array}{l} \text{mod } x = 1 \\ \text{mod } y = 1 \end{array}$$

investigate the tangent map, show that it is area-preserving and find its eigenvalues and hence determine the conditions for the stability of a given closed orbit (Chirikov (1979)).¹

¹ This map corresponds to the so-called kicked rotator model wherein a rotator with moment of inertia ma^2 is kicked with an impulse $F\Delta t \sin 2\pi x$ at equal time intervals Δt apart. $2\pi x$ denotes the angular position at the instant the impulse acts. Normalizing the angular momentum J according to $y = \frac{J\Delta t}{ma^2}$ and putting $k = \frac{F(\Delta t)^2}{ma}$ we find the following equation for the increase in angular momentum from the i th kick –

$$y_{i+1} = y_i + \frac{k}{2\pi} \sin 2\pi x_i.$$

Next, the motion between the kicks is a uniform rotation so that the increase of the angular position between the i th and $(i+1)$ -th kick is given by

$$x_{i+1} = x_i + y_{i+1}.$$

It may be noted that this model leads to the simple pendulum in an appropriate limit. Thus, in the limit, k and y both small, the differences in the above equations can be replaced by derivatives so that

$$\left. \begin{array}{l} \lim_{k,y \rightarrow 0} T \rightarrow \dot{y} = \frac{k}{2\pi} \sin 2\pi x \\ \dot{x} = y \end{array} \right\}$$

3. Establish the smoothing effect of the following mapping

$$W_n(x) = \frac{1}{2} \left[W_{n-1}\left(\frac{x}{2}\right) + W_{n-1}\left(\frac{x+1}{2}\right) \right]$$

by demonstrating that the iterations must destroy all Fourier components $e^{2\pi i l x}$ ($l = 1, 2, \dots$) describing the variation of $W_n(x)$, (Berry, (1978)).

Chapter 6

1. Construct a Cantor set as follows. Remove from the middle of a unit interval, a segment of length b , $0 < b < 1$. Repeat the process on each remaining segment of length $(1-b)/2$, ad infinitum. Calculate the fractal dimension of the resulting Cantor set S .
2. Find the fractal dimension of Smale's horseshoe attractor. Investigate the limits of negligible dissipation ($\eta \rightarrow 1$) and strong dissipation ($\eta \rightarrow \infty$).
3. Consider the transformation –

$$x_{n+1} = 2x_n \bmod 1$$

$$y_{n+1} = \begin{cases} ay_n, & 0 \leq x_n \leq \frac{1}{2} \\ ay_n + \frac{1}{2}, & \frac{1}{2} \leq x_n \leq 1 \end{cases}.$$

Show that this transformation is dissipative if $a < 1/2$. Find the fractal dimension d_y in the y -direction of the attractor of the orbit $\{x_n, y_n\}$. Show that the attractor is a Cantor set in the y -direction, i.e., after infinite iterations, the attractor occupies a region of zero length in the y -direction.

4. Consider the logistic map

$$x_{n+1} = 4\lambda x_n(1-x_n).$$

Find an exact solution for this equation for the case $\lambda = 1$ by making a simple change of variables

$$x_n = \frac{1 - \cos 2\pi\theta_n}{2}.$$

By representing the iterates for θ in binary notation, show that the solution exhibits chaotic behavior in the sense that for large n , θ_n has a value which is extremely sensitive to the exact value of θ_0 .

5. Show that the logistic map

$$x_{n+1} = 4\lambda x_n(1 - x_n)$$

has the period-2 cycle made up of the two fixed points

$$x_{1,2}^* = \frac{(4\lambda + 1) \pm \sqrt{(4\lambda - 3)(4\lambda + 1)}}{8\lambda}$$

and that this period-2 cycle becomes unstable when $\lambda > \frac{1 + \sqrt{6}}{4}$.

6. For the case $b = 2\sigma$, show that the Lorenz equations can be combined to give

$$\frac{d^2x}{dt^2} + (\sigma + 1)\frac{dx}{dt} + \sigma(1 - r)x = -\frac{x^3}{2}.$$

Determine the equilibria and their stability for this equation. Develop a description for the nonlinear approach to the steady supercritical convective flow state.

Chapter 7

1. If fluid temperature Θ is assumed to be a dynamically passive scalar, it would be randomized through advection by the turbulent fluid according to the transport equation

$$\frac{\partial \theta}{\partial t} + \nu \cdot \nabla \theta = \kappa \nabla^2 \theta$$

where κ is the thermal diffusivity of the fluid. One may then make arguments similar to those in the Kolmogorov's (1941) universal equilibrium theory for the turbulent velocity field to surmise that the small-scale structure of the temperature field has a measure of universality and, in a statistical sense, depends only weakly on the large-scale features. Experiments (Antonia *et al.* (1984) and Meneveau *et al.*

(1990)) indicated that the small-scale statistics is not Gaussian. Assuming (as suggested by Mandelbrot (1976) previously) that these intermittency effects are related to the fractal aspects of the geometry of turbulence, use the multi-fractal idea to calculate the characteristic exponent $\hat{\zeta}_p$ for the temperature structure function and the generalized fractal dimension \hat{D}_q of the scalar-variance dissipation field (Shivamoggi (1992, 1995a)).

2. Explore the possibility to describe the intermittency effects of the temperature field alternatively by generalizing the random- β model of Benzi *et al.* (1984) for the turbulent velocity field (Shivamoggi (1992, 1995a)).
3. The power-law scaling behavior via a multi-fractal model for a passive scalar diffusing in a random velocity field, mentioned in problems 1 and 2 above, breaks down in an intermediate dissipation range. Show that, upon using a suitable rescaling, however, the multi-fractal in question can still exhibit a multi-scaling behavior with certain universal features (Shivamoggi, (1995b)).

Chapter 8

1. A truncated modal expansion of the equations governing nonlinear motions in a warm electron-beam plasma leads to the following system of coupled nonlinear ordinary differential equations (Rollins and Shivamoggi, (1993)) –

$$\left. \begin{aligned} \dot{x} &= vx + (1-x)y \\ (1-x)\dot{y} &= -qx - \mu z + (1+x)y^2 + 2vxy \\ \dot{z} &= y + (v-y)z \end{aligned} \right\}$$

where μ and q are positive parameters, and v is a parameter which can be either positive or negative. Determine if this system of equations admits the Painlevé property.

2. By using a similarity reduction

$$u = t^{-2/3} F(\zeta), \quad \zeta = \frac{x}{t^{1/3}}$$

the generalized Korteweg-deVries equation

$$u_t + u^p u_x + u_{xxx} = 0$$

becomes a nonlinear ordinary differential equation (Rollins and Shivamoggi, (1994))

$$F''' + F^p F' - \frac{1}{3} \zeta F' - \frac{2}{3p} F = 0.$$

- Investigate the admission of the Painlevé property by this equation.
3. The nonlinear evolution of a modulated gravity wavetrain in deep water is governed by a nonlinear Schrödinger equation,

$$iu_t - u_{xx} + u_{yy} = \mu |u|^2 u, \quad \mu > 0.$$

By making similarity reduction,

$$u(x, y, t) = V(\xi) e^{i\lambda t + \theta(\xi)}, \quad \xi = x^2 - y^2$$

the above equation leads to the following coupled nonlinear ordinary differential equations (Shivamoggi and Rollins, (1994))

$$\left. \begin{aligned} -\lambda V - V' - \xi^2 V'' + \xi^2 V \theta'^2 &= \mu V^3 \\ -V\theta' - 2\xi^2 V'\theta' - \xi^2 V\theta'' &= 0 \end{aligned} \right\}.$$

- Investigate the admission of the Painlevé property by this system equations.
4. Use the method of Weiss *et al.* (1983) to investigate the Painlevé property directly for the modified Korteweg-deVries equation,

$$u_t - 6u^2 u_x + u_{xxx} = 0.$$

5. Use the method of Weiss *et al.* (1983) to investigate the Painlevé property directly for the Zakharov-Kuznetsov equation which describes the nonlinear propagation of ion-acoustic waves in a magnetized plasma, (Shivamoggi and Rollins, (1991)),

$$u_t + uu_x + u_{xxx} + u_{xyy} = 0.$$

References

- Abarbanel, H.D.I., Brown, R., Sidorowich, J.J. and Tsimring, L. Sh. (1993): The analysis of observed chaotic data in physical systems, *Rev. Mod. Phys.* **65**, 1331.
- Ablowitz, M.J., Ramani, A., and Segur, H. (1980): A connection between nonlinear evolution equations and ODE's of P-type I and II, *J. Math Phys.* **21**, 715 and 1006.
- Ablowitz, M.J. and Segur, H. (1981): *Solitons and the Inverse-Scattering Transform*, SIAM, Philadelphia.
- Andrews, L.C., Phillips, R.L., Shivamoggi, B.K., Beck, J.K., and Joshi, M. (1989): A statistical theory for the distribution of energy dissipation in intermittent turbulence, *Phys. Fluids A* **1**, 999.
- Anselmet, F., Hopfinger, E.J., Gagne, Y., and Antonia, R.A. (1984): High-order velocity structure functions in turbulent shear flows, *J. Fluid Mech.* **140**, 63.
- Antonia, R.A., Hopfinger, E.J. Gagne, Y., and Anselmet, F. (1984): Temperature structure functions in turbulent shear flows, *Phys. Rev. A* **30**, 2704.
- Arnol'd, V.I. (1963): Small denominators and the problem of stability of motion in classical and celestial mechanics, *Russ. Math. Surveys* **18**, 85.
- Arnol'd, V.I. (1973): *Ordinary Differential Equations*, MIT Press.
- Arnol'd, V.I. (1978): *Mathematical Methods of Classical Mechanics*, Springer-Verlag.
- Arnol'd, V.I. and Avez, A. (1968): *Ergodic Problems of Classical Mechanics*, Benjamin/Cummings, Reading, MA.
- Baker, G.L. and Gollub, J.P. (1996): *Chaotic Dynamics*, Cambridge University Press.
- Barnsley, M. (1988): *Fractals Everywhere*, Academic Press.

- Batchelor, G.K. and Townsend, A.A. (1949): The nature of turbulent motion at large wavenumbers, *Proc. Roy. Soc. (London) A* **199**, 238.
- Bender, C. and Orszag, S.A. (1978): *Advanced Mathematical Methods for Scientists and Engineers*, McGraw-Hill.
- Bennettin, G., Brambilla, R., and Galgani, L. (1977): A comment on the reliability of the Toda criterion for the existence of a stochastic transition, *Physica* **87A**, 381.
- Bennettin, G., Galgani, L., and Strelcyn, J.M. (1976): Kolmogorov entropy and numerical experiments, *Phys. Rev. A* **14**, 2338.
- Benzi, R., Ciliberto, S., Baudet, C., Massaili, F., Tripiccione, R., and Succi, S. (1993): Extended self-similarity in turbulent flows, *Phys. Rev. E* **48**, 29.
- Benzi, R., Paladin, G., Parisi, G., and Vulpiani, A. (1984): On the multifractal nature of fully-developed turbulence, *J. Phys. A* **17**, 3521.
- Bergé, P., Pomeau, Y., and Vidal, C. (1984): *Order Within Chaos: Towards a Deterministic Approach to Turbulence*, Wiley & Sons, Inc.
- Berry, M.V. (1978): Regular and irregular motion, in *Topics in Nonlinear Dynamics*, Amer. Inst. Phys. Conf. Proc. **46**, 16.
- Berry, M.V., Balazs, N.L., Tabor, M., and Voros, A. (1979): Quantum maps, *Ann. Phys. NY* **122**, 26.
- Birkhoff, G.D. (1927): *Dynamical Systems*, American Mathematical Society.
- Bountis, T., Segur, H., and Vivaldi, F. (1982): Integrable Hamiltonian systems and the Painlevé property, *Phys. Rev. A* **25**, 1257.
- Brachet, M.E., Meiron, D.I., Orszag, S.A., Nickel, B.G., Morf, R.H., and Frisch, U. (1983): Small-scale structure of the Taylor-Green vortex, *J. Fluid Mech.* **130**, 411.
- Brachet, M.E., Meneguzzi, M., Vincent, A., Politano, H., and Sulem, P.L. (1992): Numerical evidence of smooth self-similar dynamics and possibility of subsequent collapse for three-dimensional ideal flows, *Phys. Fluids A* **4**, 2845.
- Cary, J.R. (1981): Lie transforms and their use in Hamiltonian perturbation theory, *Phys. Reports* **79**, 129.

- Casati, G. and Ford, J. (1975): Stochastic transition in the unequal-mass Toda lattice, *Phys. Rev. A* **12**, 1702.
- Cerjan, C. and Reinhardt, W.P. (1979): Critical point analysis of instabilities in Hamiltonian systems, *J. Chem. Phys.* **71**, 1819.
- Chang, Y.F., Tabor, M., Weiss, J., and Corliss, C. (1981): On the analytic structure of the Hénon-Heiles system, *Phys. Lett. A* **85**, 211.
- Chen, S.S., Doolen, G., Herring, J.R., Kraichnan, R.H., Orszag, S.A., and She, Z.S. (1993): Far dissipation range of turbulence, *Phys. Rev. Lett.* **70**, 3051.
- Chirikov, B. (1979): A universal instability of many-dimensional oscillator systems, *Phys. Reports* **52**, 263.
- Collet, P. and Eckmann, J.P. (1980): *Iterated Maps of the Unit Interval as Dynamical Systems*, Birkhauser, Boston.
- Corben, H.C. and Stehle, P. (1974): *Classical Mechanics*, Krieger, Huntington, NY.
- Crawford, J.D. (1991): Introduction to bifurcation theory, *Rev. Mod. Phys.* **63**, 991.
- Devaney, R.L. (1989): *An Introduction to Chaotic Dynamical Systems*, Addison-Wesley, Reading, MA.
- Dorizzi, B., Grammaticos, B., and Ramani, A. (1984): A new class of integrable systems, *J. Math. Phys.* **25**, 481.
- Douady, S., Couder, Y., and Brachet, M.E. (1991): Direct observation of the intermittency of intense vorticity filaments in turbulence, *Phys. Rev. Lett.* **67**, 983.
- Dowell, E.H. (1984): Observation and evolution of chaos for an autonomous system, *J. Appl. Mech.* **51**, 664.
- Drazin, P.G. (1992): *Nonlinear Systems*, Cambridge University Press.
- Eckmann, J.P. (1981): Roads to turbulence in dissipative dynamical systems, *Rev. Mod. Phys.* **53**, 643.
- Eckmann, J.P. and Ruelle, D. (1985): Ergodic theory of chaos and strange attractors, *Rev. Mod. Phys.* **57**, 617.

- Ekeland, I. (1987): *Mathematics and the Unexpected*, University of Chicago Press.
- Escande, D.F. (1985): Stochasticity in classical Hamiltonian systems: universal aspects, *Phys. Reports* **121**, 165.
- Eubank, S. and Farmer, D. (1989): An introduction to chaos and randomness, in *Lectures in Complex Systems*, Ed. E. Jen, Addison Wesley, Reading, MA.
- Falconer, K. (1990): *Fractal Geometry: Mathematical Foundations and Applications*, Wiley & Sons, Inc.
- Farmer, J.D. (1982): Information dimension and the probabilistic structure of chaos, *Z. Naturforsch.* **37a**, 1304.
- Farmer, J.D., Ott, E., and Yorke, J.A. (1983): The dimension of chaotic attractors, *Physica D* **7**, 153.
- Feder, J. (1988): *Fractals*, Plenum Press.
- Feigenbaum, M.J. (1978): Quantitative universality for a class of nonlinear transformations, *J. Stat. Phys.* **19**, 25.
- Fermi, E., Pasta, J., and Ulam, S. (1955): Studies of nonlinear problems, Los Alamos Sci. Lab., Report LA-1940.
- Ford, J. and Waters, J. (1963): Computer studies of energy sharing and ergodicity for nonlinear oscillator systems, *J. Math. Phys.* **4**, 1293.
- Ford, J. (1975): The statistical mechanics of analytical dynamics, in *Fundamental Problems in Statistical Mechanics*, Ed. E.G.D. Cohen, Vol. 3, North-Holland.
- Frisch, U. (1985): Fully developed turbulence: Where do we stand, *Phys. Scripta* **T9**, 137.
- Frisch, U. and Parisi, G. (1985): On the singularity structure of fully-developed turbulence, in *Turbulence and Predictability in Geophysics and Climate Dynamics*, Ed. M. Ghil, R. Benzi and G. Parisi, p. 84, North-Holland.
- Frisch U., Sulem, P.L., and Nelkin, M. (1978): A simple dynamical model of intermittent fully developed turbulence, *J. Fluid Mech.* **87**, 719.

- Frisch, U. and Vergassola, M. (1991): A prediction of the multifractal model: The intermediate dissipation range, *Europhys. Lett.* **14**, 439.
- Froyland, J. (1992): *Introduction to Chaos and Coherence*, Inst. of Physics Publ., Bristol.
- Gibson, C.H., Stegen, G.R., and McConnell, S. (1970): Measurements of the universal constant in Kolmogorov's third hypothesis for high reynolds number turbulence, *Phys. Fluids* **13**, 2448.
- Gleick, J. (1987): *Chaos*, Penguin Books.
- Goldstein, H. (1980): *Classical Mechanics*, Addison-Wesley, Reading, MA.
- Golubov, V.V. (1953): *Lectures on Integration of the Equations of Motion of a Rigid Body About a Fixed Point*, State Publg. House, Moscow.
- Grassberger, P. and Proccacia, I. (1983): Characterization of strange attractors, *Phys. Rev. Lett.* **50**, 346.
- Grebogi, C., Ott, E., and Yorke, J.A. (1987): Chaos, strange attractors and fractal basin boundaries in nonlinear dynamics, *Science* **238**, 632.
- Greene, J.M. (1979): A method of determining a stochastic transition, *J. Math. Phys.* **20**, 1183.
- Greene, J.M., MacKay, R.S., Vivaldi, F., and Feigenbaum, M.J. (1981): Universal behavior of area-preserving maps, *Physica* **3D**, 468.
- Grimshaw, R. (1990): *Nonlinear Ordinary Differential Equations*, Blackwell, Boston.
- Guckenheimer, J. and Holmes, P. (1986): *Nonlinear Oscillations, Dynamical Systems, and Bifurcations of Vector Fields*, Springer-Verlag.
- Gulick, D. (1992): *Encounters with Chaos*, McGraw-Hill.
- Hagedorn, P. (1988): *Nonlinear Oscillations*, Oxford University Press.
- Hale, J. and Kocák, H. (1991): *Dynamics and Bifurcations*, Springer-Verlag.

- Hale, J. and Kocák, H. (1991): *Dynamics and Bifurcations*, Springer-Verlag.
- Hall, L.S. (1983): On the existence of a last invariant of conservative motion, *Physica D* **8**, 90, (1983).
- Halsey, T.C., Jensen, M.H., Kadanoff, L.P., Proccacia, I., and Shraiman, B.I. (1986): Fractal measures and their singularities: Characterization of strange sets, *Phys. Rev. A* **33**, 1141.
- Helleman, R.H.G. (1980): Self-generated chaotic behavior in nonlinear mechanics, in *Fundamental Problems in Statistical Mechanics*, Vol. 5, Ed. E.G.D. Cohen, North-Holland.
- Hénon, M. (1969): Numerical study of quadratic area-preserving mappings, *Q. Appl. Math.* **27**, 291.
- Hénon, M. (1976): A two-dimensional mapping with a strange attractor, *Commun. Math. Phys.* **50**, 69.
- Hénon, M. and Heiles, C. (1974): The applicability of the third integral of motion: Some numerical experiments, *Astron. J.* **69**, 73.
- Hentschel, H.G.E. and Proccacia, I. (1983): The infinite number of generalized dimensions of fractals and strange attractors, *Physica* **8D**, 435.
- Hilborn, R.C. (1994): *Chaos and Nonlinear Dynamics*, Oxford University Press.
- Hillé, E. (1976): *Ordinary Differential Equations in the Complex Plane*, Wiley & Sons, Inc..
- Hirsch, M. and Smale, S. (1974): *Differential Equations, Dynamical Systems and Linear Algebra*, Academic Press.
- Holton, D. and May, R.M. (1993): Chaos and one-dimensional maps, in *The Nature of Chaos*, Ed. T. Mullin, Clarendon Press.
- Hu, B.N. (1982): Introduction to real-space renormalization-group methods in critical and chaotic phenomena, *Phys. Rep.* **91**, 233.
- Ince, C.L. (1956): *Ordinary Differential Equations*, Dover.

- Jackson, E.A. (1963): Nonlinearly-coupled oscillators: I. Perturbation theory, ergodic problem; II. Comparison of theory with computer solutions, *J. Math. Phys.* **4**, 551 and 686.
- Jensen, M.H., Paladin, G., and Vulpiani, A. (1991): Multiscaling in multifractals, *Phys. Rev. Lett.* **67**, 208.
- Kabakow, H. (1968): A perturbation procedure for nonlinear oscillations, Ph.D. Thesis, California Institute of Technology.
- Kaplan, J.L. and Yorke, J.A. (1979): Chaotic behavior of multi-dimensional difference equations, in *Functional Differential Equations and Approximations of Fixed Points*, Ed. H.-O. Peitgen and H.O. Walter, *Lecture Notes in Mathematics* **730**, Springer-Verlag.
- Kerr, R.M. (1985): Higher-order derivative correlations and the alignment of small-scale structures in isotropic numerical turbulence, *J. Fluid Mech.* **153**, 31.
- Kevorkian, J. (1980): Resonance in a weakly-nonlinear system with slowly-varying parameters, *Studies Appl. Math.* **62**, 23.
- Kolmogorov, A.N. (1941): The local structure of turbulence in imcompressible viscous fluid at very large Reynolds numbers, *C.R. Acad. Sci. USSR* **30**, 299.
- Kolmogorov, A.N. (1954): On the preservation of quasi-periodic motions under a small variation of Hamilton's function, *Dokl. Akad. Nauk SSSR* **98**, 525.
- Kolmogorov, A.N. (1958): A new invariant of transitive dynamical systems, *Dokl. Akad. Nauk SSSR* **119**, 861.
- Kolmogorov, A.N. (1962): A refinement of previous hypotheses concerning the local structure of turbulence in a viscous incompressible fluid at high Reynolds numbers, *J. Fluid Mech.* **13**, 82.
- Kraichnan, R.H. (1974): On Kolmogorov's inertial range theories, *J. Fluid Mech.* **62**, 305.
- Lakshmanan, M. and Sahadevan, R. (1993): Painlevé analysis, Lie symmetries and integrability of coupled nonlinear oscillators, *Phys. Reports* **224**, 1.
- Landau, L.D. (1944): On the nature of turbulence, *Soviet Phys. Dokl.* **44**, 139.

- Landau, L.D. and Lifshitz, E.M. (1987): *Fluid Mechanics*, Pergamon Press, Oxford.
- Lanford, O.E. (1982): The strange attractor theory of turbulence, *Ann. Rev. Fluid Mech.* **14**, 347.
- Lauwerier, H. (1991): *Fractals*, Princeton University Press.
- Lebowitz, J. and Penrose, O. (1973): Modern ergodic theory, *Physics Today* **26**, 23.
- Libchaber, A., Fauve, S., and Larouche, C. (1983): Two parameter study of routes to chaos, *Physica* **7D**, 73.
- Libchaber, A. and Maurer, J. (1980): One experience de Rayleigh-Benard de geometric reduite: multiplication, accrochage, et demultiplication de frequencies, *J. Phys. Colloq.* **41**, 51.
- Lichtenberg, A.J. and Lieberman, M.A. (1992): *Regular and Chaotic Dynamics*, Springer-Verlag.
- Lighthill, M.J. (1986): The recently recognized failure of predictability in Newtonian dynamics, *Proc. Roy. Soc. (London) A* **407**, 35.
- Logan, J.D. (1987): *Applied Mathematics*, Wiley & Sons, Inc.
- Lorenz, E.N. (1963): Deterministic nonperiodic flow, *J. Atmos. Sci.* **20**, 130.
- Ma, S.K. (1976): *Modern Theory of Critical Phenomena*, Benjamin/Cummings, Reading, MA.
- MacKay, R.S. (1985): Introduction to the dynamics of area-preserving maps, *Proc. Spring College on Plasma Phys.*, Trieste, World-Scientific.
- Mandelbrot, B. (1974): Intermittent turbulence in self-similar cascades: divergence of high moments and dimension of the carrier, *J. Fluid Mech.* **62**, 331.
- Mandelbrot, B. (1976): Intermittent turbulence and fractal dimension: Kurtosis and the spectral exponent $5/3 + B$, in *Turbulence and Navier-Stokes Equations*, Ed. R. Temam, *Lecture Notes in Mathematics*, Vol. 65, p. 121, Springer-Verlag.
- Mandelbrot, B. (1983): *The Fractal Geometry of Nature*, Freeman.

- Mandelbrot, B. (1989): Multifractal measures, in *Fractals in Geophysics*, Ed. C.H. Scholz and B. Mandelbrot, Birkhauser, Boston.
- Manneville, P. and Pomeau, Y. (1979): Intermittency and the Lorenz model, *Phys. Lett.* **75A**, 1.
- Marsden, J.E. and McCracken, M(1976): *The Hopf Bifurcation and Its Applications*, Spring-Verlag.
- May, R.M. (1976): Simple mathematical models with very complicated dynamics, *Nature*, **261**, 459.
- McCauley, J.L. (1988): An introduction to nonlinear dynamics and chaos theory, *Phys. Scripta* **T20**.
- McCauley, J.L. (1990): Introduction to multifractals in dynamical systems theory and fully developed turbulence, *Phys. Reports* **189**, 225.,
- McCauley, J.L. (1993): *Chaos, Dynamics and Fractals*, Cambridge University Press.
- McLaughlin, J.B. and Martin, P.C. (1975): Transition to turbulence in a statically stressed fluid system, *Phys. Rev. A* **12**, 186.
- Melnikov, V.K. (1963): On the stability of the center for time-periodic perturbations, *Trans. Moscow Math. Soc.* **12**, 1.
- Meneveau, C. and Sreenivasan, K.R. (1987): Simple multifractal cascade model for fully developed turbulence, *Phys. Rev. Lett.* **59**, 1424.
- Meneveau, C. and Sreenivasan, K.R. (1991): The multifractal nature of turbulent energy dissipation, *J. Fluid Mech.* **224**, 429.
- Miura, R.M. (1976): The Korteweg-deVries equation: A survey of results, *SIAM Rev.* **18**, 412.
- Moser, J. (1962): On invariant curves of area-preserving mappings on an annulus, *Nachr. Akad. Wiss. Goettingen Math. Phys.* **K1**, 1.
- Moser, J. (1973): *Stable and random motions in dynamical systems*, Princeton University Press.

- Myrberg, P.J. (1958): Iteration Von quadratwurzeloperationen, *Annals. Acad. Sci. Fennicae AI Math.* **259**, 1.
- Nayfeh, A.H. and Balachandran, B. (1995): *Applied Nonlinear Dynamics*, Wiley Interscience.
- Nicolis, G. (1995): *Introduction to Nonlinear Science*, Cambridge University Press.
- Novikov, E.A. (1971): Intermittency and scale similarity in the structure of a turbulent flow, *Prikl. Mat. Mech.* **35**, 266.
- Obukhov, A.M. (1962): Some specific features of atmospheric turbulence, *J. Fluid Mech.* **13**, 77.
- Osledec, V.D. (1968): A multiplicative ergodic theorem: Liapunov characteristic numbers for dynamical systems, *Trans. Moscow Math. Soc.* **19**, 197.
- Ott, E. (1981): Strange attractors and chaotic motions of dynamical systems, *Rev. Mod. Phys.* **53**, 655.
- Ott, E. (1993): *Chaos in Dynamical Systems*, Cambridge University Press.
- Ozorio de Almeida, A.M. (1988): *Hamiltonian Systems: Chaos and Quantization*, Cambridge University Press.
- Percival, I. and Richards, D. (1982): *Introduction to Dynamics*, Cambridge University Press.
- Peitgen, H.-O., Jürgens, H., and Saupe, D. (1992): *Chaos and Fractals*, Springer-Verlag.
- Pesin, Ya.B. (1977): Characteristic Liapunov exponents and smooth ergodic theory, *Russ. Math. Surveys* **32**, 55.
- Poincaré, H. (1892): *Les Methods Nouvelles de la Mecanique Celeste*, Gauthier-Villars.
- Pomeau, Y. and Manneville, P. (1980): Intermittent transition to turbulence in dissipative dynamical systems, *Comm. Math. Phys.* **74**, 189.
- Proccacia, I. (1988): Universal properties of dynamically complex systems: Organization of chaos, *Science* **353**, 618.

- Ramani, A., Dorizzi, B., and Grammaticos, B. (1982): Painlevé conjecture revisited, *Phys. Rev. Lett.* **49**, 1539.
- Ramani, A., Dorizzi, B., Grammaticos, B. and Bountis, T. (1984): Integrability and the Painlevé property for low-dimensional systems, *J. Math. Phys.* **25**, 878.
- Ramani, A., Grammaticos, B. and Bountis, T. (1989): The Painlevé property and singularity analysis of integrable and non-integrable systems, *Phys. Reports* **180**, 159.
- Rasband, S.N. (1990): *Chaotic Dynamics of Nonlinear Systems*, Wiley & Sons, Inc.
- Rayleigh, Lord: (1916) On convection currents in a horizontal layer of fluid, when the higher temperature is on the under side, *Phil. Mag.* **32**, 529.
- Richardson, L.F. (1922): *Weather Prediction by Numerical Process*, Cambridge University Press.
- Rollins, D.K. and Shivamoggi, B.K. (1993): Nonlinear dynamics of an electron-beam plasma system, *Phys. Scripta* **48**, 367.
- Rollins, D.K. and Shivamoggi, B.K. (1994): Painlevé property and group symmetries of the generalized Kortewg-deVries equation, *Phys. Scripta* **49**, 261.
- Rowlands, G. (1988): An introduction to the properties of one-dimensional difference equations, in *Order and Chaos in Nonlinear Physical Systems*, Ed. S. Lundquist, N.H. March, and M.P. Tosi, Plenum.
- Ruelle, D. and Takens, F. (1971): On the nature of turbulence, *Commun. Math. Phys.* **20**, 167.
- Saltzman, B. (1962): Finite-amplitude free convection as an initial-value problem, *J. Atmos. Sci.* **19**, 329.
- Schuster, H.G. (1989): *Deterministic Chaos*, VCH Verlag, Weinheim.
- Shannon, C.E. and Weaver, W. (1949): *The Mathematical Theory of Information*, University of Illinois Press, Urbana.
- Shaw, R.S. (1981): Strange attractors, chaotic behavior and information flow, *Z. Naturforschung* **36a**, 80.

- Shinbrot, T., Grebogi, C., Ott, E., and Yorke, J.A. (1993): Using small perturbations to control chaos, *Nature* **363**, 411.
- Shivamoggi, B.K. (1992): Multifractal aspects of the intermittency corrections to the spectrum of temperature fluctuations in isotropic turbulence, *Phys. Lett.* **168A**, 47.
- Shivamoggi, B.K. (1995a): Multifractal aspects of the fine-scale structure of temperature fluctuations in isotropic turbulence, *Physica A* **221**, 460.
- Shivamoggi, B.K. (1995b): Intermediate dissipation range for passive scalars, *Phys. Lett.* **198A**, 209.
- Shivamoggi, B.K. and Rollins, D.K. (1991): Generalized Painlevé formulation and Lie group symmetries of the Zakharov-Kuznetsov equation, *Phys. Lett. A* **160**, 263.
- Shivamoggi, B.K. and Rollins, D.K. (1994): The Painlevé formulations and exact solutions of the nonlinear evolution equations for modulated gravity wavetrains, *J. Math. Phys.* **35**, 4779.
- Shivamoggi, B.K. and Varma, R.K. (1988): Internal resonances in nonlinearly-coupled oscillators, *Acta Mech.* **72**, 111.
- Singer, D. (1978): Stable orbits and bifurcation maps of the unit interval, *SIAM J. Appl. Math.* **35**, 260.
- Smale, S. (1967): Differentiable dynamical systems, *Bull. Amer. Math. Soc.* **73**, 747.
- Sparrow, C. (1982): *The Lorenz Equations: Bifurcations, Chaos and Strange Attractors*, Springer-Verlag.
- Sreenivasan K. and Stolovitzky, G. (1995): Turbulence cascades, *J. Stat. Phys* **78**, 311.
- Stakgold, I. (1971): Branching of solutions of nonlinear equations, *SIAM Rev.* **13**, 289.
- Stanley, H.E. and Meakin, P. (1988): Multifractal phenomena in physics and chemistry, *Nature* **335**, 405.
- Stewart, R.W., Wilson, J.R., and Burling, R.W. (1970): Some statistical properties of small-scale turbulence in atmospheric boundary layer, *J. Fluid Mech.* **41**, 141.
- Strogatz, S.H. (1994): *Nonlinear Dynamics and Chaos*, Addison-Wesley, Reading, MA.

- Struble, R.A. (1962): *Nonlinear Differential Equations*, McGraw-Hill.
- Swinney, H.L. and Gollub, J.P. (1978): The transition to turbulence, *Phys. Today* **31**, 41.
- Tabor, M. (1981): The onset of chaos in dynamical systems, *Adv. Chem. Phys.* **46**, 73.
- Tabor, M. (1984): Modern dynamics and classical analysis, *Nature* **310**, 277.
- Tabor, M. (1989): *Chaos and Integrability in Nonlinear Dynamics*, Wiley & Sons, Inc.
- Takens, F. (1981): Detecting strange attractors in turbulence, in *Lecture Notes in Mathematics* Vol. 898, Springer-Verlag.
- Tél, T. (1988): Fractals, multifractals and thermodynamics, *Z. Naturforsch.* **43a**, 1154.
- Tennekes, H. and Wyngaard, J.C. (1972): The intermittent small-scale structure of turbulence, *J. Fluid Mech.* **55**, 93.
- Toda, M. (1974): Instabilities of trajectories of the lattice with cubic nonlinearity, *Phys. Lett.* **48A**, 335.
- Townsend, A.A. (1947): The measurement of double and triple correlation derivatives in isotropic turbulence, *Proc. Camb. Phil. Soc.* **43**, 560.
- Tsonis, A.A. (1992): *Chaos*, Plenum Press.
- van Atta, C.W. and Antonia, R.A. (1980): Reynolds-number dependence of skewness and flatness factors of turbulent velocity derivatives, *Phys. Fluids* **23**, 252.
- van der Burgh, A.H.P. (1976): Studies in the asymptotic theory of nonlinear resonances, *J. Sound Vib.* **49**, 93.
- Vassiliades, D.V., Sharma, A.S., Eastman, T.E., and Papadopoulos, K. (1990): Low-dimensional chaos in magnetospheric activity from AE time series, *Geophys. Res. Lett.* **17**, 1841.
- Verhulst, F. (1979): Discrete symmetric dynamical systems at the main resonances, *Phil. Trans. Roy. Soc. A* **290**, 435.
- Vicsek, T. (1992): *Fractal Growth Phenomena*, World Scientific.

- Vincent, A. and Meneguzzi, M. (1991): The spatial structure and statistical properties of homogeneous turbulence, *J. Fluid Mech.* **225**, 1.
- von Neumann, J. (1951): Various techniques used in connection with random digits, *J. Res. Nat. Bur. Std. Appl. Math. Ser. 3*, 36.
- Walker, G.H. and Ford, J. (1969): Amplitude instability and ergodic behavior for conservative nonlinear oscillator systems, *Phys. Rev.* **188**, 416.
- Ward, R.S. (1984): The Painlevé property for the self-dual gauge-field equations, *Phys. Lett.* **102A**, 279.
- Weiss, J., Tabor, M., and Carnevale, G. (1983): The Painlevé property for partial differential equations, *J. Math. Phys.* **24**, 522.
- White, R.B. (1983): Resistive instabilities and field line reconnection, in *Handbook of Plasma Physics*, Vol. I, Ed. M.N. Rosenbluth and R.Z. Sagdeev, North-Holland.
- Whittaker, E.T. (1964): *Analytical Dynamics*, Cambridge University Press.
- Wiggins, S. (1988): *Global Bifurcations and Chaos: Analytical Methods*, Springer-Verlag.
- Wu, X.Z., Kadanoff, L.P., Libchaber, A., and Sano, M. (1990): Frequency power spectrum of temperature and fluctuations in free convection, *Phys. Rev. Lett.* **64**, 2140.

INDEX

A

Action-angle variables, 118, 129, 144
Amplitude-frequency relation, 13, 48, 59
Area-preserving mapping, 4, 108, 131, 198, 200, 205, 228, 236, 379
Tangent map, 211, 226
Twist map, 207
Arnol'd diffusion, 132
Arnol'd's cat map, 232
Asymptotic stability, 21, 225, 250
Attractor
 Basin of attraction, 5, 249
 Liapunov exponent, 225, 231, 242, 252, 293, 300, 304
 Limit cycle, 5, 84
 Poincaré-Bendixson Theorem, 52, 251
 Strange, 5, 11, 247, 250, 251, 277, 326
Auto-Bäcklund transformation, 369, 372
Auto-correlation function, 225, 231

B

Baker's transformation, 239
Basin of attraction, 5, 10, 11, 249
Bernoulli shift, 241, 302, 305
Bifurcations, 6, 28, 61, 376
 Breaking, 77, 376,
 Homoclinic, 283
 Hopf, 7, 61, 65, 77, 78, 83, 376
 One-dimensional maps, 85, 244
 Period-doubling, 290
 Pitchfork 61, 69, 71, 74, 77, 82, 290, 295, 297
 Saddle-node, 61, 65, 66, 71, 77, 307

Tangent, 307
Transcritical, 67, 70, 71, 73
Binary sequences, 240
Breakdown of integrability, 160, 198
 Global criteria, 163, 166
 Local criteria, 160
 Magnetic-island overlap, 171
 Resonance-overlap, 168, 222
Burgers equation, 367

C

Canonical transformations, 105, 144, 150, 200, 378
 Infinitesimal, 121, 122, 123, 125
Canonical perturbation theory, 140, 150, 378
Cantor's set, 6, 252, 254, 257, 284, 311, 327, 380
Center, 33
Center-manifold Theorem, 25, 375
Chaos
 Conservative systems, 3, 197
 Control, 2
 Dissipative systems, 247
 Fractal, 6, 247, 254
 Intermittency, 10, 308
 Kolmogorov entropy, 225, 229
 Liapunov exponent, 225, 231, 242, 252, 293, 300, 304
 Logistic map, 289, 380, 381
 Lorenz equations, 277, 381
 Period doubling, 8, 10, 290, 293, 295
 Renormalization group, 2, 7, 11, 298
 Stretching and folding, 3, 6, 251, 253, 284, 305, 326
 Universality, 2, 7, 9, 11, 291, 297, 314
Chirikov map, 210, 379

Cole-Hopf transformation, 370
 Conservative systems, 3, 197
 Continued fractions, 155
 Contractive map, 248
 Correlation dimension, 270, 275, 276
 Couette flow, 7
 Critical phenomena, 11

D

Deterministic systems, 14
 Diffeomorphism, 199
 Dissipative systems, 3, 4, 247
 Dufing's equation, 23, 43
 Forced, 52, 53
 Dynamical Systems, 14, 197, 198
 Center-manifold Theorem, 25, 375
 Conservative systems, 3, 197
 Dissipative systems, 3, 247
 Equilibrium points, 15
 Hartman-Grobman Theorem, 25,
 62
 Phase-plane analysis, 32
 Poincaré-Bendixson Theorem, 52
 Stability, 15, 21

E

Energy shell, 131, 132, 198
 Ensemble average, 131
 Equilibrium point, 15
 Elliptic, 33
 Focus, 36
 Hyperbolic, 25, 43
 Node, 38
 Supercritical, 51
 Ergodic system, 3, 127, 201, 226, 233,
 237

F

Fibonacci numbers, 158
 Fixed point
 Elliptic, 3, 33, 206, 210, 213, 214

Hyperbolic, 3, 207, 213, 214
 Parabolic, 213
 Fixed-point Theorem, 291
 Fractal, 6, 247, 254
 Box-counting method, 261
 Cantor set, 6, 252, 254, 257, 311, 327,
 380
 Capacity dimension, 255, 267, 312
 Correlation dimension, 270, 275, 276
 Dimension, 11, 221, 257, 380
 Entropy, 11
 Generalized fractal dimension, 263, 327,
 346, 382
 Hausdorff dimension, 221, 256, 263,
 268, 310, 327, 336, 342
 Information dimension, 268
 Koch's snowflake, 259, 311
 Lorenz attractor, 277
 Multi-fractals, 262
 Nonuniform fractals, 256
 Sierpinski triangle, 260
 Turbulence, 319, 326
 Frequency locking, 138
 Frobenius-Perron equation, 302

H

Hamiltonian dynamics, 93
 Action-angle variables, 118, 129, 144
 Area-preserving mapping, 4, 108, 131,
 147, 200, 205, 228, 239
 Canonical perturbation theoroy, 140,
 150, 278
 Canonical transformations, 105, 144,
 150, 200, 378
 Hamilton's equations, 94
 Hamilton's principal function, 94, 110
 Hamilton's principle, 93
 Hamilton-Jacobi equation, 107, 112, 127,
 133, 144, 150
 Hamiltonian, 97

- I**
- Infinitesimal canonical transformations, 121, 122, 123, 125
 - Isolating integral, 117
 - Lagrange's equations, 95
 - Lagrangian, 93, 94
 - Legendre transformation, 97, 110
 - Liouville's Theorem, 3, 101, 132, 197, 198, 247
 - Noether's Theorem, 98
 - Poincaré's Recurrence Theorem, 104, 248
 - Poisson's brackets, 122, 124, 126, 377
 - Separable systems, 127
 - Symplectic structure, 93
 - Harmonic oscillator, 32, 34, 103, 107, 115, 120
 - Hartman-Grobman Theorem, 25, 62
 - Hausdorff dimension, 221, 256, 263, 268, 310, 327, 336, 342
 - Hénon map, 222
 - Hénon-Heiles system, 162, 178, 202, 222, 362
 - Heteroclinic points, 219, 222, 238
 - Homoclinic orbits, 4, 61, 218, 219, 238, 254
 - Homeomorphism, 25
 - Hopf bifurcation, 7, 8
 - Horseshoe, 4, 221, 252, 380
 - Hysteresis, 60
- K**
- Implicit Function Theorem, 62, 66, 69, 71, 73
 - Infinitesimal canonical transformations, 121, 122, 123, 125
 - Information dimension, 268
 - Integrable systems, 3, 127, 129, 140, 219, 353
 - Canonical perturbation theory, 140, 150
- Kolmogorov-Arnol'd Moser Theorem,** 3, 149, 154, 175, 216, 217, 222
- Breakdown of integrability,** 160
- Invariant tori,** 3, 5, 127, 137, 154, 214
- Painlevé property,** 4, 353, 382
- Surface of section,** 4, 46, 198
- Intermittency,** 10, 308, 319, 382
- Internal resonances,** 152, 177
- Energy sharing in nonlinearly-coupled systems, 177, 181
 - Hénon-Heiles system, 162, 178, 202, 222, 362
 - Higher-order resonances, 178
- Invariant manifold,** 25
- Invariant measure,** 244, 249, 319
- Invariant probability distribution,** 2, 132, 301
- Invariant tori,** 3, 5, 127, 137, 154, 214
- Winding number, 201
- Iso-energetic non-degenerate system,** 139, 207
- Isolating integral,** 117
- J**
- Jump phenomena,** 13, 60
- K**
- Kaplan-Yorke conjecture, 268
 - Koch's snow flake, 259, 311
 - Kolmogorov-Arnol'd Moser Theorem, 3, 144, 154, 175, 214, 216, 217, 222
 - Kolmogorov entropy, 225, 229, 268
 - Kolmogorov theory of local similarity of turbulence, 319, 328, 381
 - Korteweg-deVries equation, 370, 382, 383
- L**
- Lagrange's equations, 95
 - Landau equation, 282
 - Lax pair, 369, 372
 - Legendre transform, 97, 110, 265, 338

- Liapunov exponent, 11, 225, 231, 242, 252, Many-body problem, 144
 293, 300, 304
 Liapunov function, 22
 Liapunov stability, 21
 Limit cycle, 5, 84, 284, 375
 Linear difference equations, 286
 Liouville equation, 243
 Liouville's Theorem, 3, 101, 132, 197, 198,
 247
 Lipschitz property, 14
 Logistic map, 289, 380, 381
 Bernoulli shift, 302, 305
 Chaos, 291, 298
 Equilibria and stability, 291
 Intermittency, 308
 Invariant probability distribution, 301
 Liapunov exponents, 299, 300, 304
 Odd period cycles, 299, 306
 Period-doubling bifurcations, 290, 293,
 295
 Pitchfork bifurcations, 290, 295, 297,
 307
 Renormalization group, 298
 Saddle-node bifurcation, 307
 Stretching and folding, 305
 Universality, 291, 297, 314
 Lorenz equations, 277, 312, 381
 Chaotic behavior, 284
 Equilibria and stability, 277, 382
 Homoclinic bifurcation, 283
 Lorenz "map", 286
 Subcritical bifurcation, 283
 Supercritical bifurcation, 280, 381
- M**
- Magnetic confinement, 171, 173
 Magnetic-island overlap, 171
 Manifold, 26, 214
 Center, 26, 82, 214
 Stable, 26, 214
 Unstable, 26, 214
- Many-body problem, 144
 Markov process, 243, 301
 Master equation, 242, 301
 Melnikov's method, 219
 Micro-canonical ensemble, 132
 Mixing, 131, 235, 236, 239
 Multi-fractals, 262
 Correlation dimension, 270, 275, 276
 Generalized fractal dimension, 263, 327,
 346, 382
 Information dimension, 268
 Kaplan-Yorke conjecture, 268
 Singularity spectrum, 266, 327, 336
 Turbulence, 319, 326
- N**
- Natural measure, 131, 228
 Newton's method, 250
 Noether's Theorem, 98
 Non-autonomous system, 51
 Non-degenerate system, 139
 Non-integrable systems, 3
 Nonlinear differential equations, 13
 Amplitude-frequency relation, 13, 48, 51
 Chaotic behavior, 52
 Hysteresis, 60
 Jump phenomena, 13, 60
 Subcritical instability, 50
 Subharmonic resonance, 60
 Supercritical equilibrium, 51
 Nonlinear Schrödinger equation, 383
 Normal form, 80
 Nyquist critical frequency, 232
- O**
- Osledec's Multiplicative Ergodic Theorem,
 226
- P**
- Painlevé property, 4, 353, 382
 Auto-Bäcklund transformation, 369, 372

- Burgers equation, 367
 Cole-Hopf transformation, 370
 Hénon-Heiles system, 362
 Integrable systems, 353
 Korteweg-deVries equation, 370, 382, 383
 Lax pair, 369, 372
 Painlevé transcendent, 356
 Partial differential equations, 367
 Singularity analysis, 357
 Zakharov-Kuznetsov equation, 383
 Partition function, 265
 Peano's space filling curve, 6
 Period doubling bifurcations, 8, 10, 290, 293, 295
 Phase-plane analysis, 32, 375
 Phase space, 3, 5, 6, 98, 127
 Average, 228
 Conservative systems, 102, 197
 Dissipative systems, 103
 Reconstruction, 275
 Symplectic structure, 93
 Phase transitions, 11
 Poincaré-Bendixson Theorem, 52, 251
 Poincaré-Birkhoff Fixed Point theorem, 3, 214, 216, 222
 Poincaré-Hopf Theorem, 129
 Poincaré's Recurrence Theorem, 104, 197, 248,
 Poisson's brackets, 122, 124, 126, 377
 Power law distribution, 254, 263
 Power spectra, 225, 232
 Predictability horizon, 6, 228
- Q**
 Quadratically irrational number, 156
 Quasi-periodic motion, 5, 138, 224, 231
- R**
 Random walk process, 244
- Rayleigh-Benard convection, 8, 10, 276, 299, 312
 Recurrence, 4, 104, 249
 Renormalization group, 2, 7, 11
 Resonance, 3
 Overlap, 4, 168, 222
 Subharmonic, 60
 Ruelle-Takens scenario, 7
- S**
 Sampling Theorem, 232
 Scale invariance, 254, 319, 328, 330
 Shannon's information theory, 229
 Sierpinski carpet, 332
 Sierpinski triangle, 260
 Simple pendulum, 45, 98, 148, 219, 375, 377, 380
 Singular point, 14
 Singularity spectrum, 266, 327, 336
 Stability
 Asymptotic, 21, 225, 250, 375
 Liapunov, 21
 Subcritical, 50
 Surface of section, 4, 46, 198, 308
 Symplectic structure, 93
- T**
 Tangent map, 211, 228
 Time series data, 7, 274, 286
 Time-delay embedding technique, 274
 Toda Hamiltonian, 163
 Turbulence, 11, 308
 β -model, 327, 331, 332, 347
 Chaotic behavior, 11
 Energy cascade, 329
 Energy dissipation, 324, 325, 330, 338, 340
 Flatness factor, 319

- F**
 Fractal dimension, 327, 332, 336, 337,
 342, 382
 Fractals, 319, 326, 382
 Gamma distribution, 326
 Generalized fractal dimension, 327, 346, Zakharov-Kuznetsov equation, 383
 382
 Intermediate dissipation range, 348, 382
 Intermittency, 308, 329, 320, 382
 Inviscid dissipation of energy, 331
 Kolmogorov microscale, 349
 Kolmogorov refined similarity
 hypothesis, 338
 Kolmogorov theory of local
 similarity, 329, 328, 381
 Logarithmic normal distribution, 326,
 347
 Multi-fractals, 319, 327, 331, 336, 382
 Multi-scaling behavior, 348, 349, 350,
 382
 Probability distribution function,
 321, 323, 329
 Random- β model, 327, 340, 382
 Reynolds number, 319, 321, 324, 325,
 329
 Ruelle-Takens scenario, 7
 Scale invariance, 328, 330
 Singularity spectrum, 327, 336
 Skewness, 322
 Statistically universal state, 319, 325
 Velocity structure function, 331, 335
 Vorticity field, 323
 Twist map, 207, 215

W
 Wiener-Khinchin Theorem, 233

Z

Mechanics

FLUID MECHANICS AND ITS APPLICATIONS

Series Editor: R. Moreau

Aims and Scope of the Series

The purpose of this series is to focus on subjects in which fluid mechanics plays a fundamental role. As well as the more traditional applications of aeronautics, hydraulics, heat and mass transfer etc., books will be published dealing with topics which are currently in a state of rapid development, such as turbulence, suspensions and multiphase fluids, super and hypersonic flows and numerical modelling techniques. It is a widely held view that it is the interdisciplinary subjects that will receive intense scientific attention, bringing them to the forefront of technological advancement. Fluids have the ability to transport matter and its properties as well as transmit force, therefore fluid mechanics is a subject that is particularly open to cross fertilisation with other sciences and disciplines of engineering. The subject of fluid mechanics will be highly relevant in domains such as chemical, metallurgical, biological and ecological engineering. This series is particularly open to such new multidisciplinary domains.

1. M. Lesieur: *Turbulence in Fluids*. 2nd rev. ed., 1990 ISBN 0-7923-0645-7
2. O. Métais and M. Lesieur (eds.): *Turbulence and Coherent Structures*. 1991 ISBN 0-7923-0646-5
3. R. Moreau: *Magnetohydrodynamics*. 1990 ISBN 0-7923-0937-5
4. E. Couston (ed.): *Turbulence Control by Passive Means*. 1990 ISBN 0-7923-1020-9
5. A.A. Borissov (ed.): *Dynamic Structure of Detonation in Gaseous and Dispersed Media*. 1991 ISBN 0-7923-1340-2
6. K.-S. Choi (ed.): *Recent Developments in Turbulence Management*. 1991 ISBN 0-7923-1477-8
7. E.P. Evans and B. Coulbeck (eds.): *Pipeline Systems*. 1992 ISBN 0-7923-1668-1
8. B. Nau (ed.): *Fluid Sealing*. 1992 ISBN 0-7923-1669-X
9. T.K.S. Murthy (ed.): *Computational Methods in Hypersonic Aerodynamics*. 1992 ISBN 0-7923-1673-8
10. R. King (ed.): *Fluid Mechanics of Mixing*. Modelling, Operations and Experimental Techniques. 1992 ISBN 0-7923-1720-3
11. Z. Han and X. Yin: *Shock Dynamics*. 1993 ISBN 0-7923-1746-7
12. L. Svarovsky and M.T. Thew (eds.): *Hydroclones*. Analysis and Applications. 1992 ISBN 0-7923-1876-5
13. A. Lichiarowicz (ed.): *Jet Cutting Technology*. 1992 ISBN 0-7923-1979-6
14. F.T.M. Nieuwstadt (ed.): *Flow Visualization and Image Analysis*. 1993 ISBN 0-7923-1994-X
15. A.J. Saul (ed.): *Floods and Flood Management*. 1992 ISBN 0-7923-2078-6
16. D.E. Ashpis, T.B. Gatski and R. Hirsh (eds.): *Instabilities and Turbulence in Engineering Flows*. 1993 ISBN 0-7923-2161-8
17. R.S. Azad: *The Atmospheric Boundary Layer for Engineers*. 1993 ISBN 0-7923-2187-1
18. F.T.M. Nieuwstadt (ed.): *Advances in Turbulence IV*. 1993 ISBN 0-7923-2282-7
19. K.K. Prasad (ed.): *Further Developments in Turbulence Management*. 1993 ISBN 0-7923-2291-6
20. Y.A. Tatarchenko: *Shaped Crystal Growth*. 1993 ISBN 0-7923-2419-6

Mechanics

FLUID MECHANICS AND ITS APPLICATIONS

Series Editor: R. Moreau

21. J.P. Bonnet and M.N. Glauser (eds.): *Eddy Structure Identification in Free Turbulent Shear Flows*. 1993 ISBN 0-7923-2449-8
22. R.S. Srivastava: *Interaction of Shock Waves*. 1994 ISBN 0-7923-2920-1
23. J.R. Blake, J.M. Boulton-Stone and N.H. Thomas (eds.): *Bubble Dynamics and Interface Phenomena*. 1994 ISBN 0-7923-3008-0
24. R. Benzi (ed.): *Advances in Turbulence V*. 1995 ISBN 0-7923-3032-3
25. B.I. Rabinovich, V.G. Lebedev and A.I. Mytarev: *Vortex Processes and Solid Body Dynamics. The Dynamic Problems of Spacecrafts and Magnetic Levitation Systems*. 1994 ISBN 0-7923-3092-7
26. P.R. Voke, L. Kleiser and J.-P. Chollet (eds.): *Direct and Large-Eddy Simulation I. Selected papers from the First ERCOFTAC Workshop on Direct and Large-Eddy Simulation*. 1994 ISBN 0-7923-3106-0
27. J.A. Sparenberg: *Hydrodynamic Propulsion and its Optimization. Analytic Theory*. 1995 ISBN 0-7923-3201-6
28. J.F. Dijksman and G.D.C. Kuiken (eds.): *IUTAM Symposium on Numerical Simulation of Non-Isothermal Flow of Viscoelastic Liquids*. Proceedings of an IUTAM Symposium held in Kerkrade, The Netherlands. 1995 ISBN 0-7923-3262-8
29. B.M. Boubnov and G.S. Golitsyn: *Convection in Rotating Fluids*. 1995 ISBN 0-7923-3371-3
30. S.I. Green (ed.): *Fluid Vortices*. 1995 ISBN 0-7923-3376-4
31. S. Morioka and L. van Wijngaarden (eds.): *IUTAM Symposium on Waves in Liquid/Gas and Liquid/Vapour Two-Phase Systems*. 1995 ISBN 0-7923-3424-8
32. A. Gyr and H.-W. Bewersdorff: *Drag Reduction of Turbulent Flows by Additives*. 1995 ISBN 0-7923-3485-X
33. Y.P. Golovachov: *Numerical Simulation of Viscous Shock Layer Flows*. 1995 ISBN 0-7923-3626-7
34. J. Grue, B. Gjevik and J.E. Weber (eds.): *Waves and Nonlinear Processes in Hydrodynamics*. 1996 ISBN 0-7923-4031-0
35. P.W. Duck and P. Hall (eds.): *IUTAM Symposium on Nonlinear Instability and Transition in Three-Dimensional Boundary Layers*. 1996 ISBN 0-7923-4079-5
36. S. Gavrilakis, L. Machiels and P.A. Monkewitz (eds.): *Advances in Turbulence VI. Proceedings of the 6th European Turbulence Conference*. 1996 ISBN 0-7923-4132-5
37. K. Gersten (ed.): *IUTAM Symposium on Asymptotic Methods for Turbulent Shear Flows at High Reynolds Numbers*. Proceedings of the IUTAM Symposium held in Bochum, Germany. 1996 ISBN 0-7923-4138-4
38. J. Verhás: *Thermodynamics and Rheology*. 1997 ISBN 0-7923-4251-8
39. M. Champion and B. Deshaies (eds.): *IUTAM Symposium on Combustion in Supersonic Flows*. Proceedings of the IUTAM Symposium held in Poitiers, France. 1997 ISBN 0-7923-4313-1
40. M. Lesieur: *Turbulence in Fluids*. Third Revised and Enlarged Edition. 1997 ISBN 0-7923-4415-4; Pb: 0-7923-4416-2

Mechanics

FLUID MECHANICS AND ITS APPLICATIONS

Series Editor: R. Moreau

41. L. Fulachier, J.L. Lumley and F. Anselmet (eds.): *IUTAM Symposium on Variable Density Low-Speed Turbulent Flows*. Proceedings of the IUTAM Symposium held in Marseille, France. 1997 ISBN 0-7923-4602-5
42. B.K. Shivamoggi: *Nonlinear Dynamics and Chaotic Phenomena*. An Introduction. 1997 ISBN 0-7923-4772-2

Mechanics

SOLID MECHANICS AND ITS APPLICATIONS

Series Editor: G.M.L. Gladwell

Aims and Scope of the Series

The fundamental questions arising in mechanics are: *Why?*, *How?*, and *How much?* The aim of this series is to provide lucid accounts written by authoritative researchers giving vision and insight in answering these questions on the subject of mechanics as it relates to solids. The scope of the series covers the entire spectrum of solid mechanics. Thus it includes the foundation of mechanics; variational formulations; computational mechanics; statics, kinematics and dynamics of rigid and elastic bodies; vibrations of solids and structures; dynamical systems and chaos; the theories of elasticity, plasticity and viscoelasticity; composite materials; rods, beams, shells and membranes; structural control and stability; soils, rocks and geomechanics; fracture; tribology; experimental mechanics; biomechanics and machine design.

1. R.T. Haftka, Z. Gürdal and M.P. Kamat: *Elements of Structural Optimization*. 2nd rev.ed., 1990 ISBN 0-7923-0608-2
2. J.J. Kalker: *Three-Dimensional Elastic Bodies in Rolling Contact*. 1990 ISBN 0-7923-0712-7
3. P. Karasudhi: *Foundations of Solid Mechanics*. 1991 ISBN 0-7923-0772-0
4. *Not published*
5. *Not published*
6. J.F. Doyle: *Static and Dynamic Analysis of Structures*. With an Emphasis on Mechanics and Computer Matrix Methods. 1991 ISBN 0-7923-1124-8; Pb 0-7923-1208-2
7. O.O. Ochoa and J.N. Reddy: *Finite Element Analysis of Composite Laminates*. ISBN 0-7923-1125-6
8. M.H. Aliabadi and D.P. Rooke: *Numerical Fracture Mechanics*. ISBN 0-7923-1175-2
9. J. Angeles and C.S. López-Cajún: *Optimization of Cam Mechanisms*. 1991 ISBN 0-7923-1355-0
10. D.E. Grierson, A. Franchi and P. Riva (eds.): *Progress in Structural Engineering*. 1991 ISBN 0-7923-1396-8
11. R.T. Haftka and Z. Gürdal: *Elements of Structural Optimization*. 3rd rev. and exp. ed. 1992 ISBN 0-7923-1504-9; Pb 0-7923-1505-7
12. J.R. Barber: *Elasticity*. 1992 ISBN 0-7923-1609-6; Pb 0-7923-1610-X
13. H.S. Tzou and G.L. Anderson (eds.): *Intelligent Structural Systems*. 1992 ISBN 0-7923-1920-6
14. E.E. Gdoutos: *Fracture Mechanics*. An Introduction. 1993 ISBN 0-7923-1932-X
15. J.P. Ward: *Solid Mechanics*. An Introduction. 1992 ISBN 0-7923-1949-4
16. M. Farshad: *Design and Analysis of Shell Structures*. 1992 ISBN 0-7923-1950-8
17. H.S. Tzou and T. Fukuda (eds.): *Precision Sensors, Actuators and Systems*. 1992 ISBN 0-7923-2015-8
18. J.R. Vinson: *The Behavior of Shells Composed of Isotropic and Composite Materials*. 1993 ISBN 0-7923-2113-8
19. H.S. Tzou: *Piezoelectric Shells*. Distributed Sensing and Control of Continua. 1993 ISBN 0-7923-2186-3

Mechanics

SOLID MECHANICS AND ITS APPLICATIONS

Series Editor: G.M.L. Gladwell

20. W. Schiehlen (ed.): *Advanced Multibody System Dynamics. Simulation and Software Tools.* 1993 ISBN 0-7923-2192-8
21. C.-W. Lee: *Vibration Analysis of Rotors.* 1993 ISBN 0-7923-2300-9
22. D.R. Smith: *An Introduction to Continuum Mechanics.* 1993 ISBN 0-7923-2454-4
23. G.M.L. Gladwell: *Inverse Problems in Scattering. An Introduction.* 1993 ISBN 0-7923-2478-1
24. G. Prathap: *The Finite Element Method in Structural Mechanics.* 1993 ISBN 0-7923-2492-7
25. J. Herskovits (ed.): *Advances in Structural Optimization.* 1995 ISBN 0-7923-2510-9
26. M.A. González-Palacios and J. Angeles: *Cam Synthesis.* 1993 ISBN 0-7923-2536-2
27. W.S. Hall: *The Boundary Element Method.* 1993 ISBN 0-7923-2580-X
28. J. Angeles, G. Hommel and P. Kovács (eds.): *Computational Kinematics.* 1993 ISBN 0-7923-2585-0
29. A. Curnier: *Computational Methods in Solid Mechanics.* 1994 ISBN 0-7923-2761-6
30. D.A. Hills and D. Nowell: *Mechanics of Fretting Fatigue.* 1994 ISBN 0-7923-2866-3
31. B. Tabarrok and F.P.J. Rimrott: *Variational Methods and Complementary Formulations in Dynamics.* 1994 ISBN 0-7923-2923-6
32. E.H. Dowell (ed.), E.F. Crawley, H.C. Curtiss Jr., D.A. Peters, R. H. Scanlan and F. Sisto: *A Modern Course in Aeroelasticity.* Third Revised and Enlarged Edition. 1995 ISBN 0-7923-2788-8; Pb: 0-7923-2789-6
33. A. Preumont: *Random Vibration and Spectral Analysis.* 1994 ISBN 0-7923-3036-6
34. J.N. Reddy (ed.): *Mechanics of Composite Materials.* Selected works of Nicholas J. Pagano. 1994 ISBN 0-7923-3041-2
35. A.P.S. Selvadurai (ed.): *Mechanics of Poroelastic Media.* 1996 ISBN 0-7923-3329-2
36. Z. Mróz, D. Weichert, S. Dorosz (eds.): *Inelastic Behaviour of Structures under Variable Loads.* 1995 ISBN 0-7923-3397-7
37. R. Pyrz (ed.): *IUTAM Symposium on Microstructure-Property Interactions in Composite Materials.* Proceedings of the IUTAM Symposium held in Aalborg, Denmark. 1995 ISBN 0-7923-3427-2
38. M.I. Friswell and J.E. Mottershead: *Finite Element Model Updating in Structural Dynamics.* 1995 ISBN 0-7923-3431-0
39. D.F. Parker and A.H. England (eds.): *IUTAM Symposium on Anisotropy, Inhomogeneity and Nonlinearity in Solid Mechanics.* Proceedings of the IUTAM Symposium held in Nottingham, U.K. 1995 ISBN 0-7923-3594-5
40. J.-P. Merlet and B. Ravani (eds.): *Computational Kinematics '95.* 1995 ISBN 0-7923-3673-9
41. L.P. Lebedev, I.I. Vorovich and G.M.L. Gladwell: *Functional Analysis. Applications in Mechanics and Inverse Problems.* 1996 ISBN 0-7923-3849-9
42. J. Menčík: *Mechanics of Components with Treated or Coated Surfaces.* 1996 ISBN 0-7923-3700-X
43. D. Bestle and W. Schiehlen (eds.): *IUTAM Symposium on Optimization of Mechanical Systems.* Proceedings of the IUTAM Symposium held in Stuttgart, Germany. 1996 ISBN 0-7923-3830-8

Mechanics

SOLID MECHANICS AND ITS APPLICATIONS

Series Editor: G.M.L. Gladwell

44. D.A. Hills, P.A. Kelly, D.N. Dai and A.M. Korsunsky: *Solution of Crack Problems. The Distributed Dislocation Technique.* 1996 ISBN 0-7923-3848-0
45. V.A. Squire, R.J. Hosking, A.D. Kerr and P.J. Langhorne: *Moving Loads on Ice Plates.* 1996 ISBN 0-7923-3953-3
46. A. Pineau and A. Zaoui (eds.): *IUTAM Symposium on Micromechanics of Plasticity and Damage of Multiphase Materials.* Proceedings of the IUTAM Symposium held in Sèvres, Paris, France. 1996 ISBN 0-7923-4188-0
47. A. Naess and S. Krenk (eds.): *IUTAM Symposium on Advances in Nonlinear Stochastic Mechanics.* Proceedings of the IUTAM Symposium held in Trondheim, Norway. 1996 ISBN 0-7923-4193-7
48. D. Ieşan and A. Scalia: *Thermoelastic Deformations.* 1996 ISBN 0-7923-4230-5
49. J. R. Willis (ed.): *IUTAM Symposium on Nonlinear Analysis of Fracture.* Proceedings of the IUTAM Symposium held in Cambridge, U.K. 1997 ISBN 0-7923-4378-6
50. A. Preumont: *Vibration Control of Active Structures. An Introduction.* 1997 ISBN 0-7923-4392-1
51. G.P. Cherepanov: *Methods of Fracture Mechanics: Solid Matter Physics.* 1997 ISBN 0-7923-4408-1
52. D.H. van Campen (ed.): *IUTAM Symposium on Interaction between Dynamics and Control in Advanced Mechanical Systems.* Proceedings of the IUTAM Symposium held in Eindhoven, The Netherlands. 1997 ISBN 0-7923-4429-4
53. N.A. Fleck and A.C.F. Cocks (eds.): *IUTAM Symposium on Mechanics of Granular and Porous Materials.* Proceedings of the IUTAM Symposium held in Cambridge, U.K. 1997 ISBN 0-7923-4553-3
54. J. Roorda and N.K. Srivastava (eds.): *Trends in Structural Mechanics. Theory, Practice, Education.* 1997 ISBN 0-7923-4603-3
55. Yu. A. Mitropolskii and N. Van Dao: *Applied Asymptotic Methods in Nonlinear Oscillations.* 1997 ISBN 0-7923-4605-X
56. C. Guedes Soares (ed.): *Probabilistic Methods for Structural Design.* 1997 ISBN 0-7923-4670-X